

TECHNICAL REPORT

**VARIATIONS IN THE THERMAL STRUCTURE
AND WIND FIELD OCCURRING IN THE
WESTERN INDIAN OCEAN DURING THE
MONSOONS**

WHOI
DOCUMENT
COLLECTION

JOHN G. BRUCE

DATA LIBRARY
Woods Hole Oceanographic Institution

AUGUST 1981

Approved for public release; distribution unlimited

PREPARED BY
COMMANDING OFFICER,
NAVAL OCEANOGRAPHIC OFFICE
NSTL STATION, BAY ST. LOUIS, MS 39522

PREPARED FOR
COMMANDER
NAVAL OCEANOGRAPHY COMMAND
NSTL STATION, BAY ST. LOUIS, MS 39529

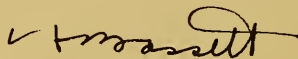


GC
1
.743
NW-TR-272

FOREWORD

A series of temperature sections from expendable bathythermographs over a 4½ year period off the Somali and Arabian coasts described in this report shows the complex eddy structure formed each year during the southwest monsoon. These eddies may be three to five times the diameter of Gulf Stream rings. Strong near-surface fronts associated with the boundaries of the larger eddies are formed.

This report gives an idea of the extreme frontal variability that occurs seasonally in this region and information about the strong wind system driving the circulation.



C. H. BASSETT
Captain, USN
Commanding Officer



WHOI
DOCUMENT
COLLECTION

REPORT DOCUMENTATION PAGE		READ INSTRUCTIONS BEFORE COMPLETING FORM
1. REPORT NUMBER TR-272	2. GOVT ACCESSION NO.	3. RECIPIENT'S CATALOG NUMBER
4. TITLE (and Subtitle) VARIATIONS IN THE THERMAL STRUCTURE AND WIND FIELD OCCURRING IN THE WESTERN INDIAN OCEAN DURING THE MONSOONS		5. TYPE OF REPORT & PERIOD COVERED
7. AUTHOR(s) John G. Bruce		6. PERFORMING ORG. REPORT NUMBER
9. PERFORMING ORGANIZATION NAME AND ADDRESS Naval Oceanographic Office (Code 9100) NSTL Station Bay St. Louis, MS 39522		8. CONTRACT OR GRANT NUMBER(s)
11. CONTROLLING OFFICE NAME AND ADDRESS		10. PROGRAM ELEMENT, PROJECT, TASK AREA & WORK UNIT NUMBERS
14. MONITORING AGENCY NAME & ADDRESS (if different from Controlling Office)		12. REPORT DATE August 1981
		13. NUMBER OF PAGES
		15. SECURITY CLASS. (of this report) UNCLASSIFIED
		15a. DECLASSIFICATION/DOWNGRADING SCHEDULE
16. DISTRIBUTION STATEMENT (of this Report) Approved for public release; distribution unlimited.		
17. DISTRIBUTION STATEMENT (of the abstract entered in Block 20, if different from Report)		
18. SUPPLEMENTARY NOTES		
19. KEY WORDS (Continue on reverse side if necessary and identify by block number)		
20. ABSTRACT (Continue on reverse side if necessary and identify by block number) The changes occurring in the temperature field in the Somali Basin and off the Arabian coast have been monitored from October 1975 through December 1979 by a time series of temperature sections obtained along the tanker sea lane offshore between 20°S and 22°N. The development and decay of the large eddy (up to roughly 600 km in diameter) in the northern Somali Basin and its smaller associated eddies were observed each southwest monsoon. Strong horizontal thermal gradients particularly in the upper 200 m occur at the eddy boundaries, and currents in this region can attain velocities of up to 7 knots. (con'd)		

WHOI
DOCUMENT
COLLECTION

MBL/WHOI
0 061997
9
0 061997
0 061997
0 061997

20. Abstract (con'd)

Monthly wind stress contoured for the western Indian Ocean clearly shows the southwest monsoon from May through September (with values over 4 dynes cm^{-2} during July) to be considerably stronger than the northeast monsoon with a maximum in January. Maps of wind stress curl during the southwest monsoon show a large region of negative curl (over -4×10^{-8} dynes cm^{-3}) to the northeast off the Somali coast, whereas a region of high positive curl occurs off the Arabian peninsula and in a small band off the Somali east coast north of 5°N . Sverdrup mass transports of up to 40×10^{12} g sec^{-1} to the north off the Somali coast are in rough agreement with observed values.

CONTENTS

		<u>Page</u>
1.	INTRODUCTION	1
2.	BACKGROUND AND RESULTS	1
3.	WIND FIELD IN THE WESTERN INDIAN OCEAN	5
4.	WIND DATA	6
5.	WESTERN INDIAN OCEAN WIND STRESS FIELD	6
6.	CURL OF WIND STRESS DURING MONSOONS	8
7.	TOTAL MERIDIONAL TRANSPORT	9
8.	CONCLUSIONS	10
	REFERENCES	12

FIGURES

Figure 1a.	14
Figure 1b.	15
Figure 2.	16-69
Figure 3.	70
Figure 4.	71
Figure 5.	72-125
Figure 6.	126
Figure 7.	127
Figure 8.	128
Figure 9.	129
Figure 10.	130
Figure 11.	131
Figure 12.	132
Figure 13.	133
Figure 14.	134-157
Figure 15.	158
Figure 16.	159
Figure 17.	160
Figure 18.	161
Figure 19.	162
Figure 20.	163
Figure 21.	164
Figure 22.	165
Figure 23.	166
Figure 24.	167
Figure 25.	168
Figure 26.	169
Figure 27.	170
Figure 28.	171

TABLE

Table 1. Number of Observations in Subdivisions	7
---	---

ACKNOWLEDGEMENTS

The author would like to express particular thanks to the EXXON Corporation for allowing us the use of their tankers. Without their generous cooperation this experiment would have been impossible. Special thanks are also due the University of Cape Town Oceanographic Department, particularly J. K. Mallory, E. S. W. Simpson, and L. Wolhuter. Data required for constructing the wind stress maps were kindly furnished by the late A. Bunker. The author is indebted to Tochiko Turner for considerable help in data analysis and to Linda-Anne Stanley for typing and help in putting this report together.

Support during the experiment was to the Woods Hole Oceanographic Institution from the Office of Naval Research under contract N00014-14-C-0262, NR-083-004 and N00014-79-C-0071, NR-083-004. The National Science Foundation furnished support also during the initial stage of the experiment under grant ATM 74-2226 A01.

1. INTRODUCTION

A program of XBT measurements in the northwestern and equatorial Indian Ocean has continued from the end of the southwest monsoon in 1975 through 1979. A series of temperature sections has been accumulated which, combined with other surveys in the area, has given a considerable amount of information about this region. The long-range scientific objectives have been to attempt an understanding of the circulation characteristics particularly in the Somali Basin and off the Arabian coast, in order to examine the time variations and horizontal scale of the eddy circulation associated with the commencement of the dominant southwest monsoon, the variation during an entire season and also that from year to year. It is important to know whether certain preferred modes exist in the current patterns, the decline of the flow upon cessation of the monsoon winds, the changes in the heat content of the mixed layer, the variations in the region of strong upwelling off the Somali and Arabian coasts, and the changes occurring in the near-equatorial dynamic topography as a result of the Somali circulation.

These studies in the western Indian Ocean are important to the Navy because considerable information about the unusually strong horizontal temperature gradients which develop during northern summer off the Somali and Arabian coasts within a relatively short period (two to three months for full strength) has been obtained. The surface currents associated with these gradients are on the order of twice those found in the Gulf Stream, and volume transports in the upper 200 m exceed that of the Gulf Stream. Variation in acoustic patterns should be expected in this area.

This program was set up for monitoring the thermal structure in the northwestern Indian Ocean by means of XBT observations from tankers and other available ships. It is a cooperative effort originated and managed by the Woods Hole Oceanographic Institution and shared during 1979 by the U. S. Naval Oceanographic Office. The University of Cape Town, South Africa, has cooperated with and aided the observational program. This study has been part of INDEX (Indian Ocean Experiment), a program designed for examining the circulation dynamics by a series of oceanographic studies associated with the First GARP Global Experiment (FGGE).

2. BACKGROUND AND RESULTS

A series of temperature sections along the tanker sea lane (figure 1a) off the East African and Arabian coasts has allowed the observation of the seasonal development of large eddies which occur during the period of strong southwest monsoon winds in the northwestern Indian Ocean. For five consecutive years (1975-1979), a large eddy described by Bruce (1968) was formed in the northern Somali Basin between approximately 4°N and 12°N .

This eddy appears to be the first to form in the region upon commencement of the southwest monsoon; it is considerably larger and more energetic than other eddies formed there during the year; and it has been observed to remain in this location at least three months after cessation of the southwest monsoon. It is first discernable from sections in late May or early June in the near surface waters (0-100 m) and continues to intensify until late September or early October at the end of the southwest monsoon. The fully developed eddy

is clearly evident as indicated by the depressed isotherms of the temperature sections in figure 1. The horizontal dimensions across the prime eddy are 400 to 600 km with variations occurring during a single monsoon season (Bruce, 1970) as well as yearly differences which will be described here.

An eddy of smaller horizontal dimensions which appears to be associated with the prime eddy was found each year (1979-1979) off Socotra between 12°N to 15°N. During some years such as 1976 and 1979 [also 1970 (Bruce, 1973)] an eddy was observed south of about 5°N and adjacent to the southern boundary of the prime eddy and to the east African coast.

Observations during several surveys within the last fifteen years indicate that the northeastward current flowing alongshore (Somali Current) is clearly part of the eddy field found each southwest monsoon off the Somali coast (Swallow and Bruce, 1966; Bruce, 1968, 1973). The current diverges from the coast turning eastward about 9°N to 10°N each year and during some years also at 3°N to 5°N forming a southern eddy. Farther offshore (55°E to 58°E), it turns southward and then back toward the shore. All past measurements known to the author indicate that during the southwest monsoon, a clockwise "warm" eddy (prime eddy) of this general description occurs within the Somali Basin. Pronounced upwelling with surface temperatures as low as 13°C (Warren et al., 1966) is found in the region where the strong coastal current turns offshore.

The program has utilized ships of opportunity (EXXON tankers) en route along the sea lane between the Persian Gulf and South Africa. These obtained a temperature-depth (0-450 m) section with expendable bathythermograph probes (XBTs) on an average of approximately every three weeks along essentially the same track. The track location is extremely fortuitous in that it passes directly through the central region of the eddy field and thus provides an excellent means of monitoring the growth and decay of the eddies formed during each southwest monsoon. The measurements were obtained by special observers who were placed aboard at Cape Town, South Africa, and made a round trip to the Persian Gulf, thus obtaining two sections per trip. Altogether 55 sections were completed (figure 2). The closely spaced stations (20-30 km apart) necessary to observe the small scale features of the temperature structure essentially require a full time observer who was also needed to maintain good quality control of the data and record, at each station, wind velocity, ship's set by currents, surface salinity samples, etc.

With each of the sections shown in figure 1 (which represents the fully developed southwest monsoon eddy system) is given a schematic representation of the circulation pattern of the near-surface water (upper 150 m). This estimate is aided by previous surveys in this area (Bruce, 1968, 1970) during which time the structure of the eddies to the east and west of the tanker track was observed. The complete time sequence showing the changes occurring in the thermal structure of the eddy field is given in figure 2. In late March and April no large scale horizontal gradients generally are evident in the upper thermocline, whereas in the late June - early July sections the prime eddy is clearly discernible roughly between 5°N to 10°N. Then during July and August (the periods of maximum wind strength) the development intensifies with a deepening of the mixed layer in the central regions of the prime eddy (centered approximately 8°N) and the Socotra eddy (12°N to 14°N). By

December a relaxation of the eddy field is evident. During some years, however, the prime eddy is still discernible in the upper layer as late as January (i.e., January 1976).

Although a large eddy is found each year within the northern Somali Basin, there are some differences from year to year. Probably the most evident is the formation of a southern loop or eddy in 1976 and 1979. The pattern at that time was similar to that found in 1970 (Bruce, 1973). The coastal surface current turned offshore about 5°N to the south of the prime eddy. Normally in the case of a single large eddy as observed during 1976 and 1977 the strong upwelling associated with the divergence of the coastal current from the coast occurs at approximately 9°N to 11°N . When the southern circulation or eddy forms and becomes well developed, strong upwelling also occurs at 4°N to 6°N . Although this circulation is termed an eddy, some of the flow extends south of the equator and may in fact not all return to the coastal current regime.

Judging from XBT data from 1975 through July 1979, it appeared that once the general pattern of circulation becomes established during the monsoon, it then tends to continue throughout the duration of the monsoon. For example, between late May and mid-October 1976 (see figure 2), all eight tanker XBT sections obtained throughout this period indicate that both the southern eddy and prime eddy were present. However, this might not always hold true. During late August 1979 (figure 2), a northward shift in the northern boundary of the southern eddy near 5°N occurred. This shift occurred in the following manner: during the early stages of the development of the 1979 southwest monsoon eddies, a large southern eddy and the northern prime eddy were both clearly established by June in the Somali Basin. This circulation resulted in the current turning offshore and forming a wedge of cold upwelled water in two locations: 4°N to 5°N , and 9°N to 10°N . The general location and size of the eddies tended to remain approximately the same through early August. The ESSO HONOLULU XBT section, 14-18 July 1979 (figure 2), is representative of the temperature structure along the tanker sea lane. The strong gradients above 150 m depth near 4°N occur at the northern edge of the southern eddy. The cold near-surface water advected offshore by the anticyclonic eddy extends through the section here. It may be seen that the southern eddy is relatively shallow whereas the northern prime eddy (4°N to 10°N) exhibits horizontal temperature gradients at least to 400-500 m depth. The upwelled cold water also extends offshore through the section near 10°N . As found in each previous southwest monsoon during which data in this region have been collected (Bruce, 1979), the Socotra eddy also occurred in 1979 (10°N to 14°N). Because of the relatively fresh ($35.135.3$ ‰) near-surface water entrained in the system of eddies from the Somali coastal current, a surface salinity map serves as a remarkably good method for examining the circulation pattern. By mid-August the northern front and cold wedge associated with the southern eddy began a northward translation at a rate of $15\text{-}30$ cm s^{-1} . By late August the southern eddy apparently had merged with the northern prime eddy as indicated by the temperature section taken 25-31 August 1979 from the ESSO CARRIBBEAN (figure 2) and a map of surface salinity (figure 3) obtained during the survey aboard USNS WILKES. The satellite imagery of sea surface temperature also indicated this translation during August. The coalescence of the southern eddy with the northern prime eddy is somewhat similar to that observed during August and September 1970 by Bruce (1973), although for 1979 the data was obtained more frequently during the occurrence.

Data collected from WILKES during August and September included 415 XBTs and 27 STD stations. In addition to observing the shift of the southern eddy, the prime or northern eddy was surveyed. Also a more detailed study of the Socotra eddy was obtained than has been made to date.

In 1975, 1977, and 1978, whereas a well-developed southern eddy was not evident, still there appear to be variations in the near-surface (0-100 m) structure that suggest that some offshore flow might occur between 3°N and 5°N. For example, along the 19-23 October 1975 section (figure 1b) at 4°N to 5°N, there are small scale temperature gradients which suggest a weak eastward flow in the upper 100 m. It seems possible that the returning onshore flow (2°N to 5°N) of the prime eddy or northern eddy might well affect changes in the alongshore current flow. Similar observations are described in laboratory scale models for fluidics research (Carbonare *et al.*, 1970). A small southern eddy was found during the early stage of the southwest monsoon 1978 (Bruce *et al.*, 1980) although it did not appear to attain the size or strong horizontal gradients occurring during 1976 or 1979.

The time series of sections following the development of the eddy structure through the early stages of the southwest monsoon (March through June) indicate that the prime eddy first forms between 5°N to 10°N in the Somali Basin, with the center at approximately 8°N, 53°E. The data do not suggest that the northern eddy is formed at the equator and then translates northeastward along the coast as postulated by the numerical models of Cox (1976), and Hurlburt and Thompson (1976).

The strong signal during the southwest monsoon in the surface dynamic topography (7°N to 10°N) of the sea surface within the prime eddy is evident in figure 4 and the complete series in figure 5. The same temperature-salinity relationship for the Somali Basin during the southwest monsoon (a mean temperature-salinity curve determined by values obtained from previous surveys during the southwest monsoon period) was used for all the determinations shown. The density gradients that occur in the Somali eddies, as in the Gulf Stream, are largely a function of temperature. The pronounced downward slope of the surface dynamic topography to the north in figure 4 occurs between 8°N to 12°N with values on the order of 2×10^{-3} dynes g^{-1} (about the same as found across the Gulf Stream at 36°N). The volume transport of the prime eddy to the east offshore amounts to 38 to 42×10^6 m^3 sec^{-1} (0-400 dbar, rel. 400 dbar) with a comparable return flow inshore to the south between 4°N to 8°N. To the north of the prime eddy, the Socotra eddy occurs each of the five observation years with transports on the order of 9 to 15×10^6 m^3 sec^{-1} . The temperature sections and surface dynamic topography show that this eddy during 1979 (center of eddy along sections is about 12°N) was well developed from July through October (figures 2 and 5).

The surface temperature (figure 6) and salinity (figure 7) characteristics of the western Indian Ocean, particularly in the region of the Somali Basin, are changed considerably during the southwest monsoon as a result of several factors: 1) the advection into the basin by the Somali Current of relatively cool and fresh South Equatorial Current water, 2) high evaporation, 3) advection of upwelled water (also relatively fresh and cool) off the Somali Coast, 4) vertical mixing resulting from the very large wind stress at the sea surface during the southwest monsoon, and 5) horizontal mixing within the

anticyclonic eddies. Within the upper 100 m (approximation of the mixed layer depth) along the tanker sea lane between 2°N and 12°N during the monsoon period (approximately three months) there was a heat loss of approximately 3×10^{12} to 5×10^{12} cal/cm as determined from the XBT temperature stations (figure 8). Now the area of the region influenced by entrainment within the eddy circulation where relatively good mixing is found (Bruce, 1968) extends roughly 400 km offshore. Thus the total heat loss of the area would be about 10^{20} cal if the tanker section is assumed to be representative of the area. The rate of heat loss during the southwest monsoon is the same order of magnitude as that found in the western North Atlantic on an annual average (Bunker and Worthington, 1976), although in the Somali region the loss occurs only over the monsoon period and is regained again in the interim northern fall and spring warming period between the northeast and southwest monsoons.

Although there is a heat loss in the upper 100 m during the southwest monsoon, at the same time because of the deepening of the isotherms below the prime eddy there is a heat gain in the layers deeper than the mixed layer (figures 9, 10 and 11). Thus the amount of actual heat lost to the atmosphere would be reduced by the transfer of heat to deeper layers. After the southwest monsoon as the eddy slowly weakens, as shown by the series of XBT temperature sections, heat is released from these layers for three to four months after the monsoon. There is evidence from the sections that the prime eddy in fact might have been maintained from 1975 to 1976 (in particular see 22-27 January 1976, figure 2) through the northeast monsoon as suggested from earlier measurements by Bruce and Volkmann (1969); however, it is not clear that the continuity occurred during other years.

The data indicate that the temperature of the mixed layer of the equatorial water in the Somali Basin as well changes at the time the eddy field is built up. Between 1°N to 1°S during the southwest monsoon the near-surface water along the tanker lane (48°E to 50°E) becomes cooler resulting in a corresponding drop in sea surface dynamic height (relative to 400 dbar) on the order of 0.10 to 0.15 dynamic meters (figure 12). In figure 2 the reduction of temperature in the mixed layer can be seen to occur after the spring warming period each year. During the warming period the layer normally reaches 28°C to 30°C. By July and August after the eddy field has developed the temperature drops to about 25°C to 26°C in this region. After the cessation of the southwest monsoon by November the layer had again warmed (27°C to 28°C). These changes are clearly shown in the surface temperature values given in figure 6. It seems that this change might well influence the strength and/or direction of the equatorial undercurrent because a local slope of the sea surface which is negative westward might occur. Taft and Knauss (1967) found no evidence of the undercurrent on the western side of the Indian Ocean during the months of the southwest monsoon. It should be noted that although there are only surface salinity observations from these XBT sections, it turns out that the hydrographic data from this equatorial region indicate that the probable seasonal salinity variations would produce changes in the sea surface dynamic height of only about 0.01 dynamic meters.

3. WIND FIELD IN THE WESTERN INDIAN OCEAN

Recent interest in the effect of monsoonal winds on the circulation of the Indian Ocean has resulted in several programs of oceanographic measurement

both of the Somali current and equatorial dynamics in the western and central Indian Ocean. As part of the oceanographic participation (INDEX, Indian Ocean Experiment) during FGGE, the eddy structure and current system off the Somali coast was studied during the 1979 southwest monsoon (May-September) with particular emphasis on the commencing stage of the monsoon. Since considerable data have been made available from the National Climatic Center (NCC) on past wind measurements throughout this region, it is felt that some discussion of these observations would be worthwhile.

4. WIND DATA

Using the NCC ship observations from the TDF-11 tapes, Bunker (1976) prepared a program for calculating sea surface energy fluxes. From these determinations the values of wind stress over the western Indian Ocean kindly were made available by him. Using these values, maps of monthly averages of τ_x and τ_y were contoured in order to observe the patterns occurring during the southwest (May through September) and northeast (December through February) monsoons.

The values of C_D in the equation $\tau = \rho C_D U_{10}^2$ (ρ is air density, U_{10} is average wind speed at 10 m or ship's anemometer level) were selected by Bunker (1979, table 2) using various classes of air-sea temperature differences and wind speed ranges from the work of several investigators. Monthly averages for the period 1922-1972 were obtained for subdivisions of the Marsden squares as shown in figure 13 which gives the center of gravity of the observation positions. The total number of observations for each subdivision is given in table 1. The remoteness of some regions of the Indian Ocean results in a number of lesser traveled sea lanes as may be seen by comparing the volume of observations in table 1 with that of the North Atlantic in Bunker (1976, figure 3). The subdivisions of the Marsden squares have been adjusted in an attempt to include sufficient monthly observations to be significant. Averages for periods greater than a month would be of considerably less value in depicting the relatively rapid seasonal changes occurring during the monsoons.

5. WESTERN INDIAN OCEAN WIND STRESS FIELD

The maps of wind stress (figure 14) have been contoured with the same interval, $0.2 \text{ dynes cm}^{-2}$, for all months with τ_x and τ_y positive to the east and north respectively. Perhaps the most outstanding characteristic of the monthly maps is the large difference in magnitude of the wind stress field between the two monsoons. The southwest monsoon reaches its greatest strength during July and the northeast monsoon during January. In the early stage of the southwest monsoon the components become positive by May off the Somali coast around 5°N to 10°N with the largest values ($> 1 \text{ dyne cm}^{-2}$) near 8°N . This region is where the first evidence of upwelling at the sea surface is observed from the maps of Wyrтки (1971) with near coastal temperatures falling below 27°C . The June and July averages indicate the rapid development of the areas of high positive stress values, particularly off northeast Somali at about 10°N to 12°N . June averages greater than 2 dynes cm^{-2} extend over half the distance to the Indian coast and meridionally between 5°N to 15°N . During July areas with over 4 dynes cm^{-2} occur, and the band encompassing the strong

TABLE I
Number of Observations in Subdivisions, Figure
for Period 1922-1972

Mar. Sq.	103	102	068	067	066	065	032	031	030	029	331	330	329	328
Lat.	20-30N	10-20N	10-20N	10-20N	20-20N	10-20N	0-10N	0-10N	0-10N	0-10N	0-10S	0-10S	0-10S	0-10S
Long (E)	50-60E	60-70E	40-50E	50-60E	60-70E	70-80E	40-50E	50-60E	60-70E	70-80E	40-50E	50-60E	60-70E	70-80E
1	18598	1031	2352	23134	3442	1318	551	898	7819	4852	2477	2632	1862	2529
2	23090	858	7155	15929	5279	1809	707	3611	11001	5093	3779	3134	2642	1290
3	7869	915	7313	11345	3014	1225	870	5895	959	5212	2972	2257	1705	3607
4		5151	6929	6858	7766	1625	881	4549	6985	10737	4471	1245	1093	707
5		2569	6845	4632	1649	3150	661	916	1245	5790	2288	1410	902	2036
6		1331	9875	4456	6282	3712	858	923	1116	16557	4938	1516	3538	
7		5118	8812	4349	2354	3909	860	3506	599	2679	2659	514	968	
8		3687	13734	8682	4362	3850	755	3327	1026	13387	3963	1682	5945	
9		2167	15104	6927	3525	3988	814	2038	1114	3650	4314	189	4241	
10			2528	10931	1846	4767	936	1733	1141	3651	3113	1149	2417	
11								1306	679					
12								962	384					
13								406						
14								796						
15								350						
16								883						
	49,557	22,827	80,647	97,243	39,519	29,353	7,893	29,664	36,503	71,608	34,974	10,678	13,254	27,278

Total 550,998 observations

gradient south of the region of the maximum stress values extends northeastwards from the African coast to about 65°E. The general pattern of the contours is similar for August and September, however, with a continued weakening of stress to 0.2 dynes cm⁻² or less by October.

There are apparently fluctuations of a shorter duration than could be shown by monthly averages during the build-up of the southwest monsoon wind field. Schott and Fernandez-Partagas (1980) have found that the wind for May and June 1979 varies over a period of a few days in both speed and direction. The variations were evident in three-day averaged ship observations as well as records from shore stations and cloud-level winds from satellite data.

The first evidence of wind reversal and the commencing of the northeast monsoon is also indicated off the Somali coast about 6°N to 10°N during November. By January at the maximum strength of this monsoon values of -1.0 dynes cm⁻² occur, these being along the Somali coast approximately between 0°N and 10°N. The wind stress then diminishes by March. April and October, the months falling between monsoons, have relatively low values over most of the northwestern Indian Ocean.

6. CURL OF WIND STRESS DURING MONSOONS

The increase of the curl of the wind stress during the commencement of the southwest monsoon starting in May and reaching maximum values in July is shown in the maps of figures 15, 16, and 17. The curl maps were constructed using the gradients of the wind stress field given in figure 14 with a grid spacing of 2° for both latitude and longitude.

The most negative values first appear in the Somali Basin (5°N to 8°N, 53°E) by May and increase through July. They tend to lie in a band extending from the central Somali Basin on toward the northeast to about 65°E.

Values during July of -6×10^{-8} dynes cm⁻³ in the region, 5°N to 10°N, 54°E to 59°E, occur approximately where the thermocline deepens in the central part of the large Somali anticyclonic eddy observed each southwest monsoon (Bruce, 1968, 1979). There is insufficient data concerning the prevalence and structure of the eddy field to the northeast of the Somali Basin, 10°N to 15°N, 60°E to 65°E, where the curl values up to -10×10^{-8} dynes cm⁻³ are shown for July, to estimate the probable location of these mid-ocean eddies. However, there is evidence from the near-surface dynamic topography that they occur here (Bruce, 1968). Also from Robinson *et al.* (1979) (figures 18 and 19) the depth to the top of the thermocline reaches a maximum during the southwest monsoon in the region of large negative curl values and the patterns of the maps of curl and thermocline depth are somewhat similar.

A region of positive curl to the north of this band is found off the Arabian coast (values over 10×10^{-8} dynes cm⁻³) and extends down to the southwest just off the Somali coast to about 4°N. The region where the Somali current turns offshore has been observed to be between about 4°N to 9°N (Bruce, 1979) within the area of positive curl. Here upwelling and the upward vertical velocity reaches a maximum in the near surface water (calculated by Swallow and Bruce (1966) to be 7×10^{-3} cm sec⁻¹ while the thickness of the mixed layer decreases.

During the period of maximum strength of the northeast monsoon in January, the values of curl are substantially less than those of July. Over much of the Somali Basin the curl becomes positive (figure 20) up to $>1 \times 10^{-8}$ dynes cm^{-3} with a small area about 10°N just off the Somali coast which is $>2 \times 10^{-8}$ dynes cm^{-3} . In the region to the north of the contour of zero curl between the Somali east coast and the Indian west coast (which has positive curl during the southwest monsoon), the curl during the northeast monsoon becomes negative. A similar reversal of sign occurs to the south of the zero contour. Although in general there is a change of sign of the curl between monsoons, the magnitude of the values in most regions is considerably less during the northeast monsoon.

7. TOTAL MERIDIONAL TRANSPORT

From the July and January values of curl (representing the maximum values for each monsoon) the meridional mass transport (Sverdrup transport), $M_y = \beta^{-1} \text{curl } \bar{\tau}$ can be determined (Stommel, 1965). M_y is the sum of the geostrophic and Ekman transports. Values were summed over areas of 2° latitude and longitude (figures 21 and 22) from the eastern boundary (transport function considered zero here), i.e., the west coast of India and Sri Lanka and from 80°E for the region south of Sri Lanka down to 2°N , toward the west approaching the Somali and Arabian Coasts.

In the Somali Basin during July the transport is greater than 30×10^{12} g sec^{-1} and in two regions near 6°N and 12°N greater than 40×10^{12} g sec^{-1} to the south. For continuity this would require a northward current of equal magnitude along the Somali coast and off the island of Socotra (12°N , 54°E). The transport around 6°N is in agreement with direct measurements here which amount to 40 to 50×10^{12} g sec^{-1} (Swallow and Bruce, 1966) (figure 22), however, a more northerly section (up to $8^{\circ} 40'\text{N}$) of direct measurements where the current turns offshore during the same cruise had a transport over 60×10^{12} g sec^{-1} . It was also found that in the North Atlantic the computations of transport failed to account for the large observed transports in the Gulf Stream after it leaves the coast (Leetmaa and Bunker, 1978). The Somali Basin, as in this area of the Atlantic, has a strong eddy field which in part might account for the greater transport. The northwestern Indian Ocean is subjected to large seasonal changes in wind stress, particularly with the onset and build-up of the southwest monsoon, and it is not clear whether the mean stress curl for a period as short as a month would account for the transport which is a function of both barotropic and baroclinic processes (Hantel, 1971). However, once the onset of the monsoons has occurred, the wind direction tends to be relatively steady compared to most ocean regions, thus conceivably a shorter response time would be required in this part of the Indian Ocean as suggested by the agreement with direct current observations. A lag of the order of magnitude of a month between the build-up in the wind stress field (greatest in July) and the oceanic response is indicated in figures 6 and 7 where the greatest monthly mean depths of the top of the thermocline are attained during August (Robinson et al., 1979).

The fact that there are two areas in figure 21 with transports greater than 40×10^{12} g sec^{-1} suggests the formation of two eddies. Such a circulation has been observed each southwest monsoon during the period 1975-1979 (Bruce, 1979): a large eddy off the Somali coast and a somewhat smaller one to the east of

Socotra. Note that the mass transport calculations suggest that the Socotra eddy is the larger. Observations also show that during certain years (as 1970, 1976, 1979) (Bruce, 1973, 1979; Brown *et al.*, 1980; Düing *et al.*, 1980) a portion of the Somali current may turn offshore about 4°N to 6°N forming a separate near-equatorial eddy or loop. There is no indication of this mode of circulation in the mass transport map.

To the east of the Somali Basin observations from earlier hydrographic surveys (sections along 5°N and 10°N) (Bruce, 1968) give evidence for the occurrence of other eddies formed during the southwest monsoon. The geostrophic velocity and transport across these sections are shown in figures 23, 24, 25, and 26. Drawing from these data and previous studies of the southwest monsoon circulation (Bruce, 1968; Düing, 1970) a schematic drawing indicating a possible circulation pattern of the eddy field which occurs is given in figure 27.

Off the Arabian coast during July (figure 21) a southward transport would be required. From hydrographic observations (Bruce, 1968) it is not clear that such might be the case. The section along 15°N during early August 1963 (Bruce, 1968) indicates a northward geostrophic near-surface current along the coast with a transport amounting to approximately 12×10^{12} g sec⁻¹. Pilot charts and the Dutch atlas (1952) show a northward current along the coast.

During January the Sverdrup transport (figure 22) values are relatively weak compared with that of July. A southward transport along the Somali coast south of about 5°N amounting to greater than 10×10^{12} g⁻¹ sec would be required. This flow is in good agreement with the pilot charts (H.O. Pub. 566) which show southward coastal currents ranging up to 125 cm sec⁻¹. The meridional geostrophic transport across a 5°N section just after the northeast monsoon (figure 28) gives relatively low values compared with the transports during the southwest monsoon (figure 24) as well as indicating a small northward transport off the Somali coast.

8. CONCLUSIONS

From the evidence on hand to date, it appears that both the northern (or "prime") eddy in the Somali Basin and the eddy east of Socotra are probably generated each southwest monsoon. These eddies have been observed for five consecutive years (1975 through 1979) by XBT temperature sections along the tanker sea lane. They have also been present during all known earlier surveys (Bruce, 1979). During some years (1970, 1976, 1979) the Somali current has been found to turn offshore between about 4°N to 6°N forming a southern loop or eddy. When this circulation pattern is established, a region of cold upwelled water occurs both at the location where the northern eddy turns offshore (approximately 8°N to 10°N) and where the southern turnoff is observed (approximately 4°N to 6°N) along the coast. During late August and early September during 1970 and 1979 the southern eddy was observed to flow into and coalesce with the northern one.

During the southwest monsoon the strong signal in the sea surface dynamic topography of the northern eddy develops each year. The slope on the northern edge of the eddy (8°N to 12°N) amounts to about 2×10^{-3} dynes g⁻¹ (comparable

to the Gulf Stream at 36°N). The volume transport offshore during the southwest monsoon can reach 38 to 42 x 10⁶ m³ sec⁻¹ (0-400 dbar, rel. 400 dbar).

In the mixed layer (upper 100 m) along the XBT section (2°N to 12°N) heat is gained in late Spring until the commencement of the southwest monsoon, after which a rapid heat loss occurs. At the same time the loss takes place in the mixed layer, however, there is a comparable gain in heat in the 100 to 200 m layer caused by a deepening of the isotherms, thus the heat loss for 0 to 200 m appears to be small, if any, during the southwest monsoon. After the southwest monsoon at the end of the year both layers show a heat loss.

The surface dynamic topography of western Indian Ocean equatorial water (48°E to 50°E) shows strong seasonal signals: an increase in dynamic height during each interim between monsoons (at the times the Wyrtkie jet should occur) and a decrease during the northwest and southwest monsoons.

The patterns of the monthly averages of the wind stress show the magnitude of values during the southwest monsoon (July, off Socotra, > 4 dynes cm⁻²) are large relative to that of the northeast monsoon (January, off northern Somalia, > 1 dynes cm⁻²). Sverdrup mass transport determined from values of curl of the wind stress shows agreement (values up to 40 x 10¹² g sec⁻¹ to the north) with observations during the southwest monsoon off the Somali coast (6°N). During the northeast monsoon the Sverdrup transport requires a southward flow along the Somali coast south of about 5°N (up to 10 x 10¹² g⁻¹ sec).

REFERENCES

- Brown, O.B., J.G. Bruce, and R.H. Evans, Evolution of sea surface temperature in the Somali Basin during the southwest monsoon of 1979, Science, 209, 595-597, 1980.
- Bruce, J.G., Comparison of near-surface dynamic topography during the two monsoons in the western Indian Ocean, Deep-Sea Research, 15, 665-678, 1968.
- Bruce, J.G., Notes on the Somali Current system during the southwest monsoon, Journal of Geophysical Research, 75, 4170-4173, 1970.
- Bruce, J.G., Large-scale variations of the Somali Current during the southwest monsoon, 1970, Deep-Sea Research, 20, 837-846, 1973.
- Bruce, J.G., Eddies off the Somali Coast during the southwest monsoon, Journal of Geophysical Research, 84, 7742-7748, 1979.
- Bruce, J.G., D.R. Quadfasel, and J.C. Swallow, Somali eddy formation during the commencement of the southwest monsoon, 1978, Journal of Geophysical Research, 85, 6654-6660, 1980.
- Bruce, J.G. and G.H. Volkmann, Some measurements of current off the Somali coast during the northwest monsoon, Journal of Geophysical Research, 74, 1958-1967, 1969.
- Bunker, A.F. and L.V. Worthington, Energy exchange charts of the North Atlantic Ocean, Bulletin of the American Meteorological Society, 57, 670-678, 1976.
- Carbonaro, M., P.E. Colin, and D. Olivari, The deflection of a jet by a cross-flowing stream and its application to anemometry, The von Karman Institute for Fluid Dynamics, Rhode-Saint-Genese, Belgium, 1970.
- Cox, M.D., Equatorially trapped waves and the generation of the Somali Current, Deep-Sea Research, 23 (12), 1139-1152, 1976.
- Düing, W., The monsoon regime of the currents in the Indian Ocean, East-West Center Books, Honolulu, 1970.
- Düing, W., R.L. Molinari, J.C. Swallow, Somali current: Evolution of surface current, Science, 209, 588, 1980.
- Hantel, M., Wind stress curl - the forcing function for ocean motions. Studies in Physical Oceanography, Gordon and Breach, New York, 124-136, 1971.
- Hurlburt, H.E. and J.D. Thompson, A numerical model of the Somali current, Journal of Physical Oceanography, 6 (5), 646-664, 1976.
- Koninklijk Nederlands Meteorologisch Instituut, Indische Oceaan, Oceanografische in Meteorologische gegevens, (Dutch Atlas), 2nd Ed., Publ. No. 135, Vol. 1, Test 31 pp., Vol 2, 24 Charts, 1952.

- Leetmaa, A. and A.F. Bunker, Updated charts of the mean annual wind stress, convergences in the Ekman layers, and Sverdrup transports in the North Atlantic, Journal of Marine Science, 36 (2), 311-322, 1978.
- Robinson, M.K., R.A. Bauer, and E.H. Schroeder, Atlas of North Atlantic - Indian Ocean monthly mean temperatures and mean salinities of the surface layer, Naval Oceanographic Office Ref. Pub. 18, Dept. of the Navy, Washington, DC, 1979.
- Schott, F. and J. Fernandez-Partagas, The onset of the summer monsoon during the FGGE 1979 experiment off the East African coast: a comparison of wind data collected by different means, Journal of Geophysical Research, in press, 1980.
- Stommel, H., The Gulf Stream, University of California Press, Berkeley, 248 pp., 1965.
- Swallow, J.C. and J.G. Bruce, Current measurements off the Somali Coast during the southwest monsoon of 1964, Deep-Sea Research, 13, 861-888, 1966.
- Taft, B.A. and J.A. Knauss, The equatorial undercurrent of the Indian Ocean as observed by the Lusiad expedition, Bulletin of Scripps Institution of Oceanography, 9, 19-26, 1967.
- U.S. Navy Hydrographic Office, Atlas of surface currents, Indian Ocean, H.O. Pub. No. 566, 1958.
- Warren, B.A., H. Stommel and J.C. Swallow, Water masses and patterns of flow in the Somali Basin during the southwest monsoon of 1964, Deep-Sea Research, 13, 825-860, 1966.
- Wyrski, K., Oceanographic Atlas of the International Indian Ocean Expedition, The National Science Foundation, Washington, D.C., 531 pp., 1971.

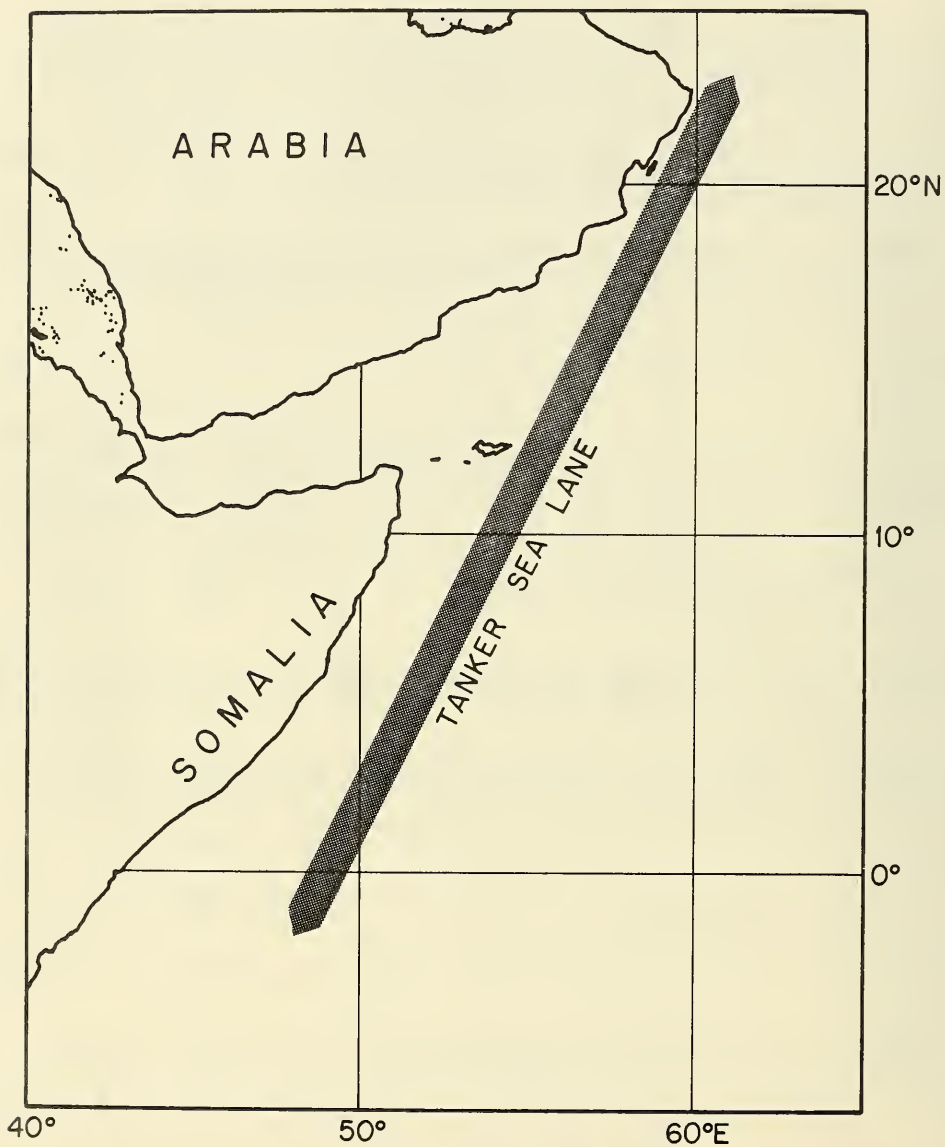


Figure 1a. Sea lane used by tankers en route between Persian Gulf and Atlantic ports along which XBT sections are obtained.

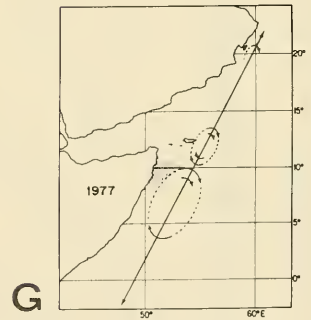
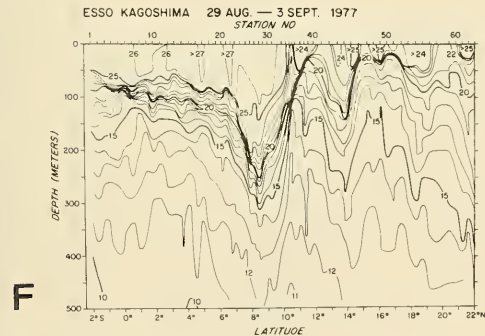
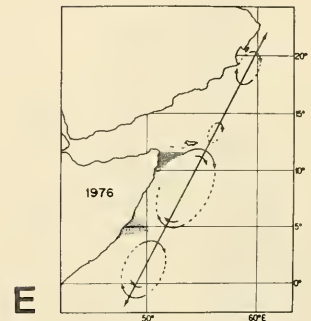
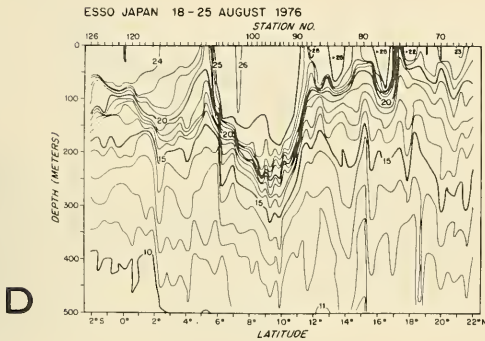
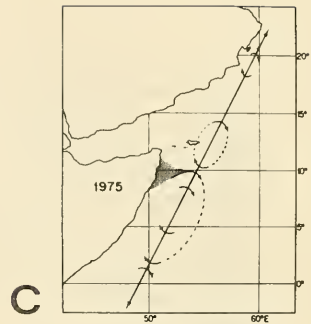
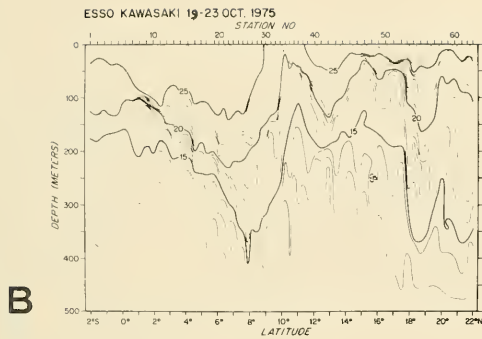


Figure 1b - 1g. Temperature ($^{\circ}\text{C}$) sections along the (a) tanker sea lane from XBTs for three successive southwest monsoons: (b), (c) 1975, (d), (e) 1976, and (f), (g) 1977. The large Somali prime eddy is clearly discernible (4°N to 12°N) with the smaller Socotra eddy to the north (right).

ESSO KAWASAKI 15-23 OCT. 1975

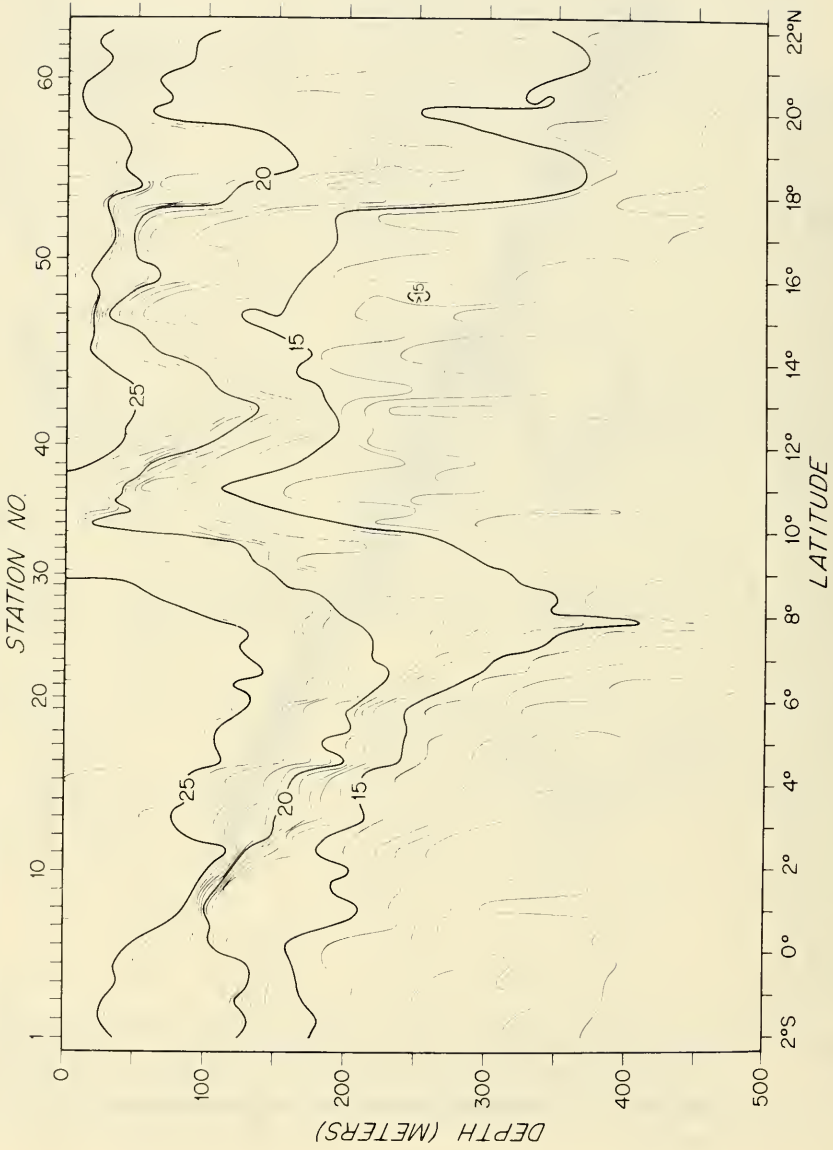


Figure 2. Temperature ($^{\circ}\text{C}$) from XBT sections each along tanker sea lane (see Figure 1a) from October 1975 through December 1979.

ESSO KAWASAKI 30 OCT. - 4 NOV. 1975

STATION NO.

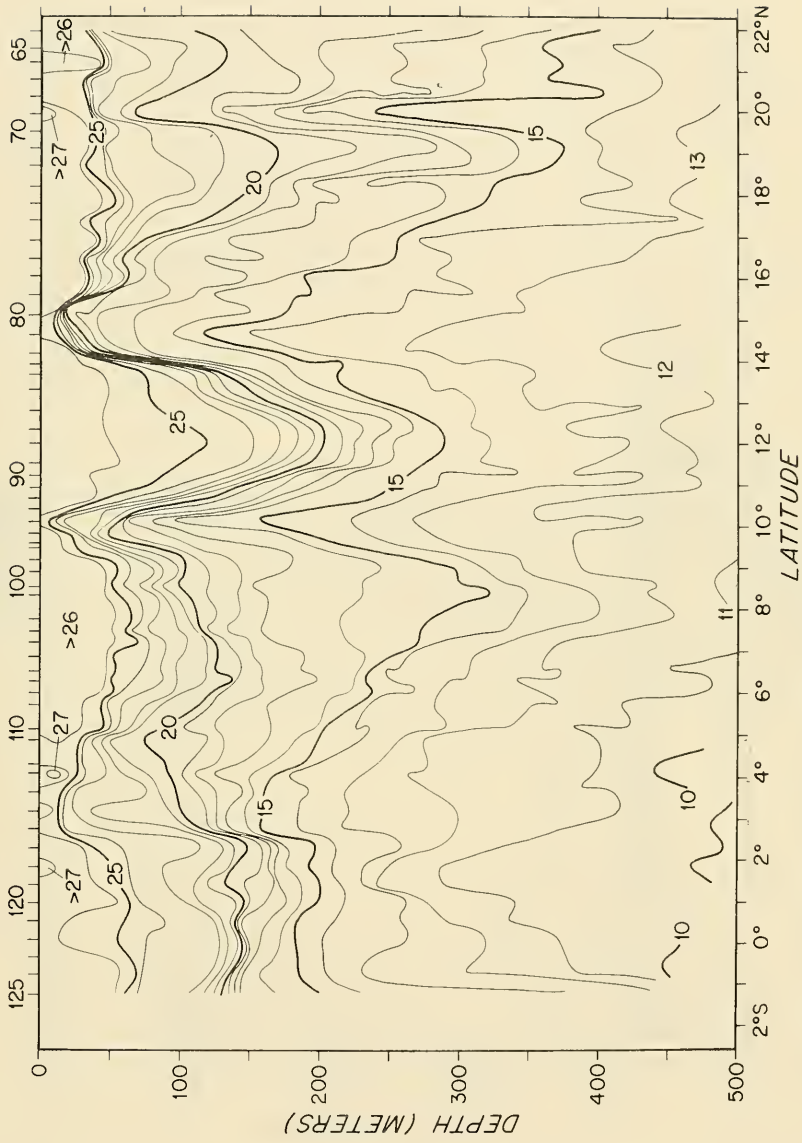


Figure 2. (cont.)

ESSO AFRICA 22-27 JAN. 1976

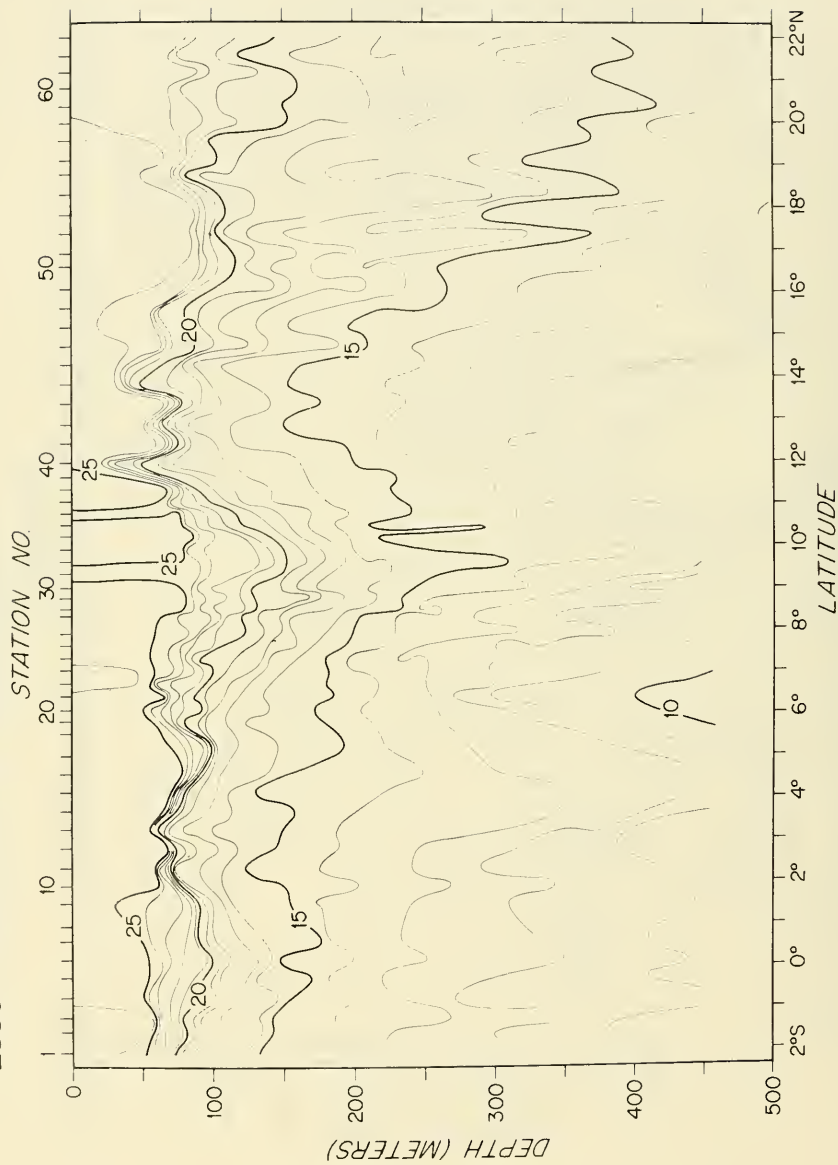


Figure 2. (cont.)

ESSO AFRICA 5-9 FEBRUARY 1976

STATION NO.

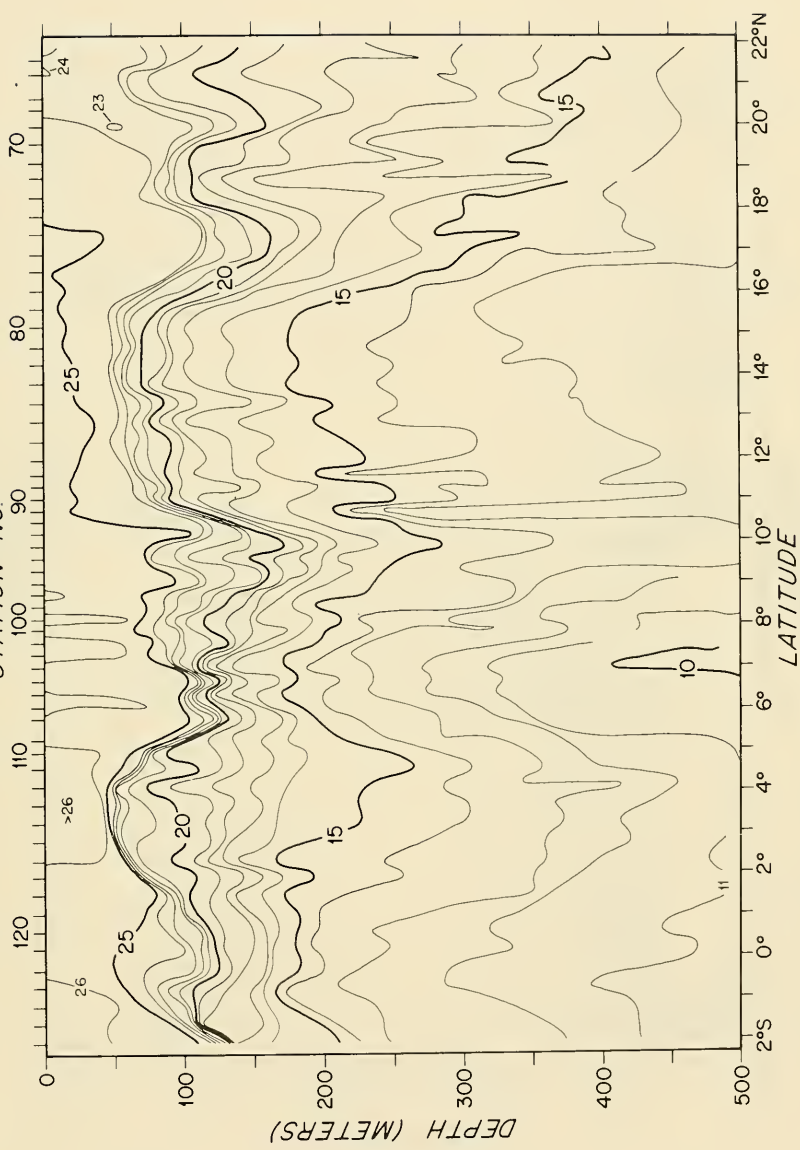


Figure 2. (cont.)

ESSO WILHELMSHAVEN 20-24 APRIL 1976
STATION NO

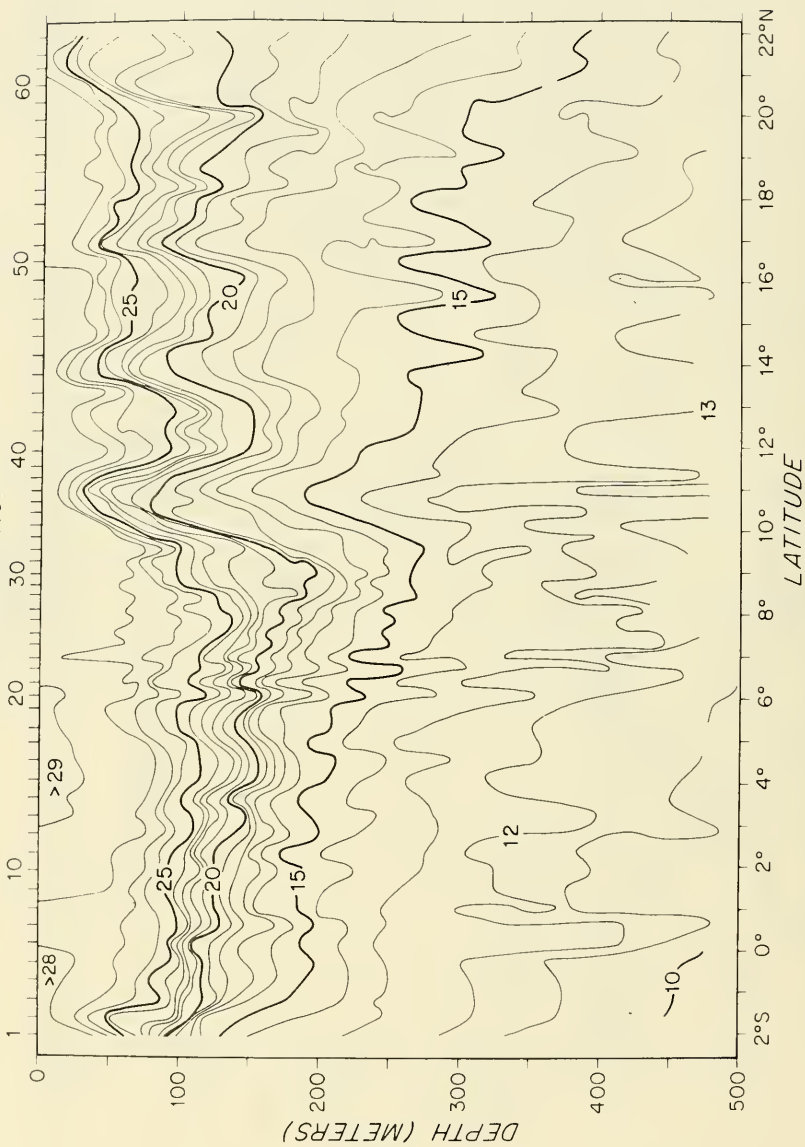


Figure 2. (cont.)

ESSO WILHELMSHAVEN 3-9 MAY 1976
STATION NO.

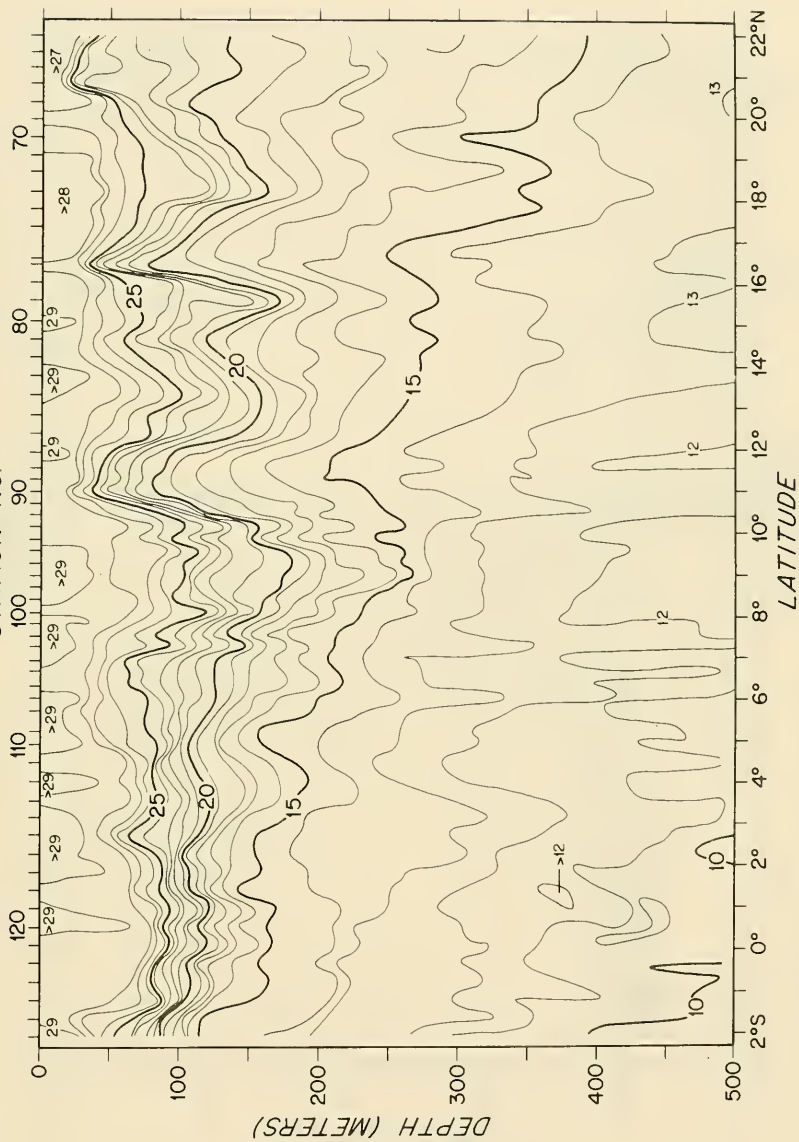


Figure 2. (cont.)

ESSO HONOLULU 22-26 MAY 1976

STATION NO.

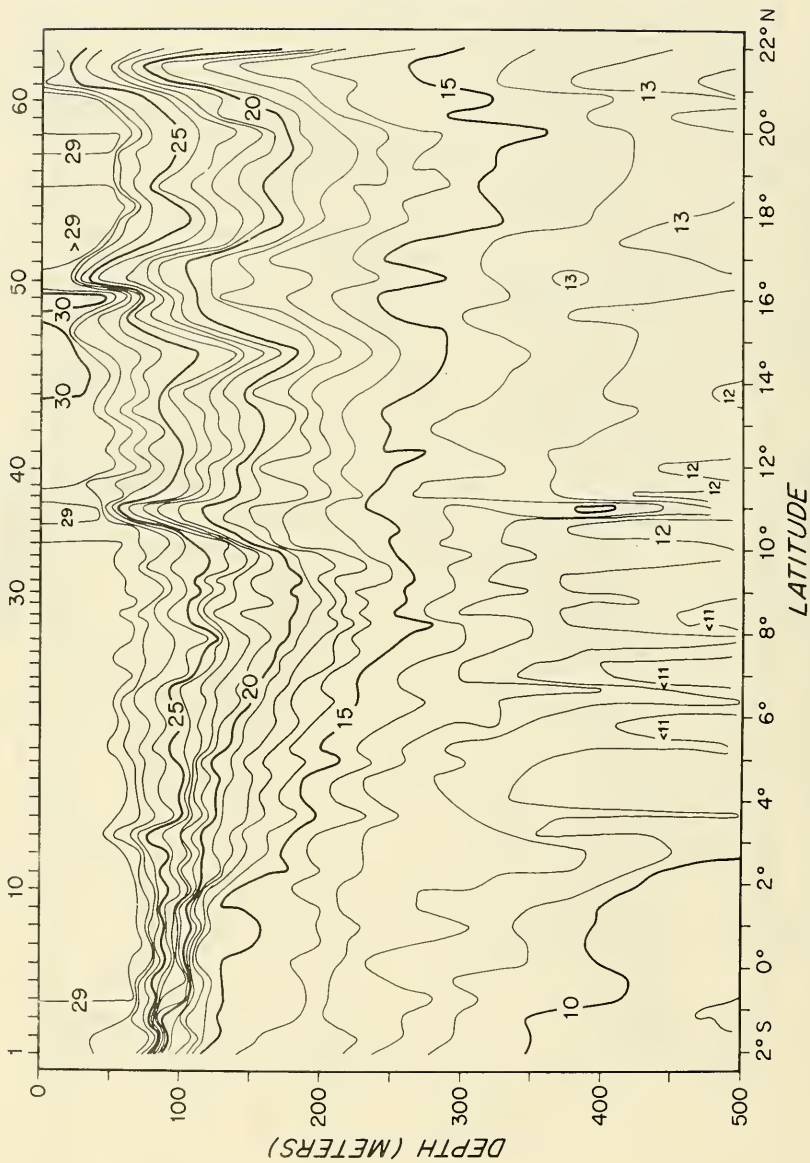


Figure 2. (cont.)

ESSO HONOLULU 2 - 8 JUNE 1976

STATION NO.

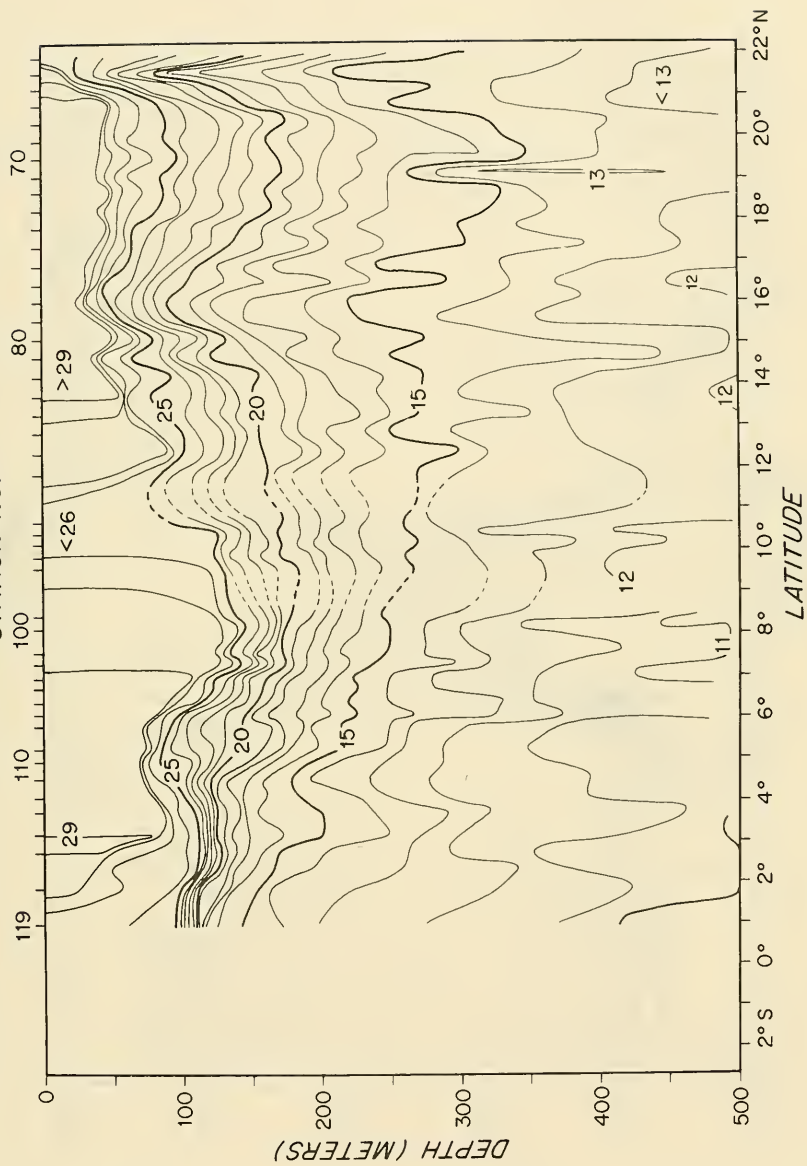


Figure 2. (cont.)

ESSO JAPAN 7-11 AUGUST 1976

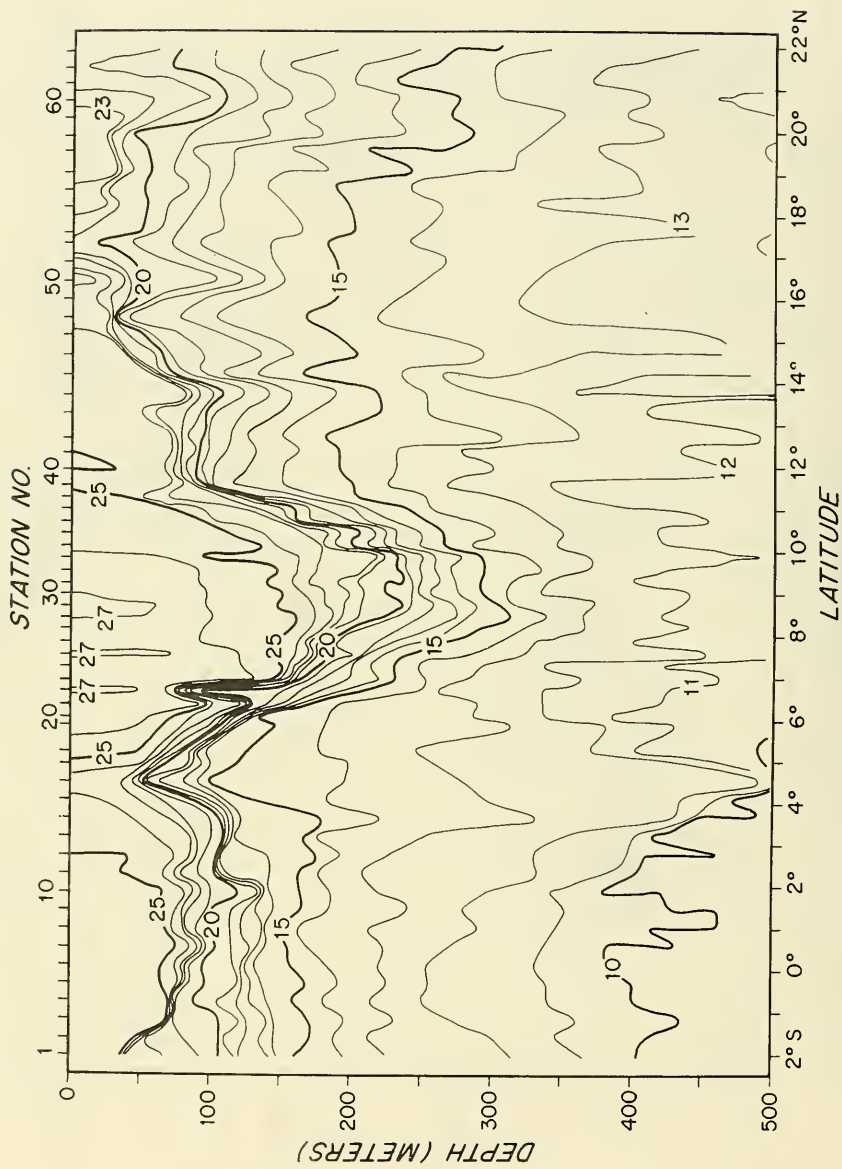


Figure 2. (cont.)

ESSO JAPAN 18 - 25 AUGUST 1976

STATION NO.

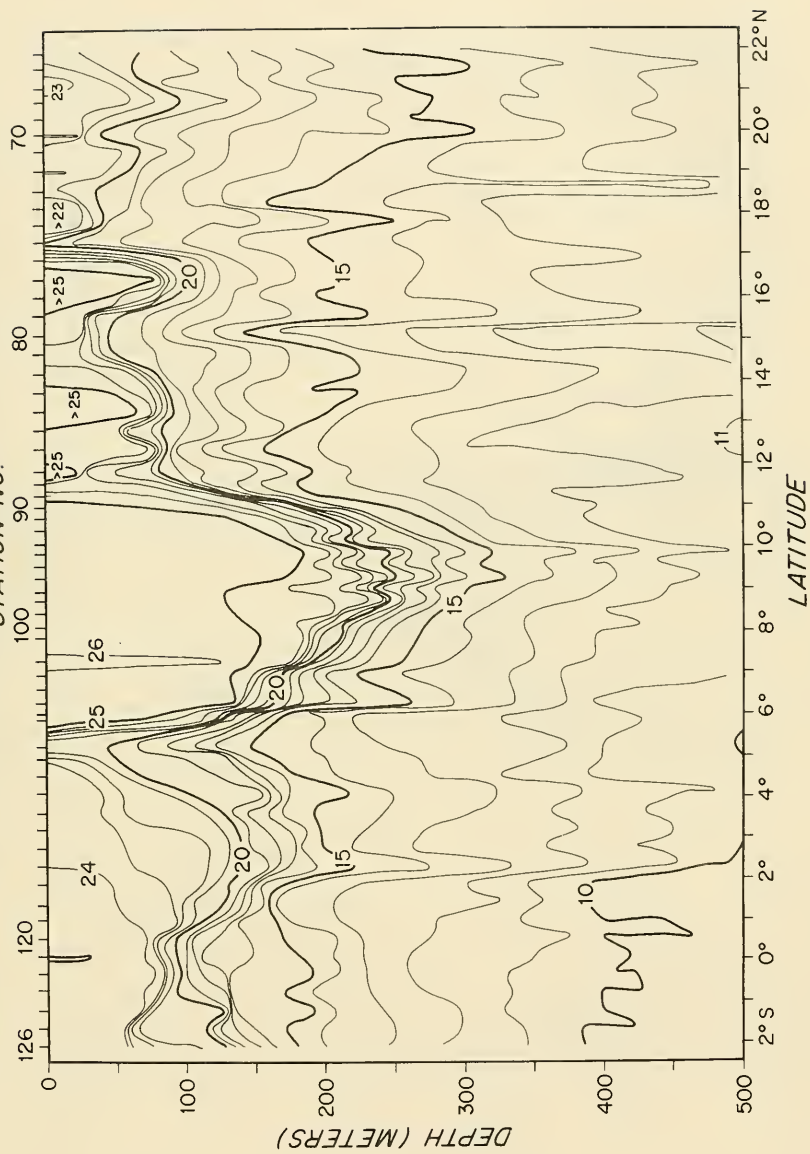


Figure 2. (cont.)

ESSO GENEVA 9-14 SEPT. 1976

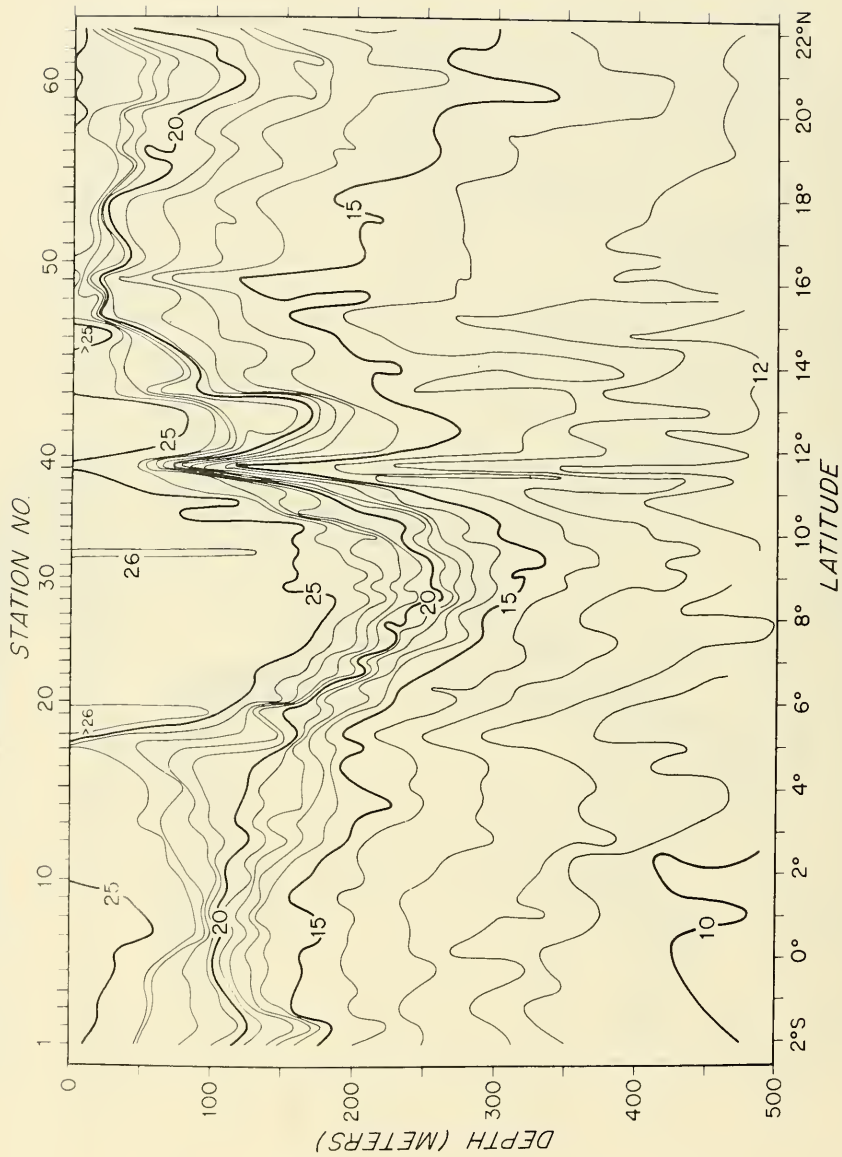


Figure 2. (cont.)

ESSO GENEVA 25-30 SEPTEMBER 1976

STATION NO.

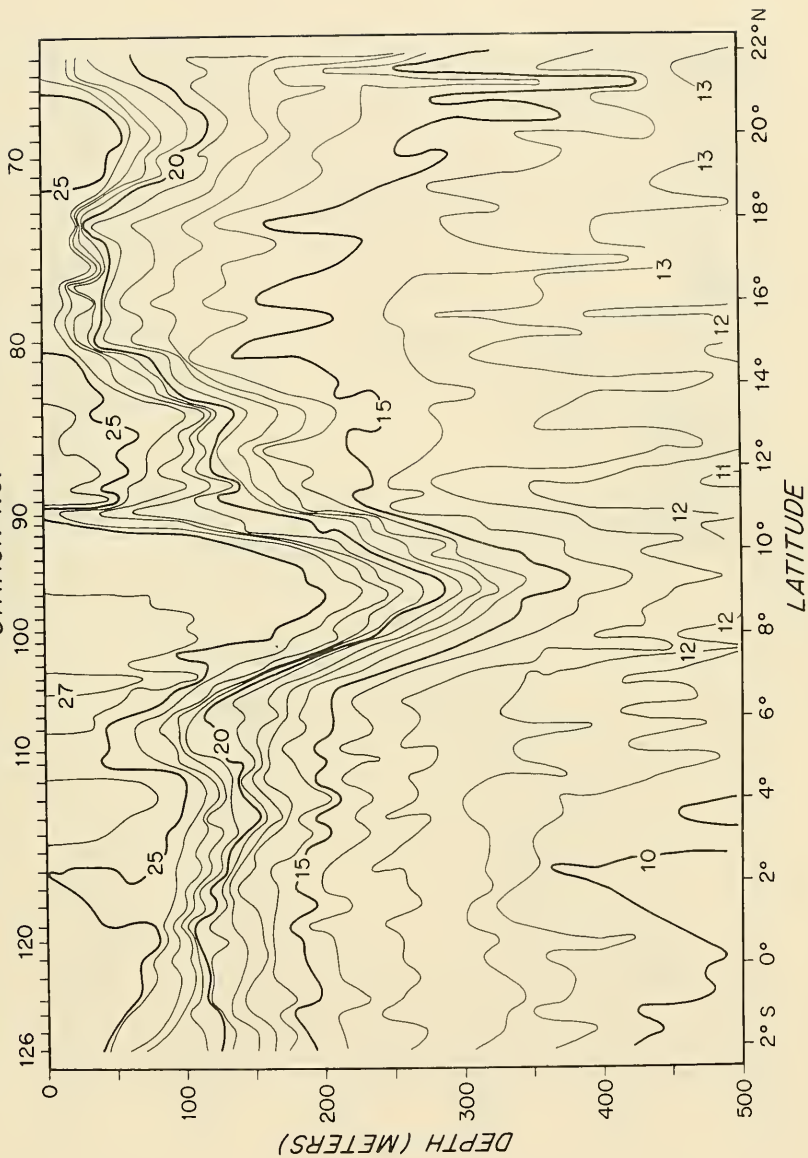


Figure 2. (cont.)

ESSO MADRID 17-23 OCT. 1976

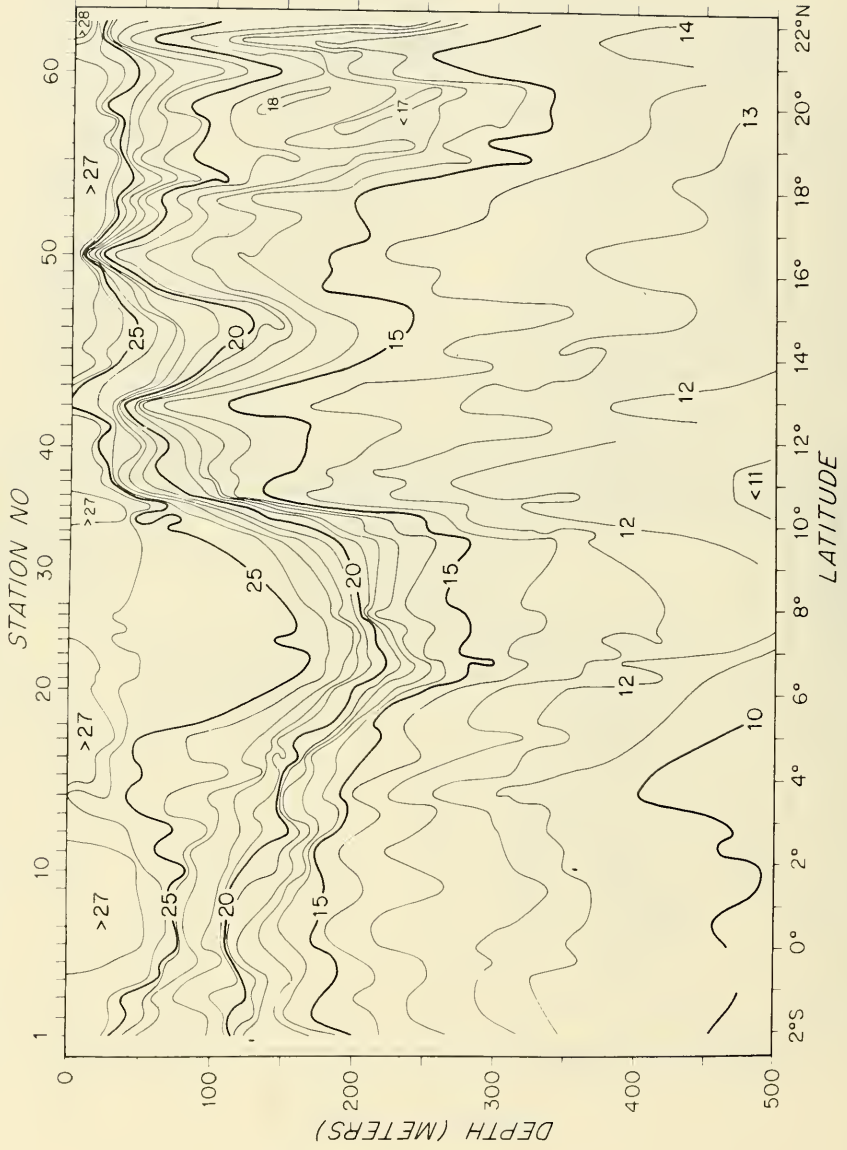


Figure 2. (cont.)

ESSO MADRID 28 OCTOBER - 2 NOVEMBER 1976

STATION NO.

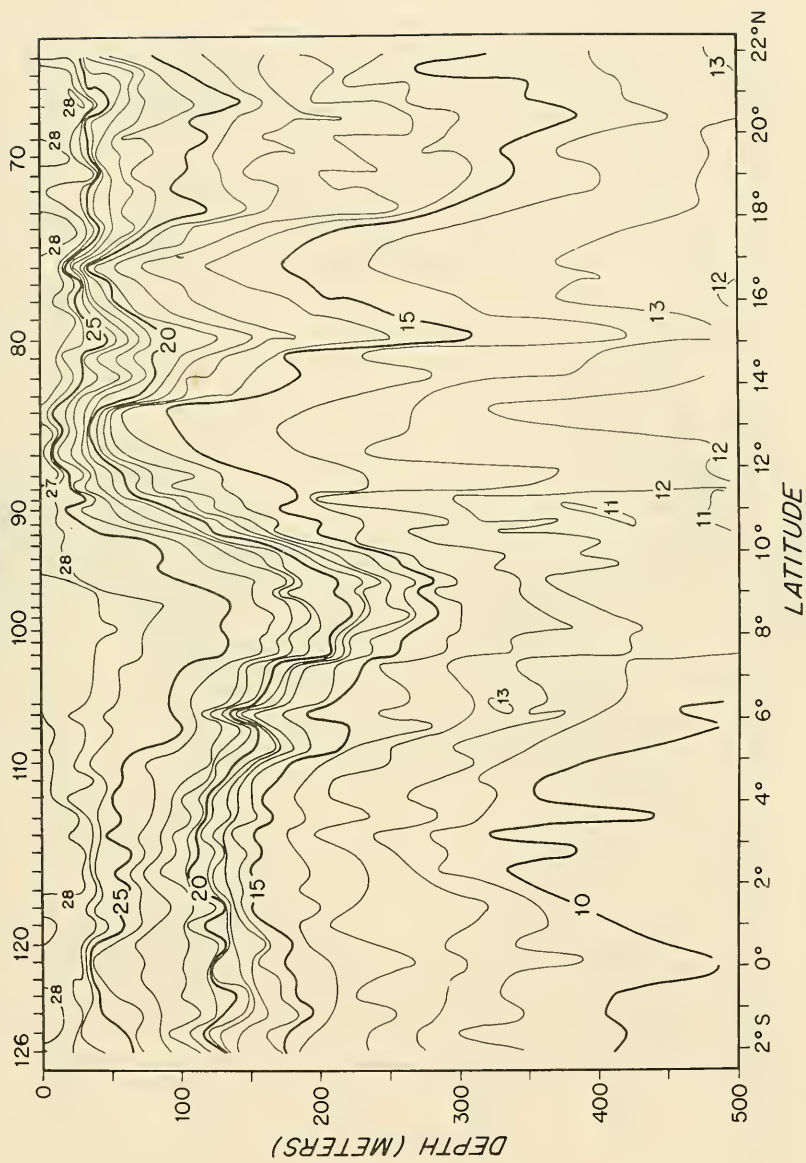


Figure 2. (cont.)

ESSO GENEVA 5-9 DEC. 1976

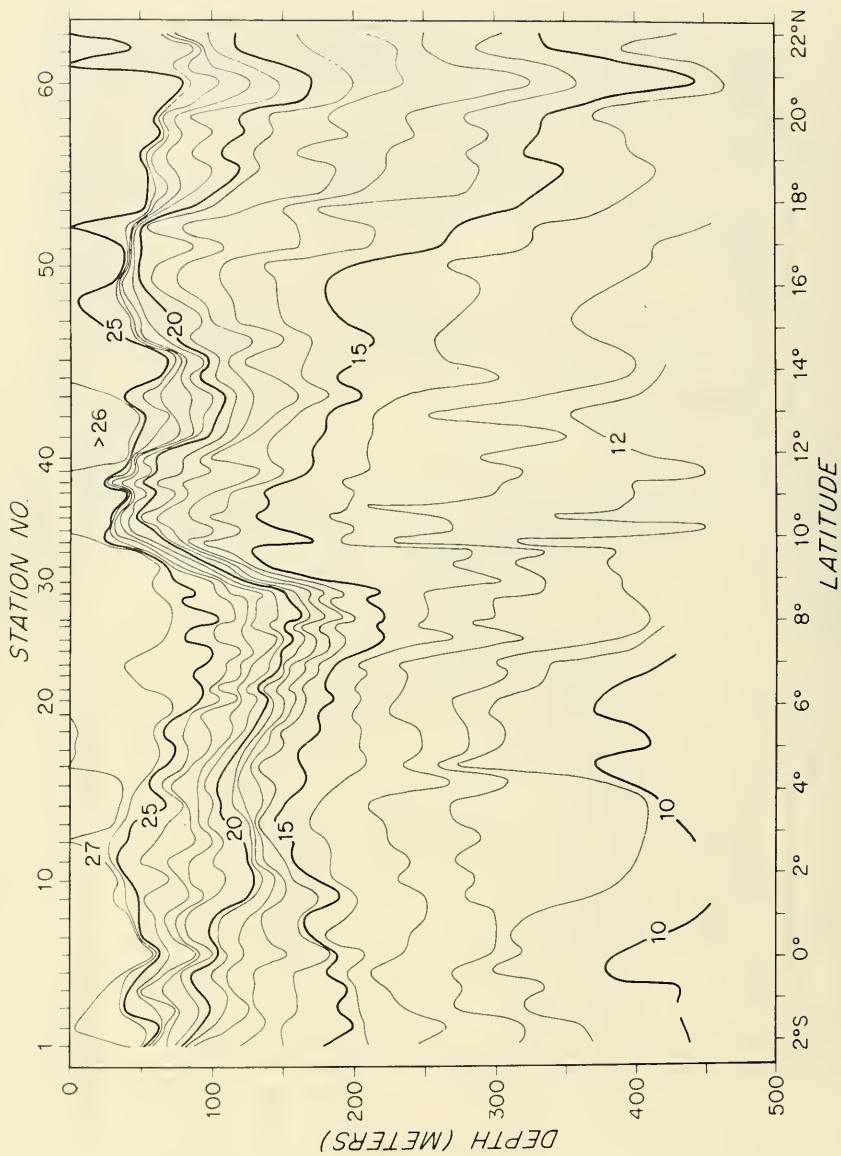


Figure 2. (cont.)

ESSO GENEVA 18 - 22 DECEMBER 1976

STATION NO.

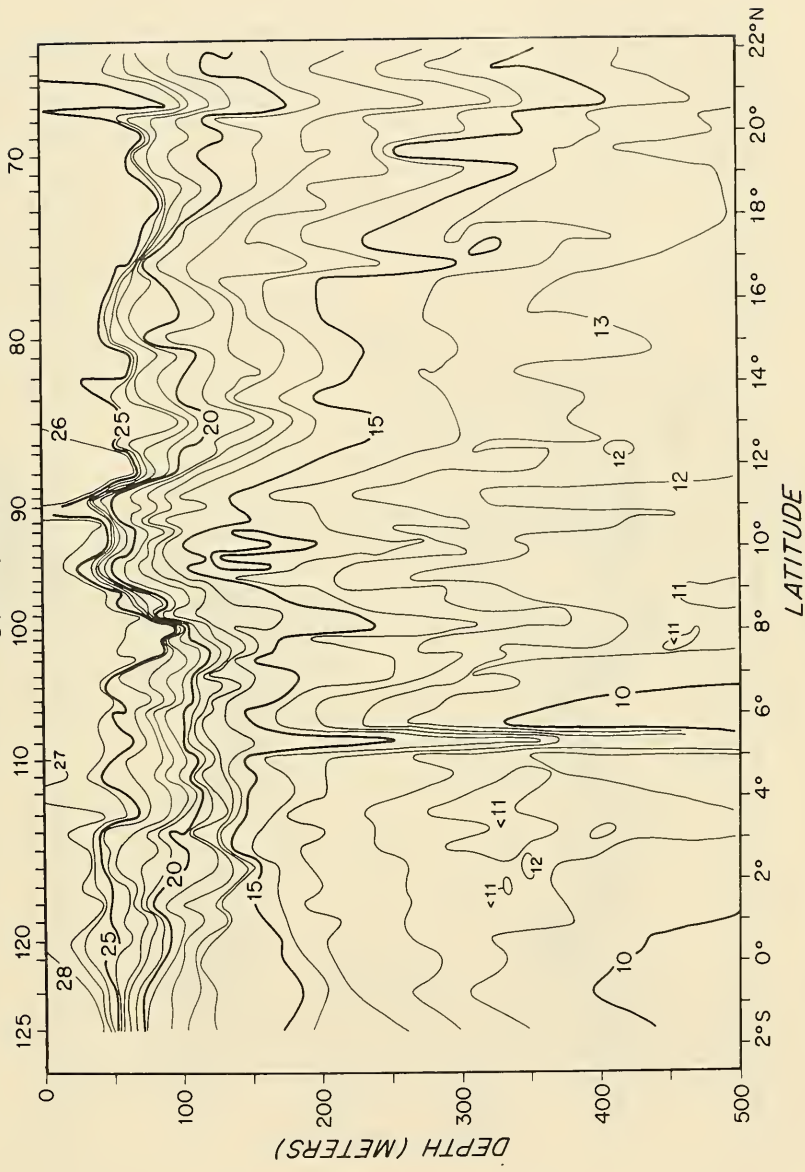


Figure 2. (cont.)

ESSO GENEVA 27 FEB. - 5 MARCH 1977

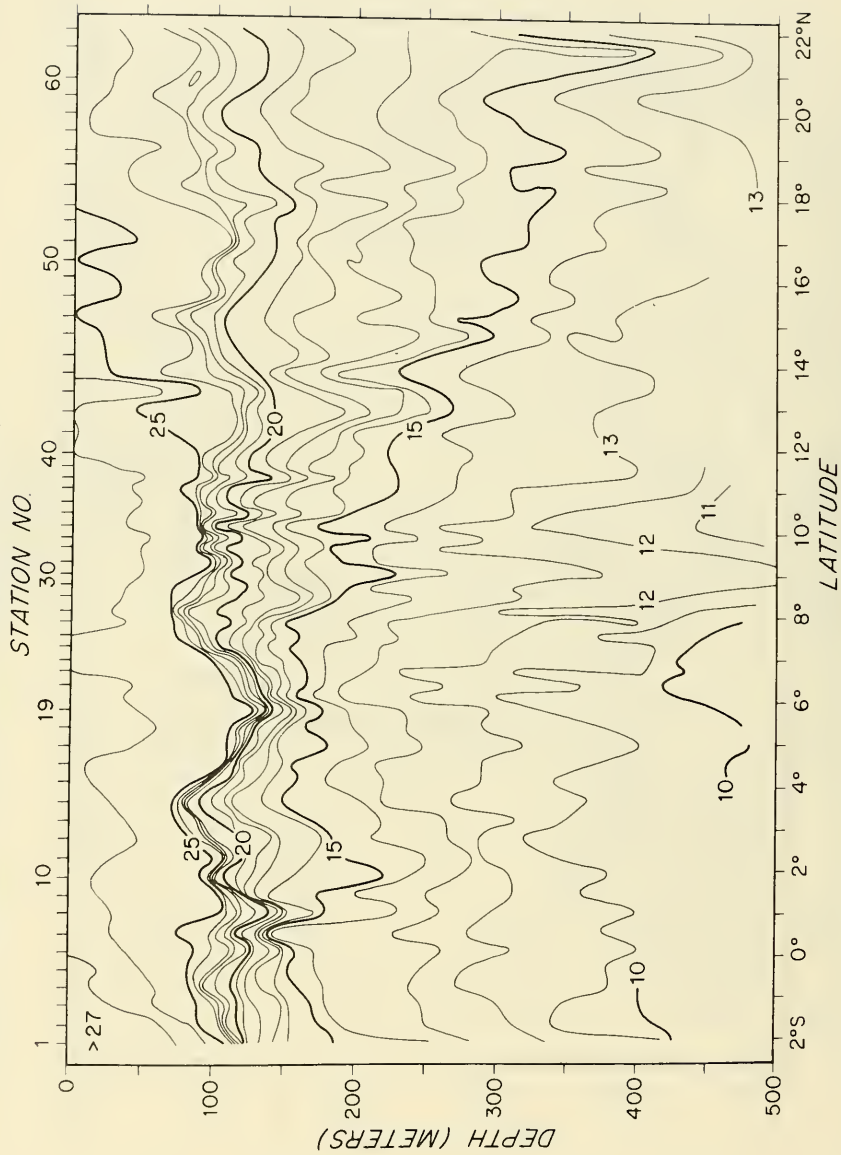


Figure 2. (cont.)

ESSO GENEVA 13-18 MARCH 1977
STATION NO.

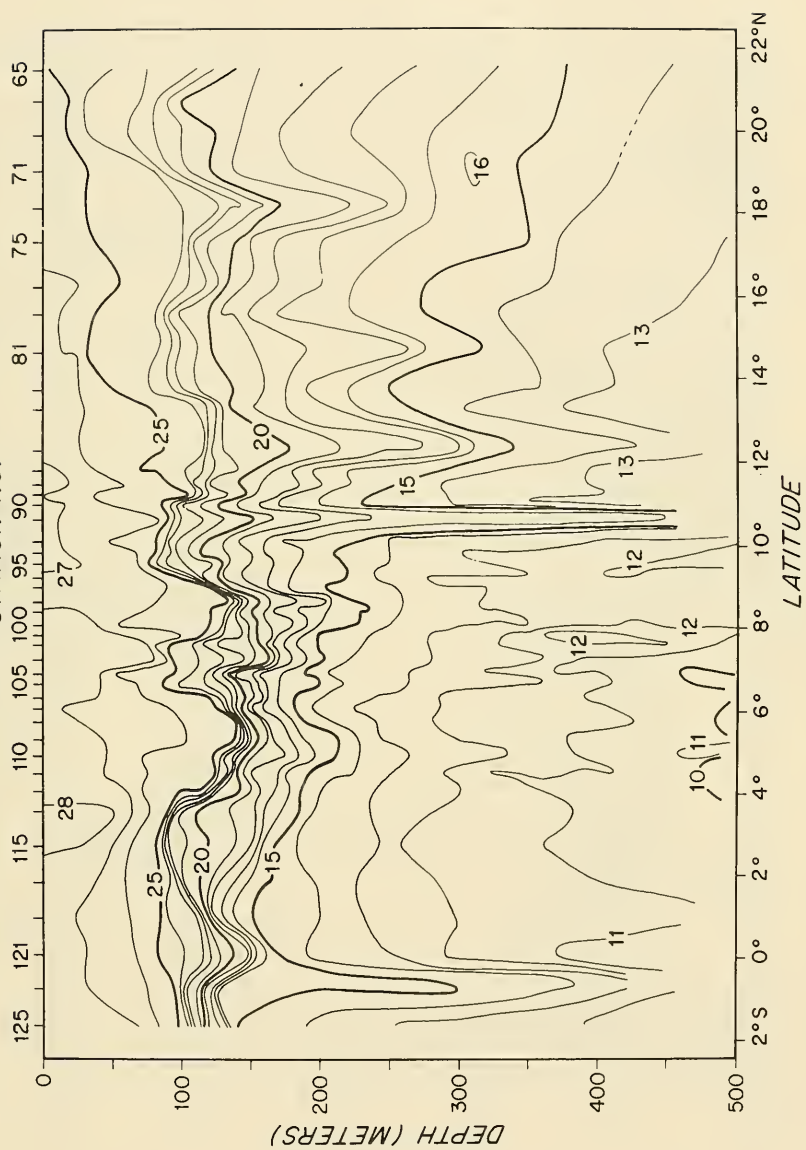


Figure 2. (cont.)

ESSO HAWAII 5 - 12 MAY 1977

STATION NO.

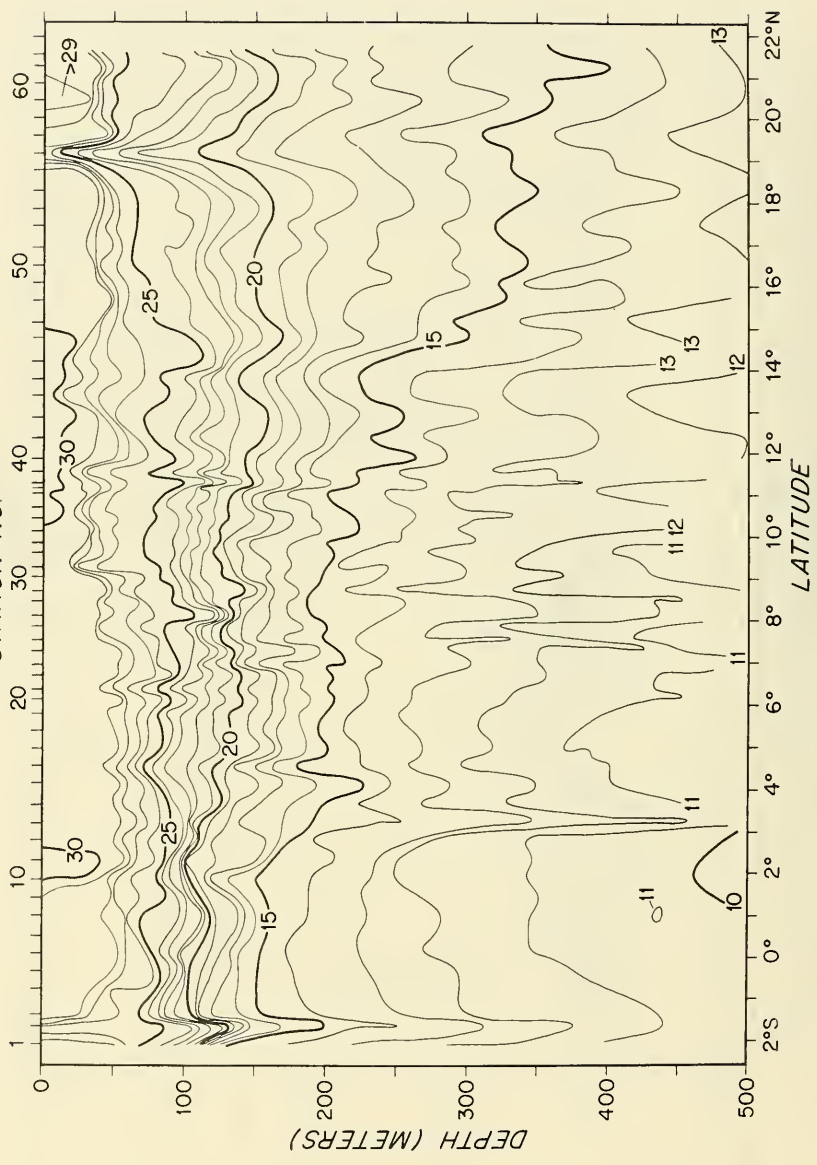


Figure 2. (cont.)

ESSO HAWAII 27 MAY - 6 JUNE 1977

STATION NO.

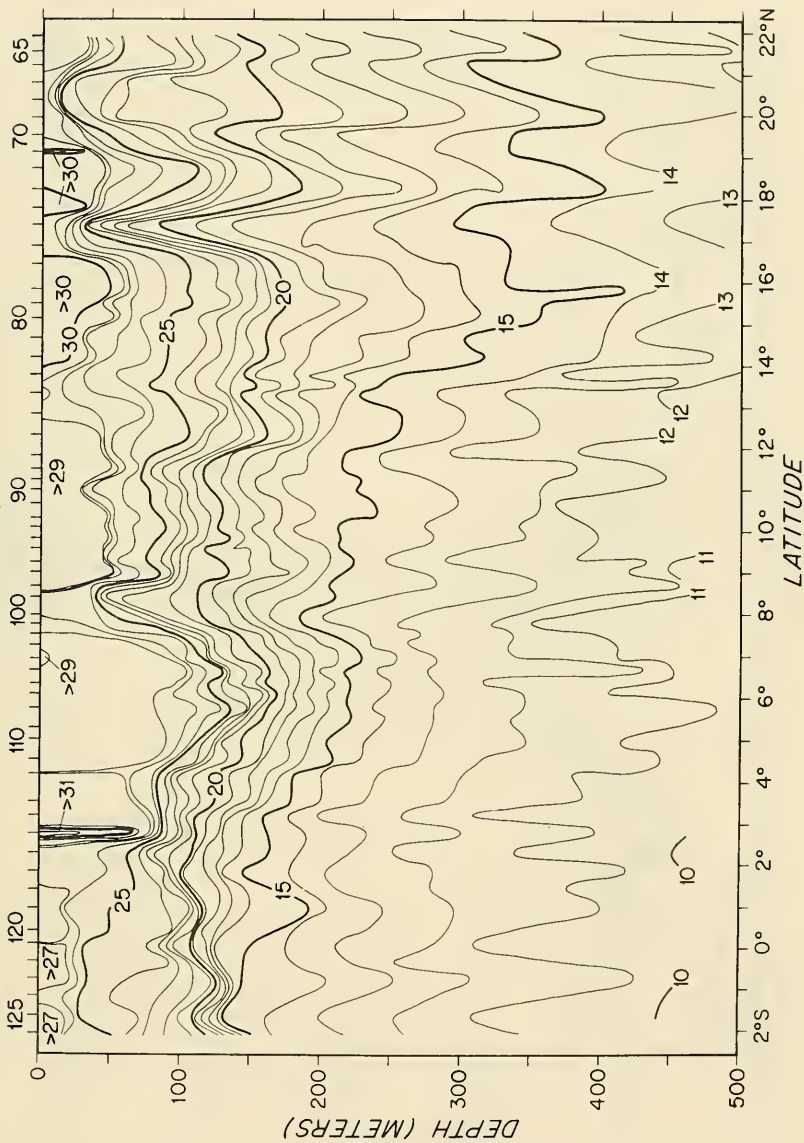


Figure 2. (cont.)

ESSO KAWASAKI 10 - 18 JUNE 1977
STATION NO.

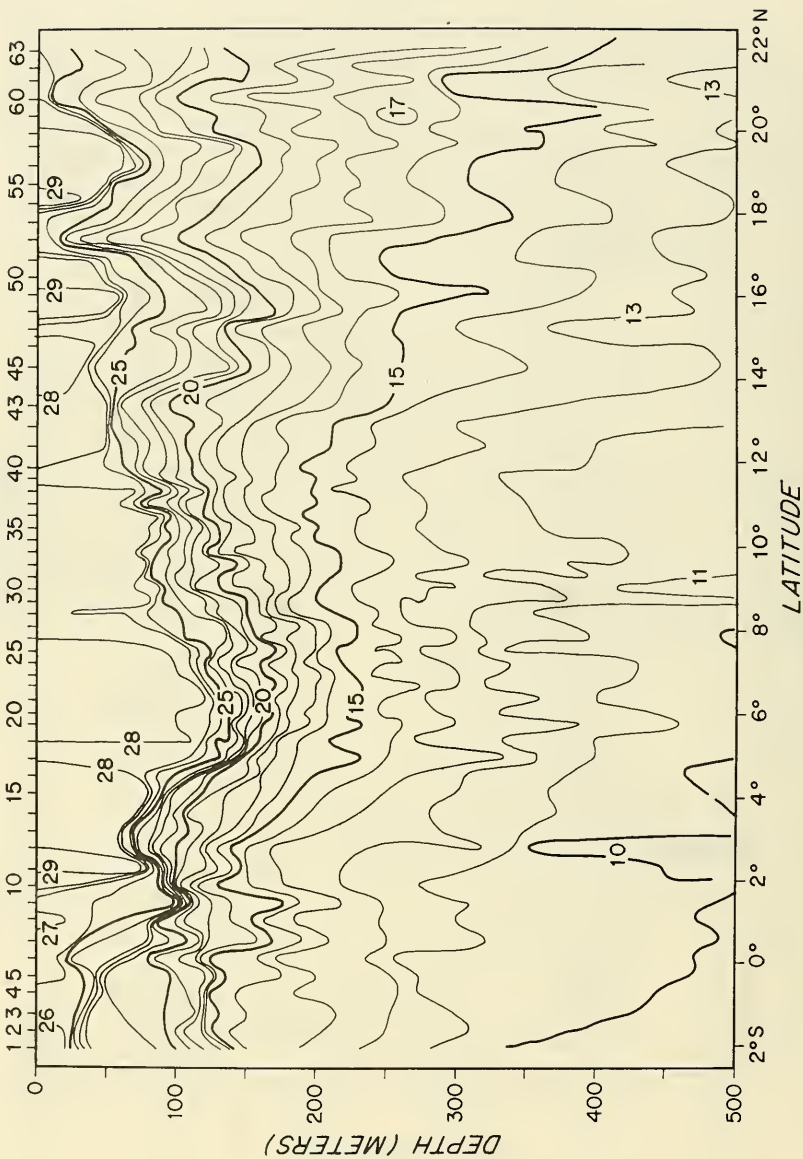


Figure 2. (cont.)

ESSO KAWASAKI 28 JUNE - 4 JULY 1977

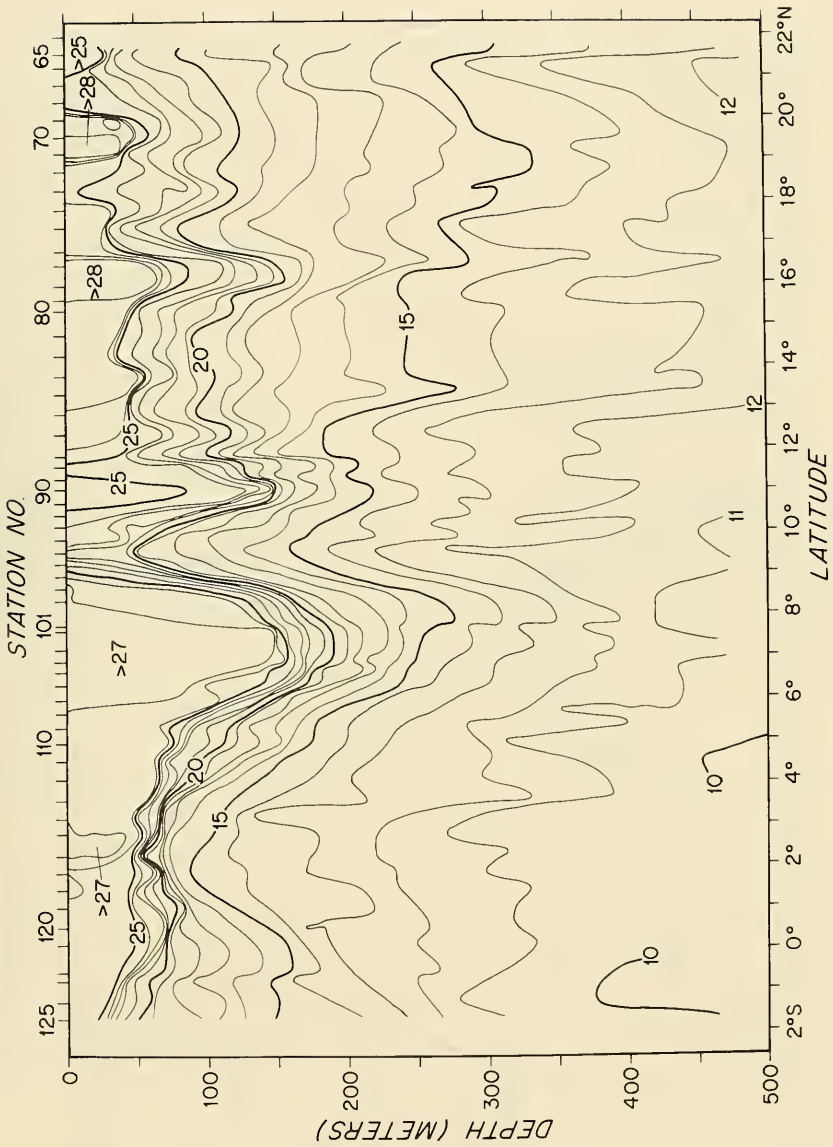


Figure 2. (cont.)

ESSO MADRID 15-19 JULY 1977

STATION NO.

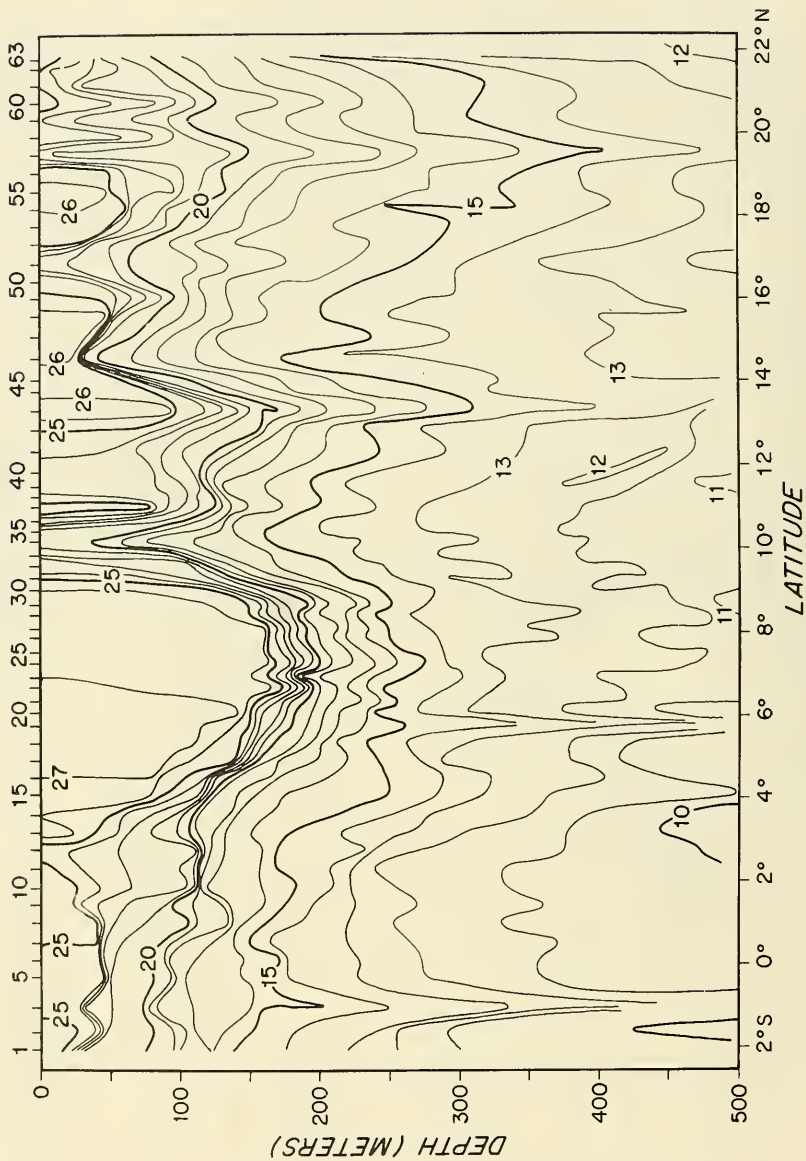


Figure 2. (cont.)

ESSO MADRID 28 JULY - 2 AUGUST 1977

STATION NO.

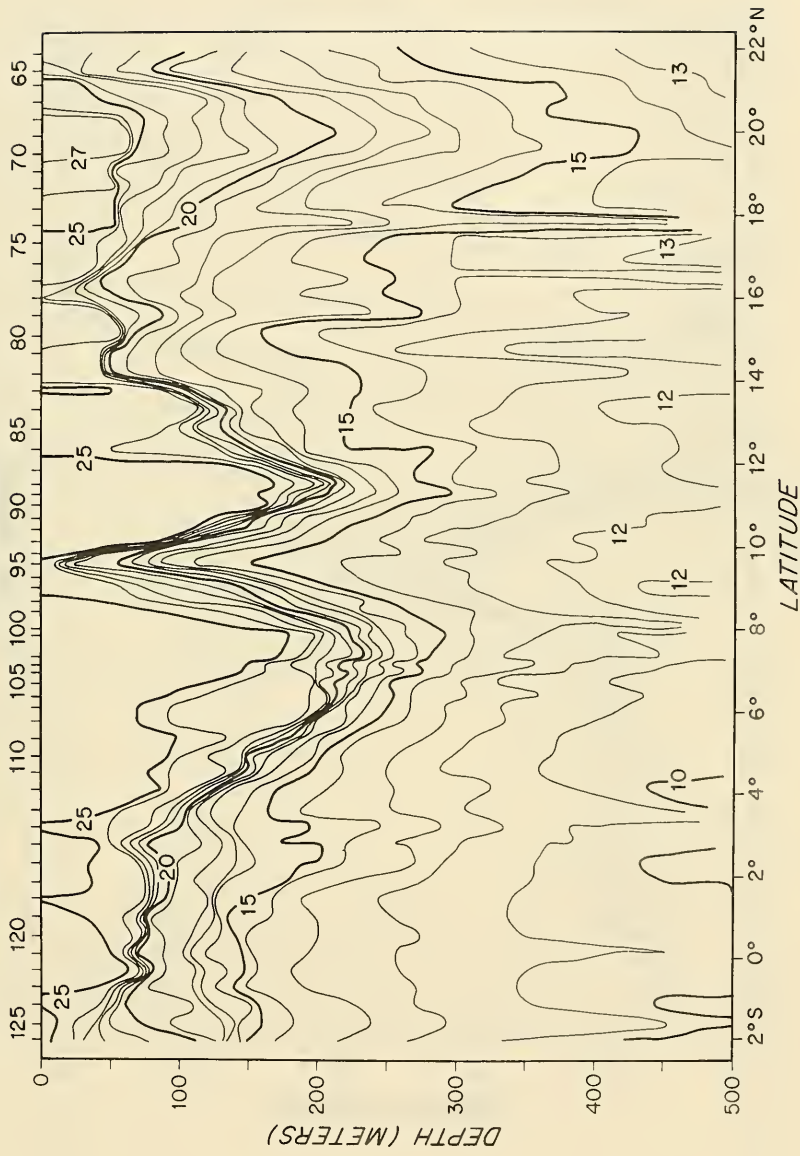


Figure 2. (cont.)

ESSO KAGOSHIMA 29 AUG. — 3 SEPT. 1977

STATION NO.

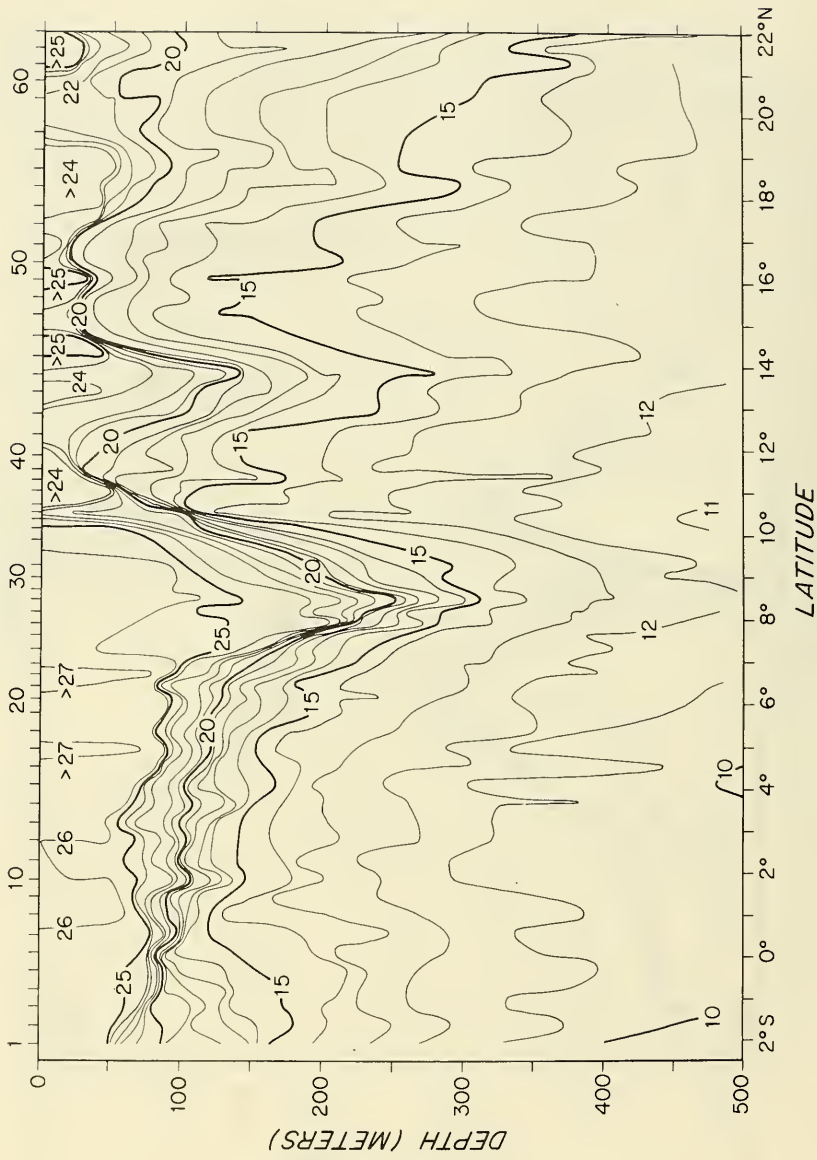


Figure 2. (cont.)

ESSO KAGOSHIMA 19-27 SEPTEMBER 1977

STATION NO.

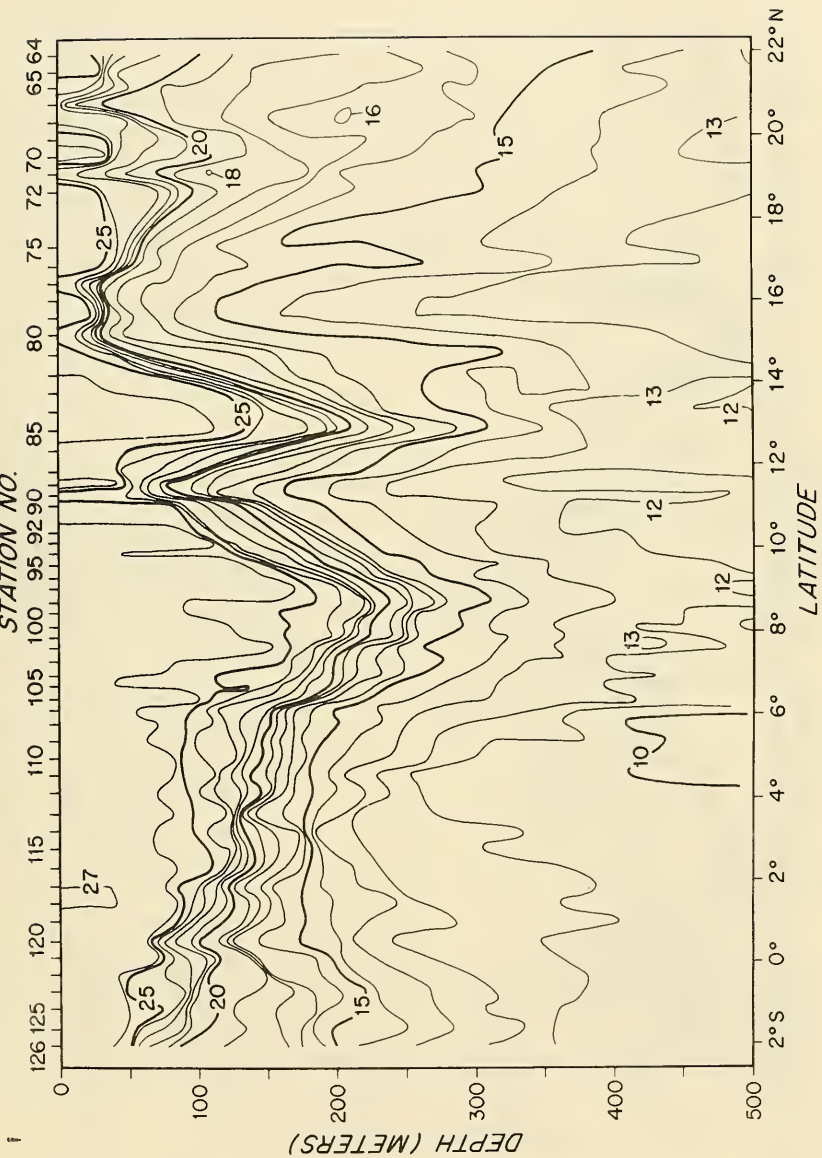


Figure 2. (cont.)

ESSO WILHELMSHAVEN 28 NOVEMBER - 3 DECEMBER 1977

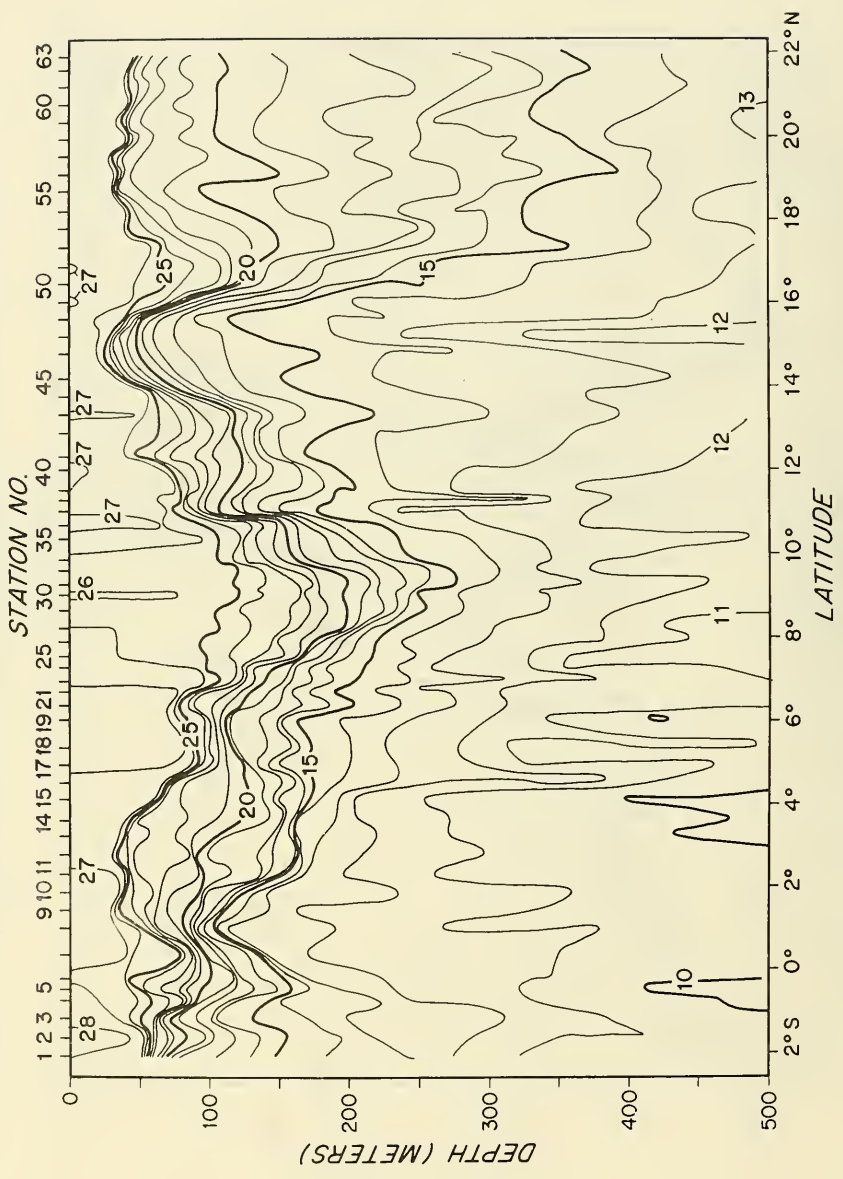


Figure 2. (cont.)

ESSO WILHELMSHAVEN 11 - 17 DECEMBER 1977

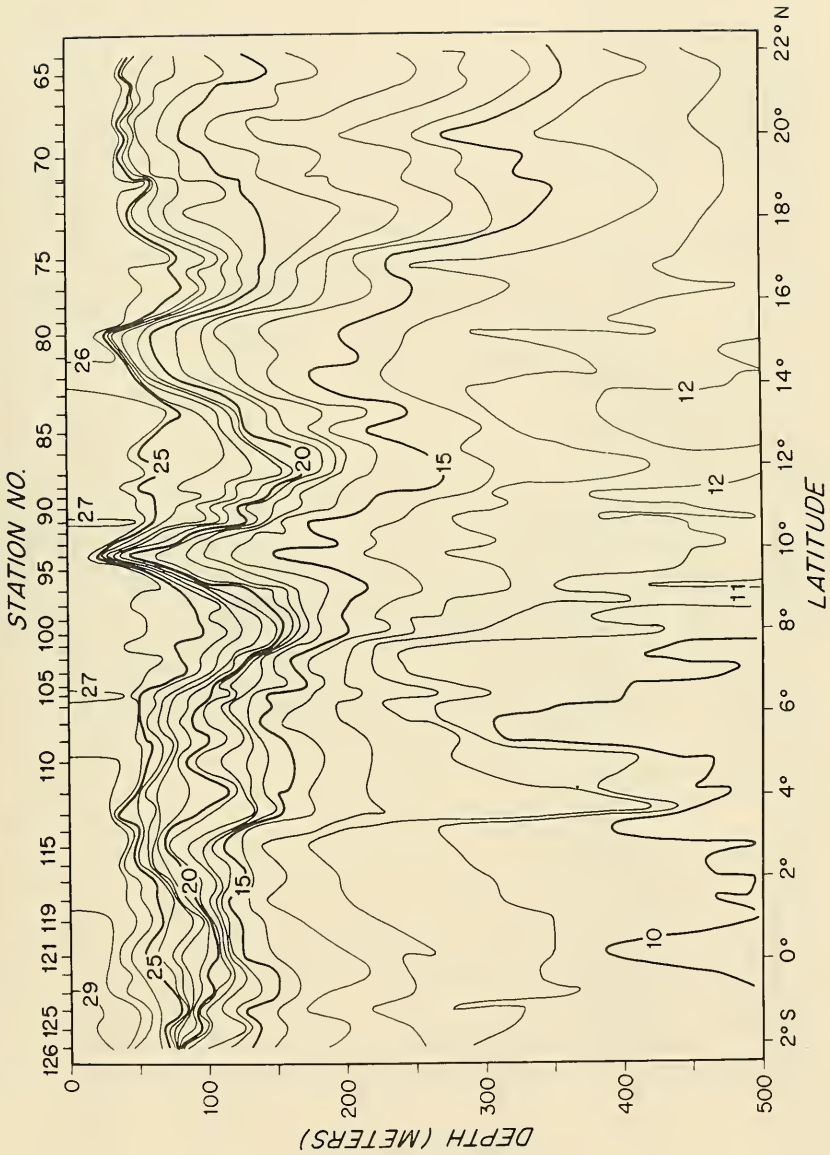


Figure 2. (cont.)

ESSO PACIFIC 26 MARCH - 1 APRIL 1978

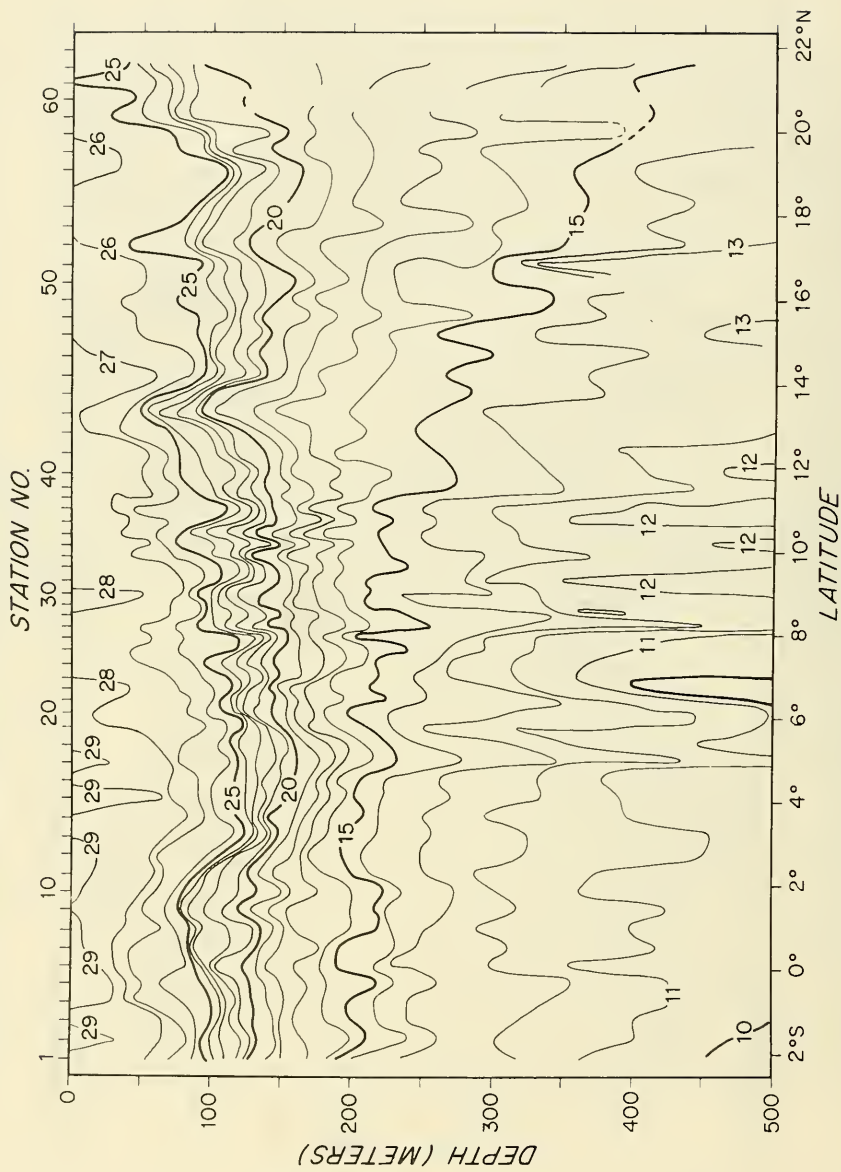


Figure 2. (cont.)

ESSO PACIFIC 10 - 13 APRIL 1978

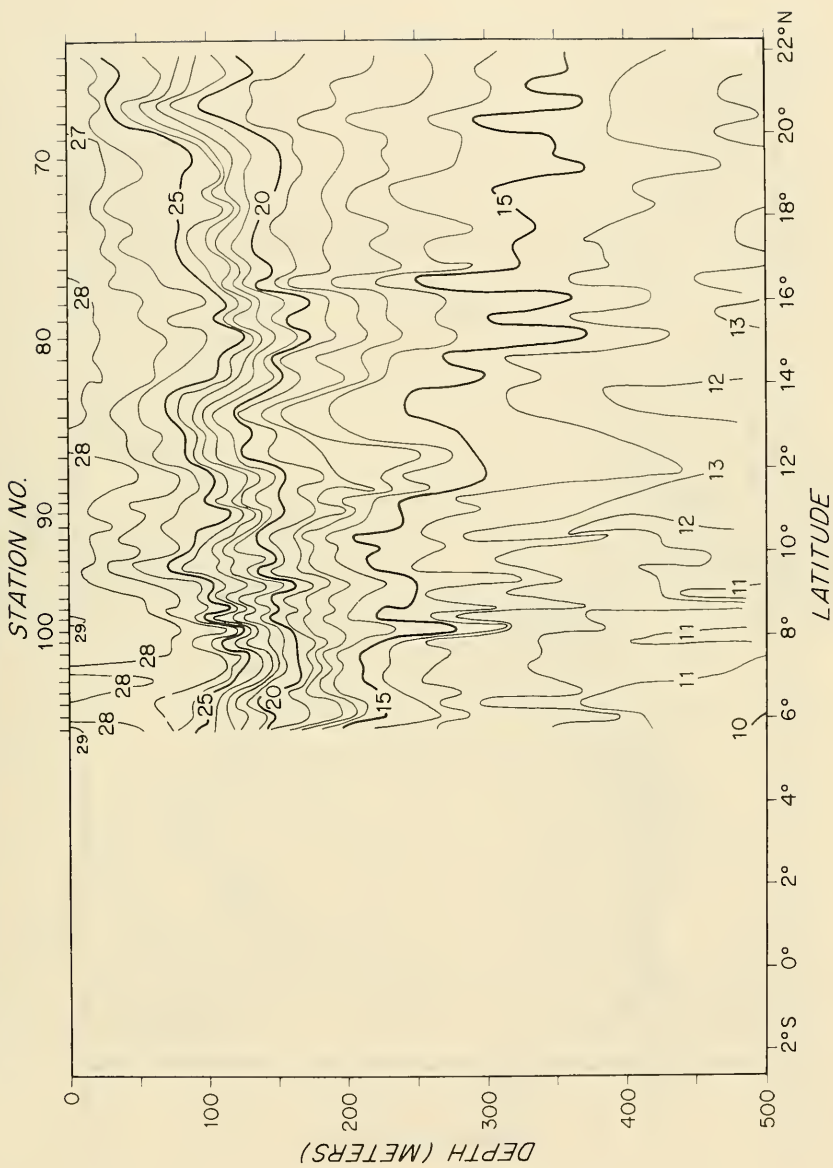


Figure 2. (cont.)

ESSO OSAKA 18 - 24 MAY 1978

STATION NO.

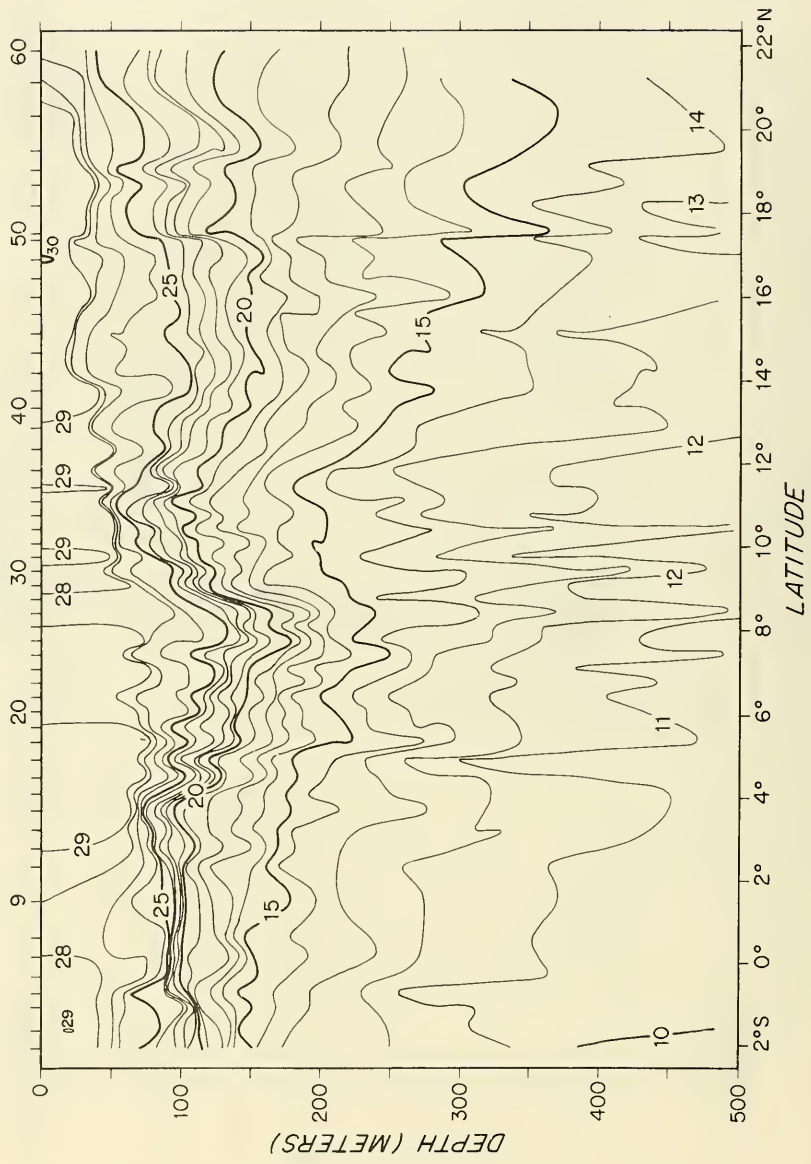


Figure 2. (cont.)

AL DURIYAH 7-13 JUNE 1978

STATION NO.

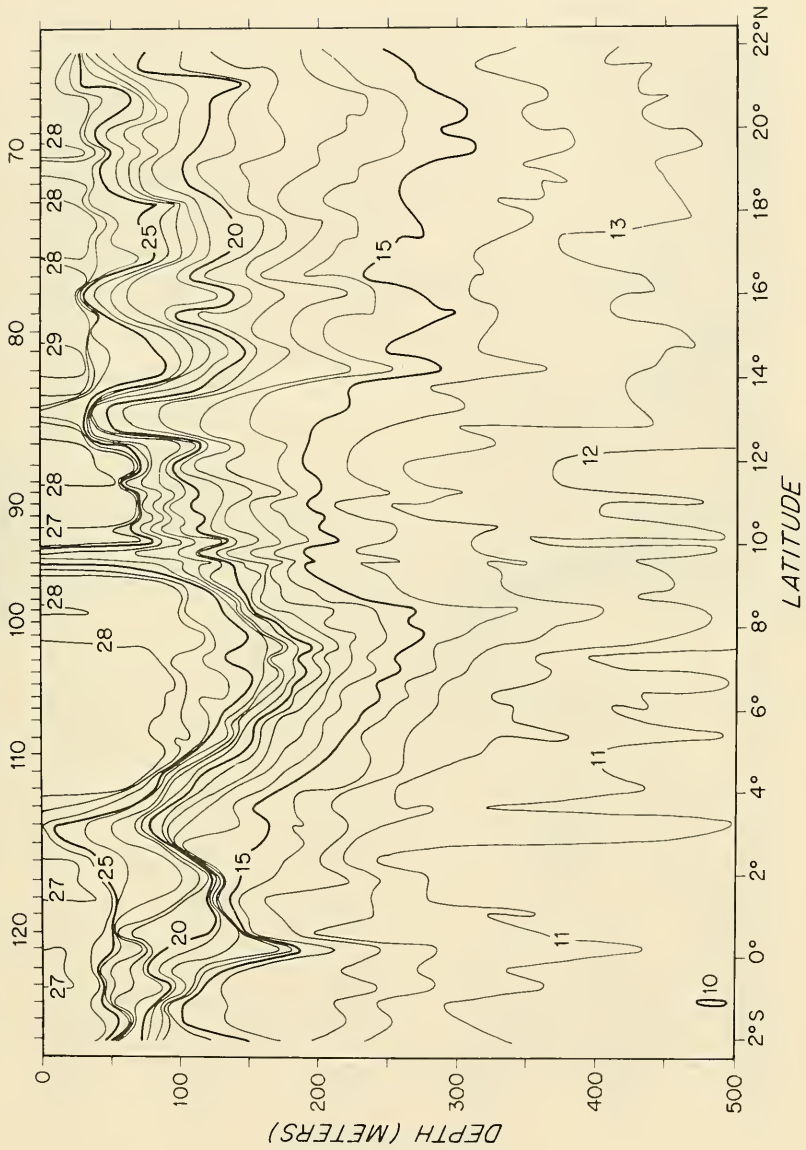


Figure 2. (cont.)

ESSO ATLANTIC 6-11 JULY 1978

STATION NO.

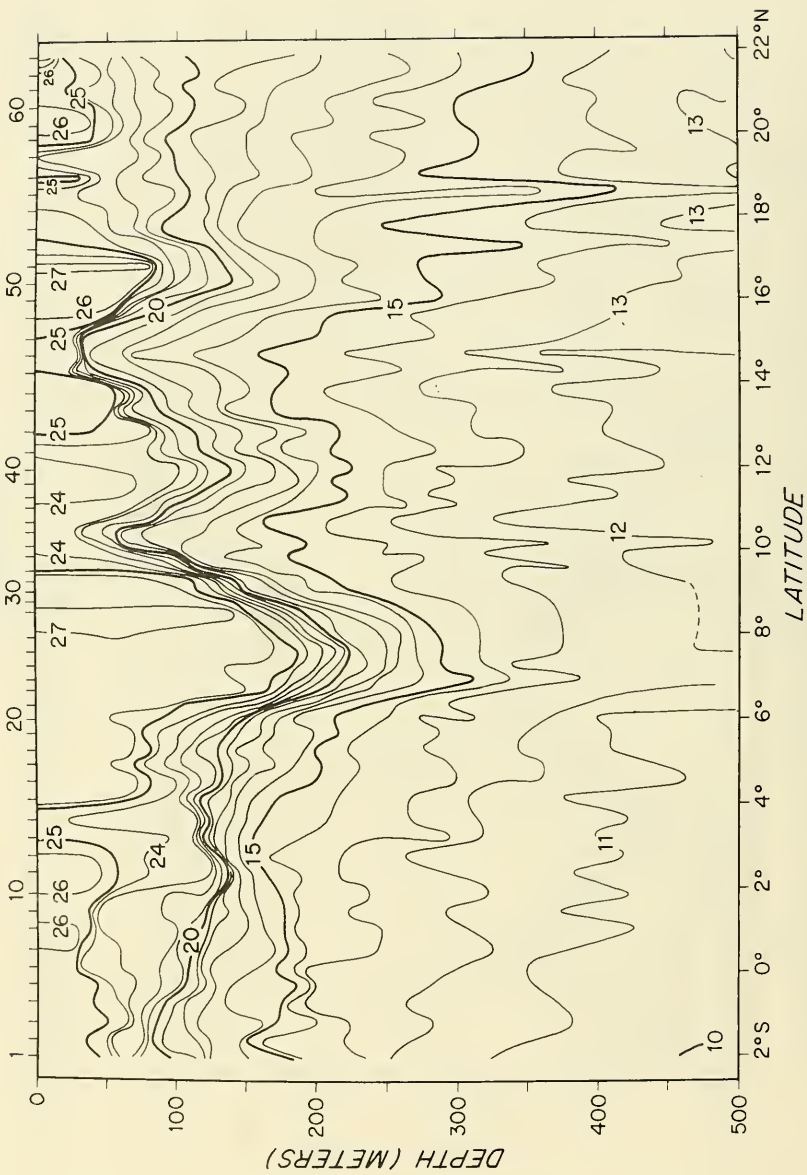


Figure 2. (cont.)

ESSO ATLANTIC 25 - 31 JULY 1978

STATION NO.

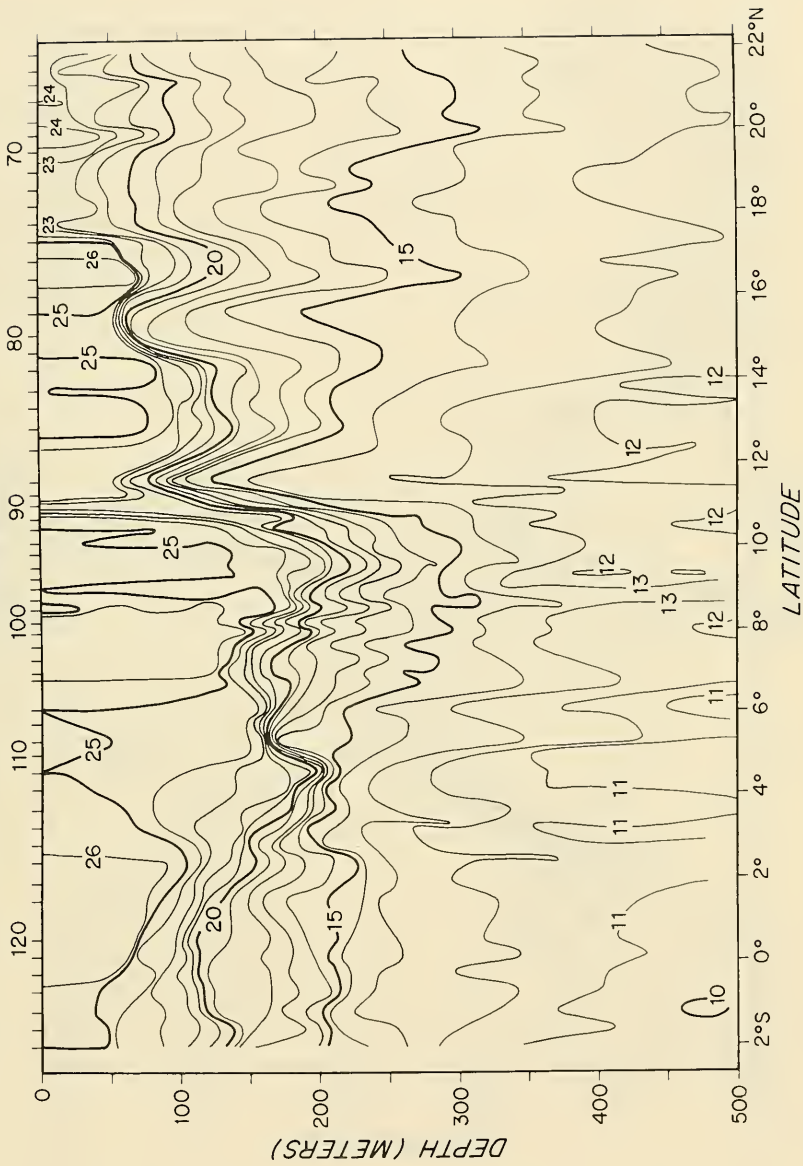


Figure 2. (cont.)

ESSO NEDERLAND 22-27 AUG. 1978

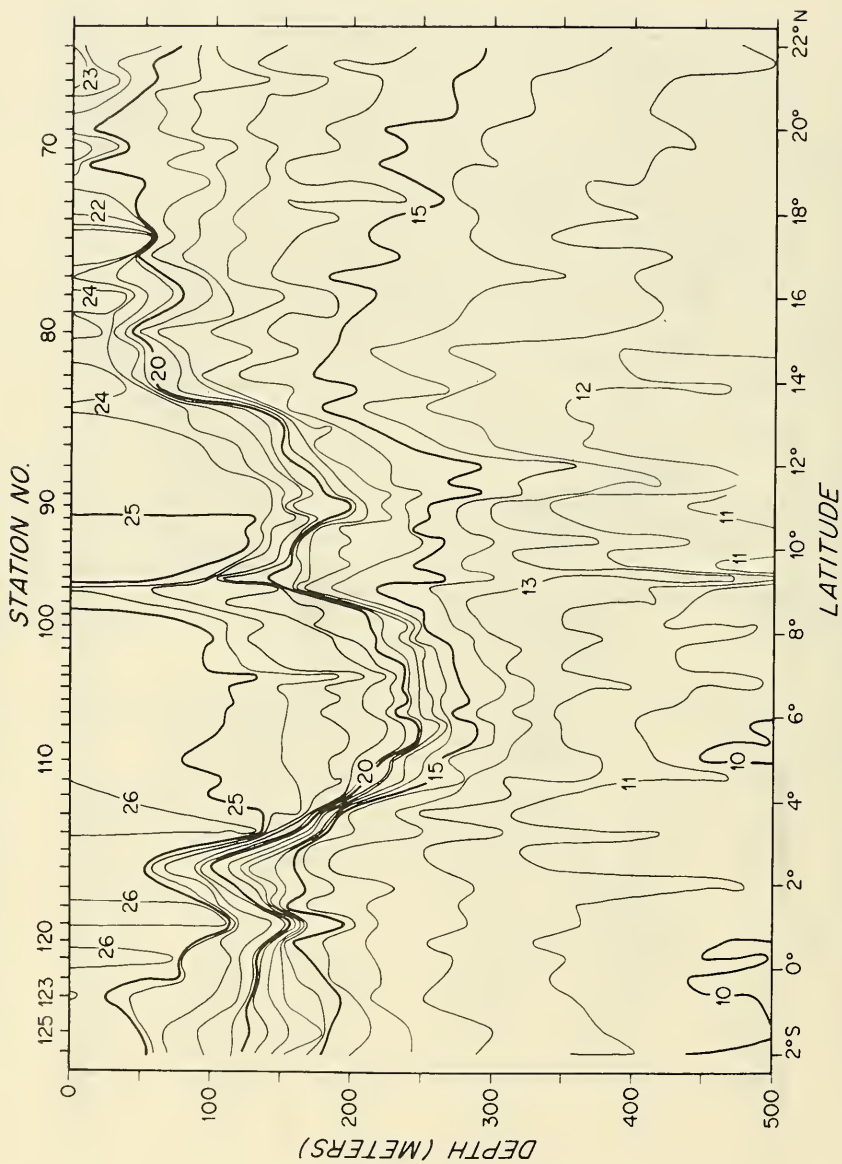


Figure 2. (cont.)

ESSO TOKYO 27 SEPT. - 1 OCT. 1978

STATION NO.

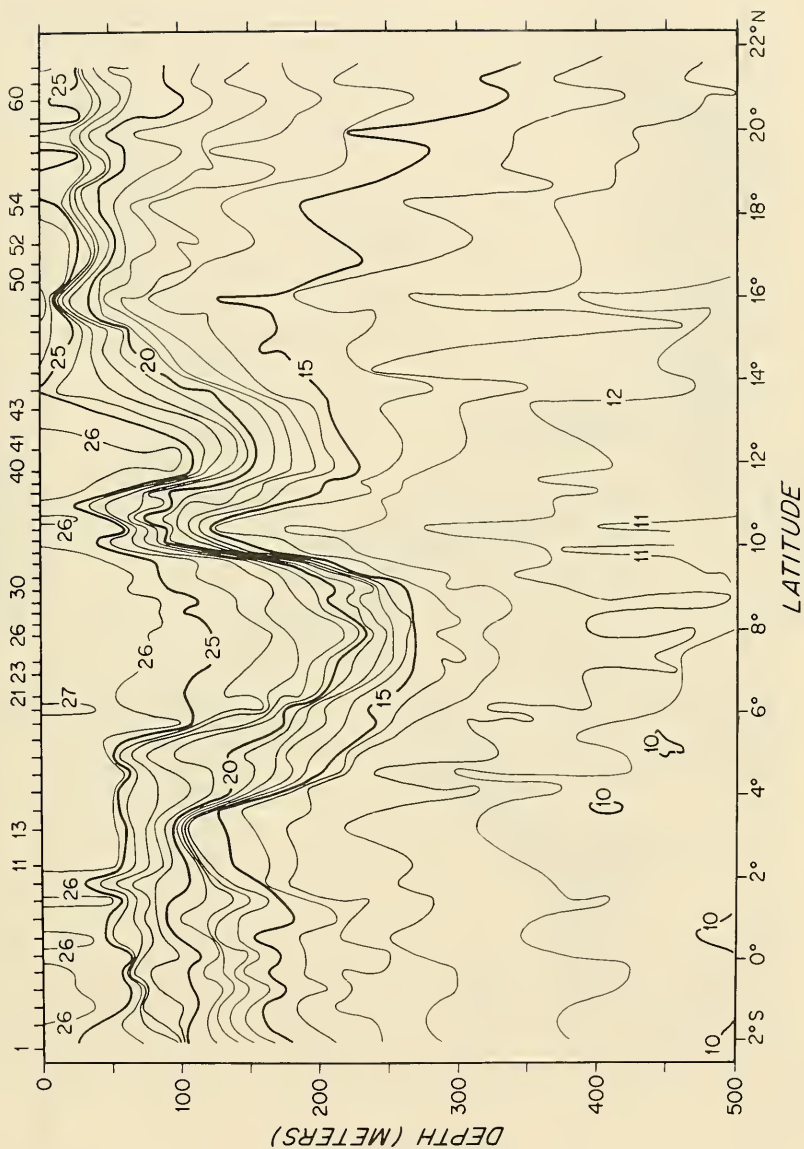


Figure 2. (cont.)

ESSO TOKYO 9-14 OCT. 1978

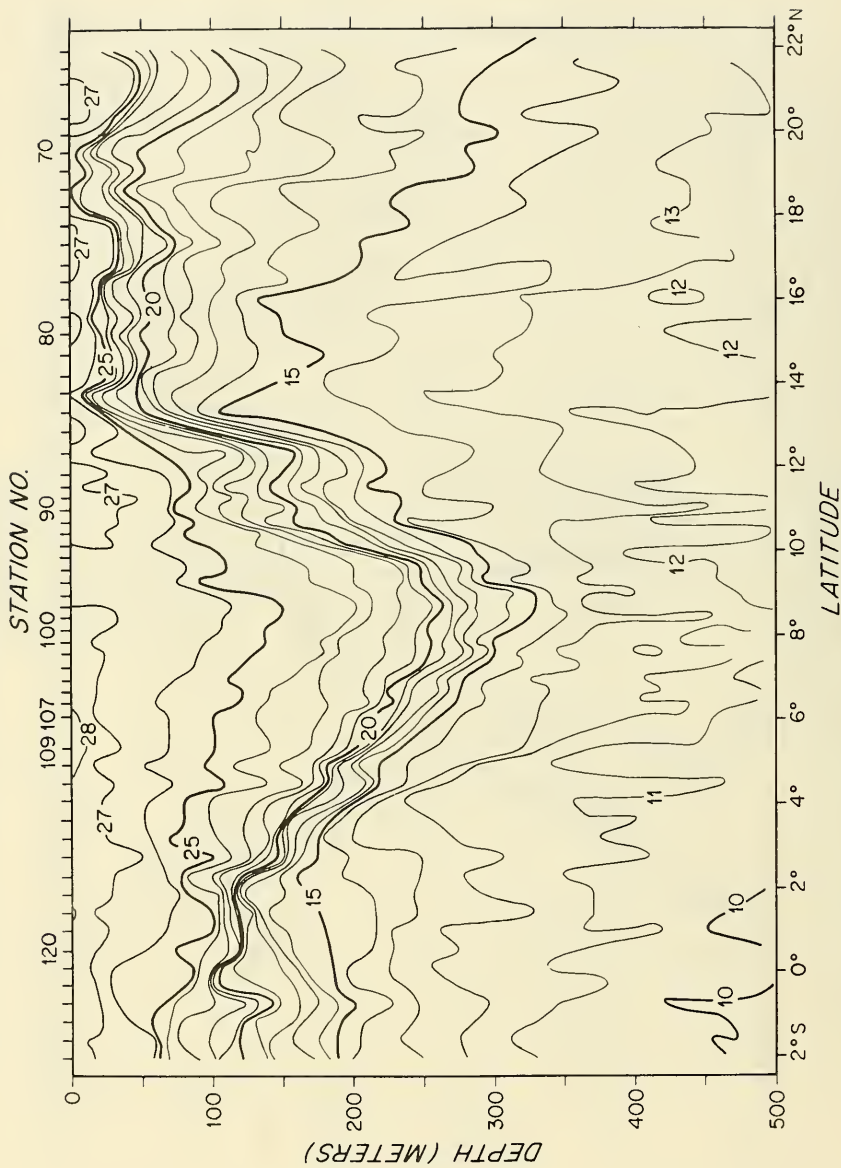


Figure 2. (cont.)

ESSO WILHELMSHAVEN 20-26 NOV. 1978
STATION NO.

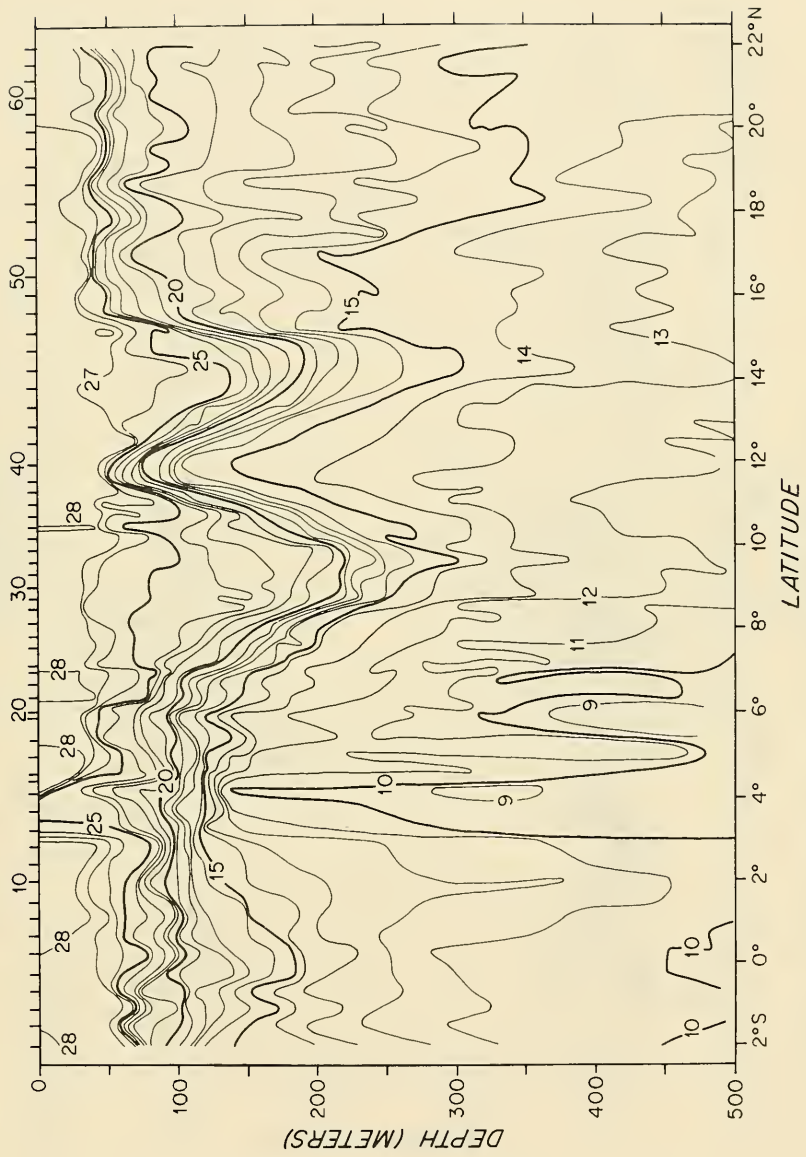


Figure 2. (cont.)

ESSO WILHELMSHAVEN 24-29 DEC. 1978

STATION NO

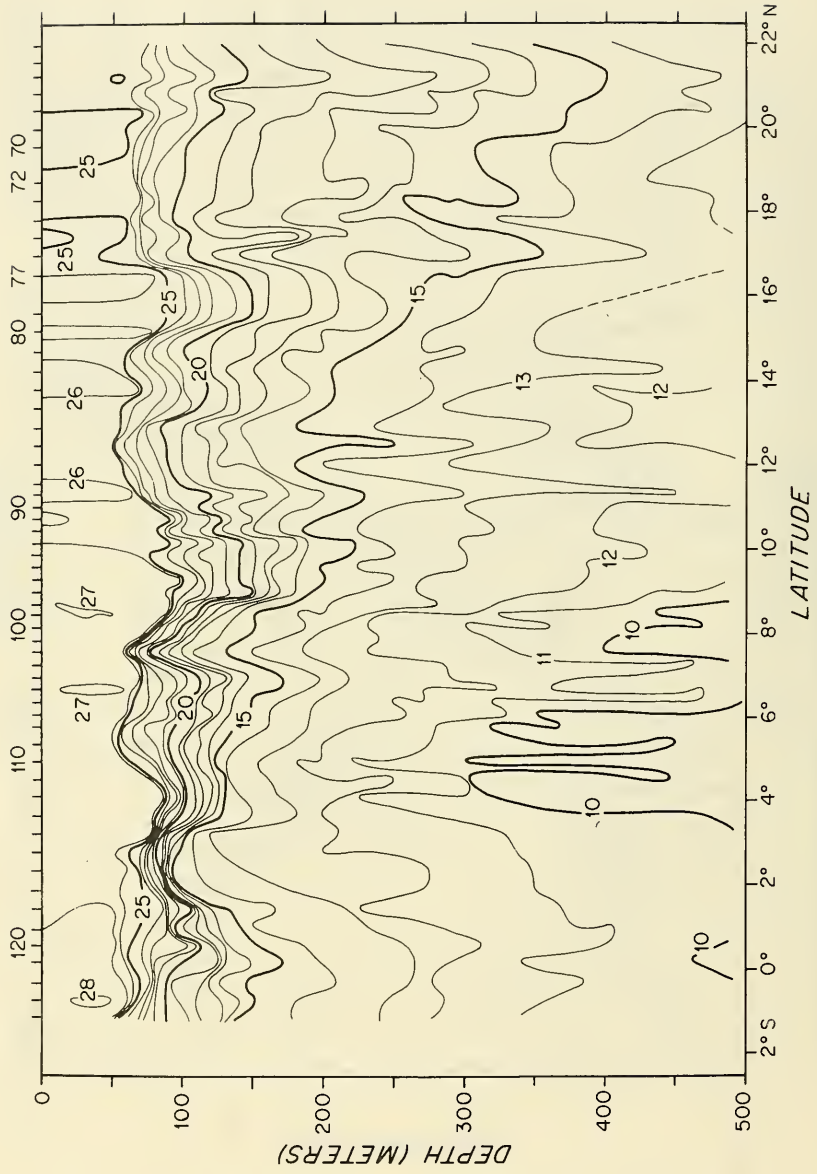


Figure 2. (cont.)

ESSO CARIBBEAN 22-27 JAN 1979

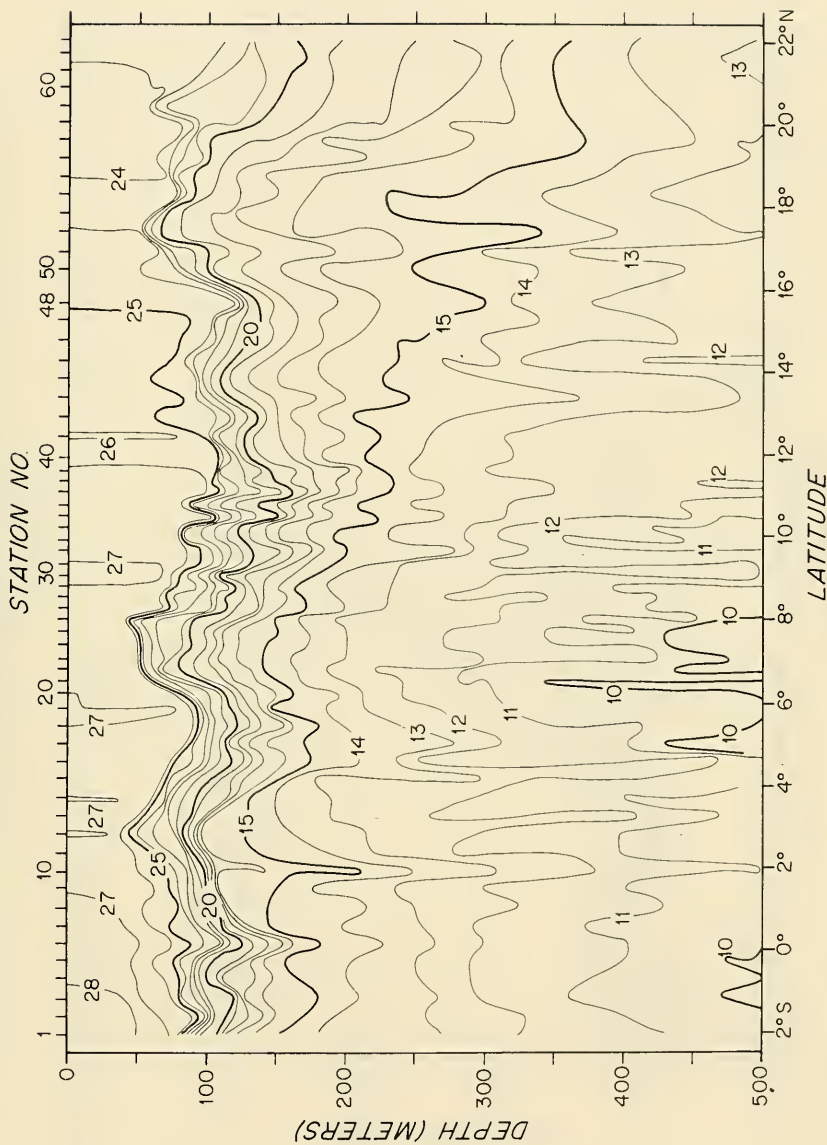


Figure 2. (cont.)

ESSO CARIBBEAN 6-11 FEB 1979

STATION NO.

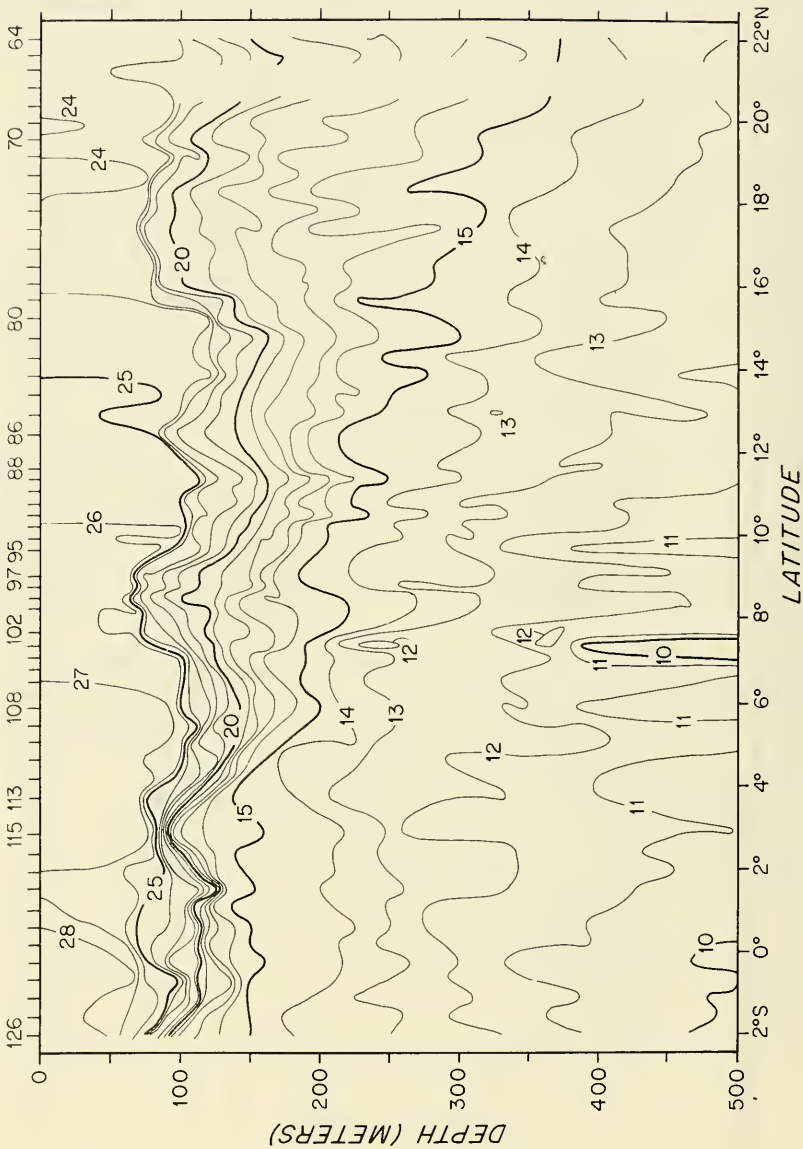


Figure 2. (cont.)

AL DURIYAH 5-10 MARCH 1979

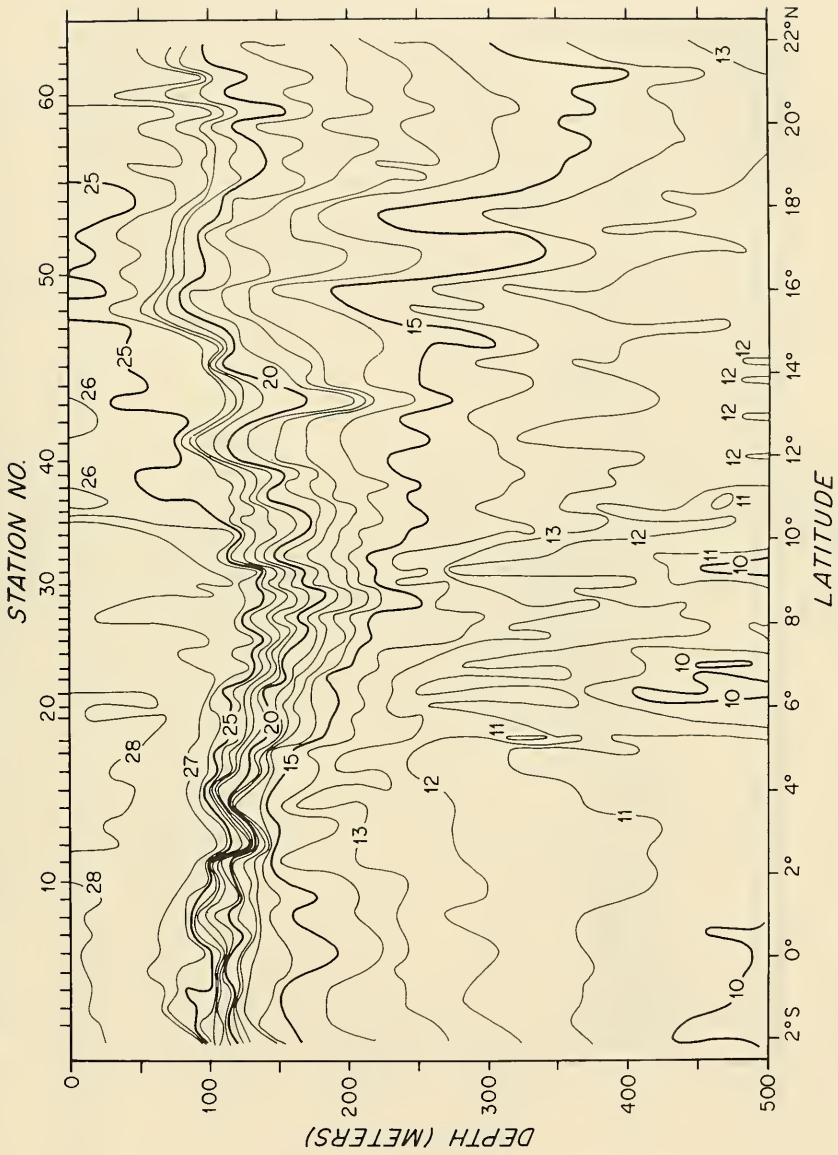


Figure 2. (cont.)

AL DURIYAH 24-30 MARCH 1979

STATION NO.

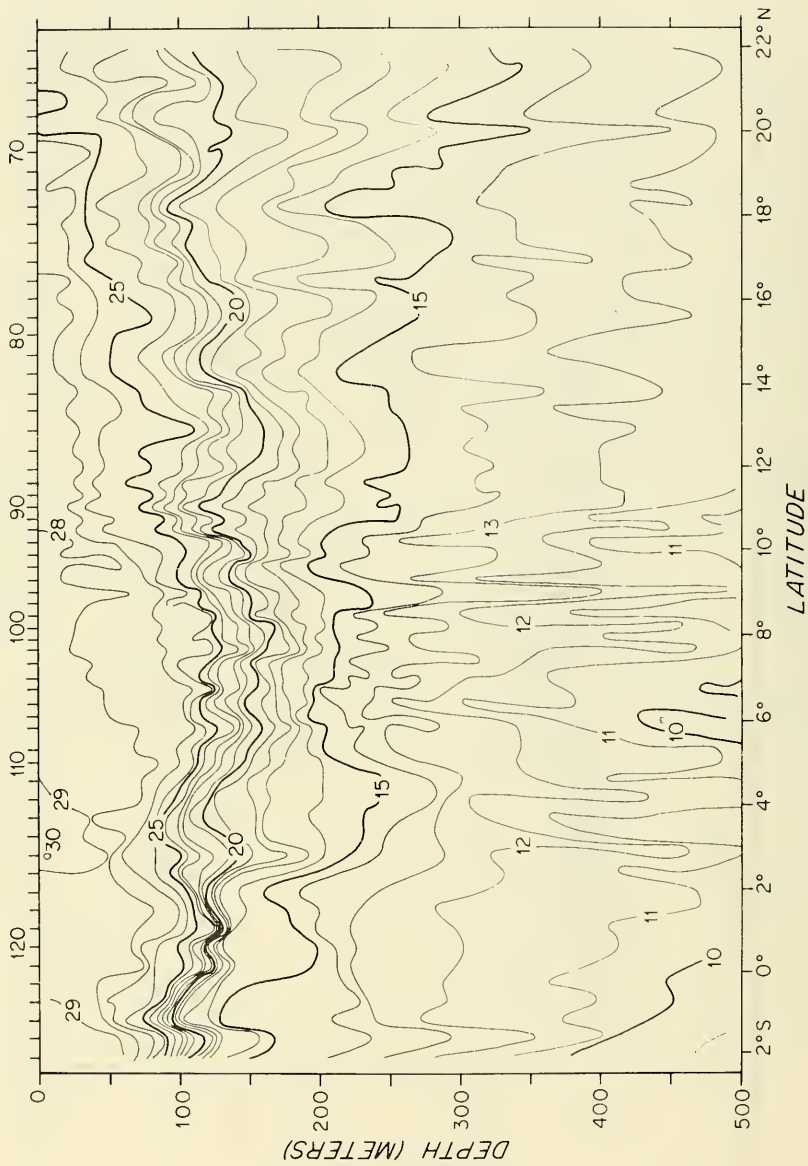


Figure 2. (cont.)

ESSO CARIBBEAN 18 - 24 APRIL 1979

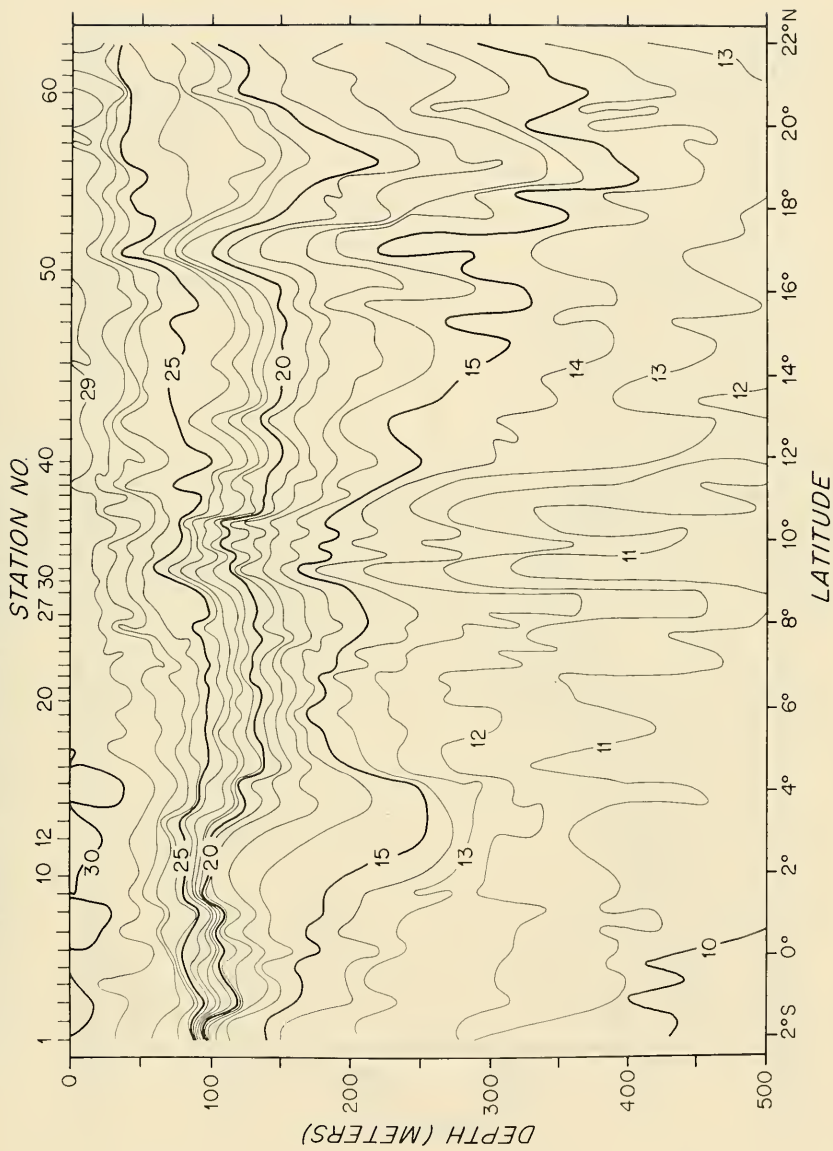


Figure 2. (cont.)

ESSO CARIBBEAN 6-10 MAY 1979

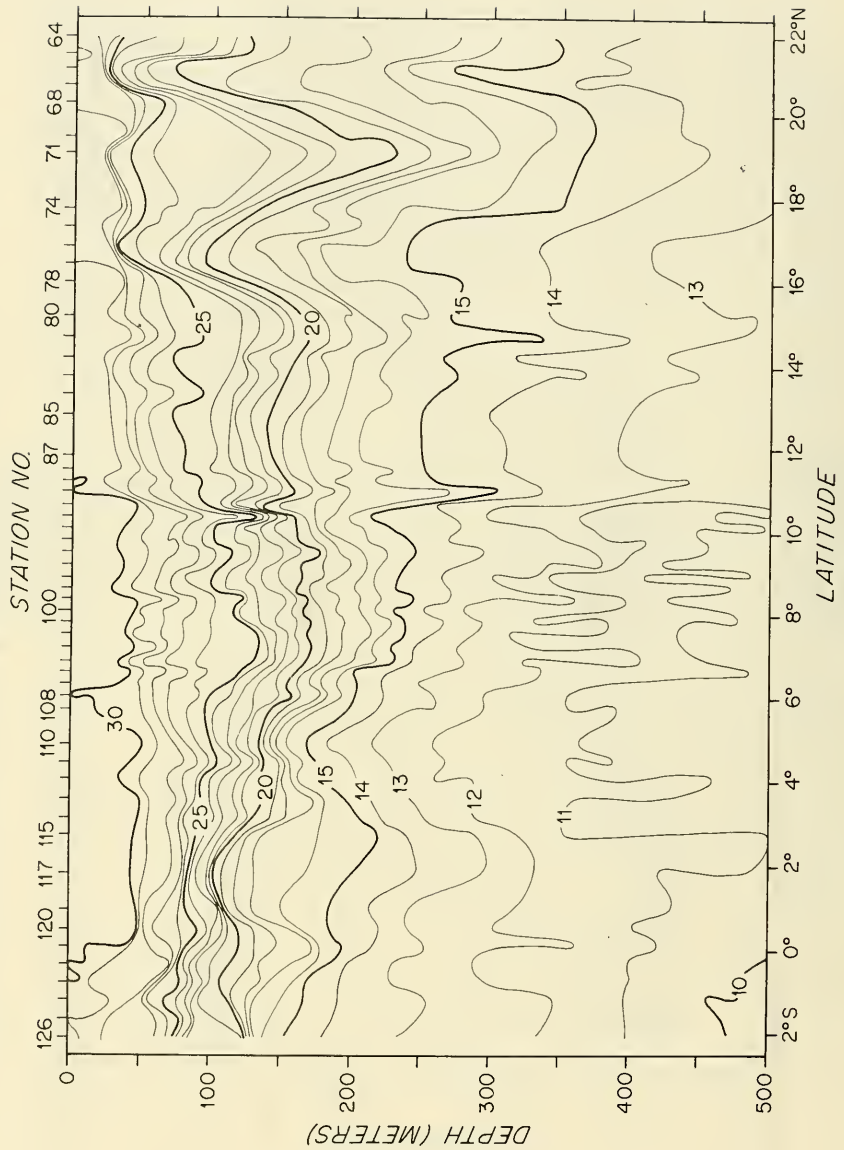


Figure 2. (cont.)

AL DURIYAH 5-10 JUNE 1979

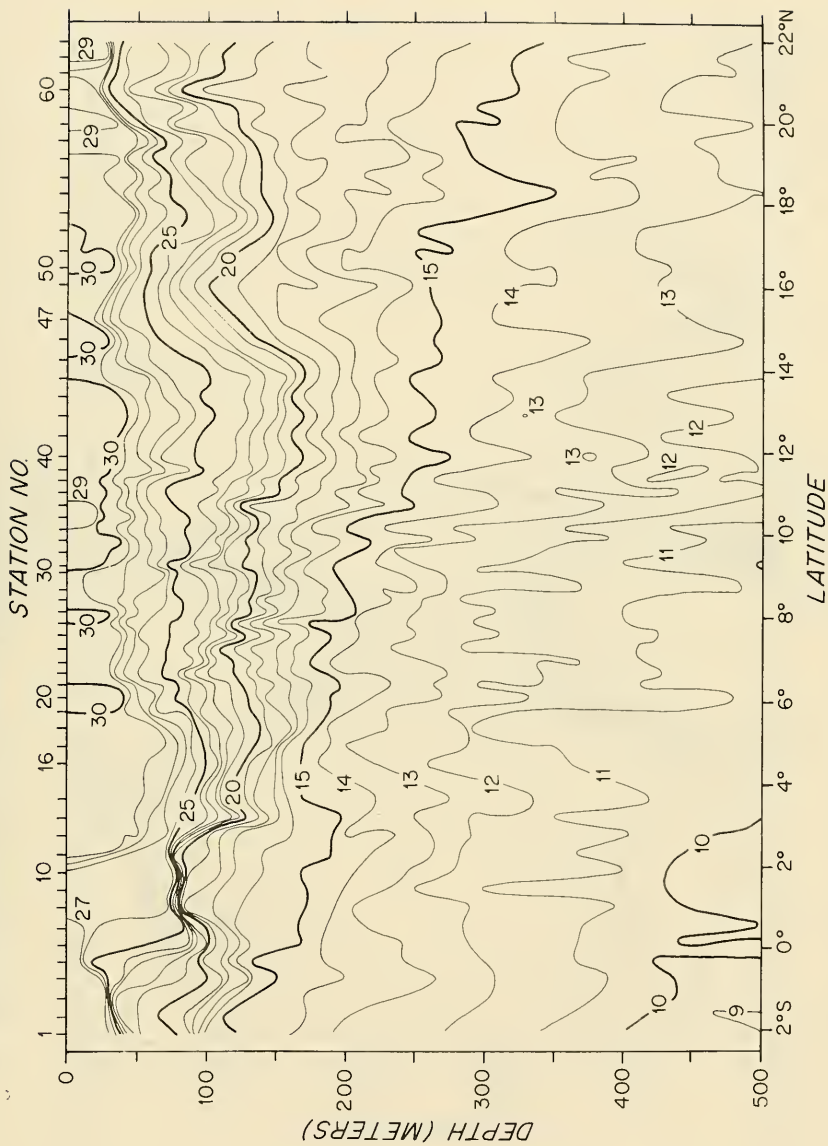


Figure 2. (cont.)

AL DURIYAH 28 JUNE - 3 JULY 1979

STATION NO.

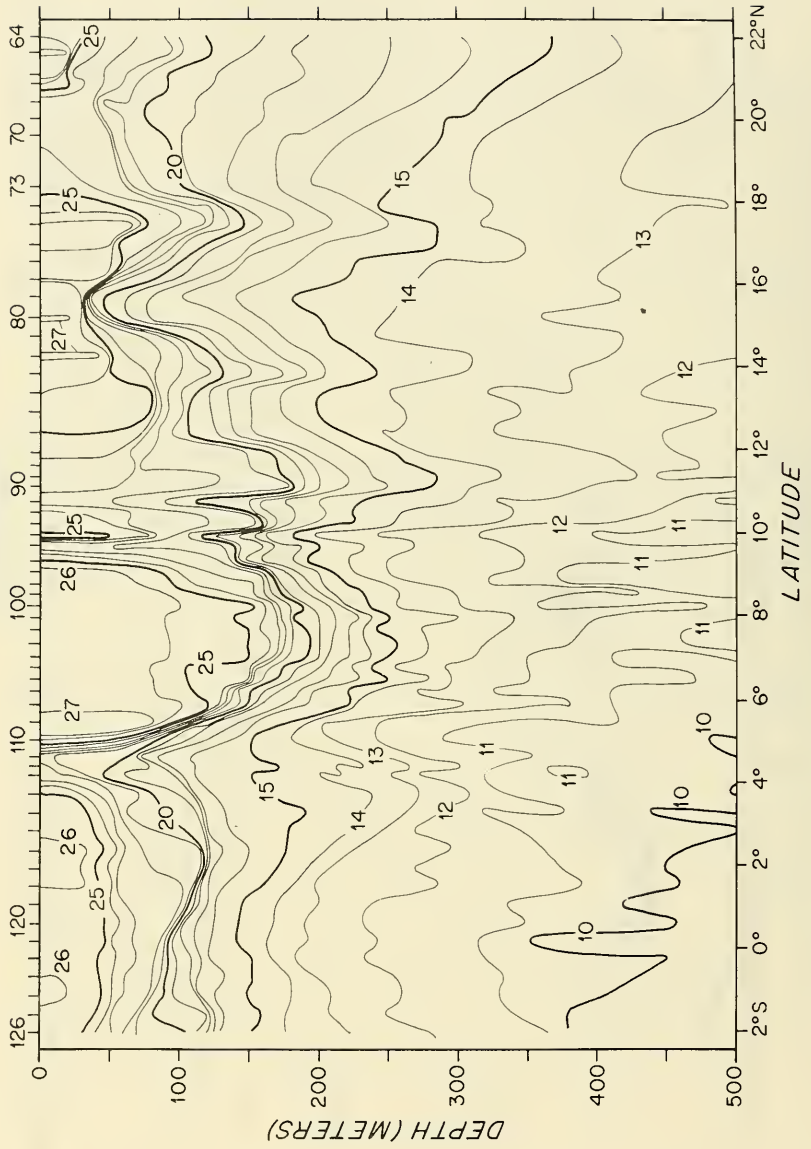


Figure 2. (cont.)

ESSO HONOLULU 14-18 JULY 1979

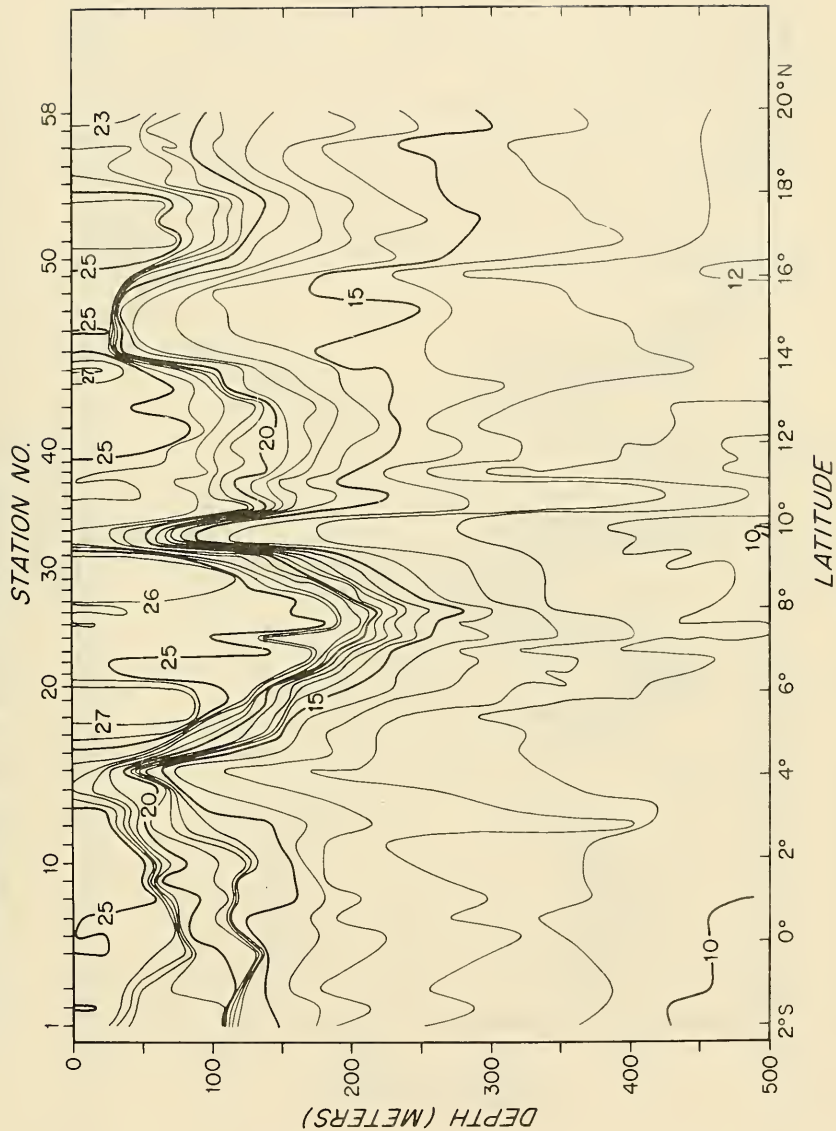


Figure 2. (cont.)

ESSO CARIBBEAN 10-17 AUG. 1979

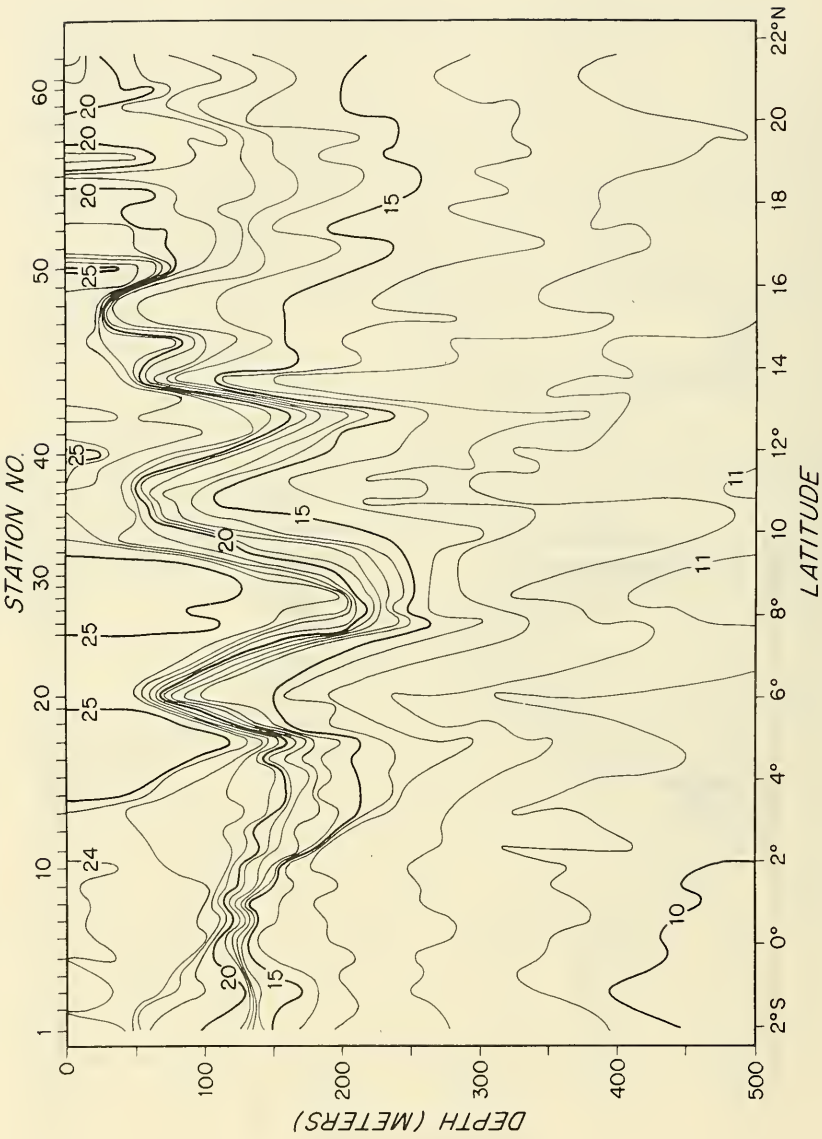


Figure 2. (cont.)

ESSO CARIBBEAN 25-31 AUG. 1979
STATION NO.

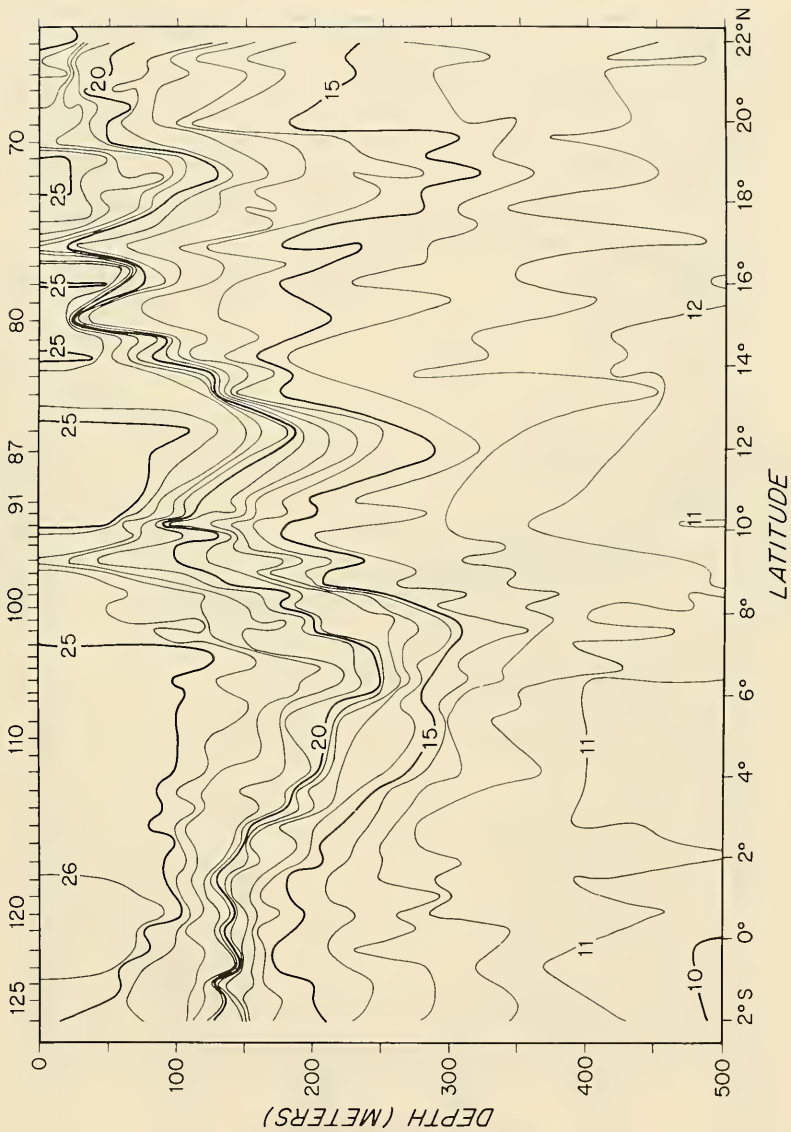


Figure 2. (cont.)

ESSO COPENHAGEN 17-21 OCT 1979

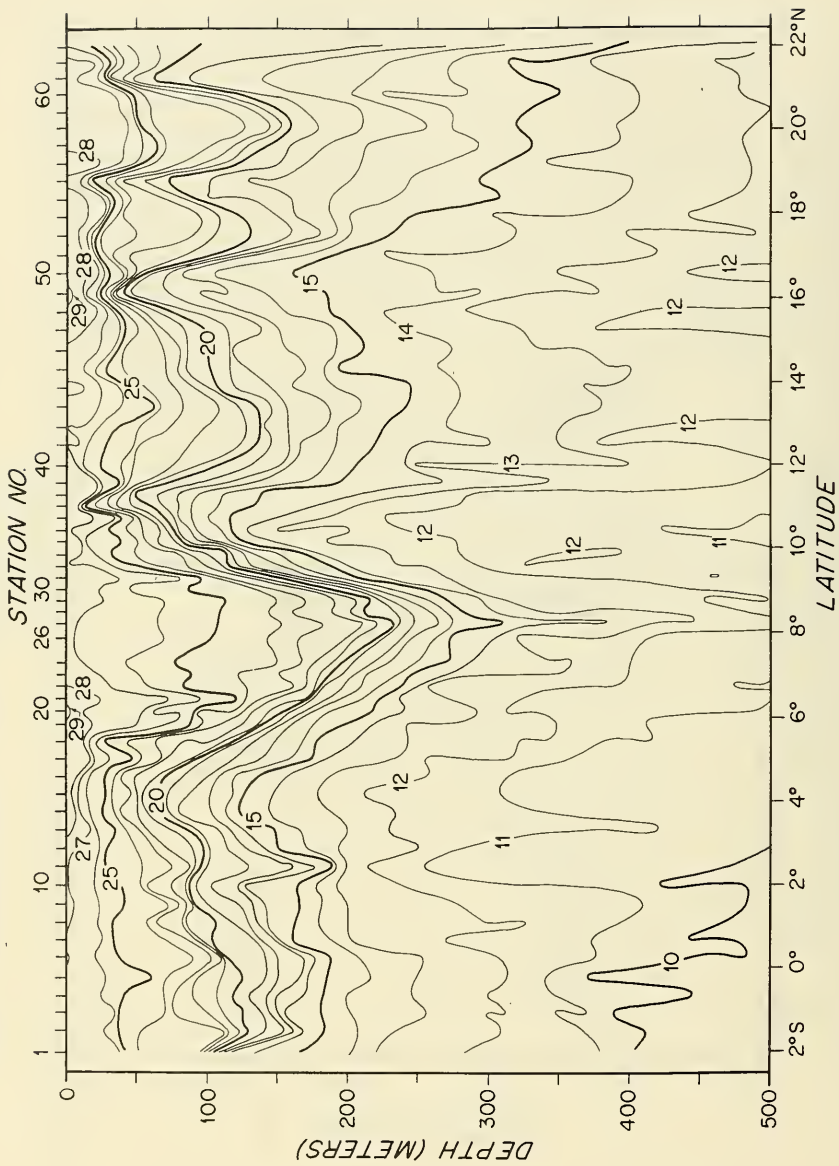


Figure 2. (cont.)

ESSO TOKYO 23-27 NOV 1979

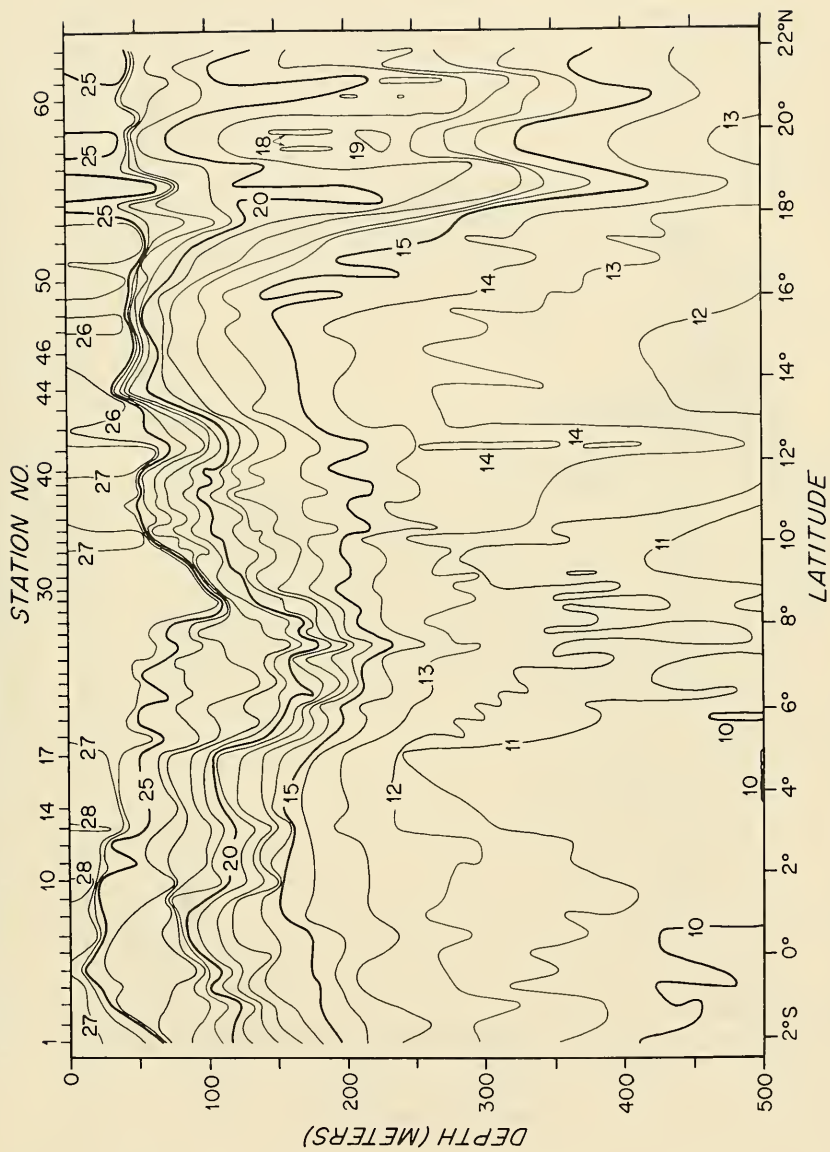


Figure 2. (cont.)

ESSO COPENHAGEN 28 NOV - 4 DEC 1979

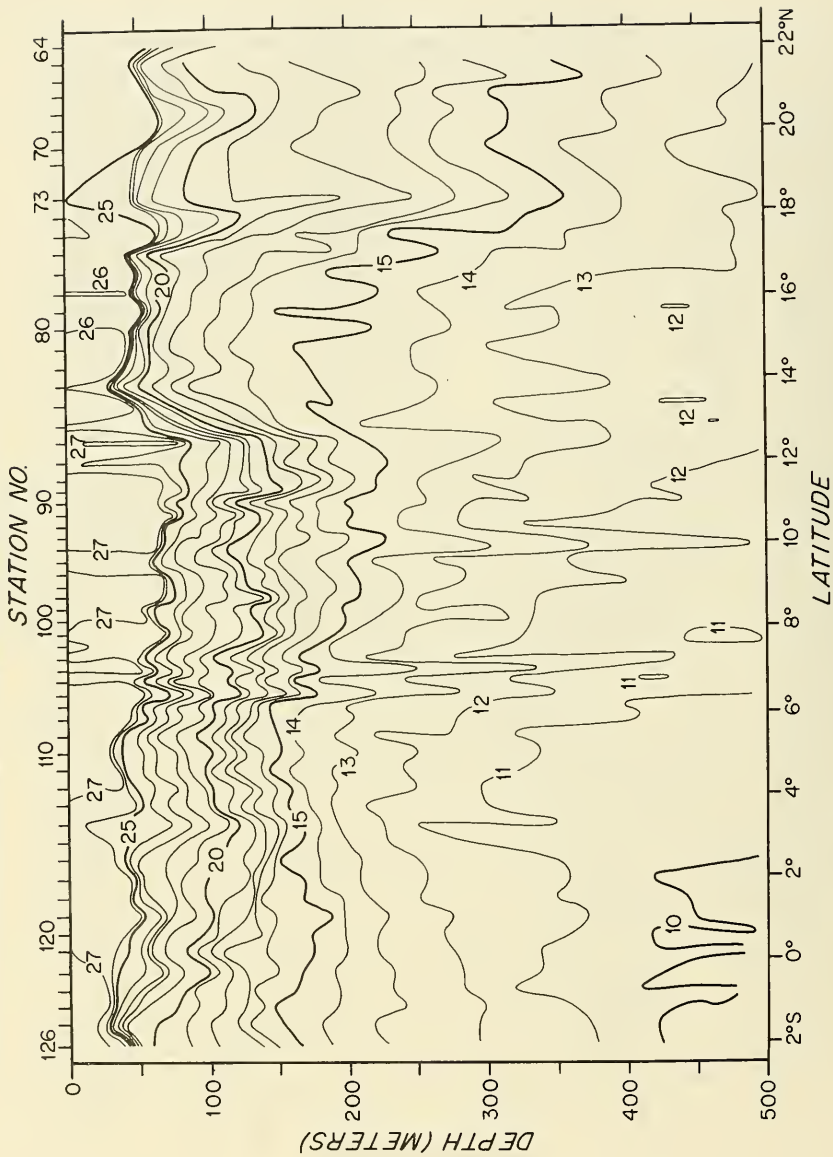


Figure 2. (cont.)

ESSO TOKYO 7-13 DEC 1979

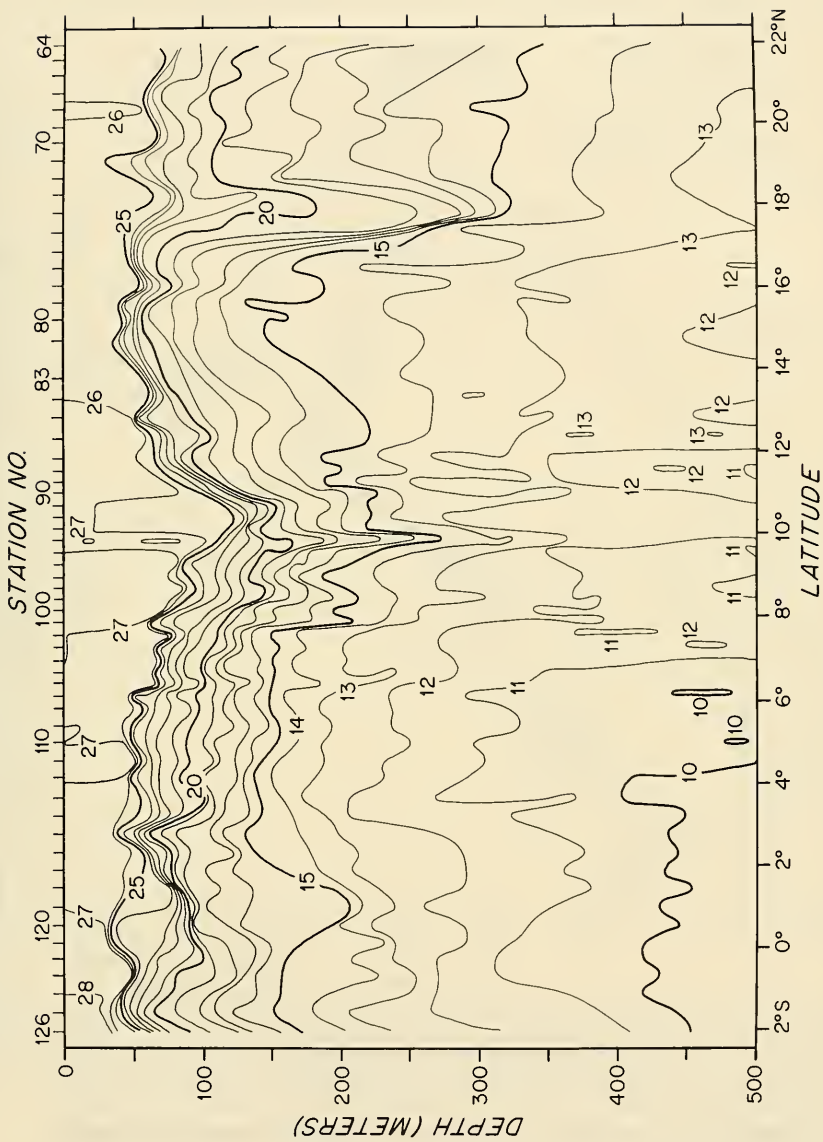


Figure 2. (cont.)

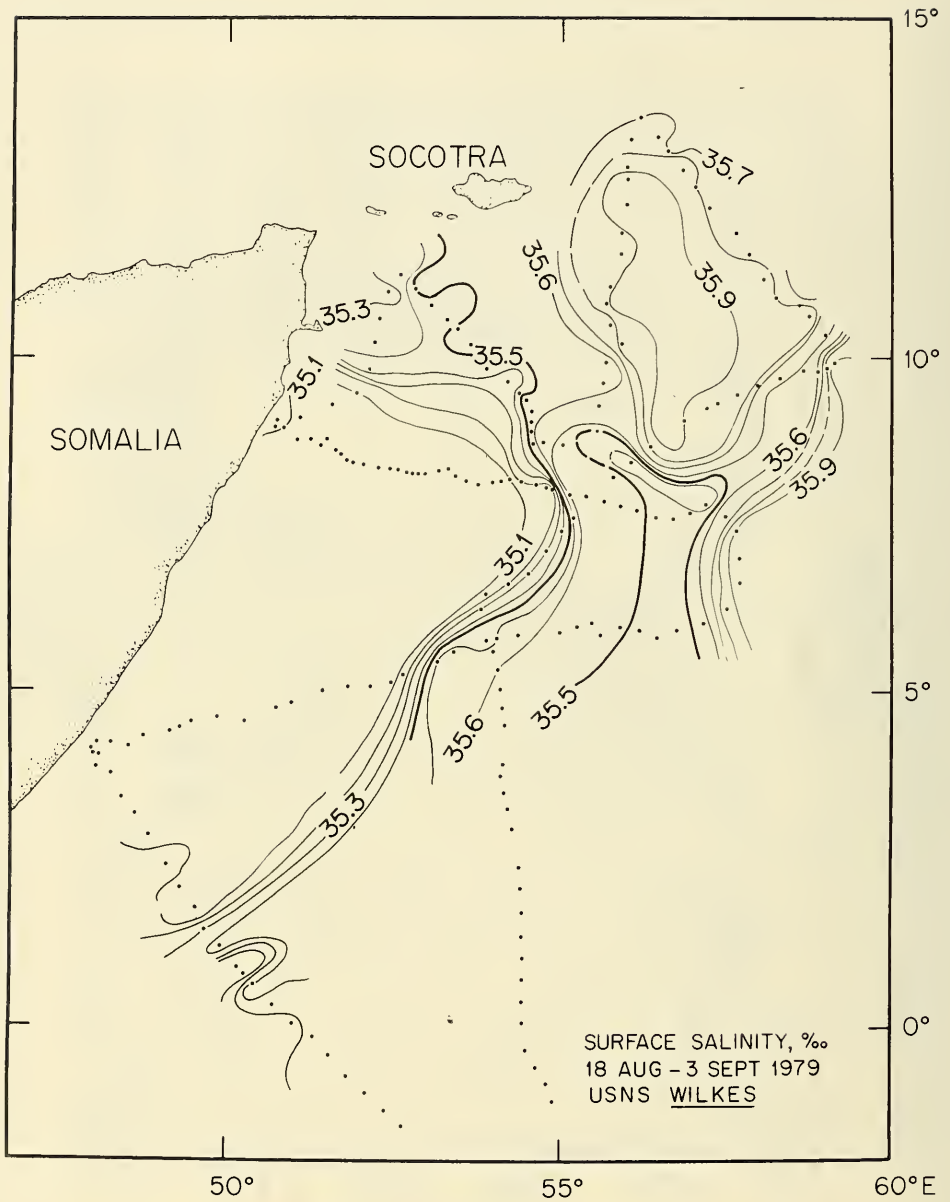


Figure 3. Surface salinity (‰), 18 August - 3 September 1979, from USNS WILKES.

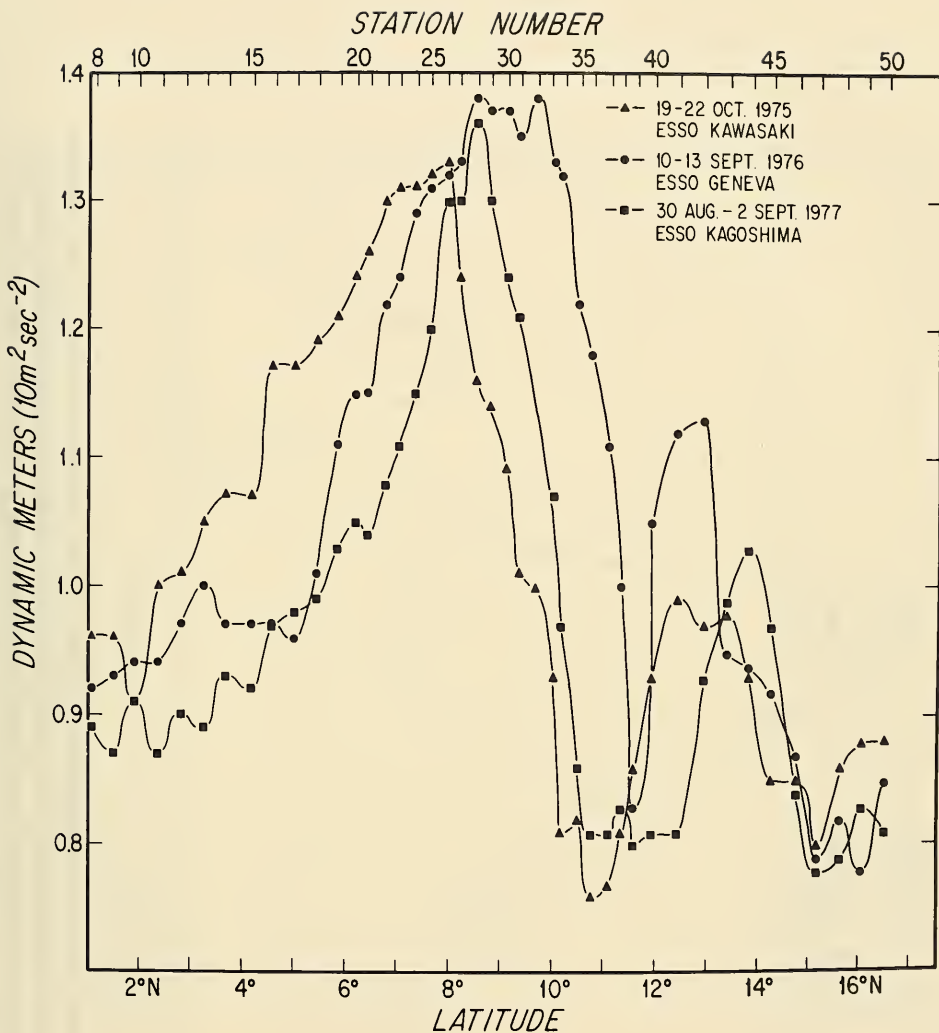


Figure 4. Sea surface dynamic height relative to 400 dbar during the southwest monsoons 1975, 1976, and 1977 constructed from XBT stations along the tanker sea lane (Figure 1a). For each year the strong signal of the prime eddy occurs from 8°N to 10°N with a deep trough to the north (11°N to 12°N) between it and the Socotra eddy 12°N to 14°N. Mean temperature-salinity relationship determined from previous data in this region (same temperature-salinity distribution used for all stations) was used with XBT temperatures to determine the specific volume values needed to produce these curves.

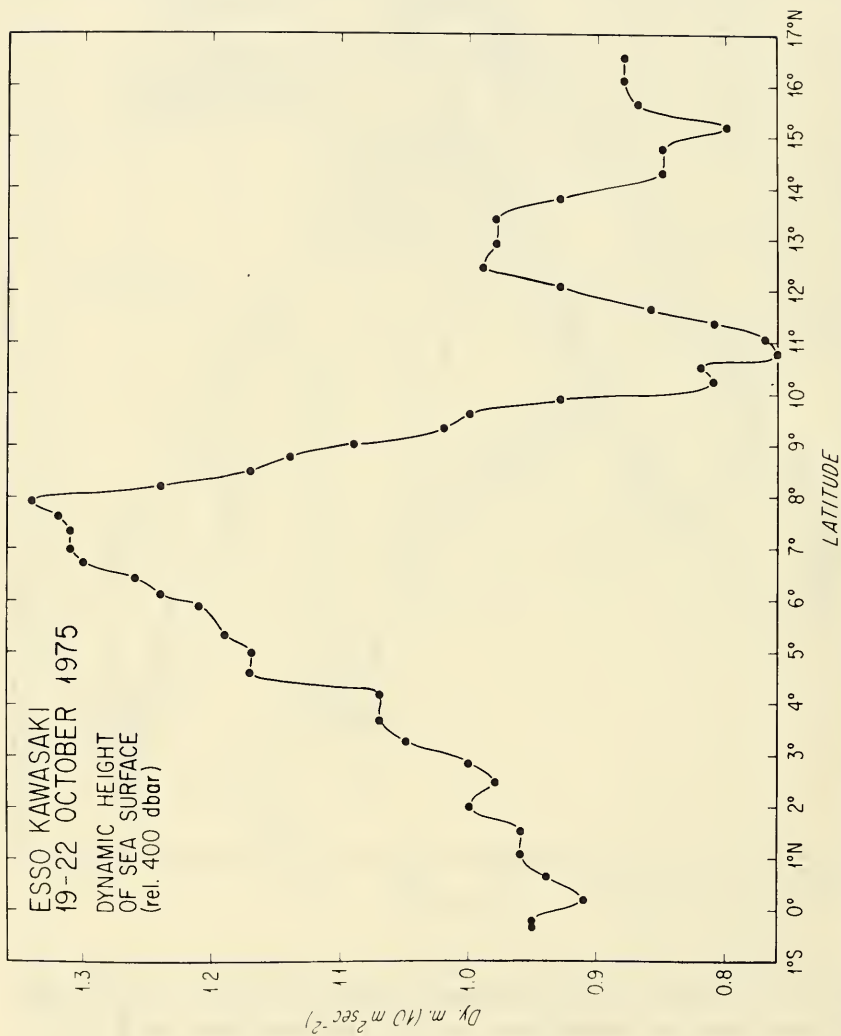


Figure 5. Sea surface dynamic height relative to 400 dbars each along tanker sea lane (figure 1a) from temperature sections shown in Figure 2. Mean temperature-salinity relationship determined from previous data in the region (same temperature-salinity distribution used for all stations) was used with XBT temperatures to determine the specific volume values needed to produce these curves.

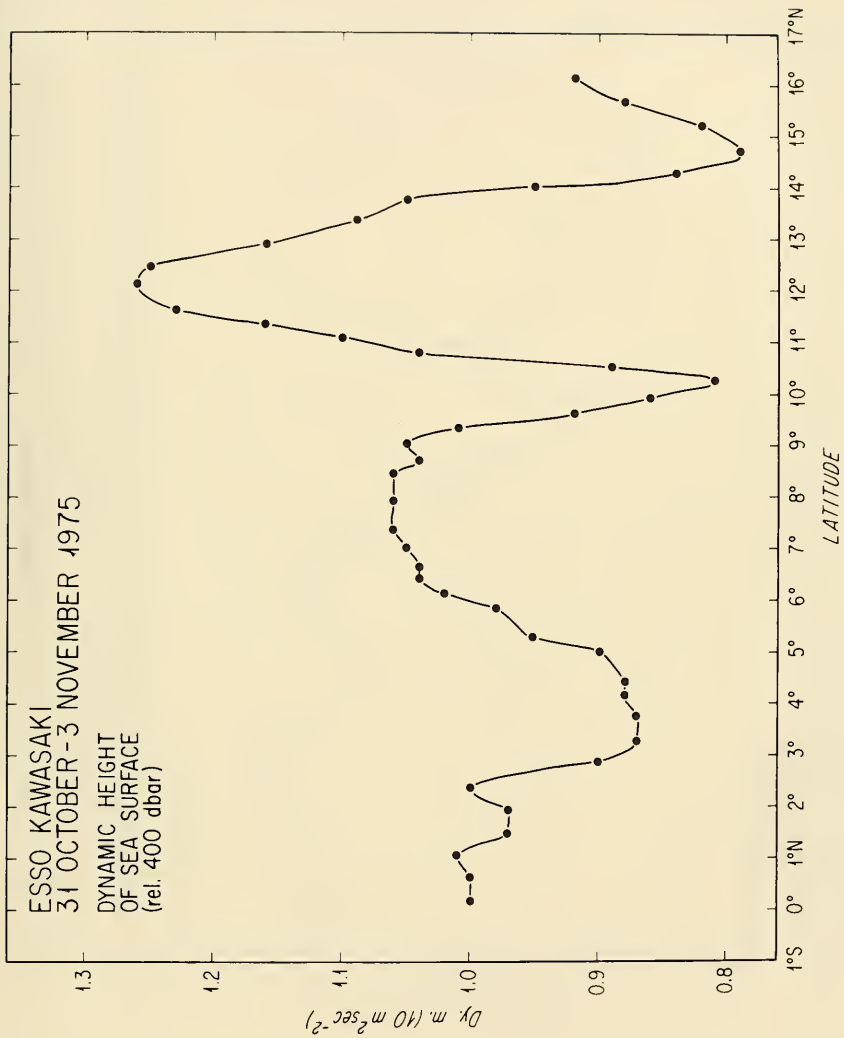


Figure 5. (cont.)

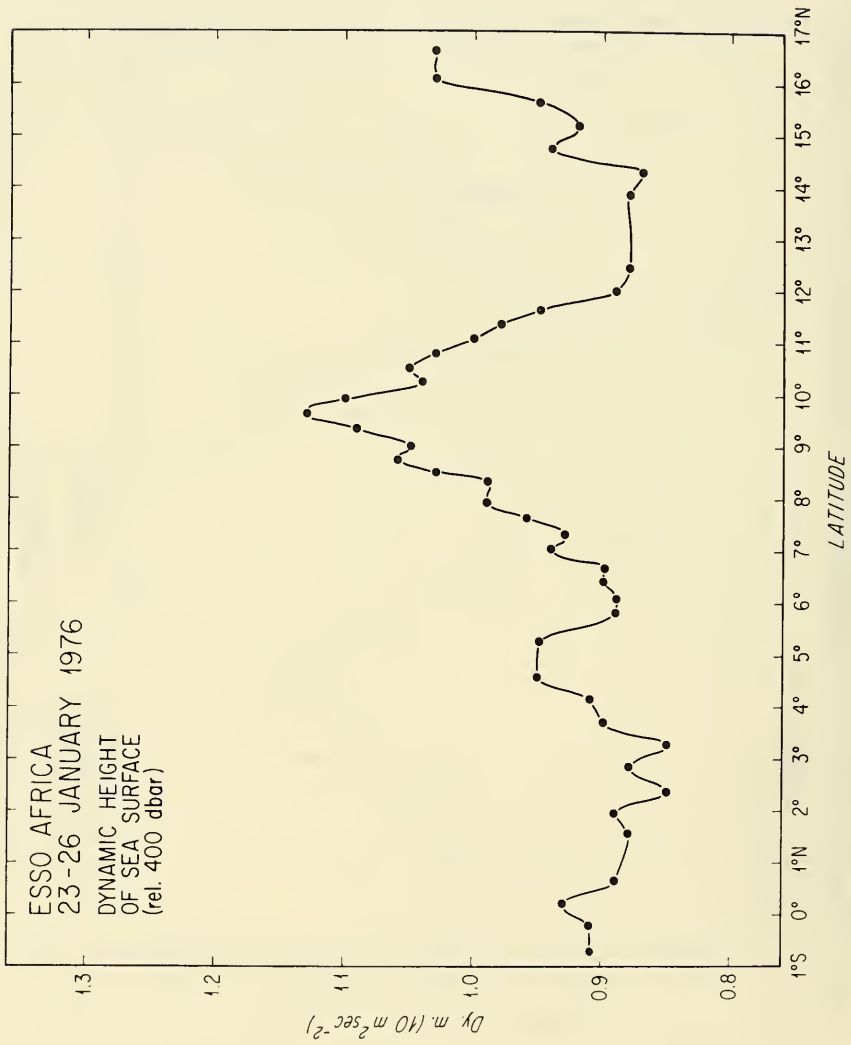


Figure 5. (cont.)

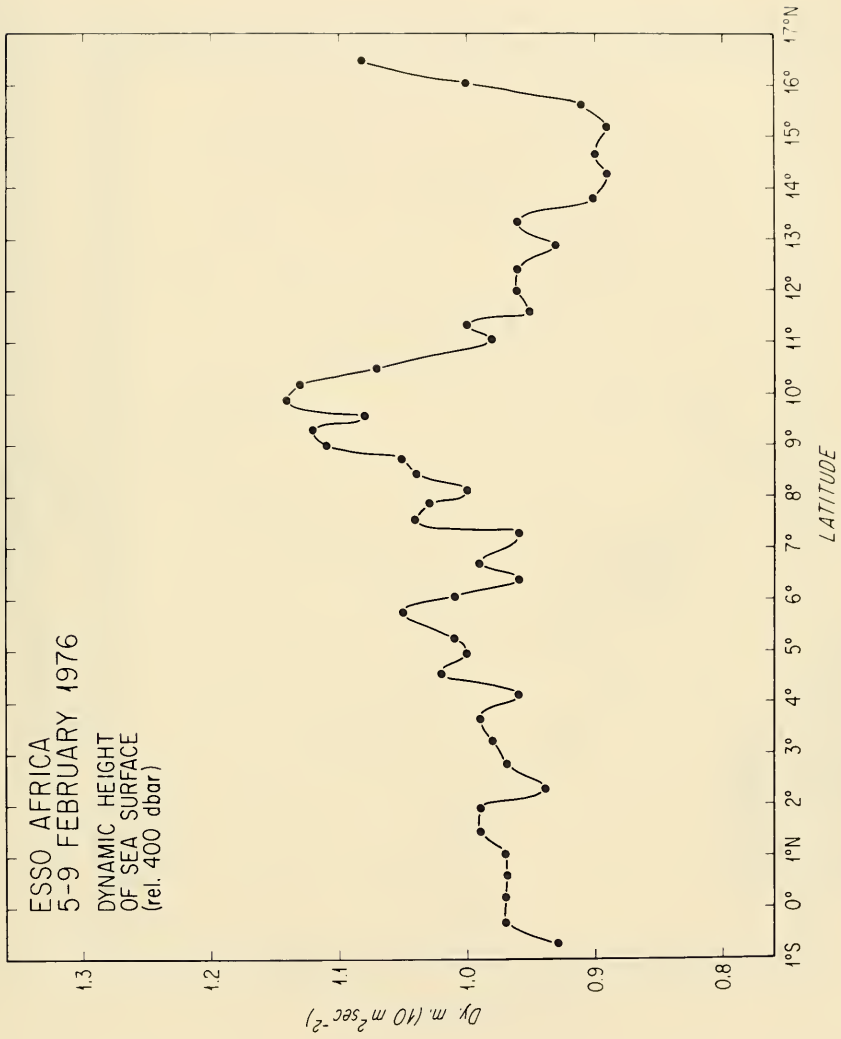


Figure 5. (cont.)

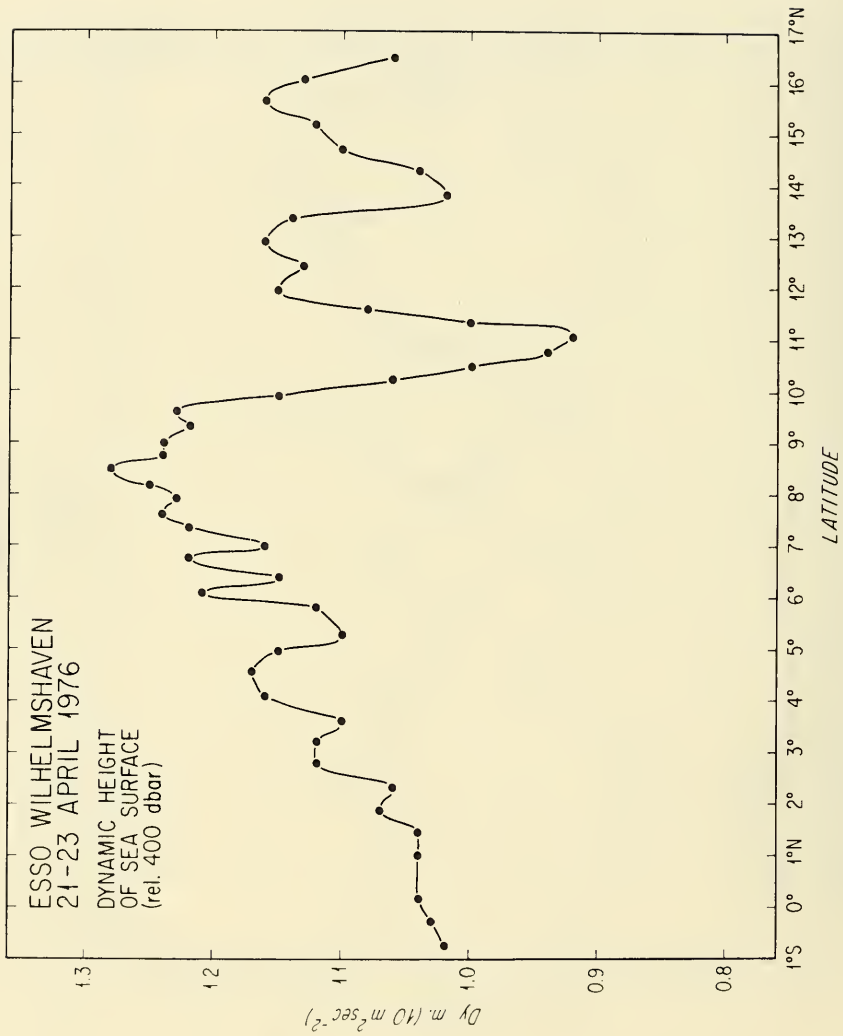


Figure 5. (cont.)

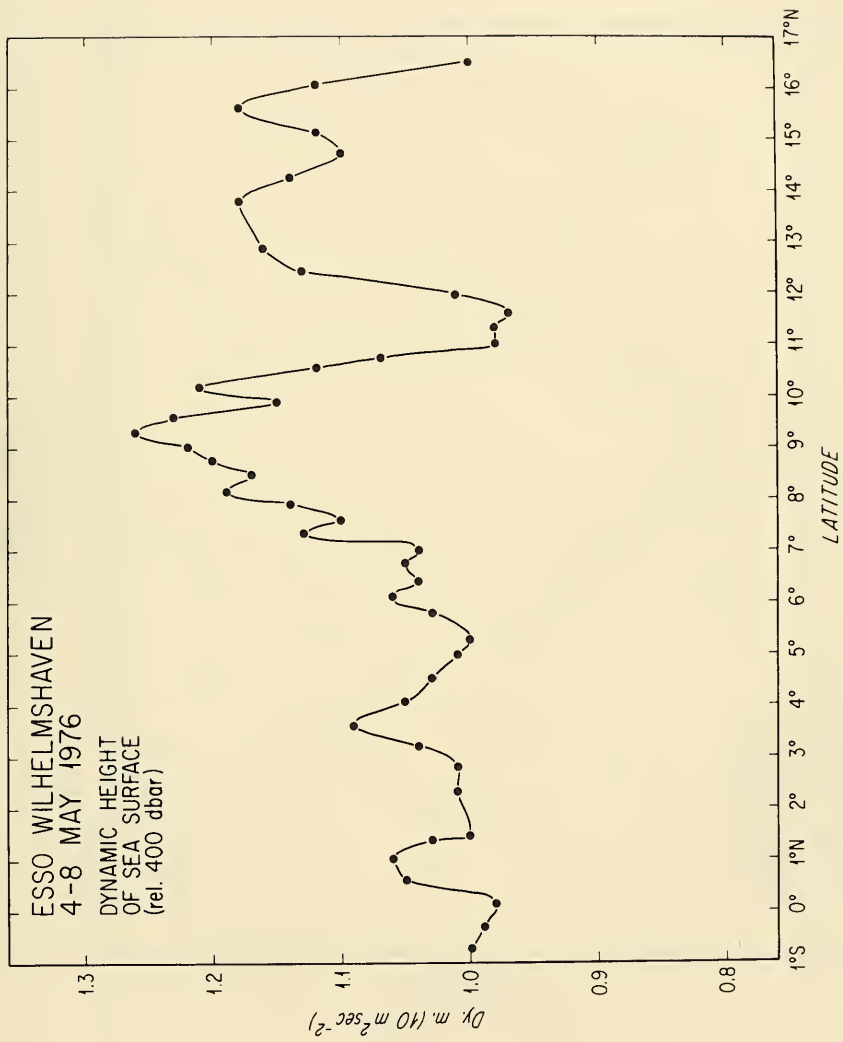


Figure 5. (cont.)

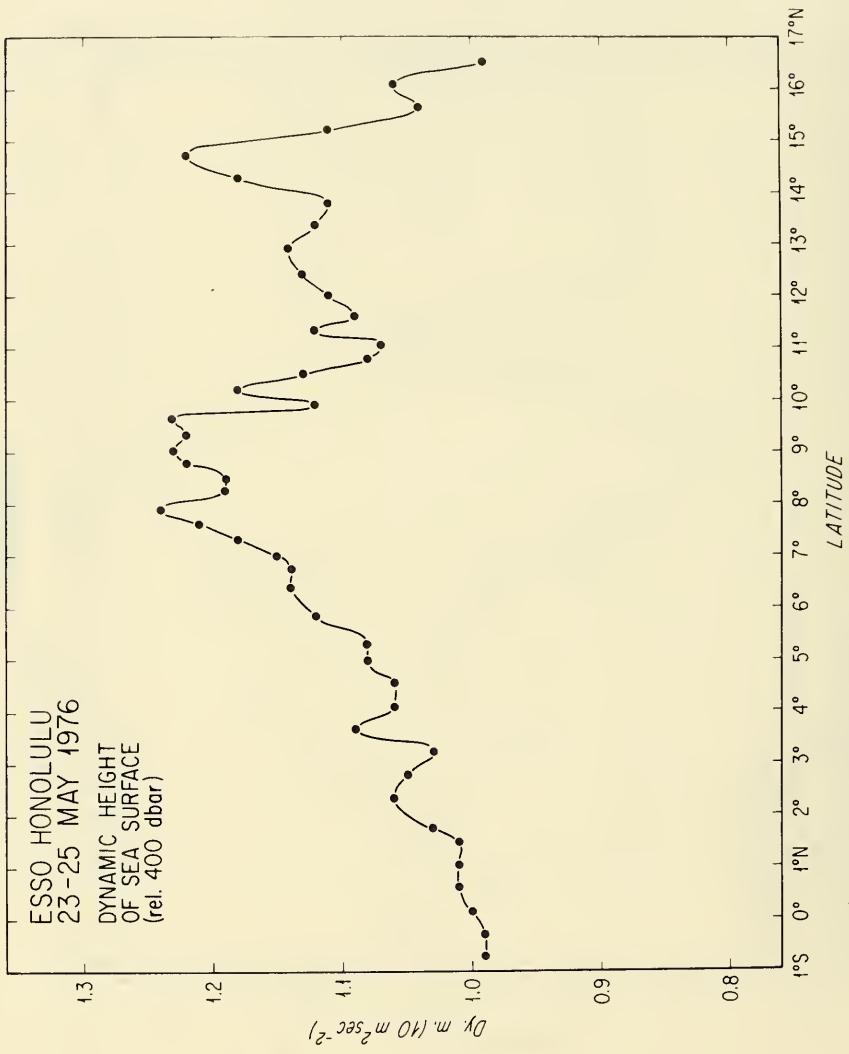


Figure 5. (cont.)

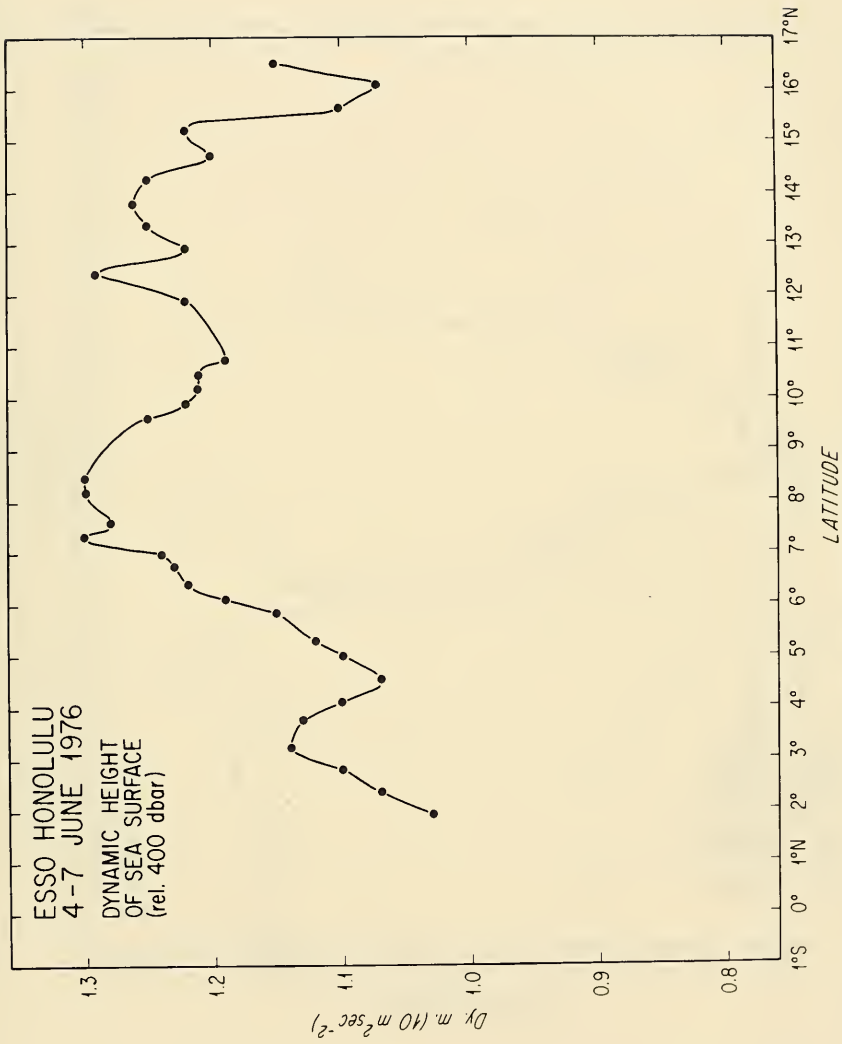


Figure 5. (cont.)

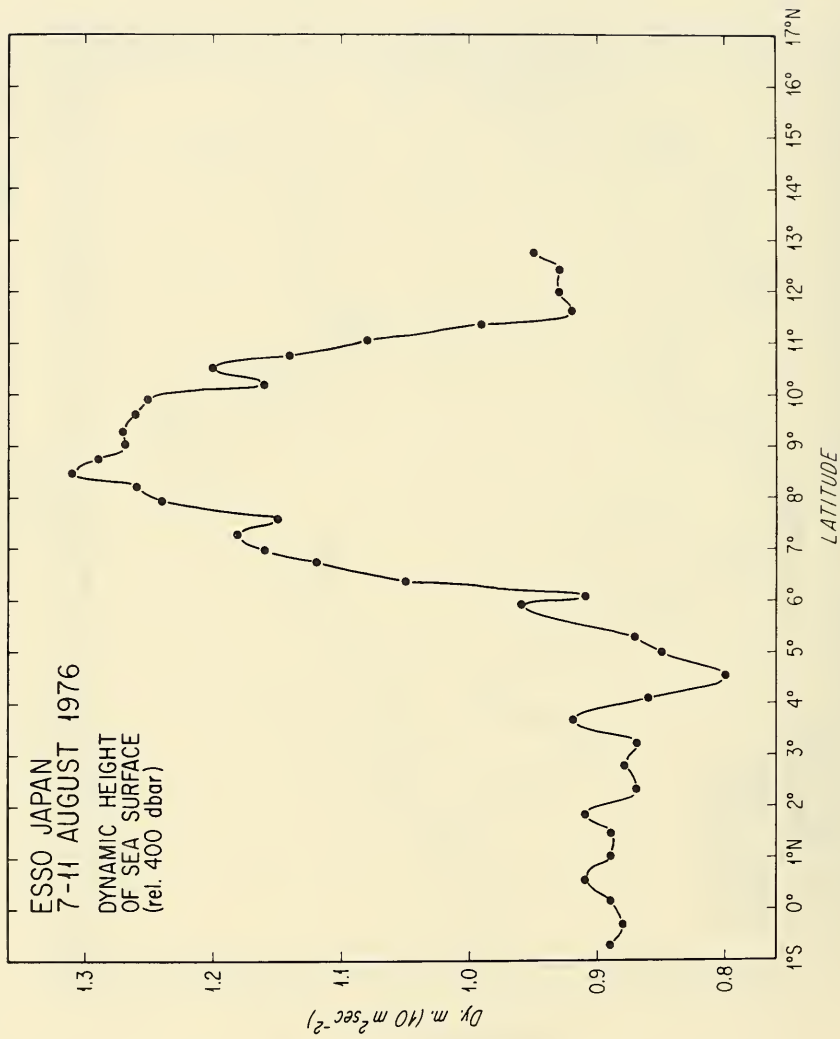


Figure 5. (cont.)

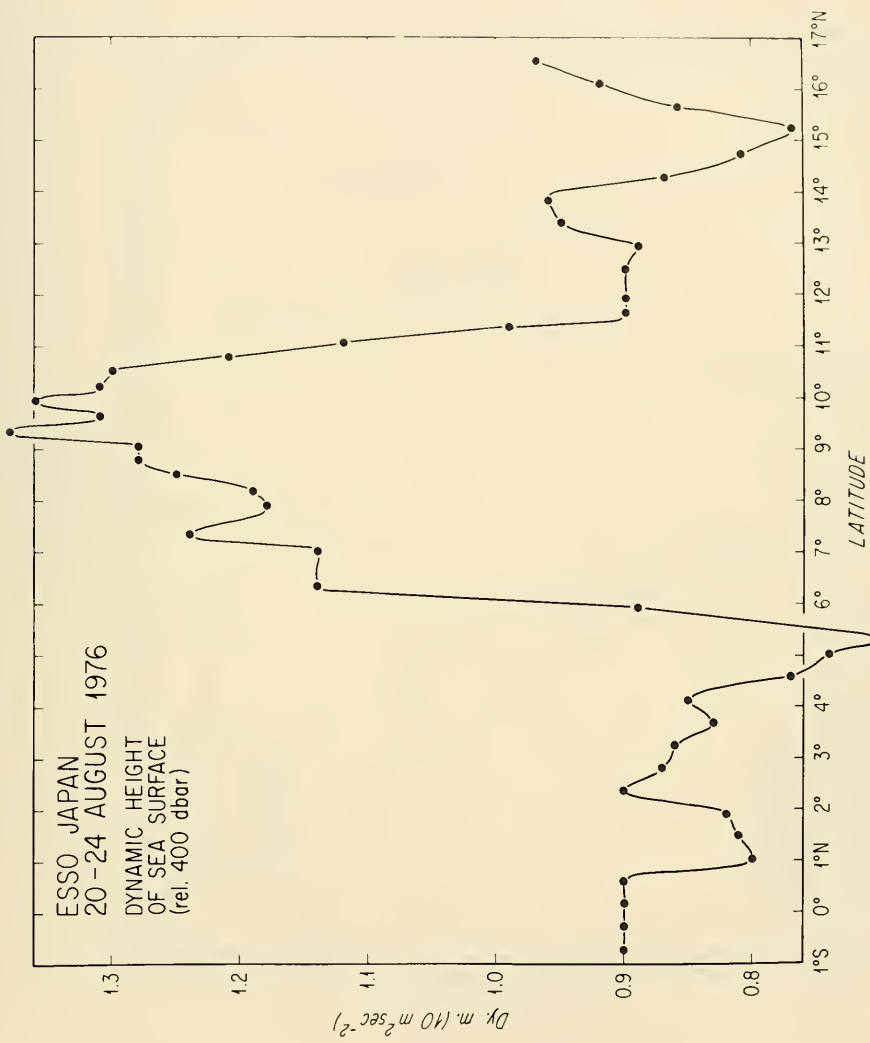


Figure 5. (cont.)

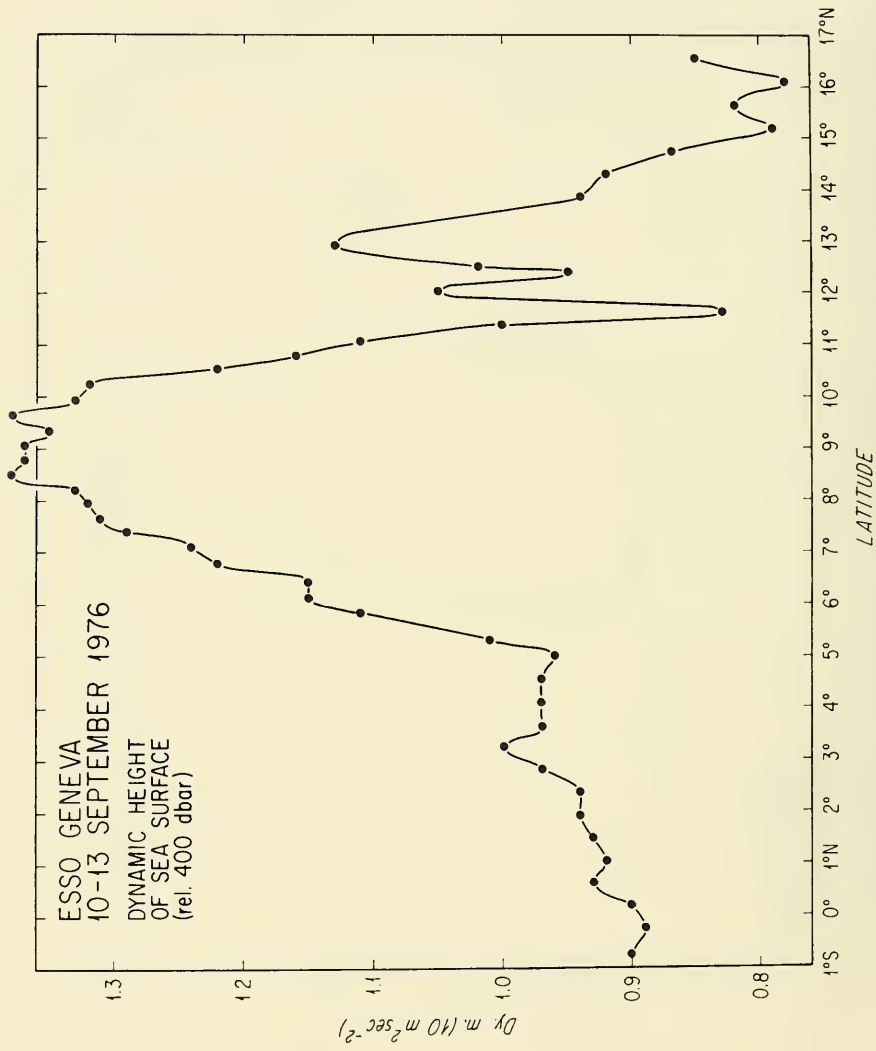


Figure 5. (cont.)

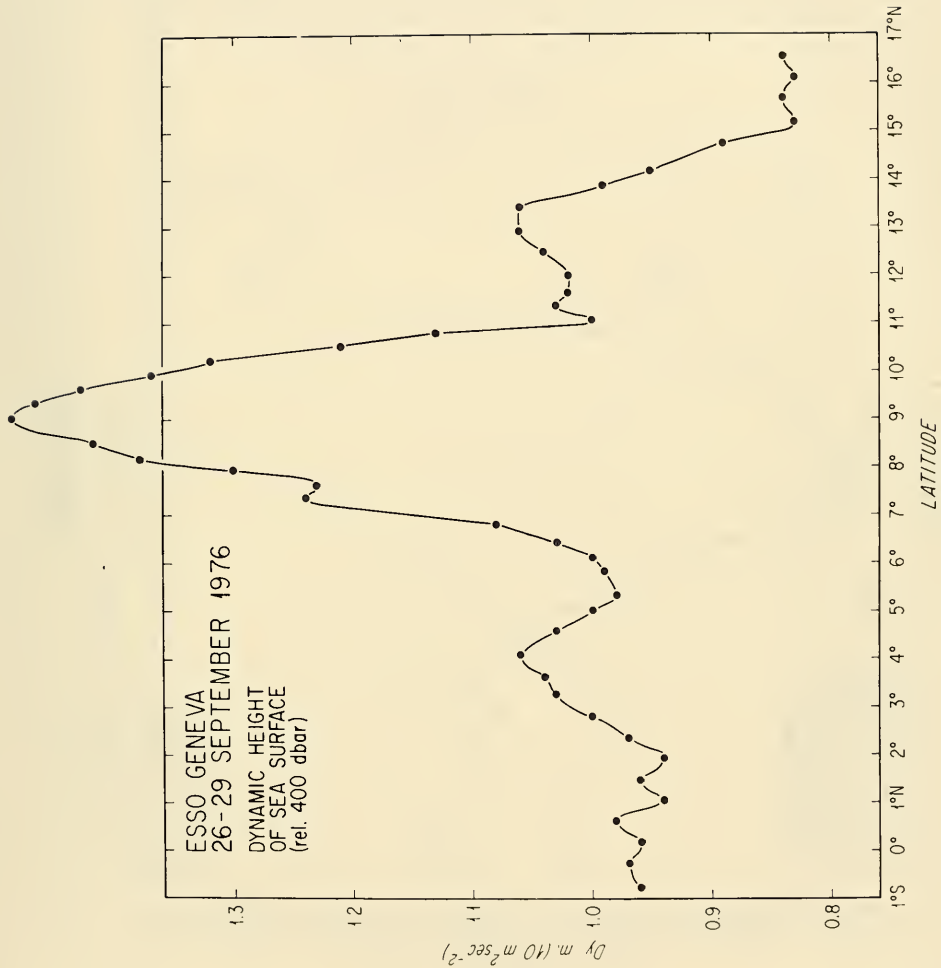


Figure 5. (cont.)

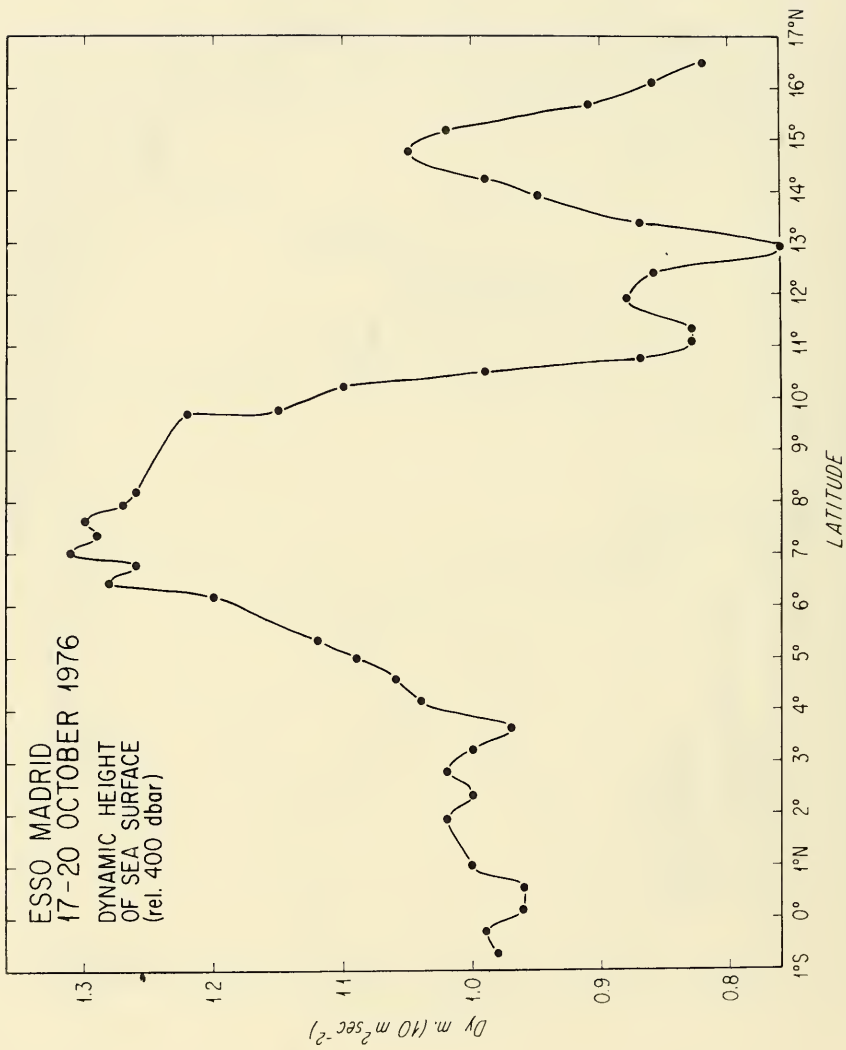


Figure 5. (cont.)

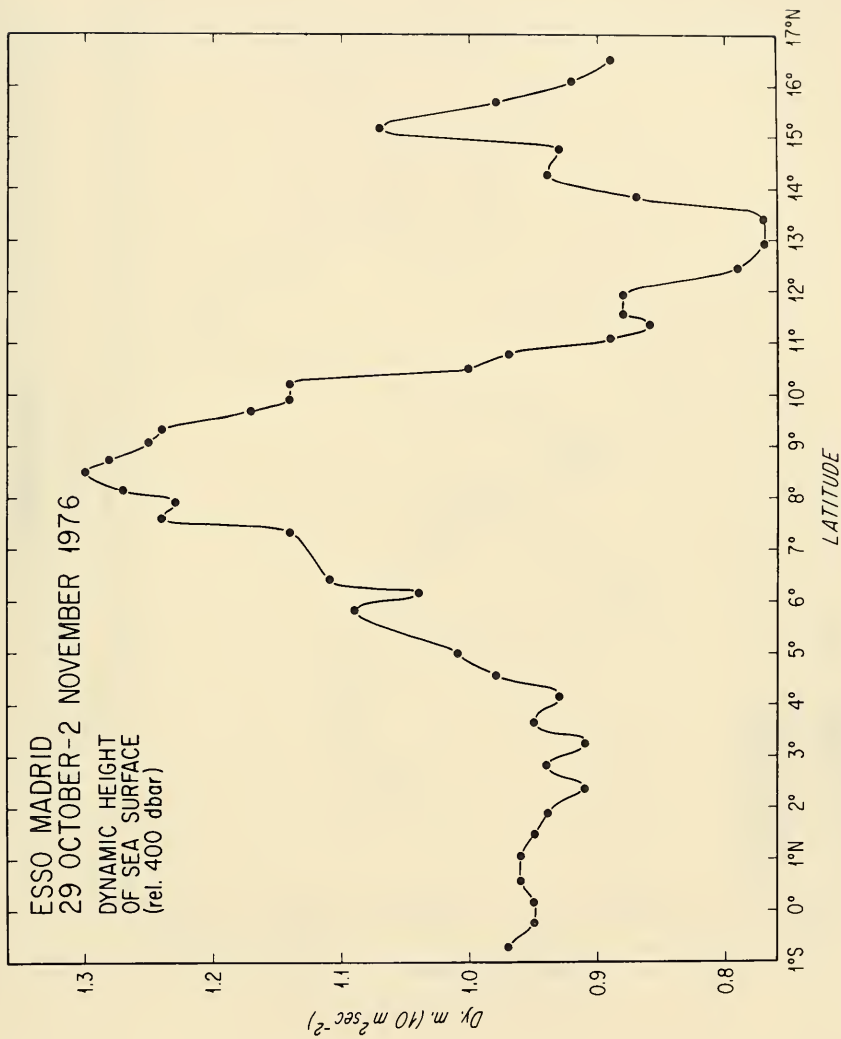


Figure 5. (cont.)

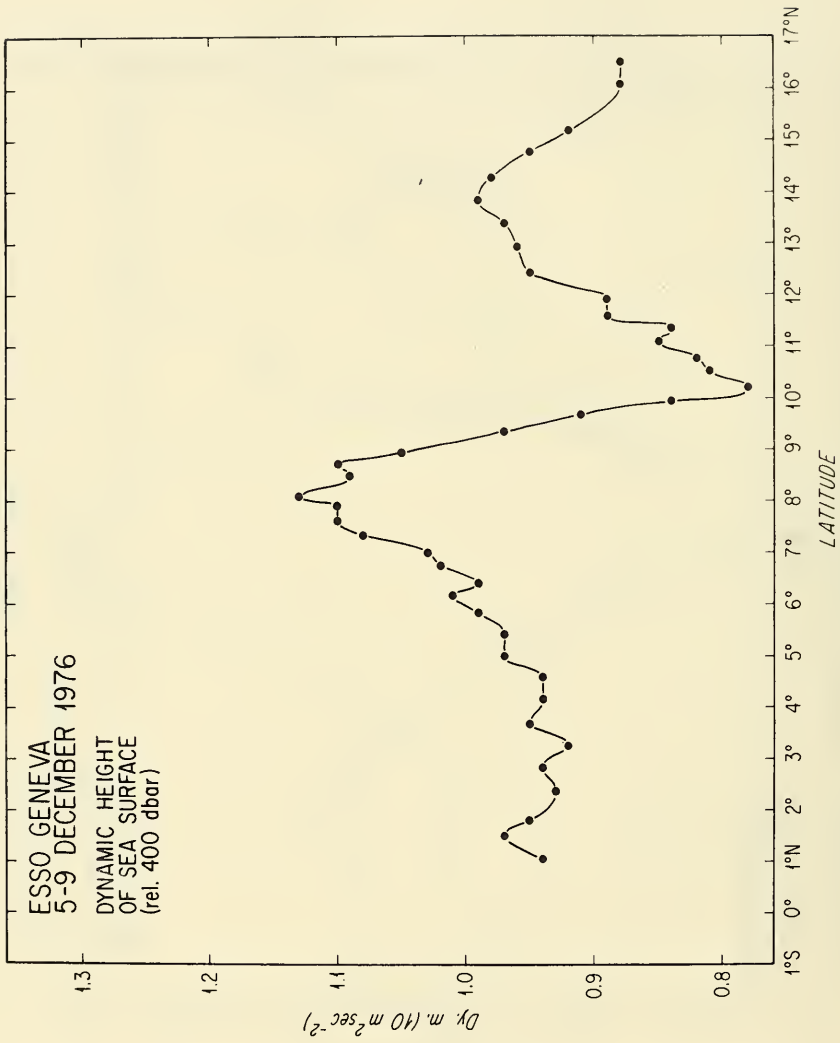


Figure 5. (cont.)

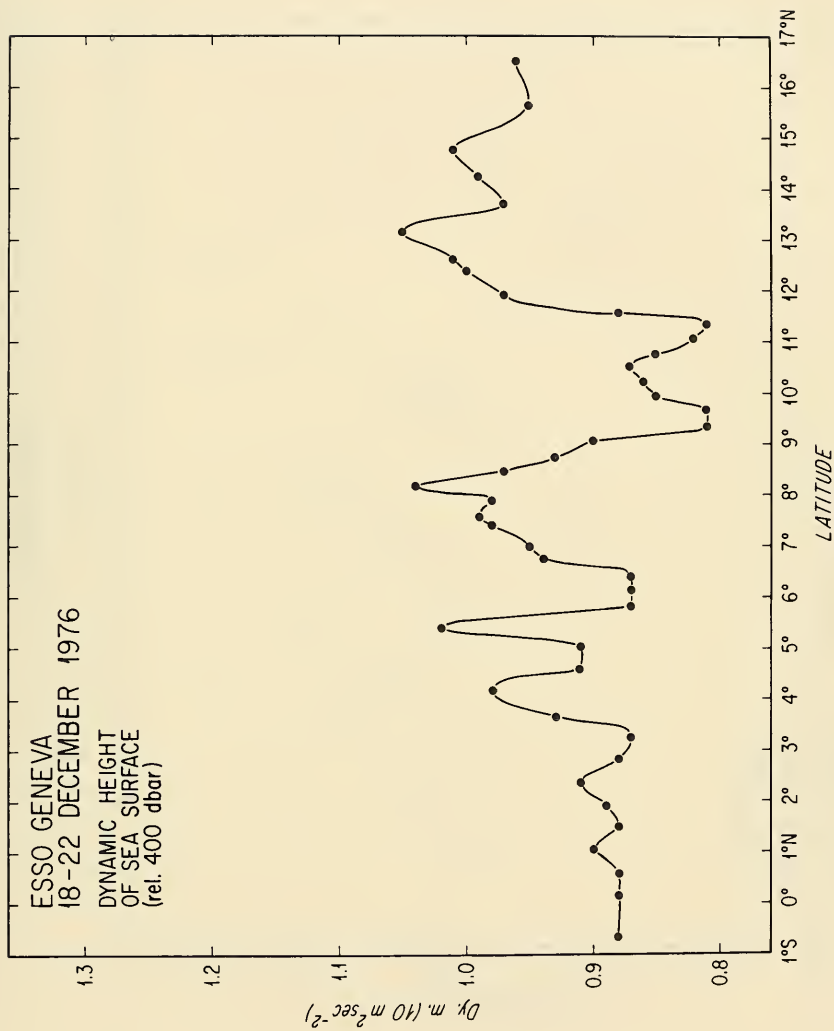


Figure 5. (cont.)

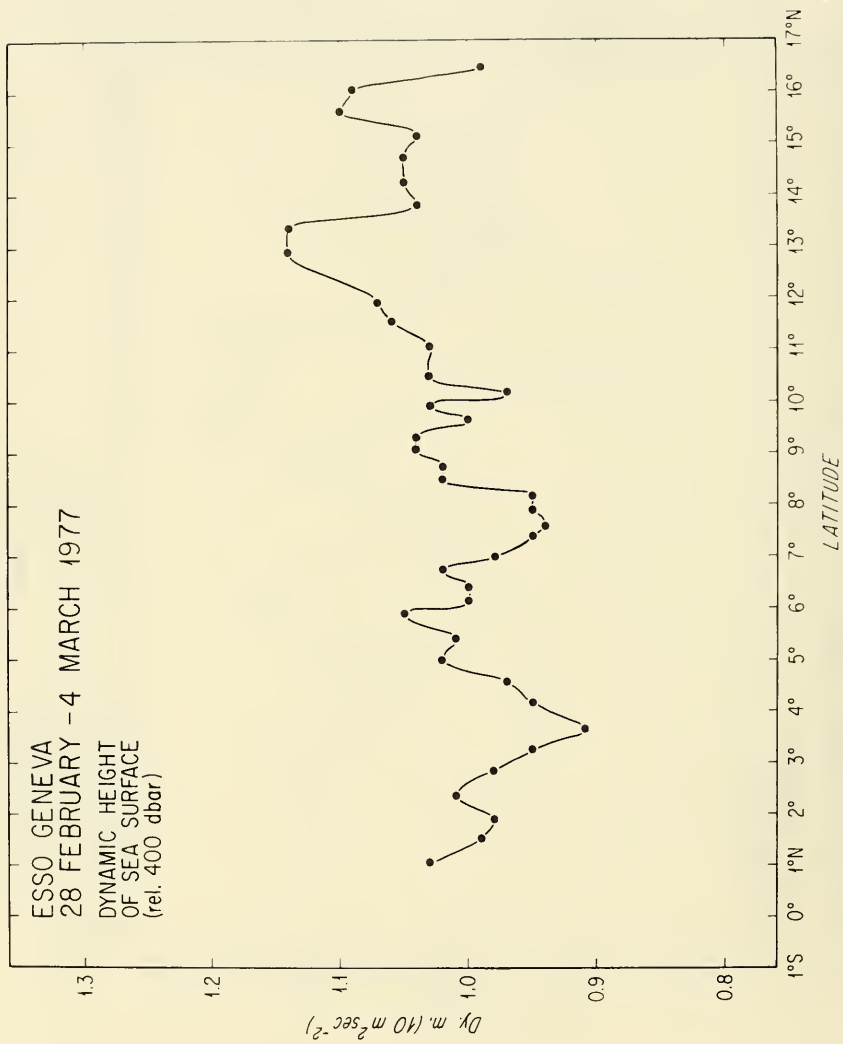


Figure 5. (cont.)

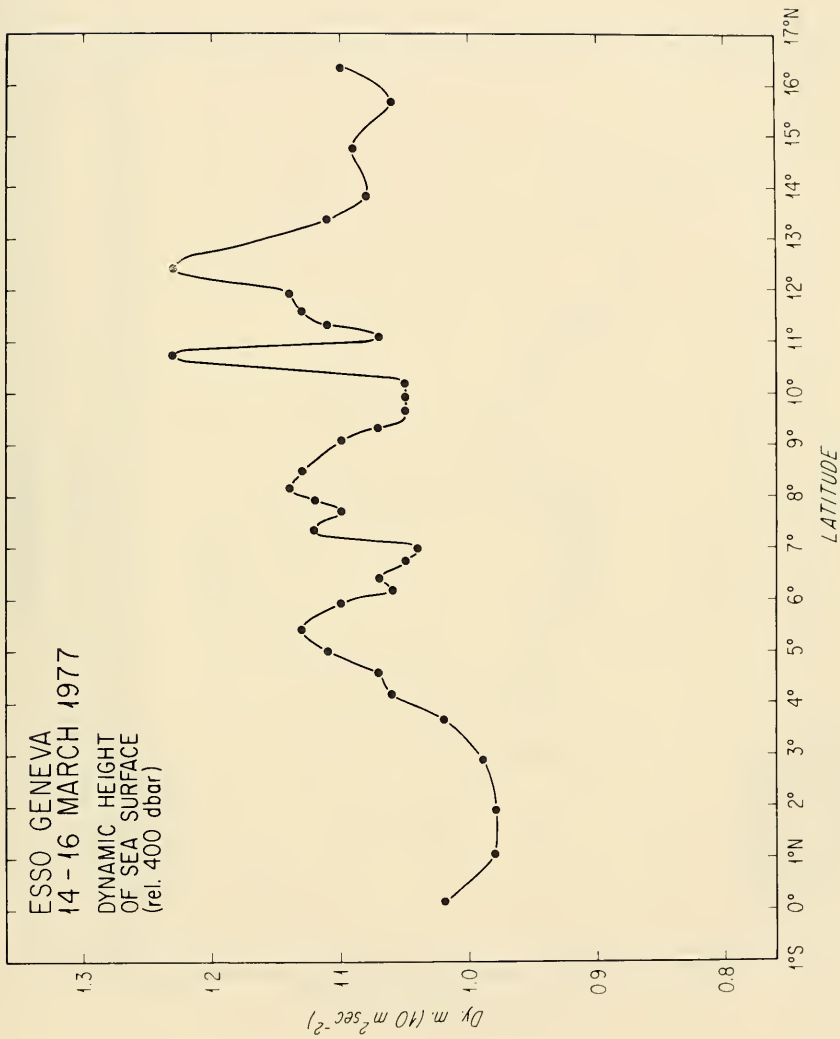


Figure 5. (cont.)

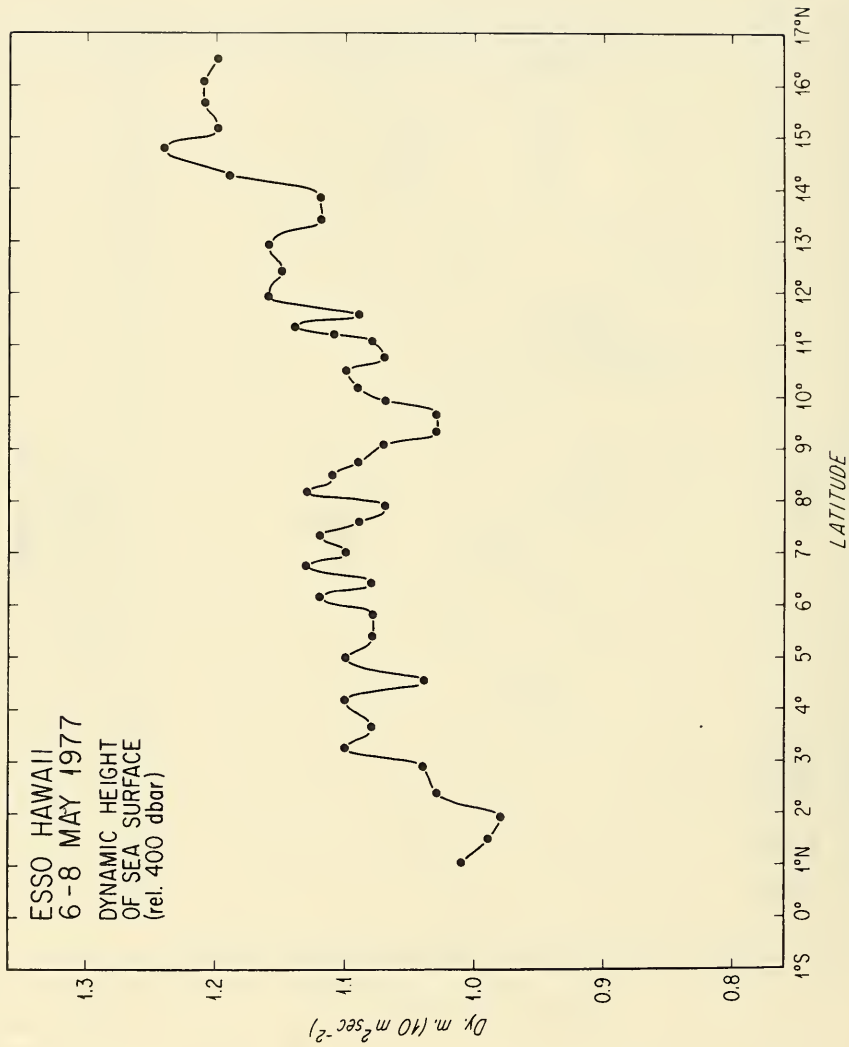


Figure 5. (cont.)

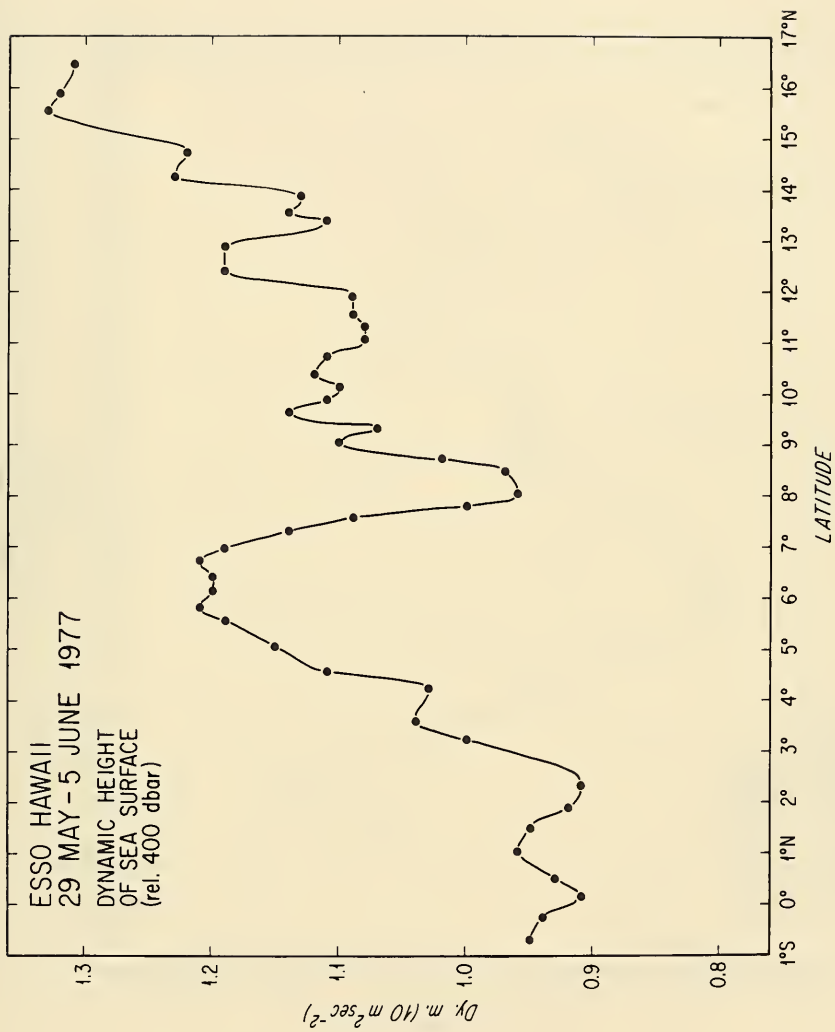


Figure 5. (cont.)

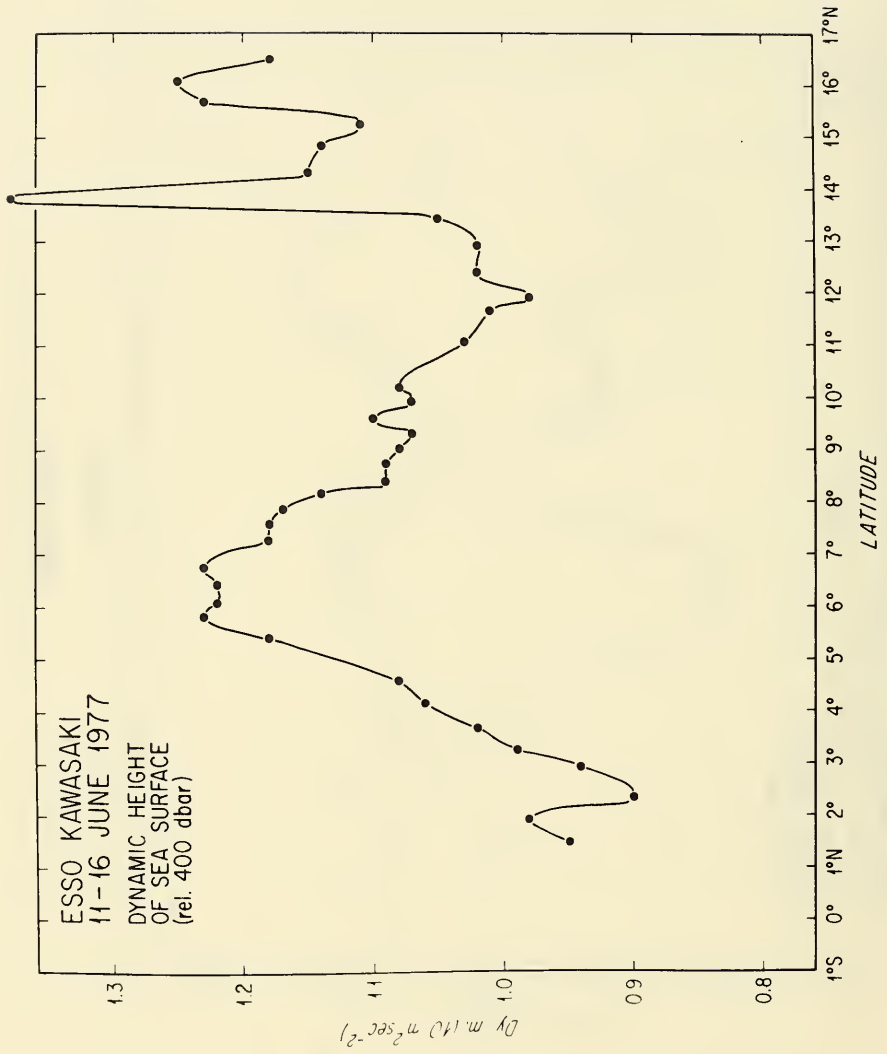


Figure 5. (cont.)

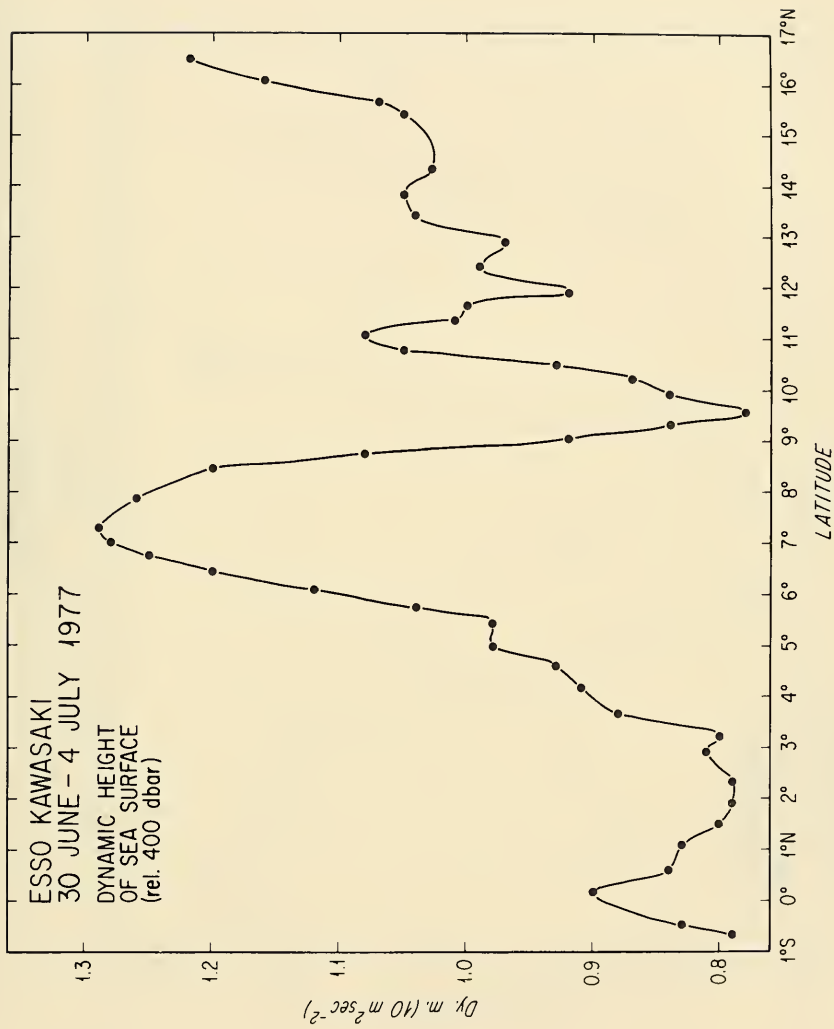


Figure 5. (cont.)

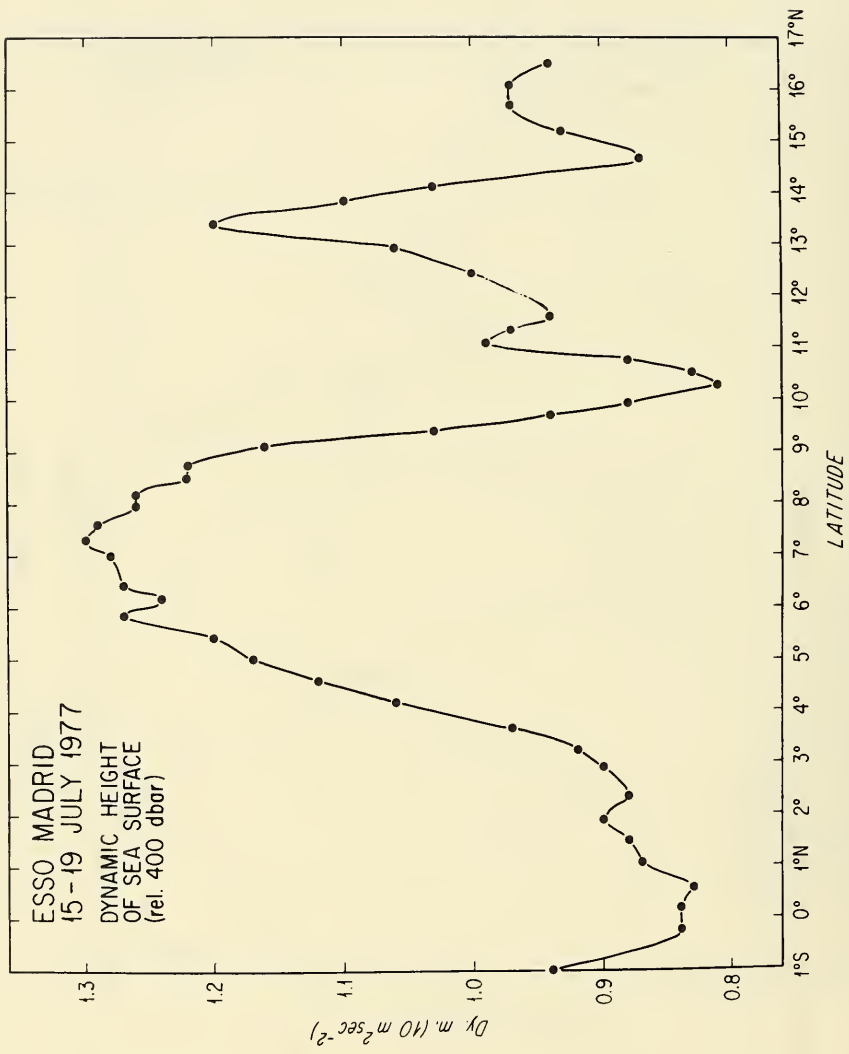


Figure 5. (cont.)

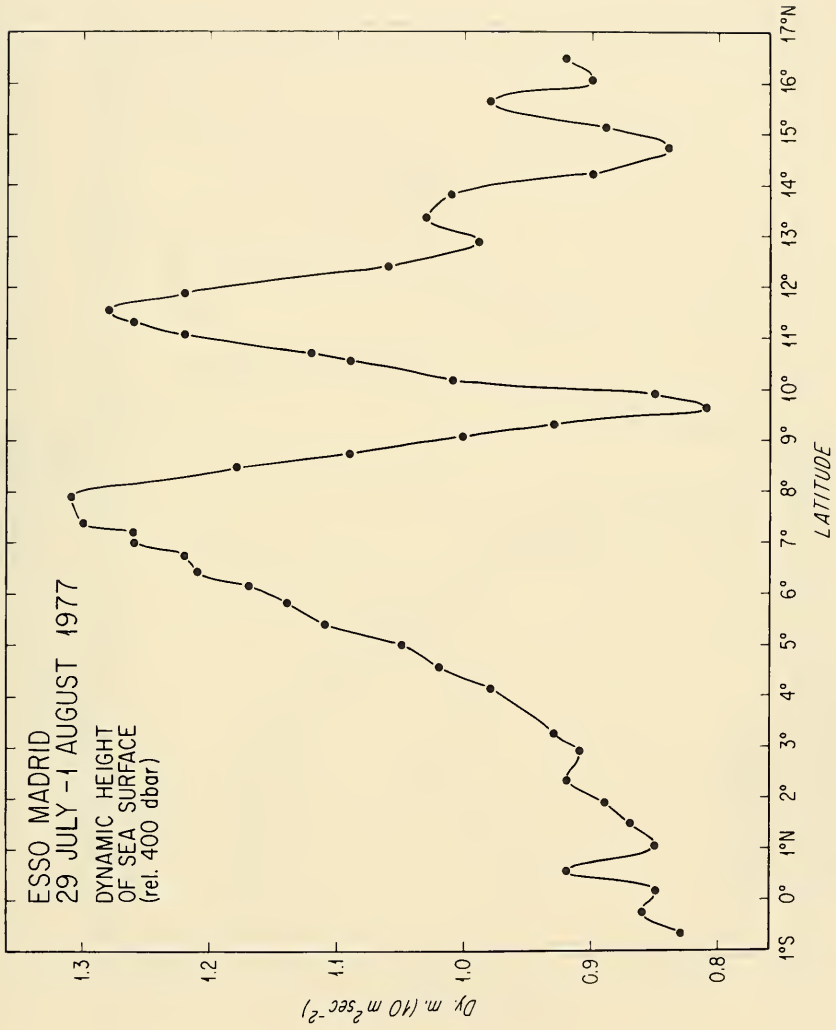


Figure 5. (cont.)

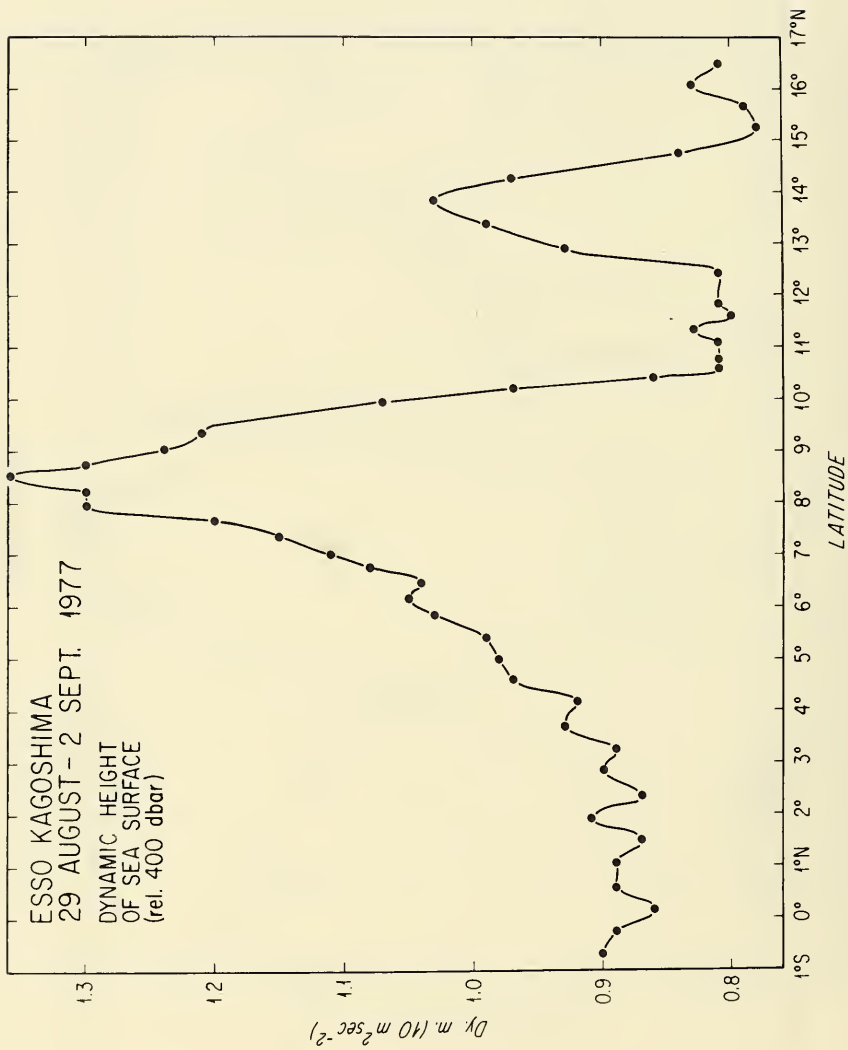


Figure 5. (cont.)

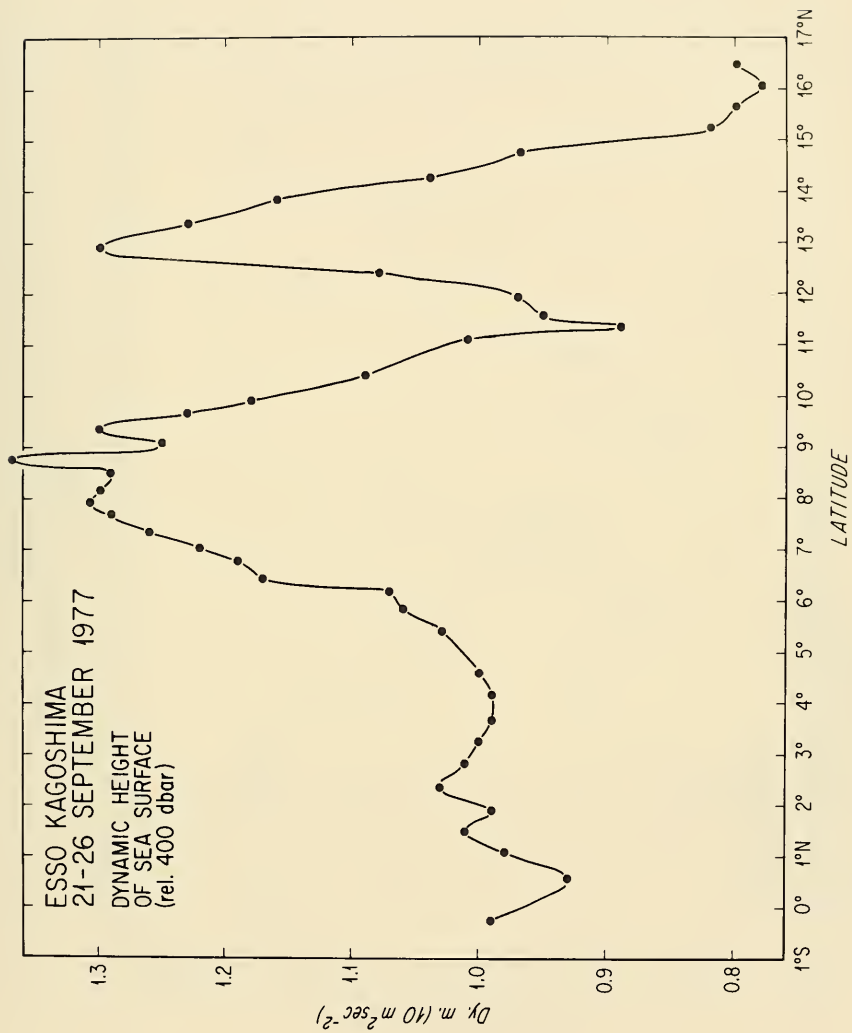


Figure 5. (cont.)

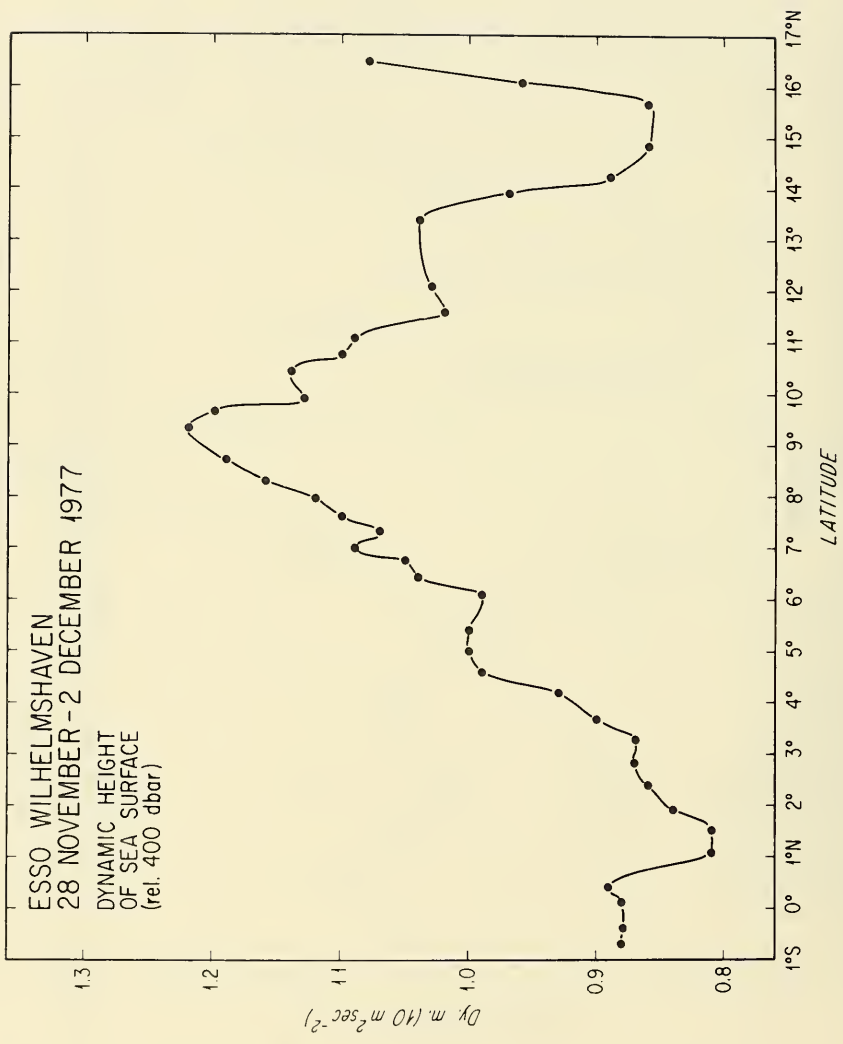


Figure 5. (cont.)

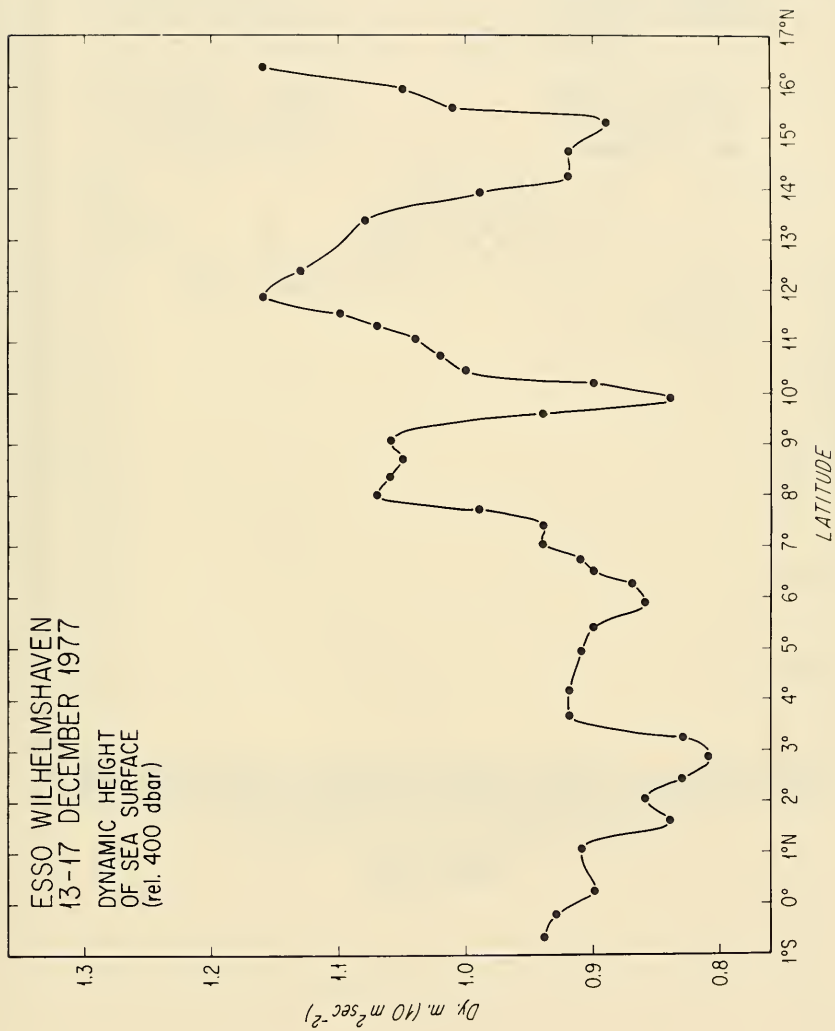


Figure 5. (cont.)

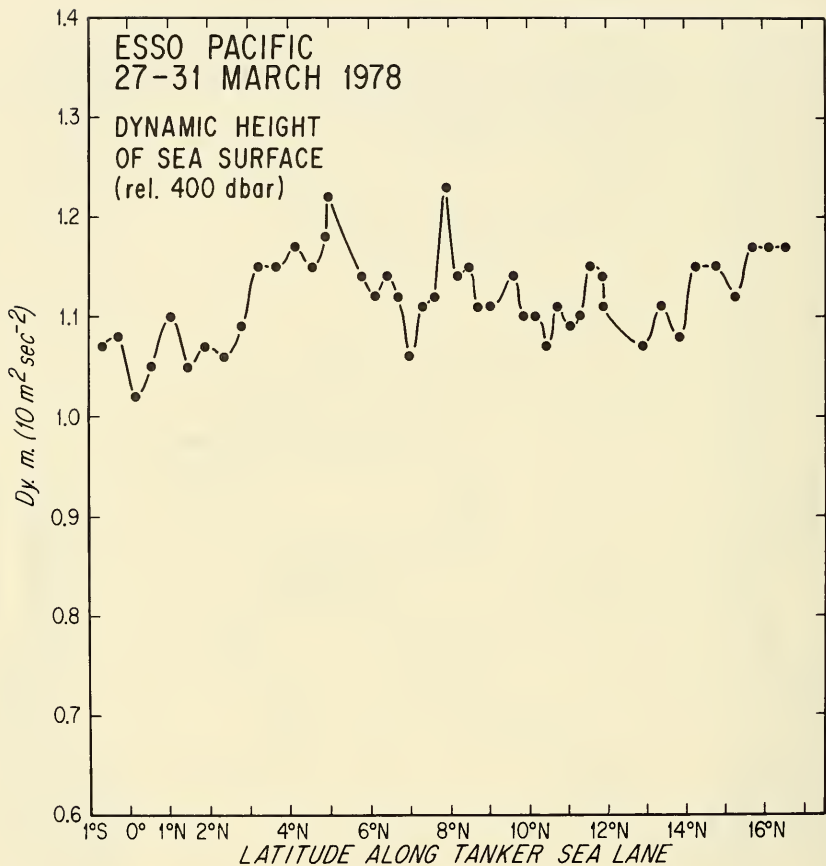


Figure 5. (cont.)

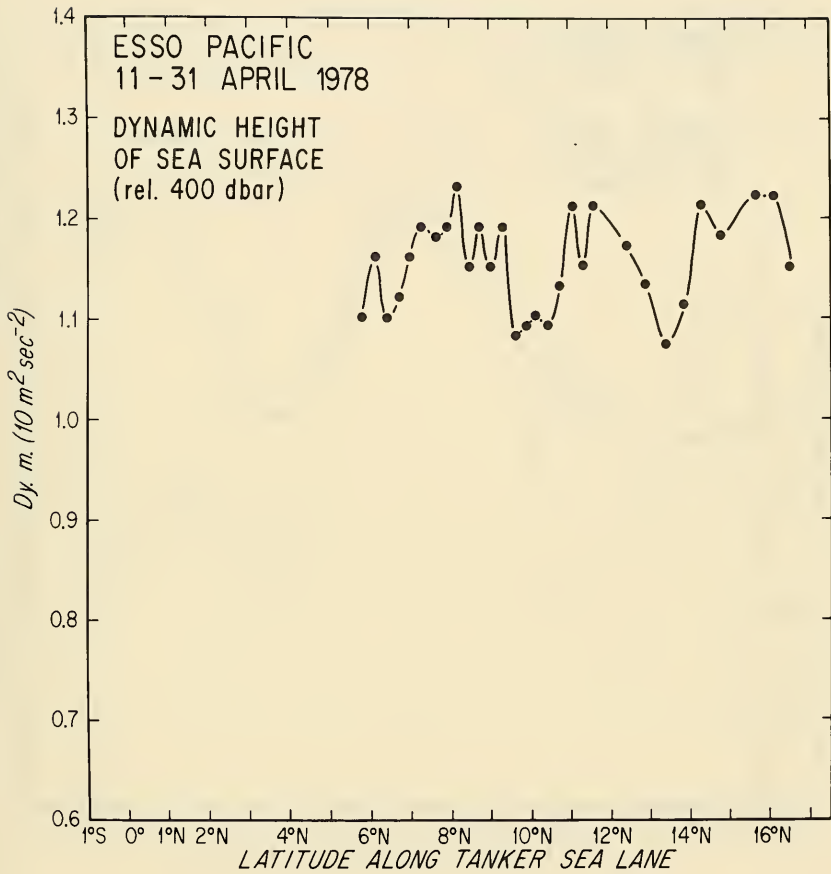


Figure 5. (cont.)

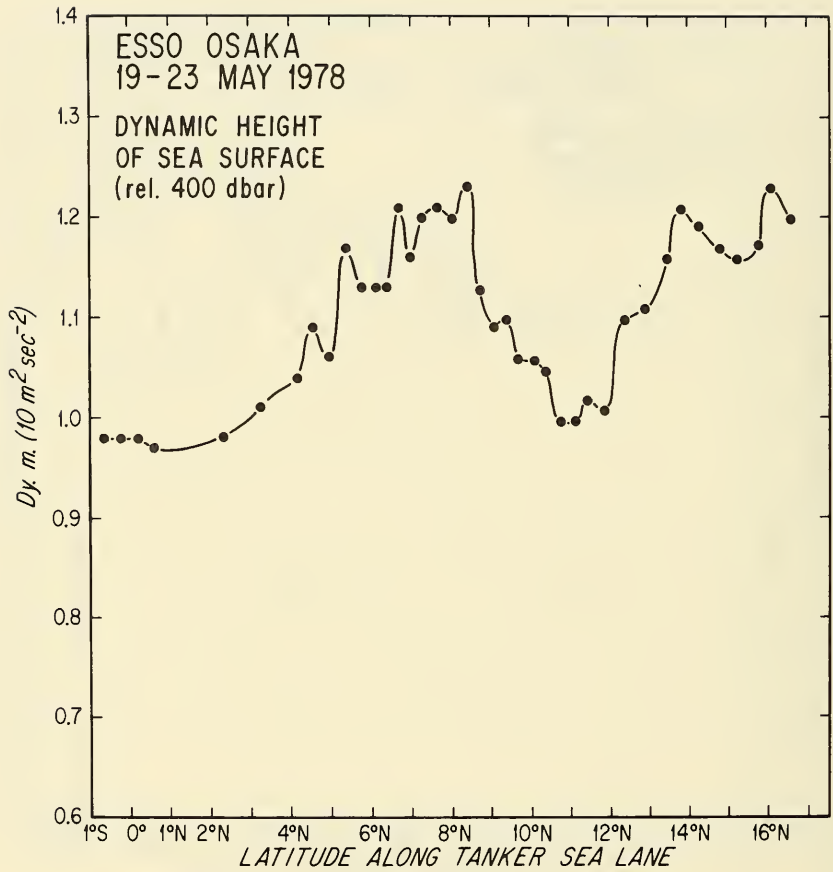


Figure 5. (cont.)

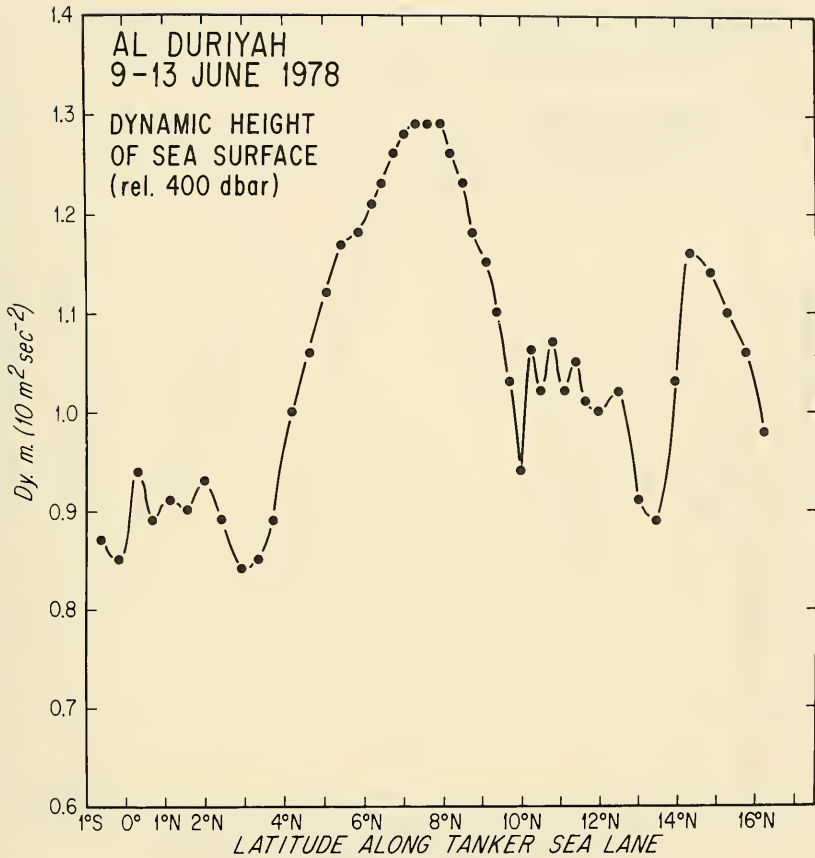


Figure 5. (cont.)

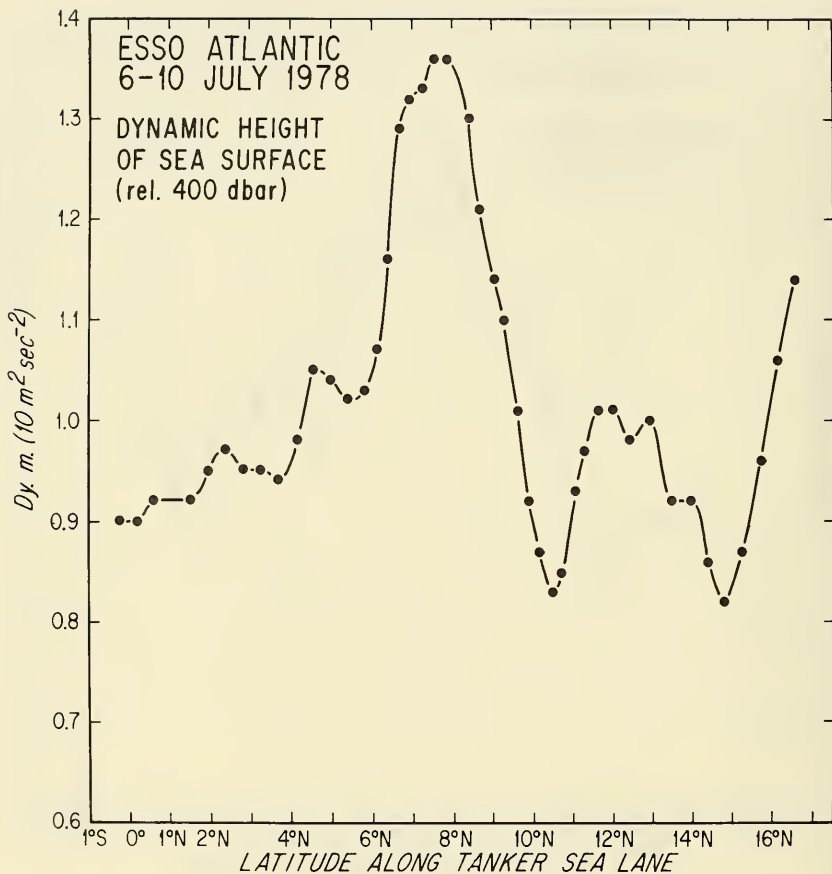


Figure 5. (cont.)

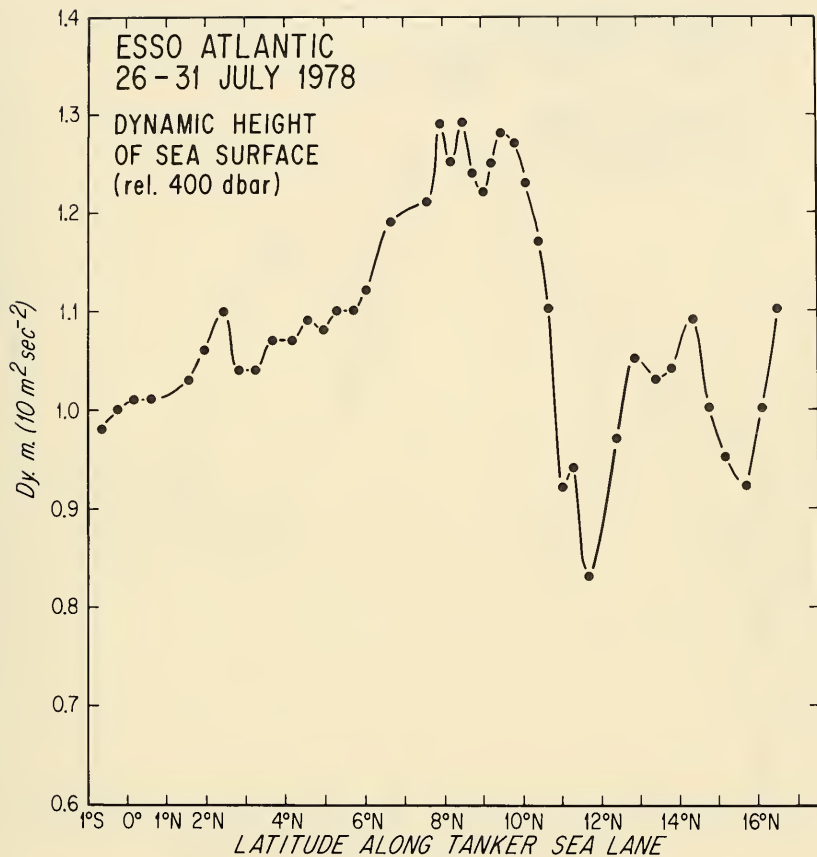


Figure 5. (cont.)

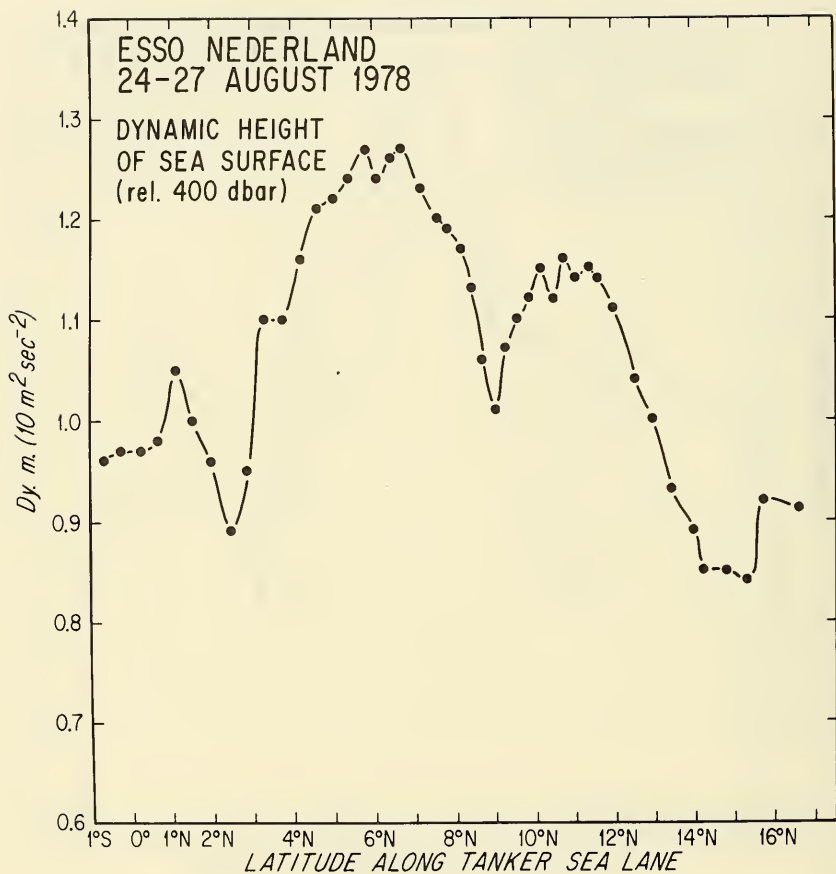


Figure 5. (cont.)

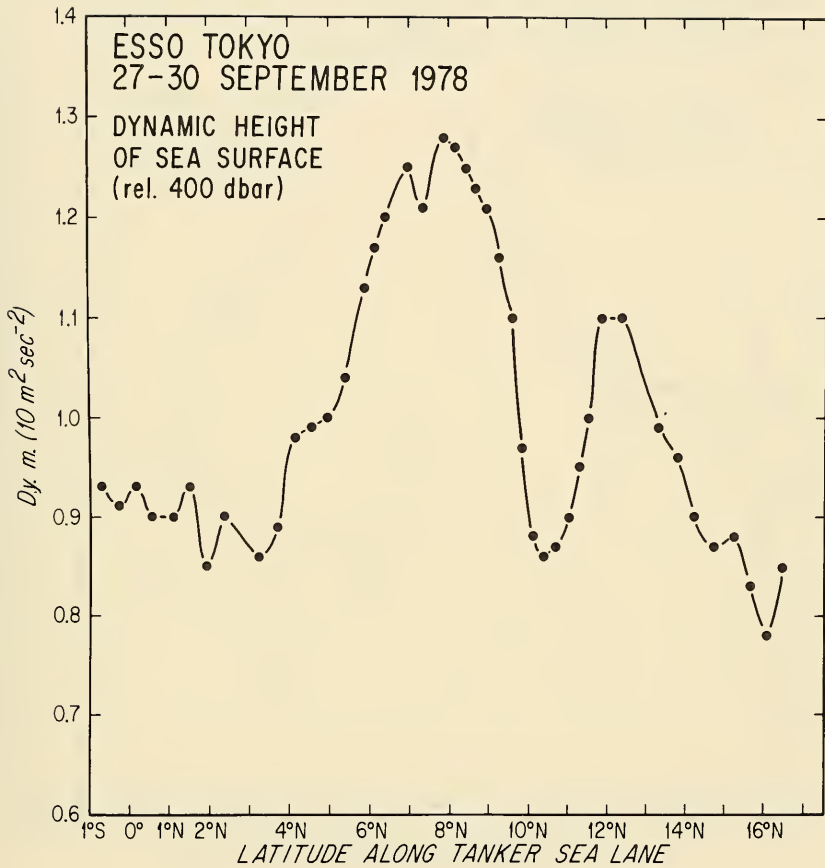


Figure 5. (cont.)

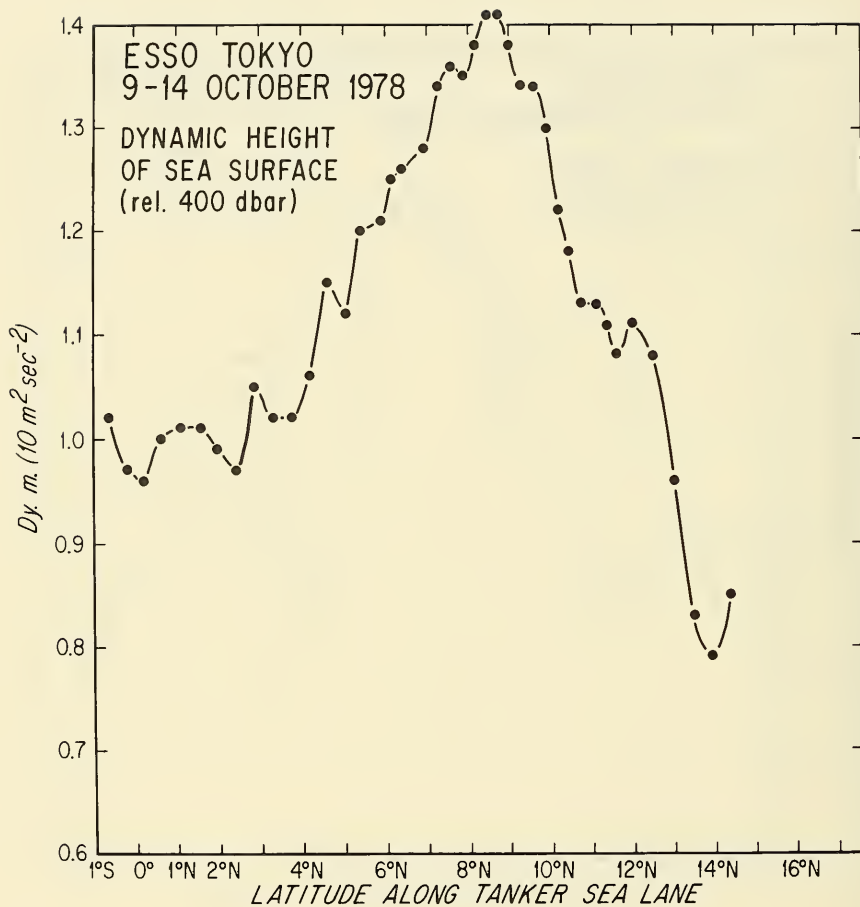


Figure 5. (cont.)

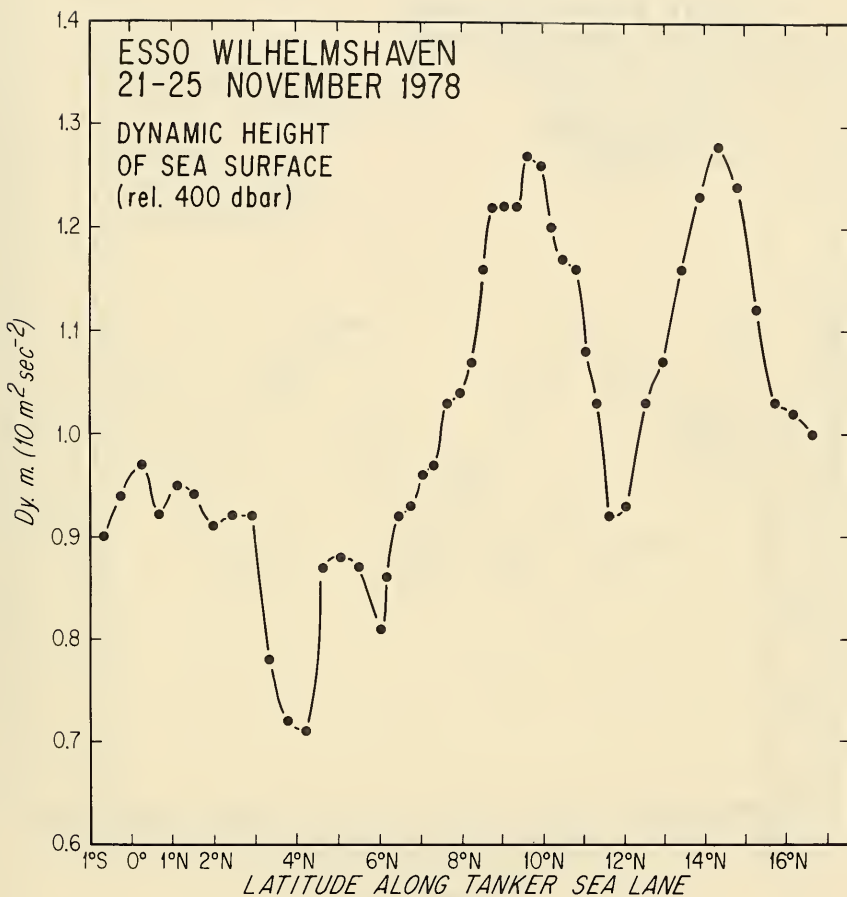


Figure 5. (cont.)

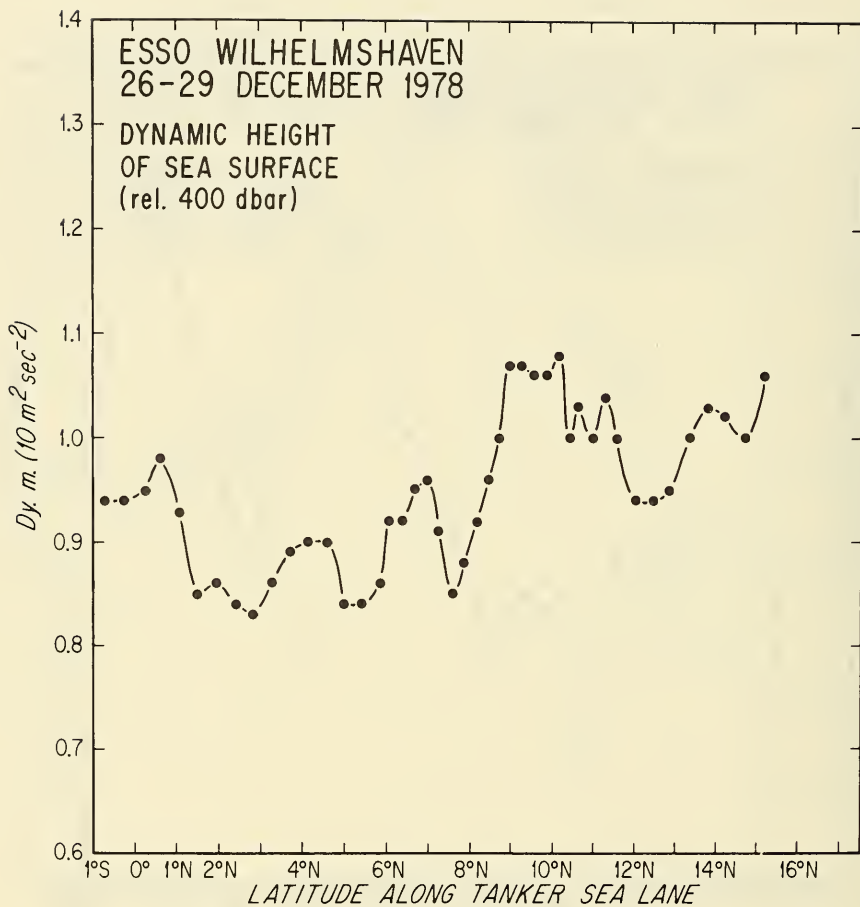


Figure 5. (cont.)

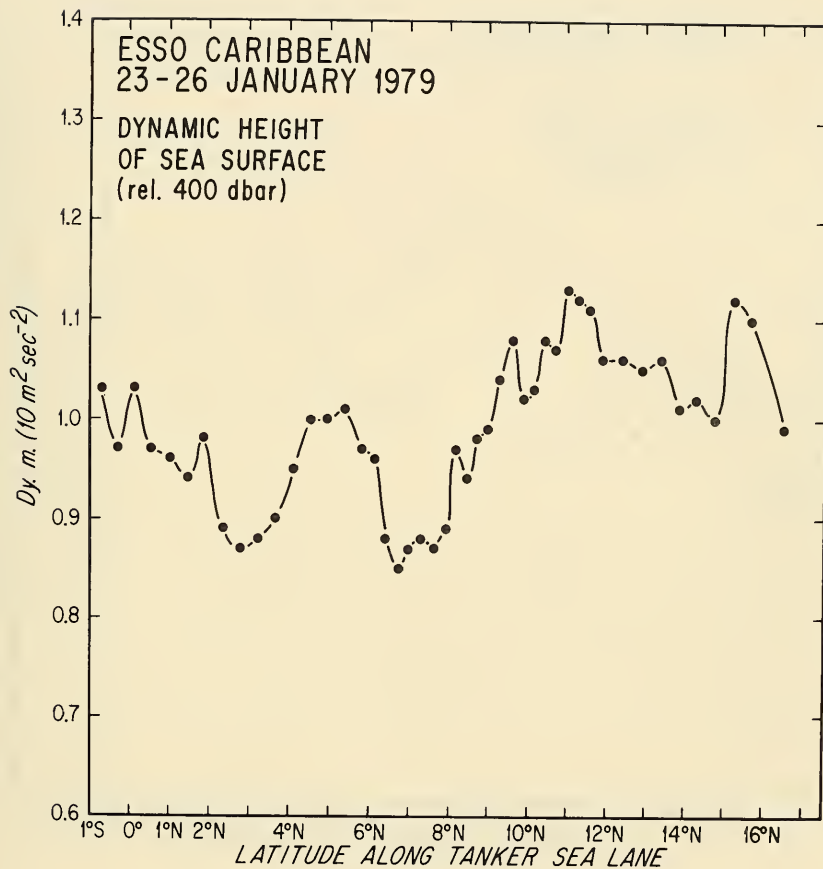


Figure 5. (cont.)

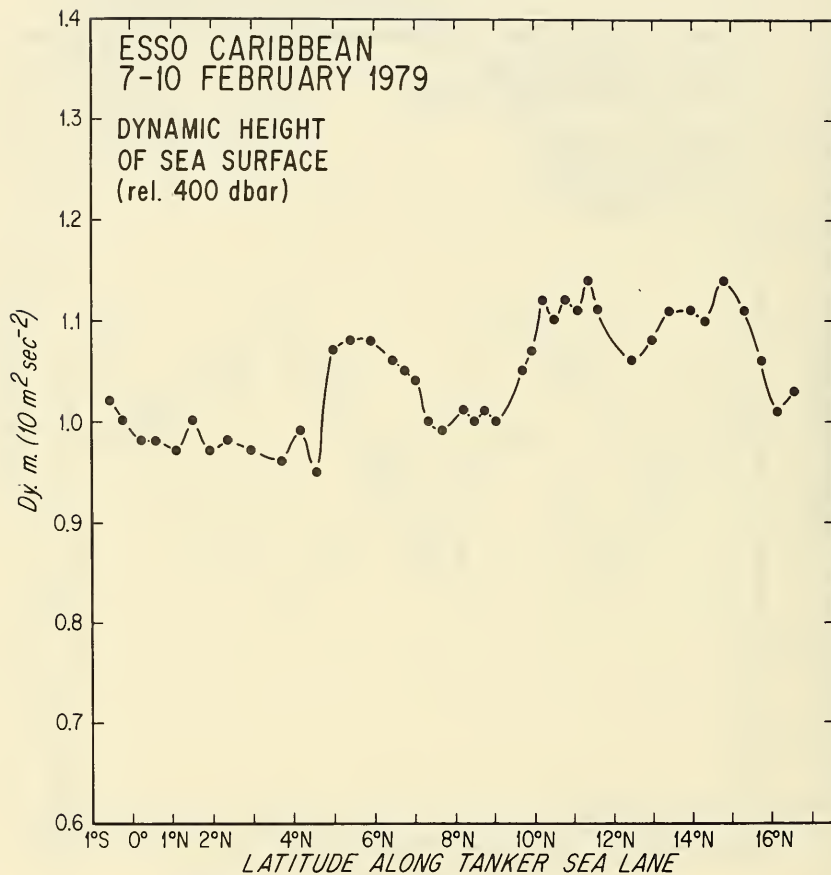


Figure 5. (cont.)

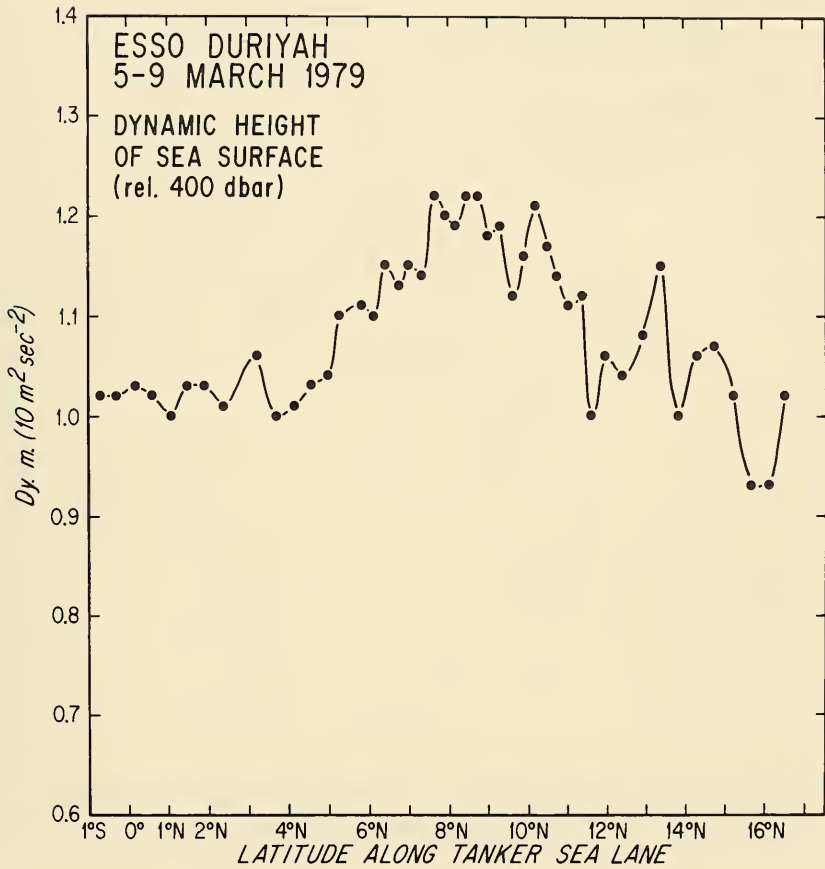


Figure 5. (cont.)

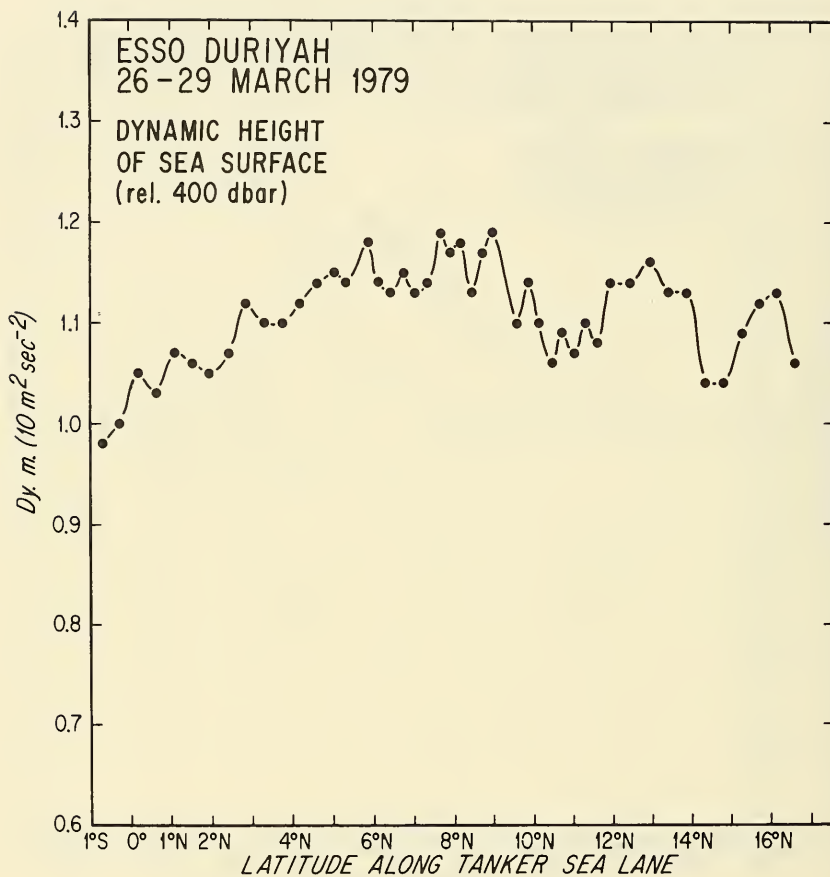


Figure 5. (cont.)

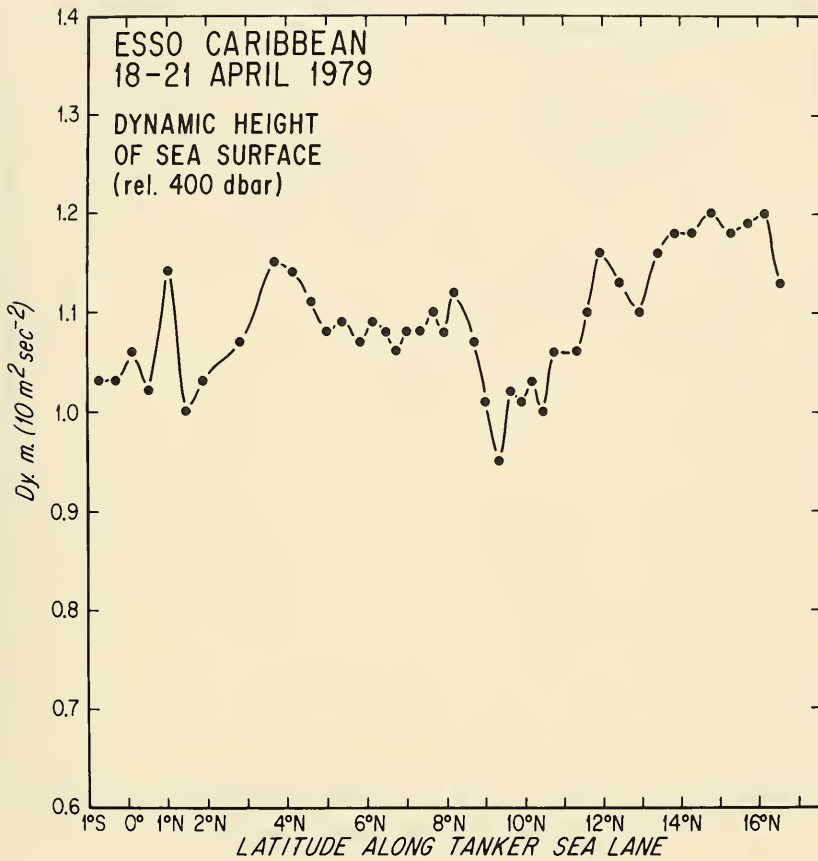


Figure 5. (cont.)

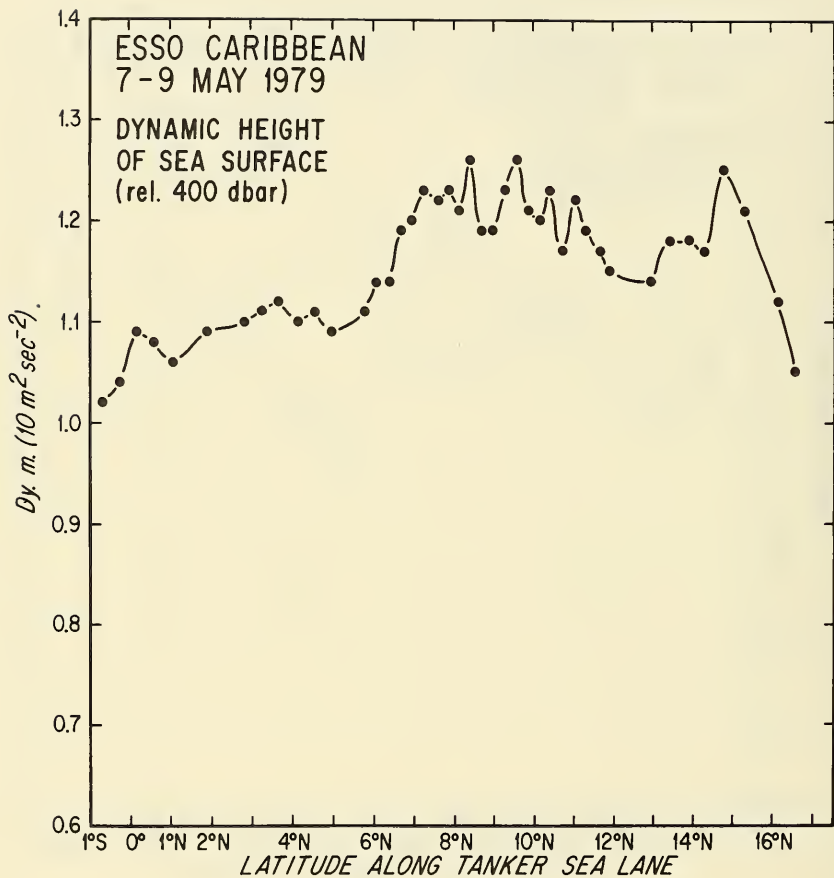


Figure 5. (cont.)

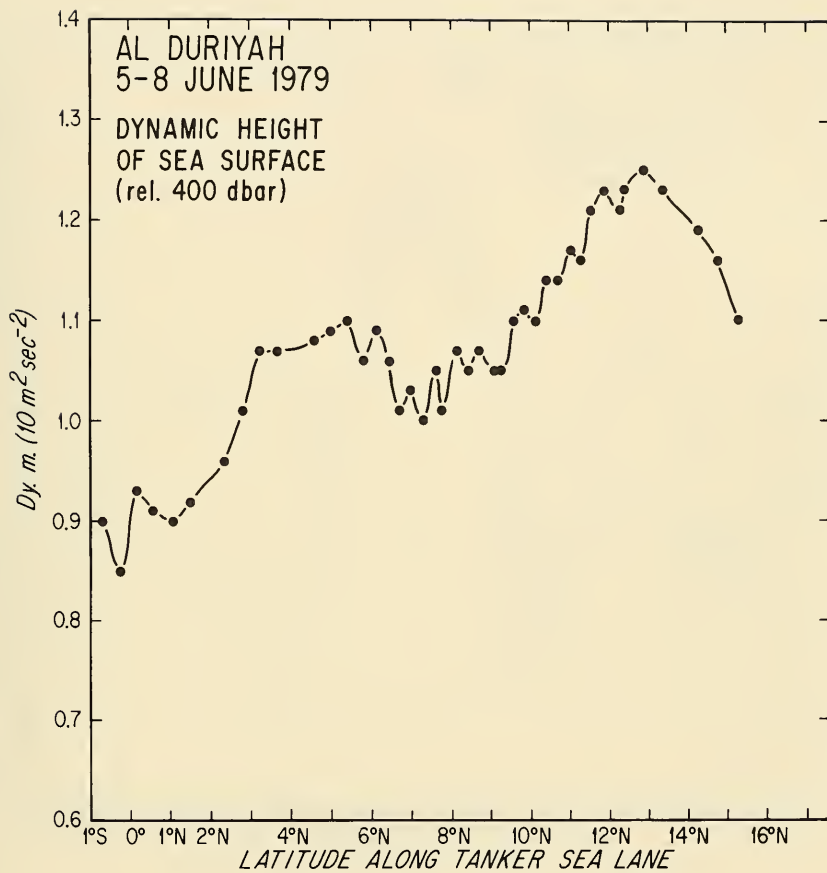


Figure 5. (cont.)

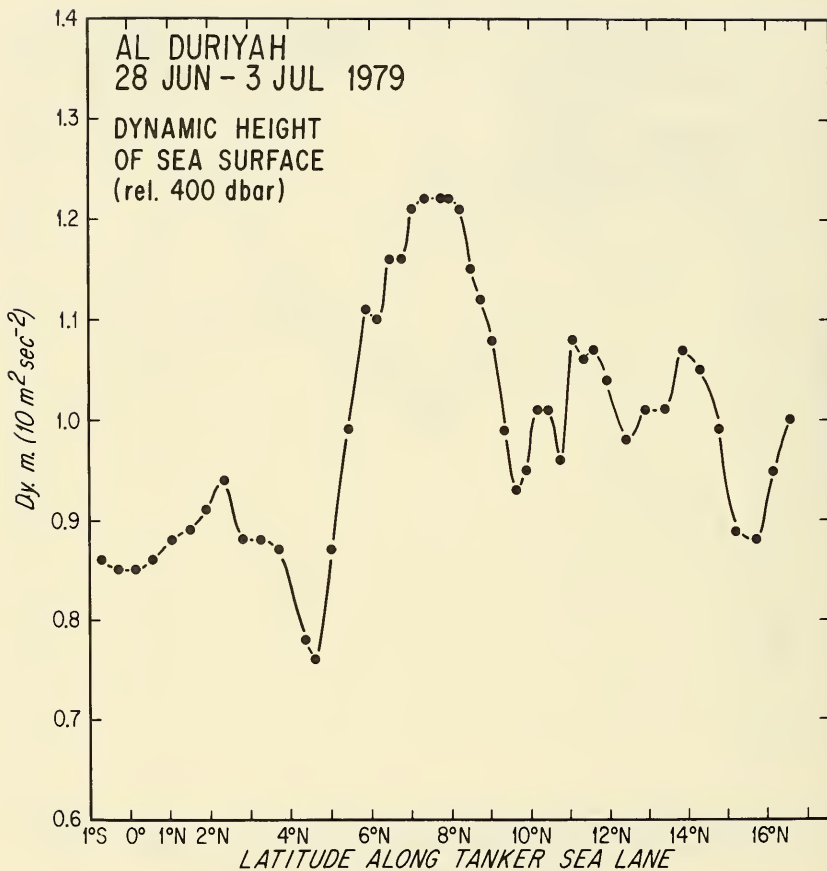


Figure 5. (cont.)

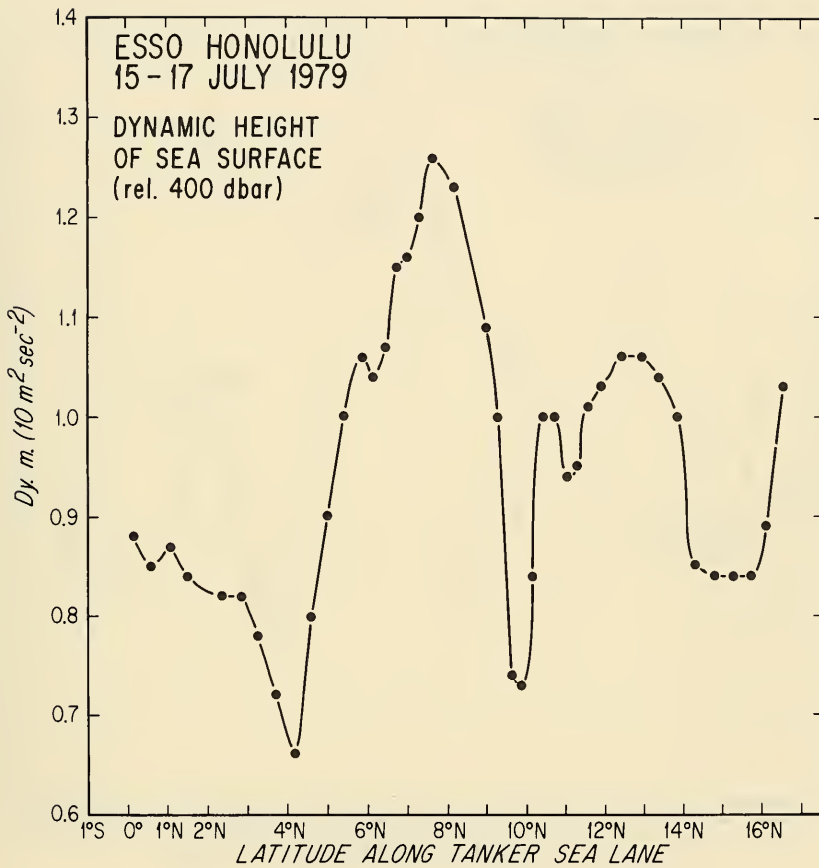


Figure 5. (cont.)

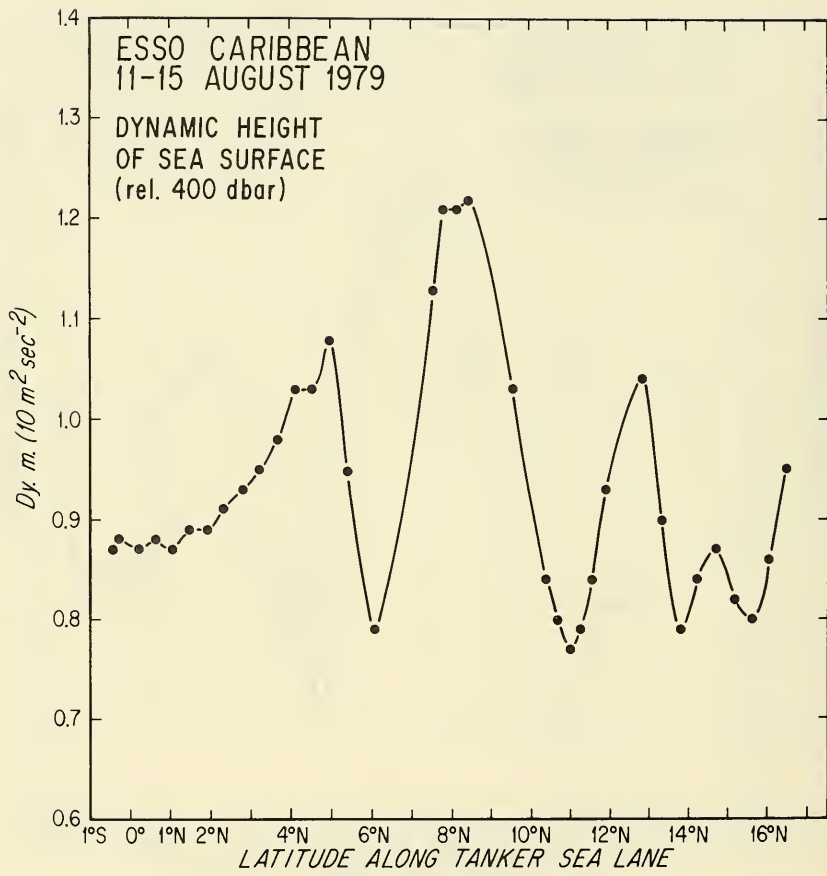


Figure 5. (cont.)

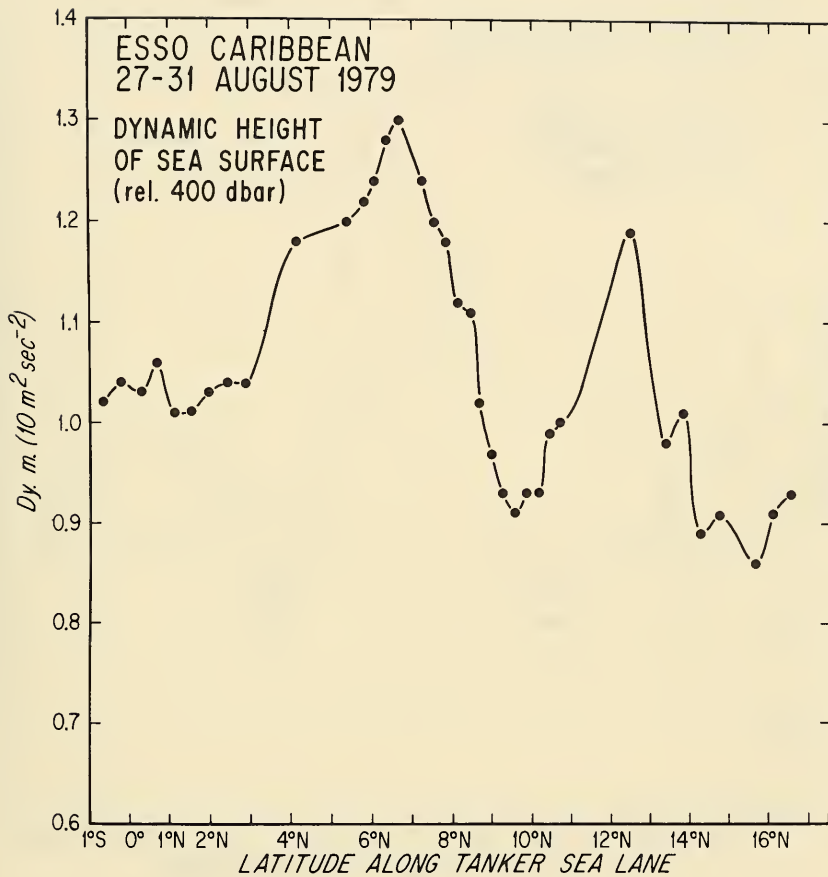


Figure 5. (cont.)

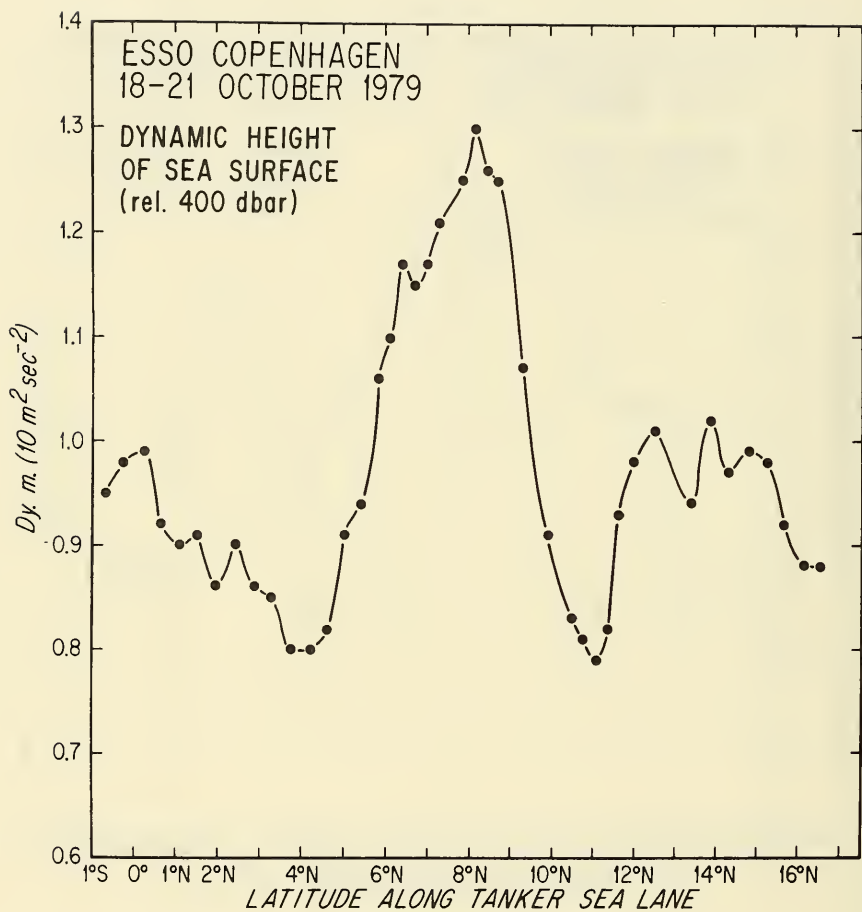


Figure 5. (cont.)

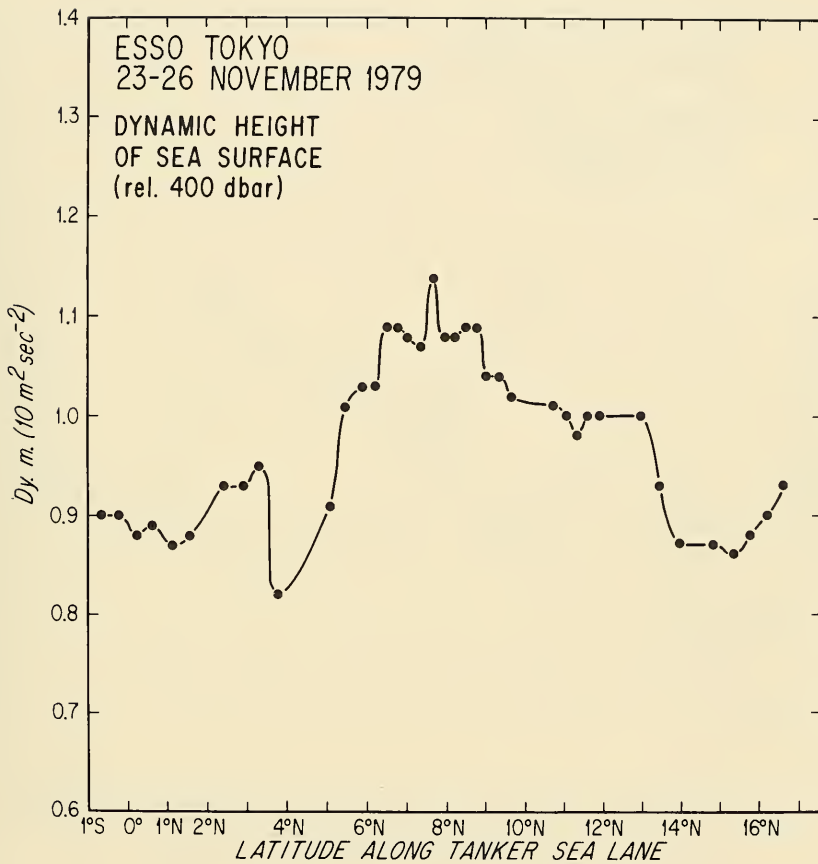


Figure 5. (cont.)

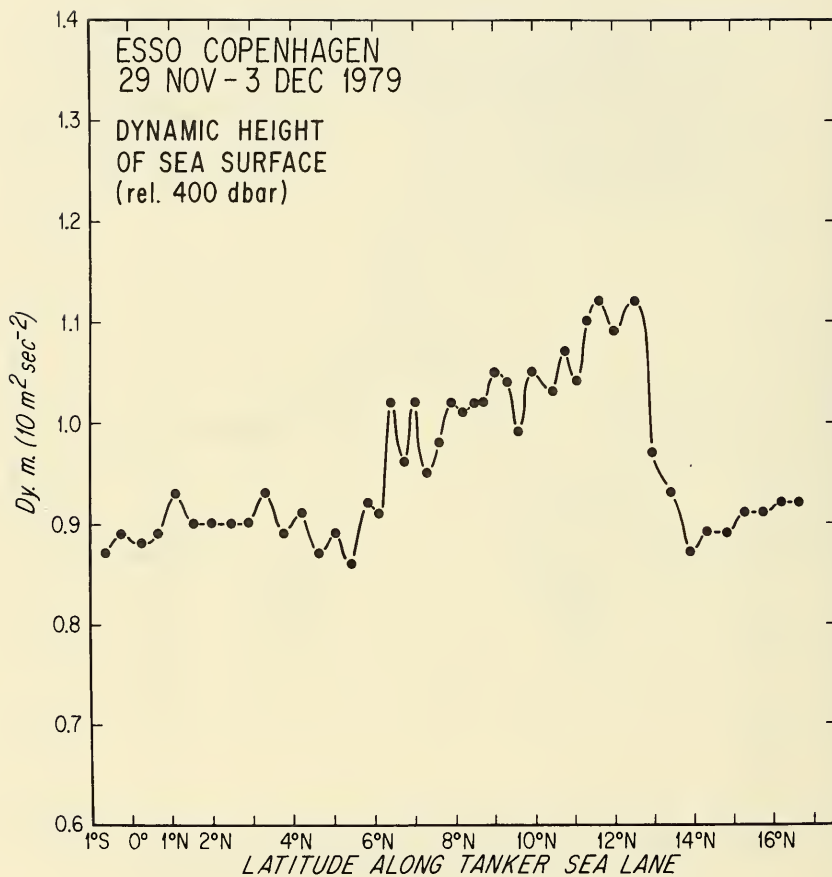


Figure 5. (cont.)

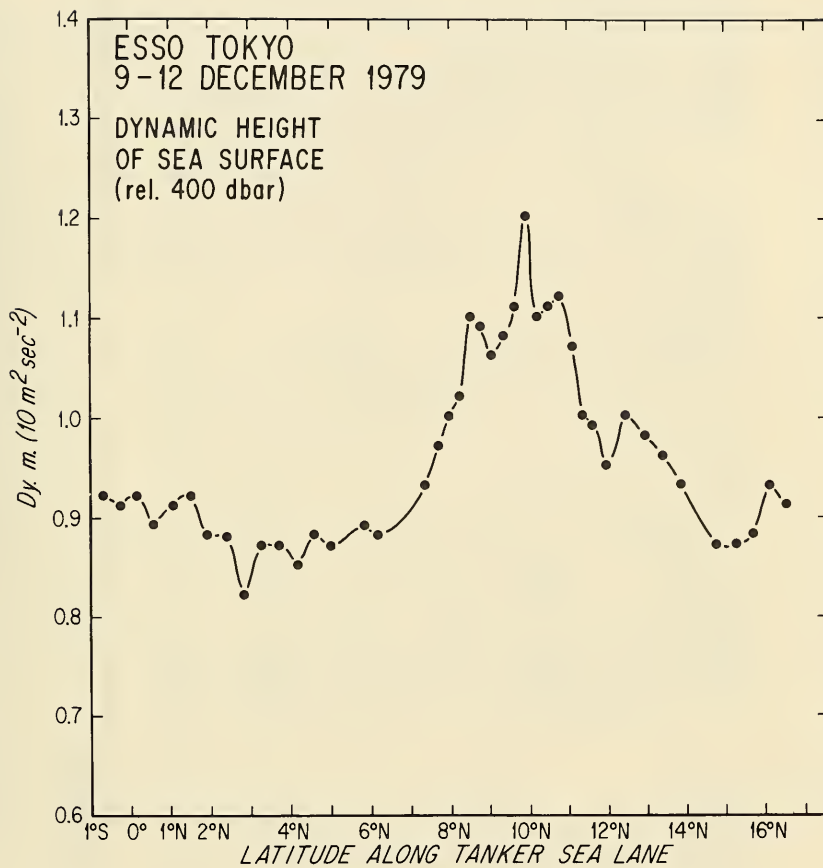


Figure 5. (cont.)

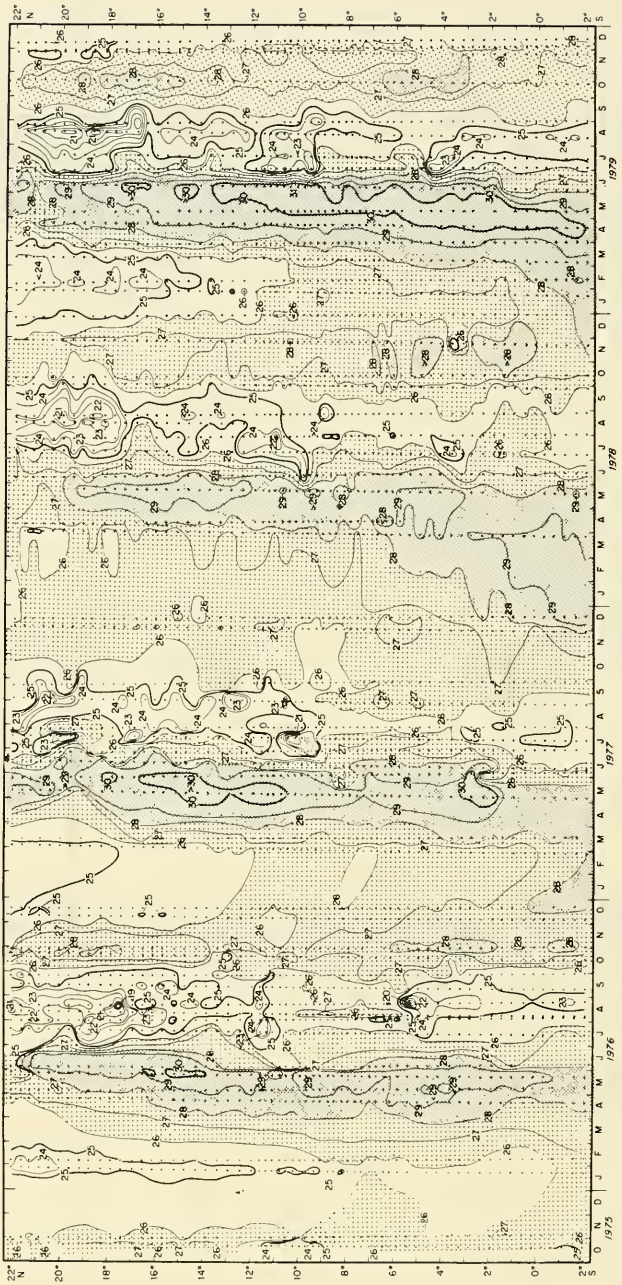


Figure 6. Surface temperature ($^{\circ}\text{C}$) from XBT sections along tanker sea lane (Figure 1a) 2°S to 22°N off Somali and Arabian coasts, October 1975 to December 1979.

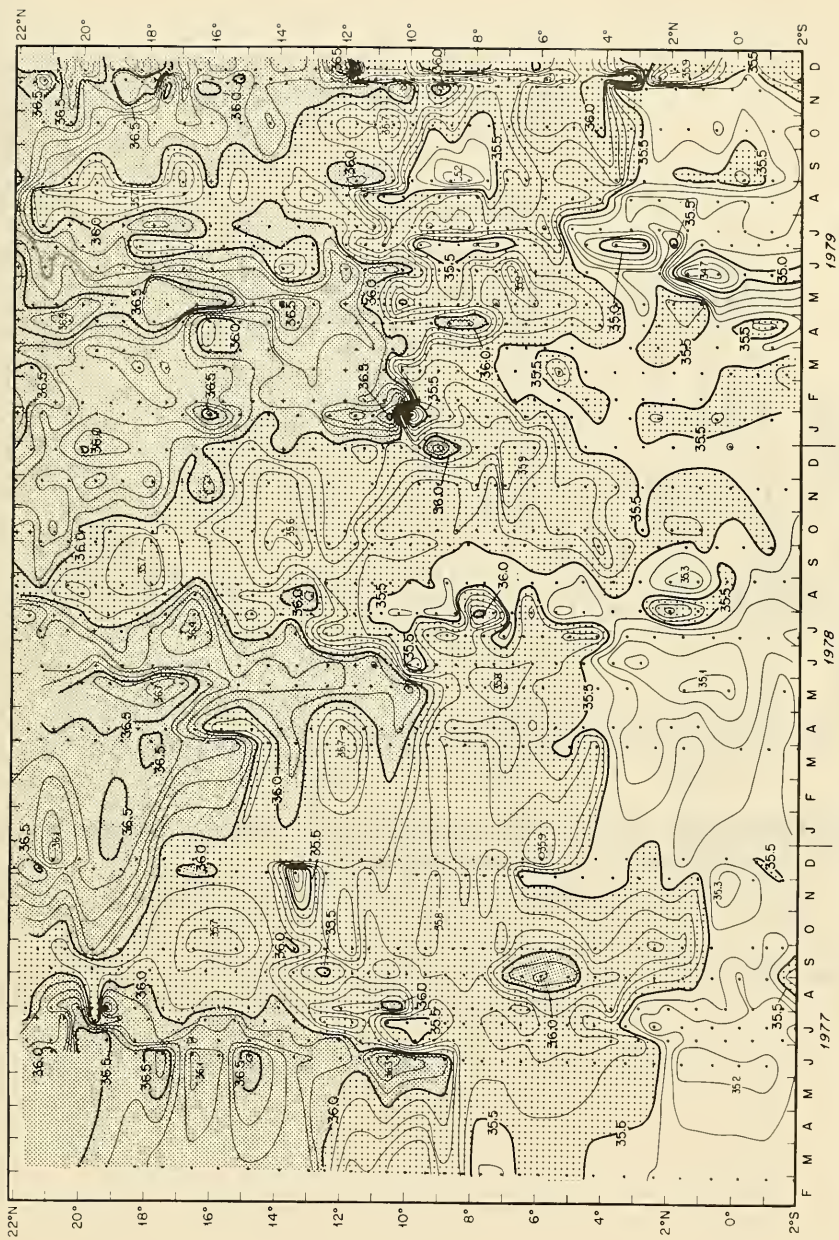


Figure 7. Surface salinity (‰) contemporaneous with XBT sections along tanker sea lane (Figure 1a) 2°S to 22°N off Somali and Arabian coasts, February 1977 to December 1979.

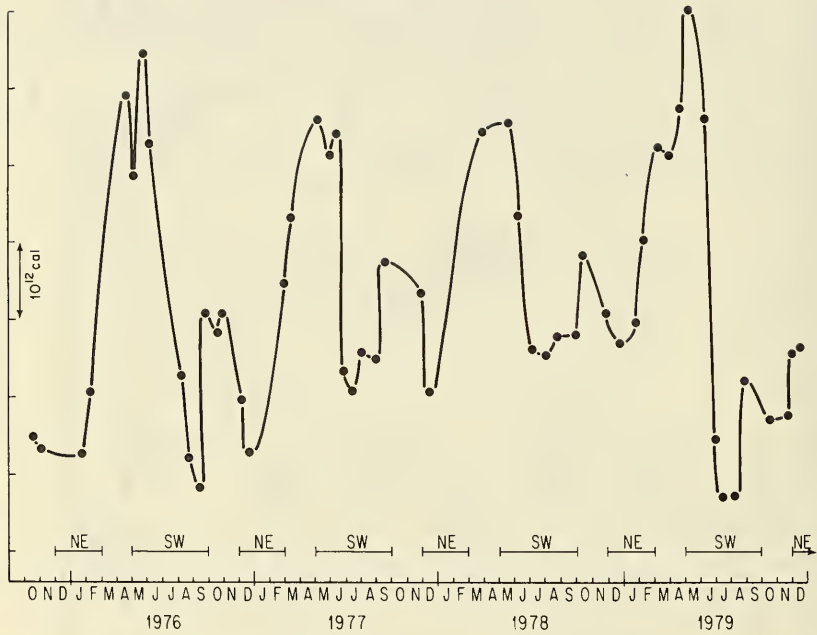


Figure 8. Heat content (cal) for 0 - 100 m layer between 2°N to 12°N from XBT temperature sections (Figure 2) along tanker sea lane (Figure 1a).

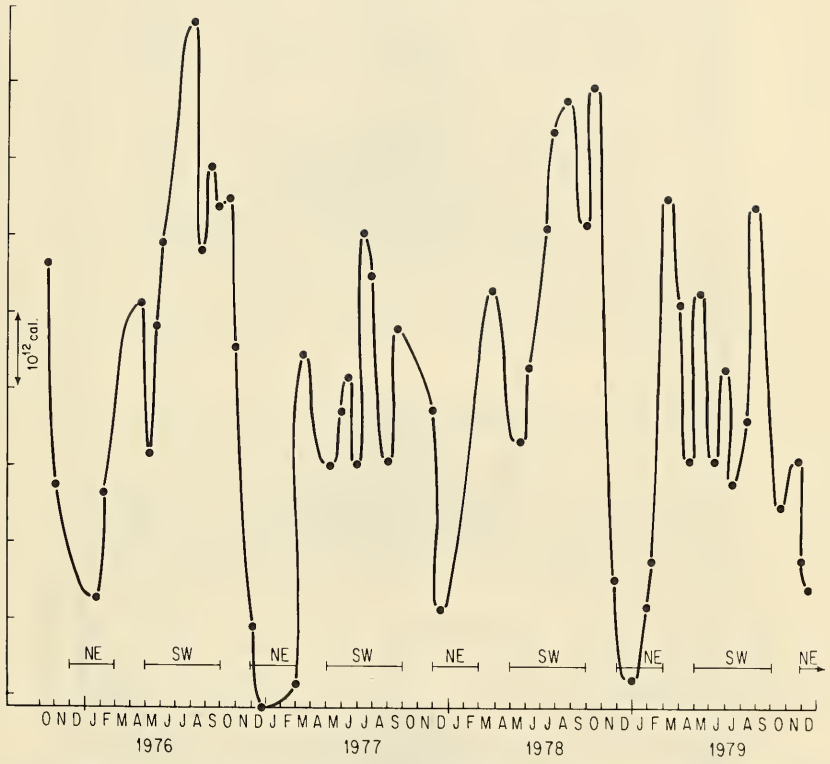


Figure 9. Heat content (cal) for 100 - 200 m layer between 2°N to 12°N from XBT temperature sections (Figure 2) along tanker sea lane (Figure 1a).

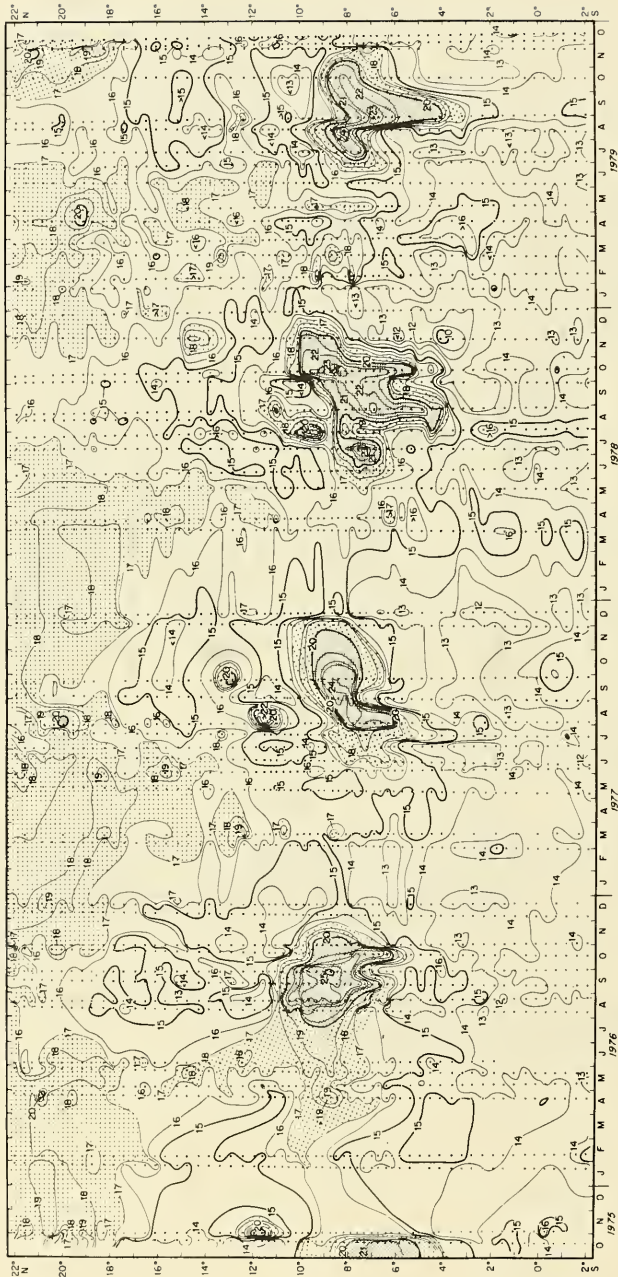


Figure 10. Temperature ($^{\circ}\text{C}$) at 200 m depth from XBT sections along tanker sea lane (Figure 1a) 2 $^{\circ}\text{S}$ to 22 $^{\circ}\text{N}$ off Somali and Arabian coasts, October 1975 to December 1979.

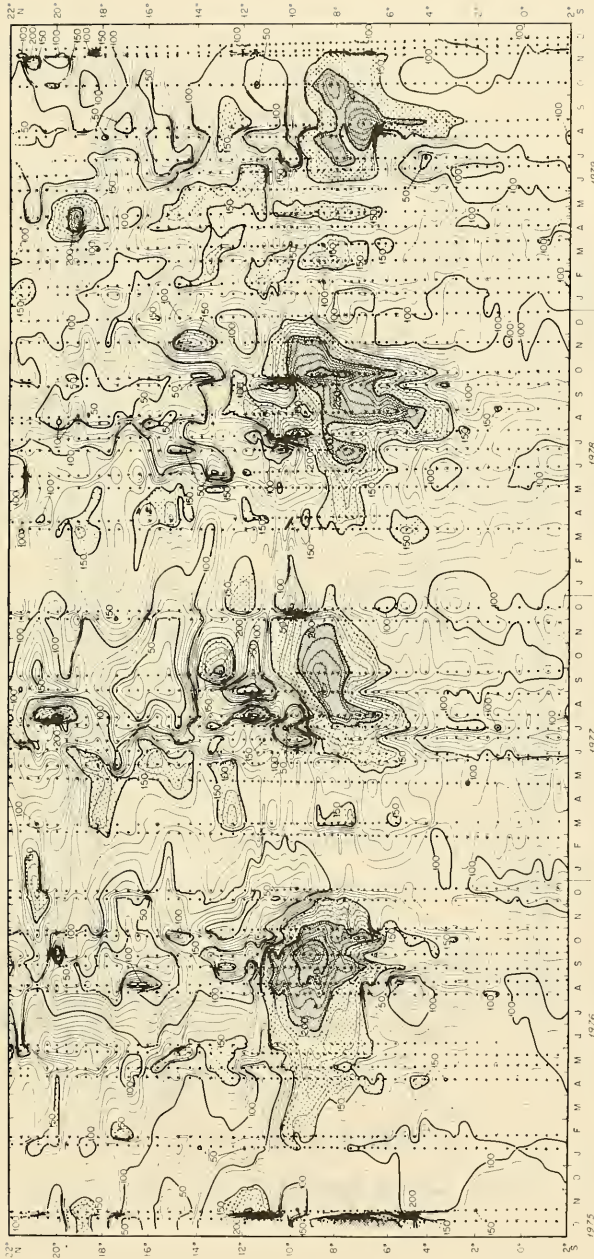


Figure 11. Depth (m) of 20°C isotherm from XBT sections along tanker sea lane (Figure 1a) 2°S to 22°N off Somali and Arabian coasts, October 1975 to December 1979.

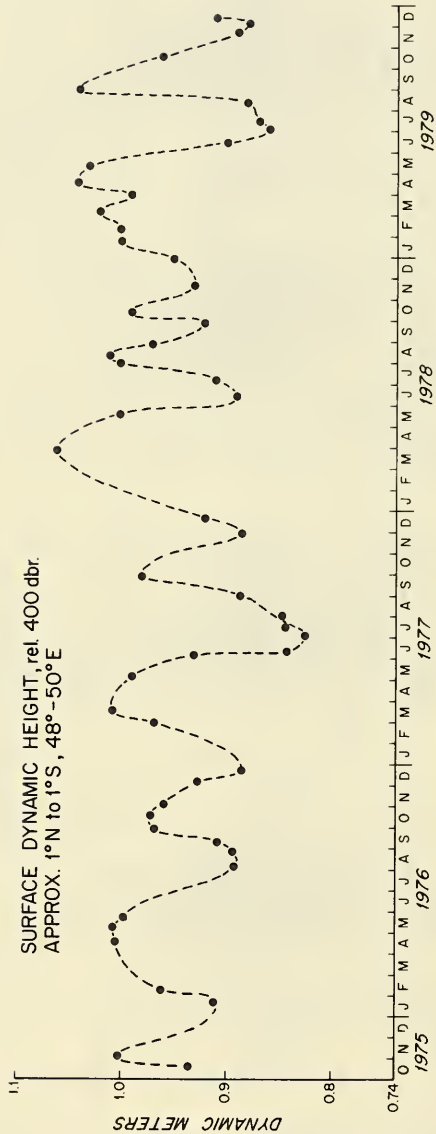


Figure 12. Equatorial surface dynamic height relative to 400 dbar averaged from stations between 1°N to 1°S, from XBT data along tanker sea lane (figure 1a) crossing the equator at approximately 49°E from October 1975 to December 1979.

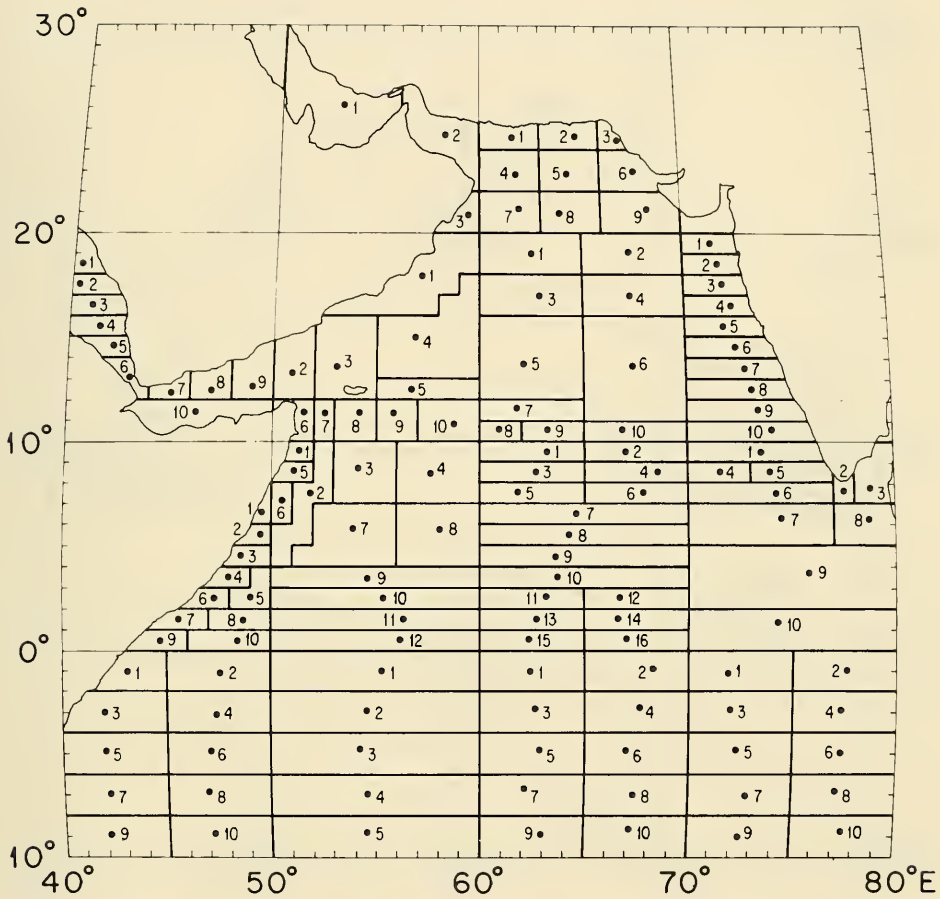


Figure 13. Subdivisions of Marsden squares within which monthly averages of wind stress were calculated for Figure 14. Dot gives center of gravity of observations. Number of observations for each subdivision is given in Table 1.

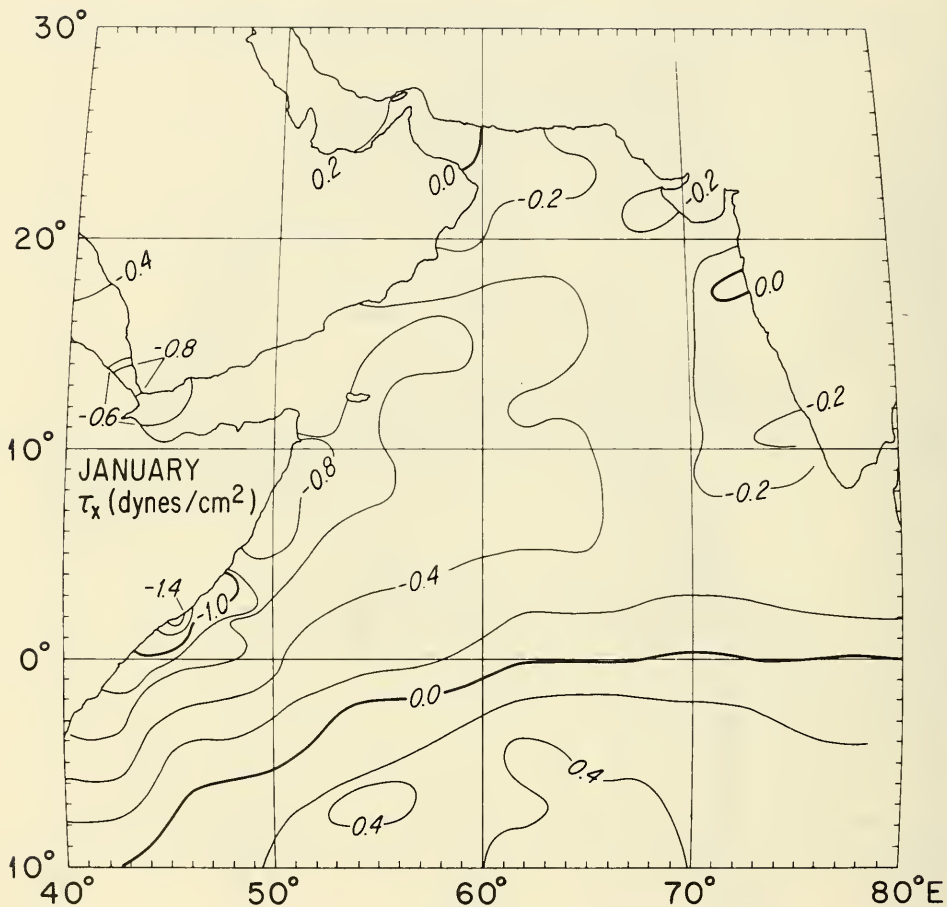


Figure 14. Monthly averages of zonal, τ_x , and meridional, τ_y , wind stress for the western Indian Ocean. The contour increment of 0.2 dynes cm⁻² is the same for all monthly maps. Values are positive to east and north.

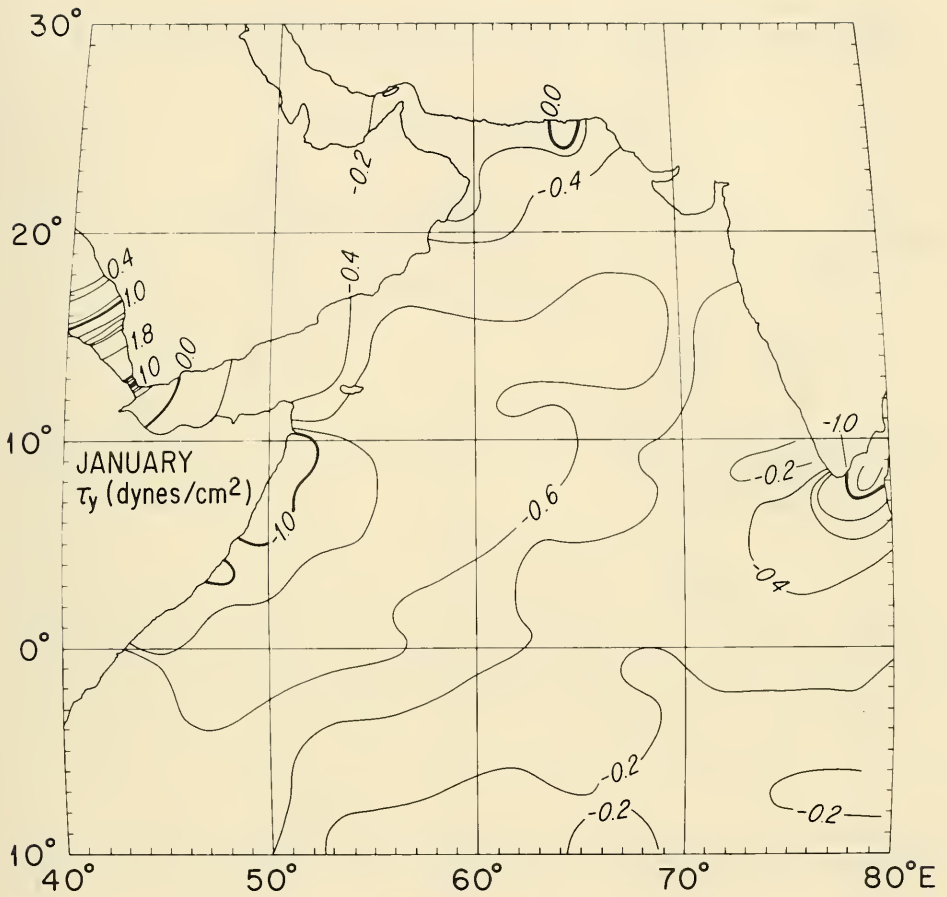


Figure 14. (cont.)

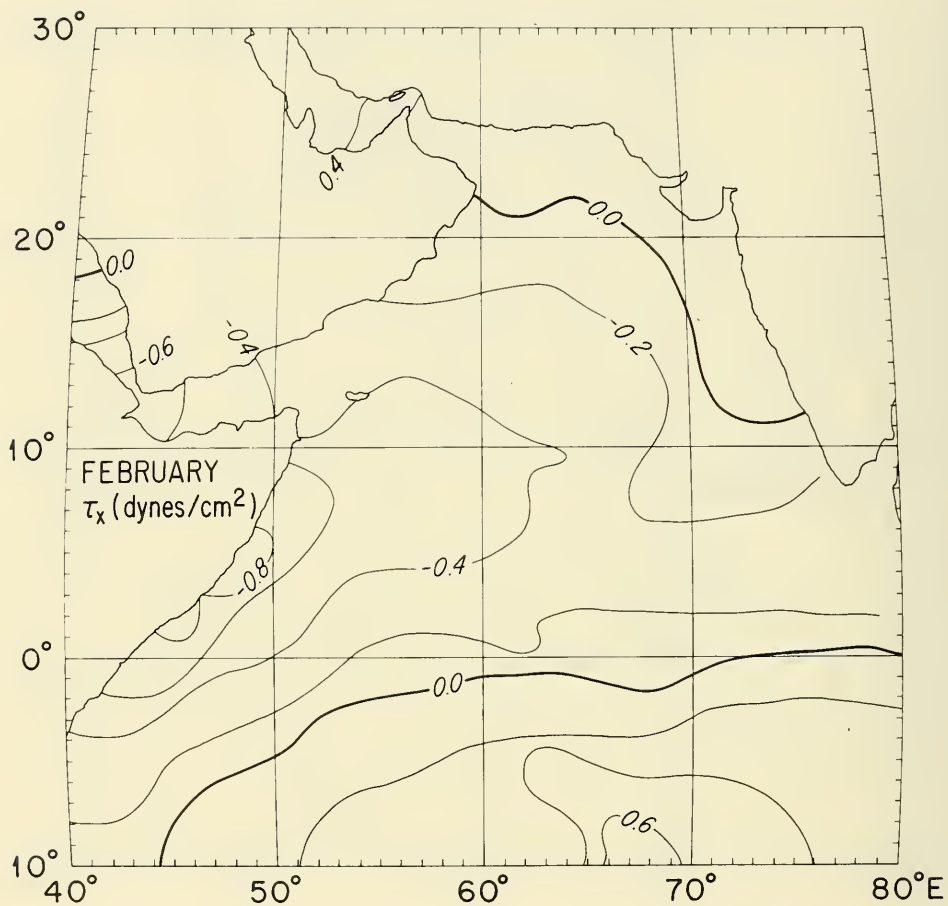


Figure 14. (cont.)

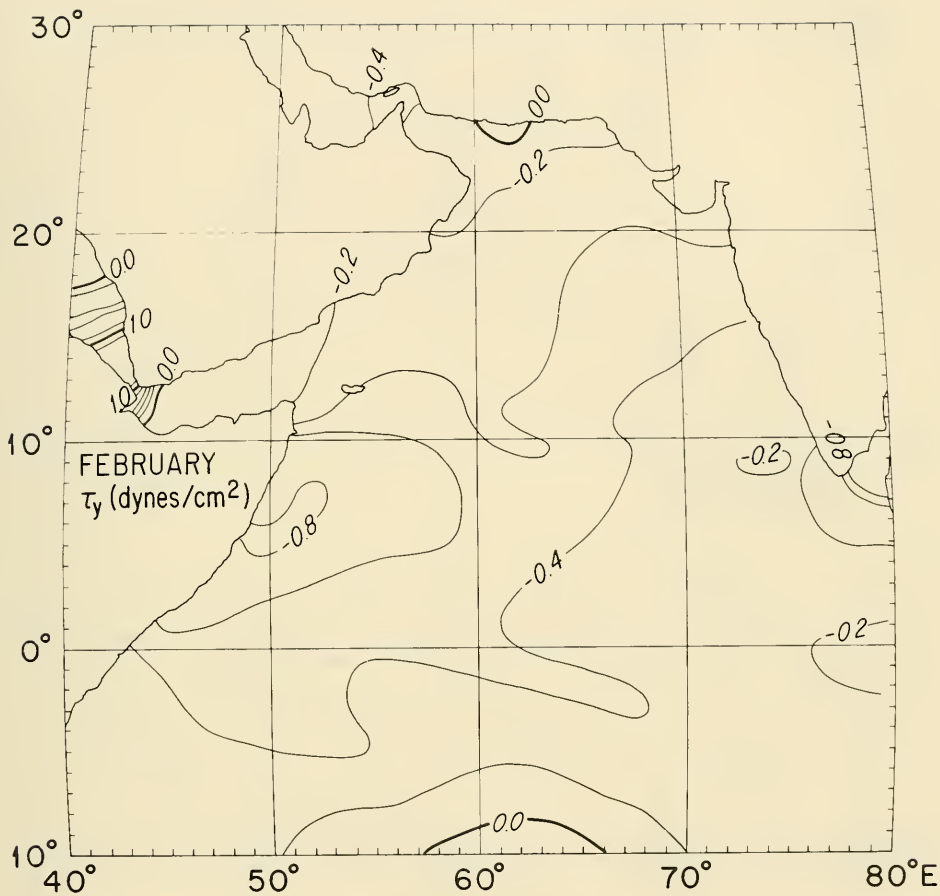


Figure 14. (cont.)

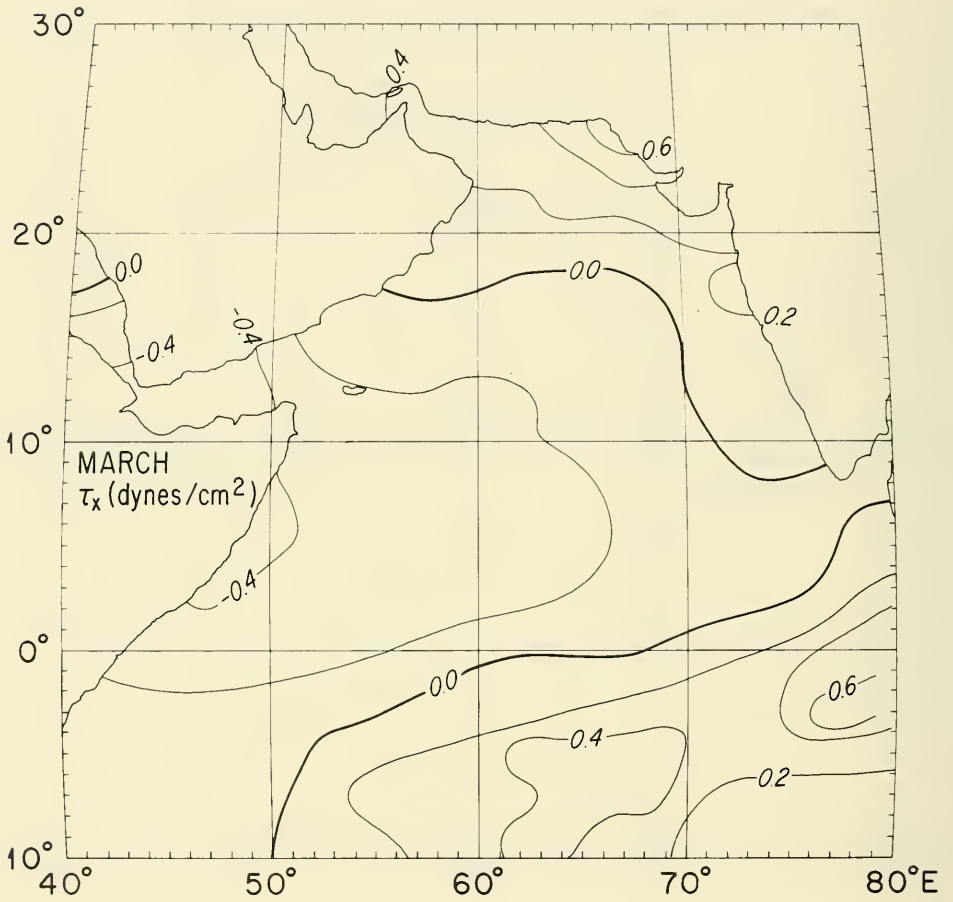


Figure 14. (cont.)

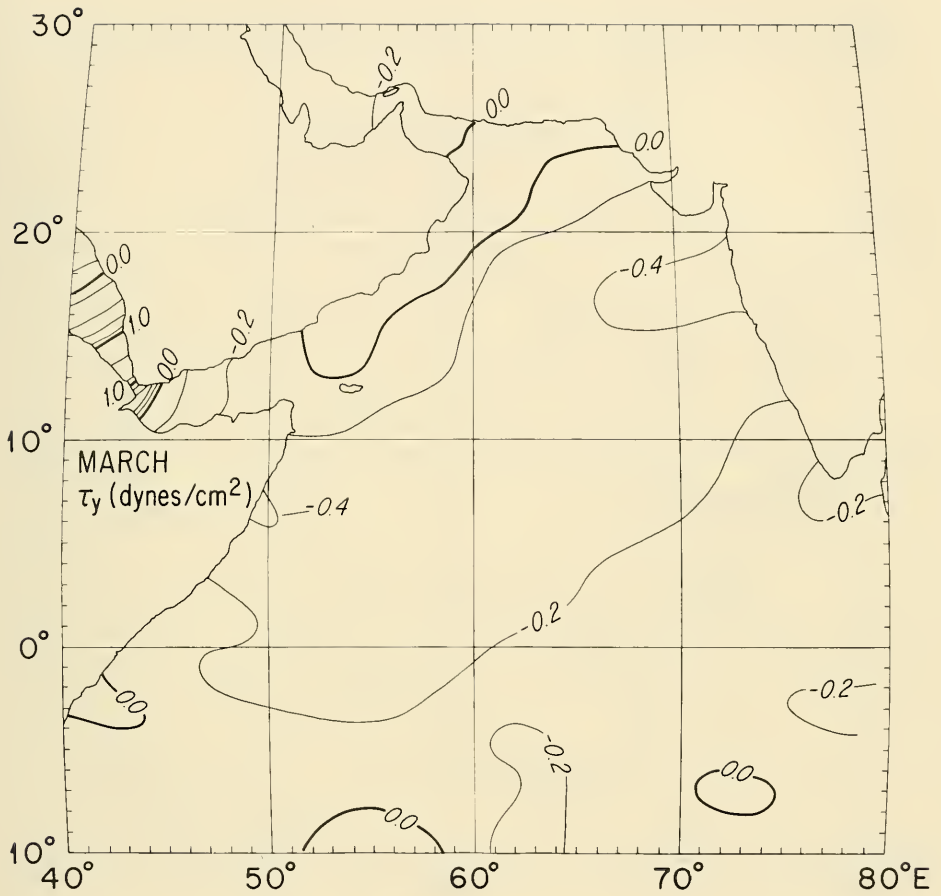


Figure 14. (cont.)

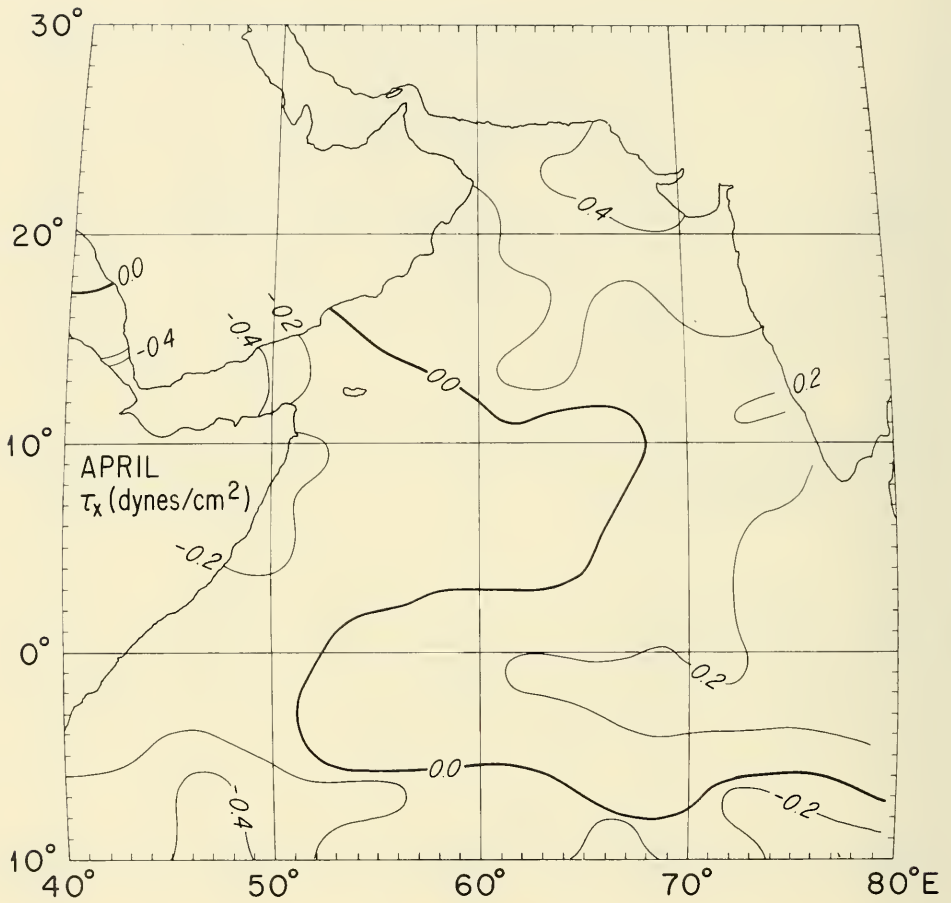


Figure 14. (cont.)

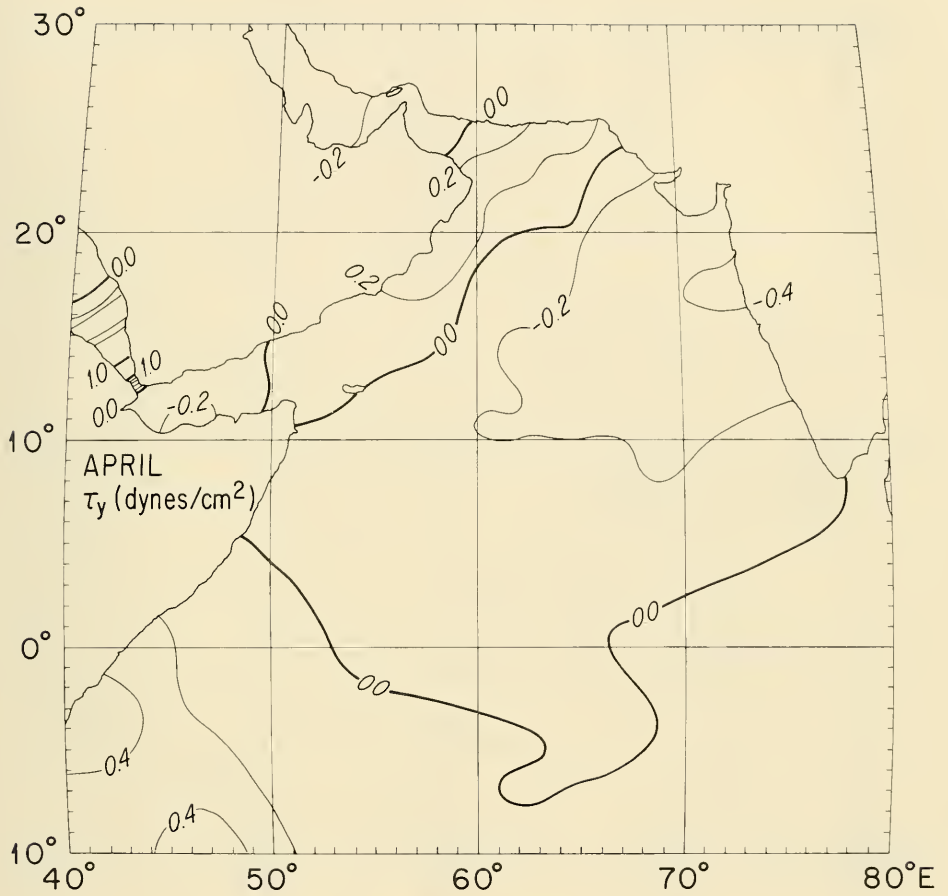


Figure 14. (cont.)

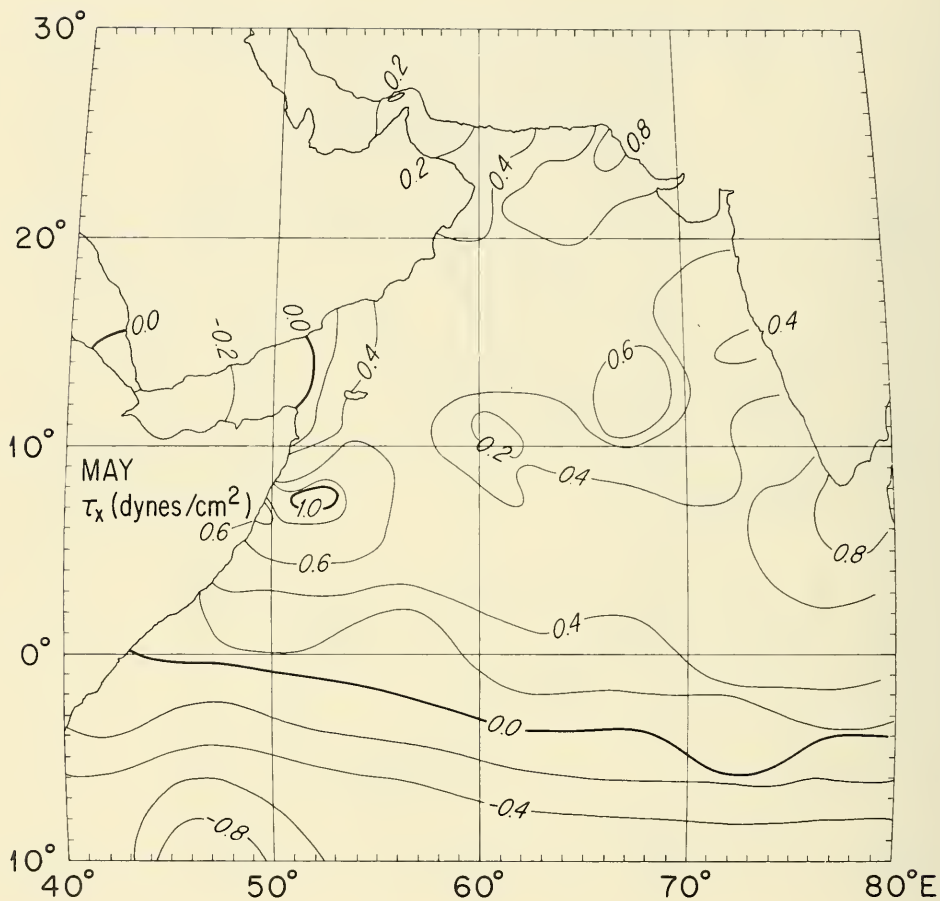


Figure 14. (cont.)

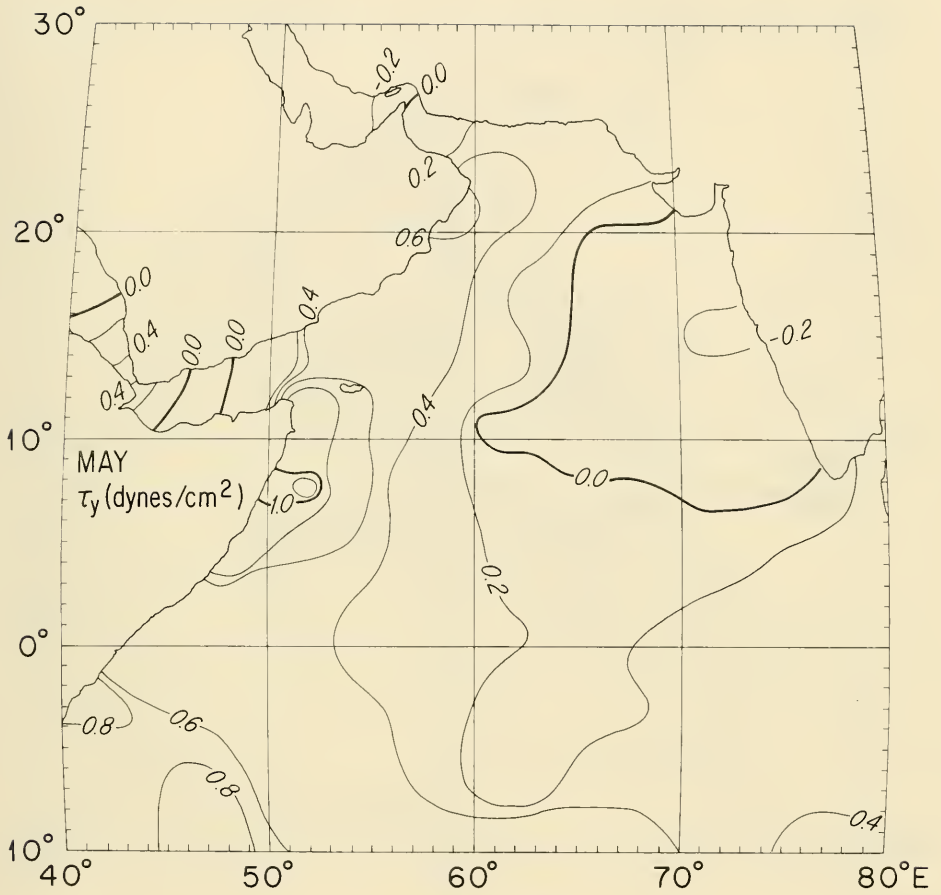


Figure 14. (cont.)

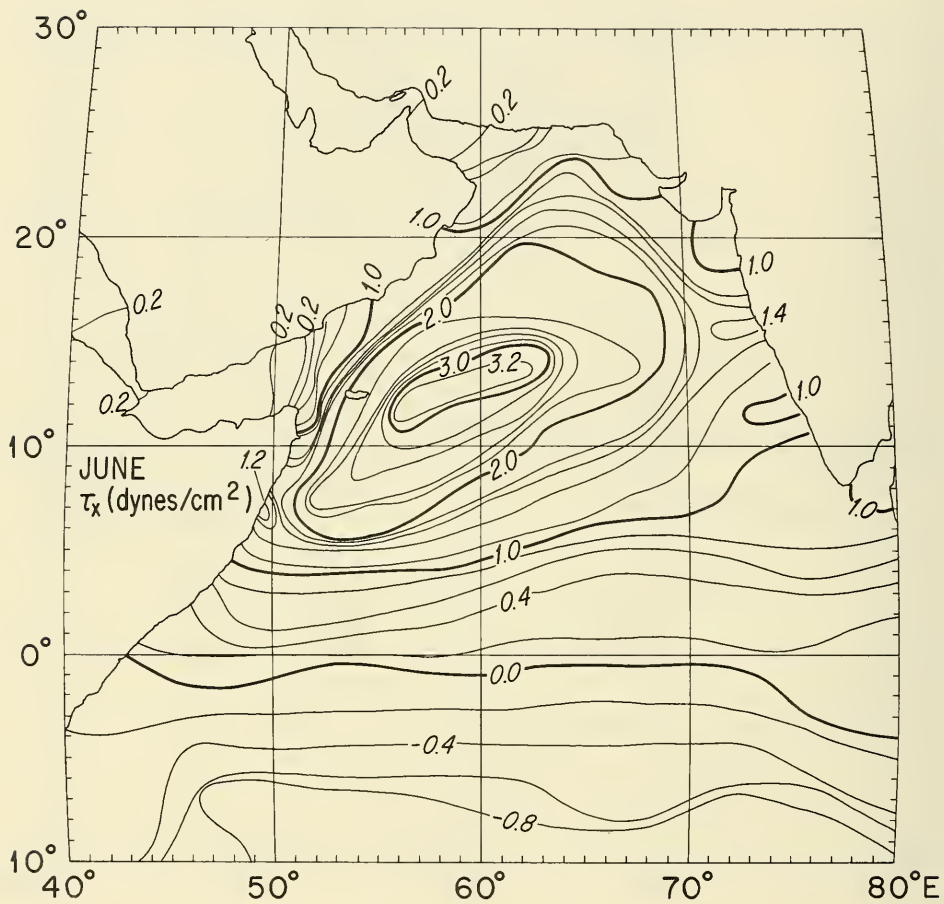


Figure 14. (cont.)

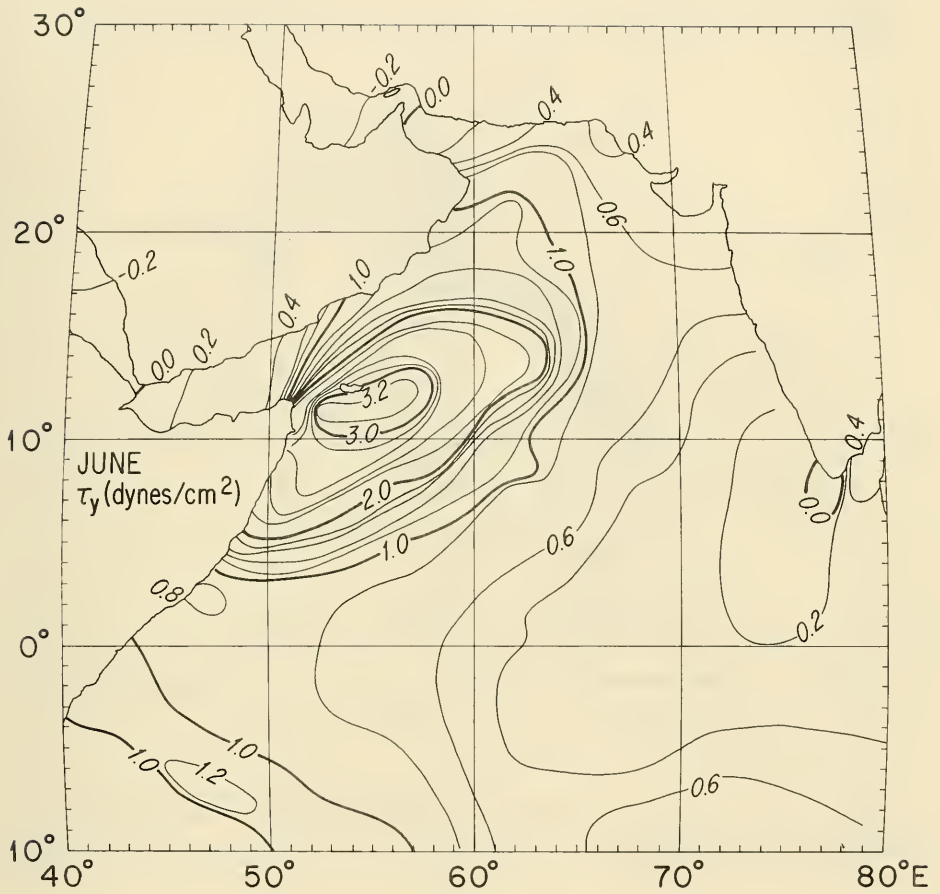


Figure 14. (cont.)

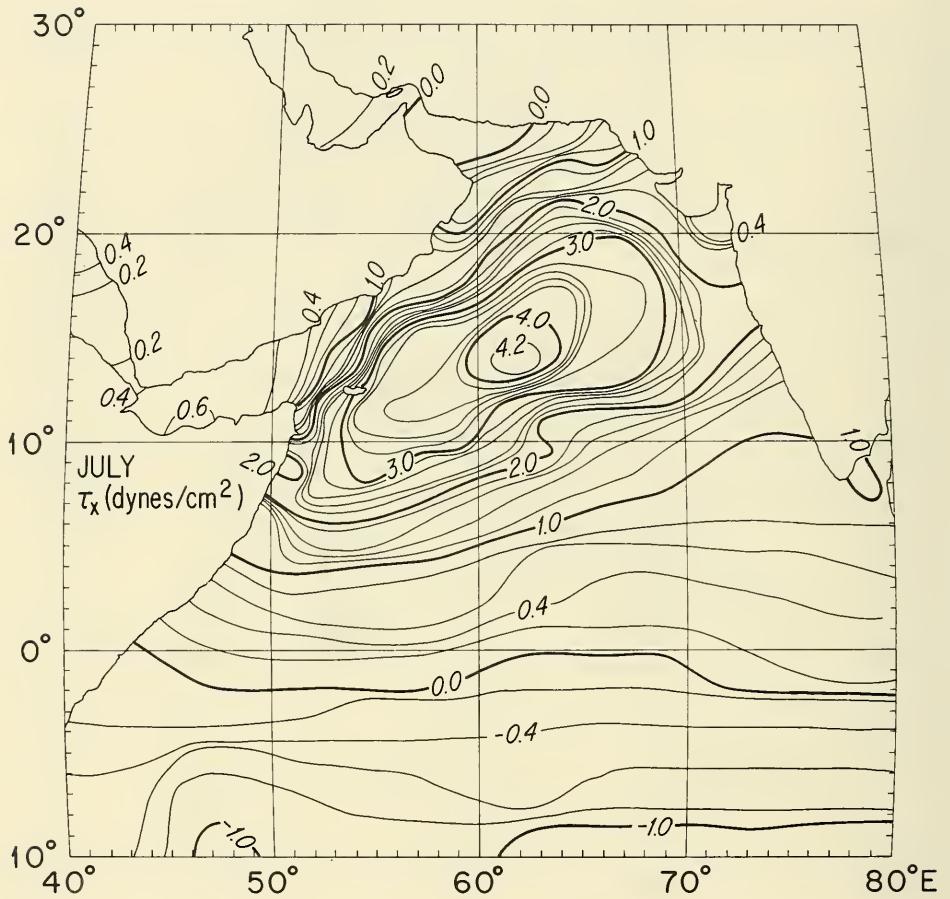


Figure 14. (cont.)

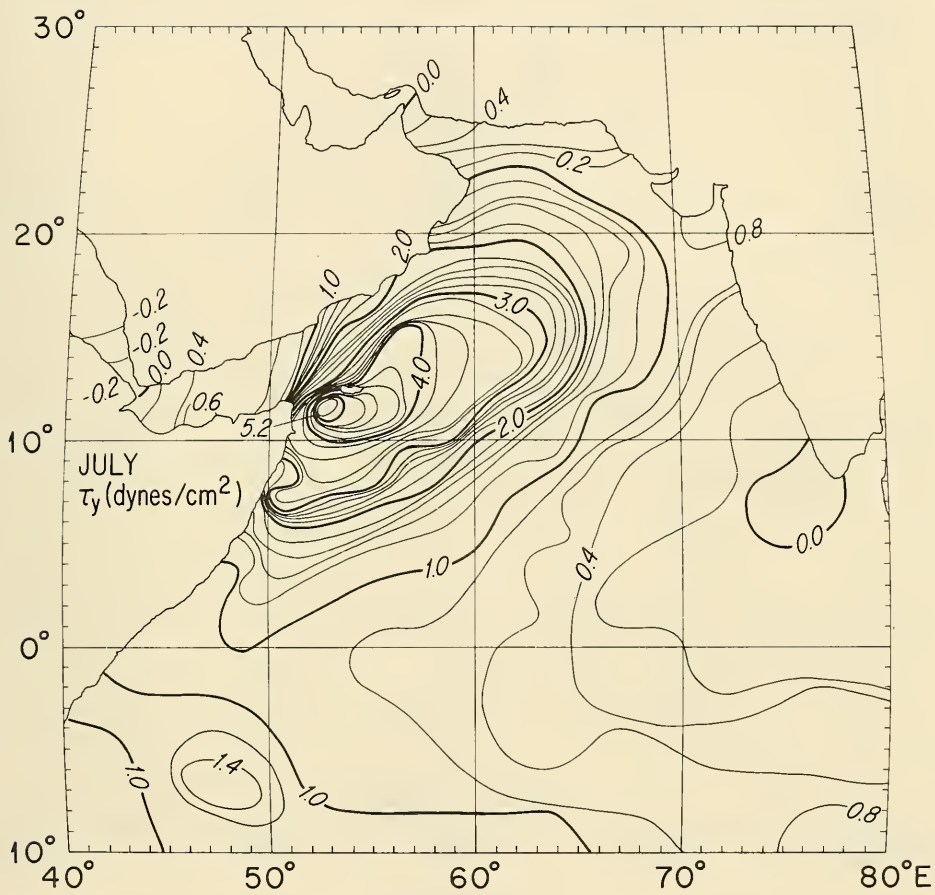


Figure 14. (cont.)

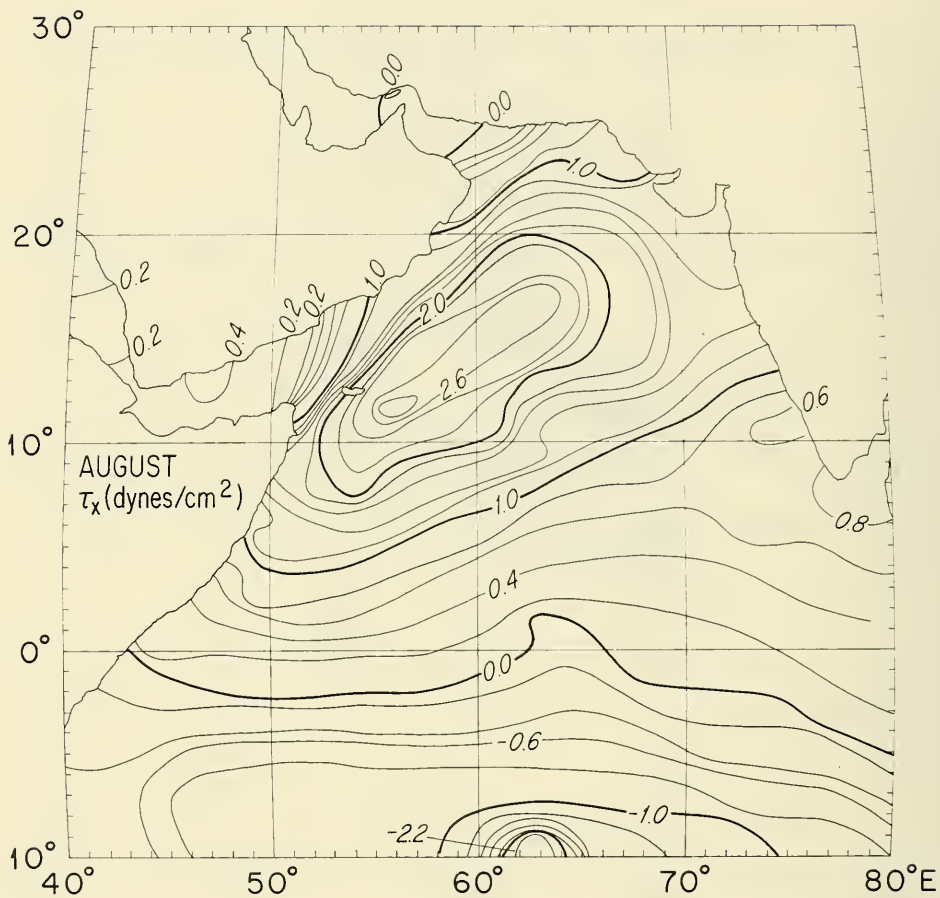


Figure 14. (cont.)

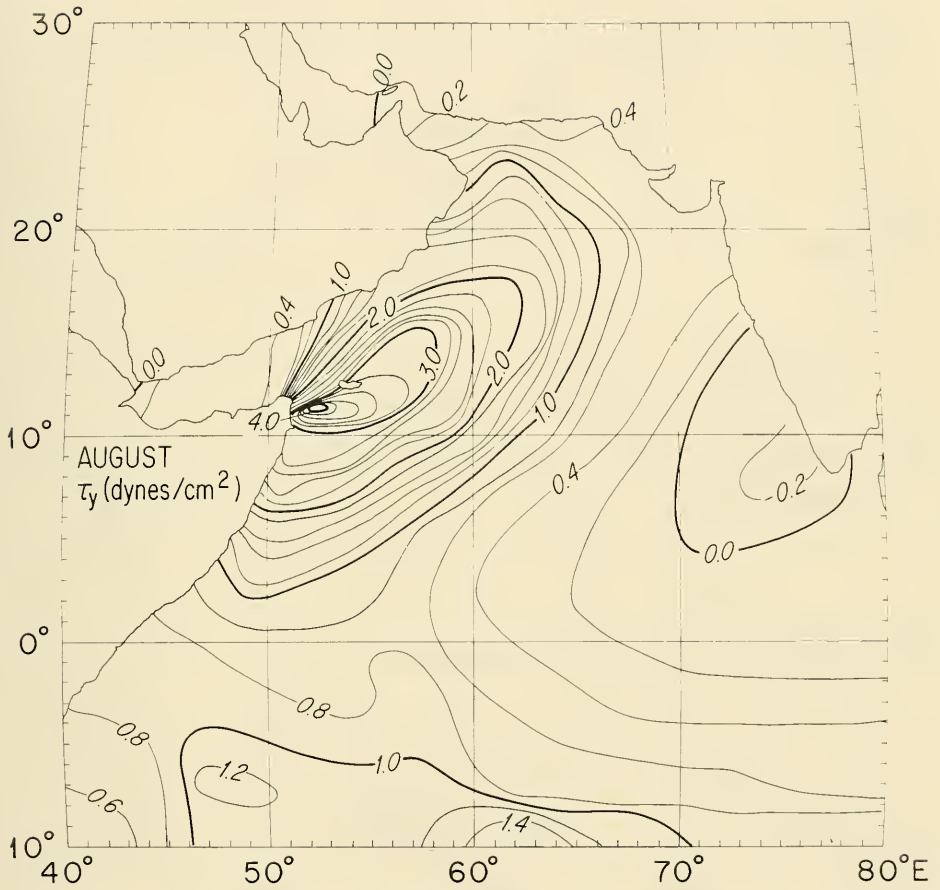


Figure 14. (cont.)

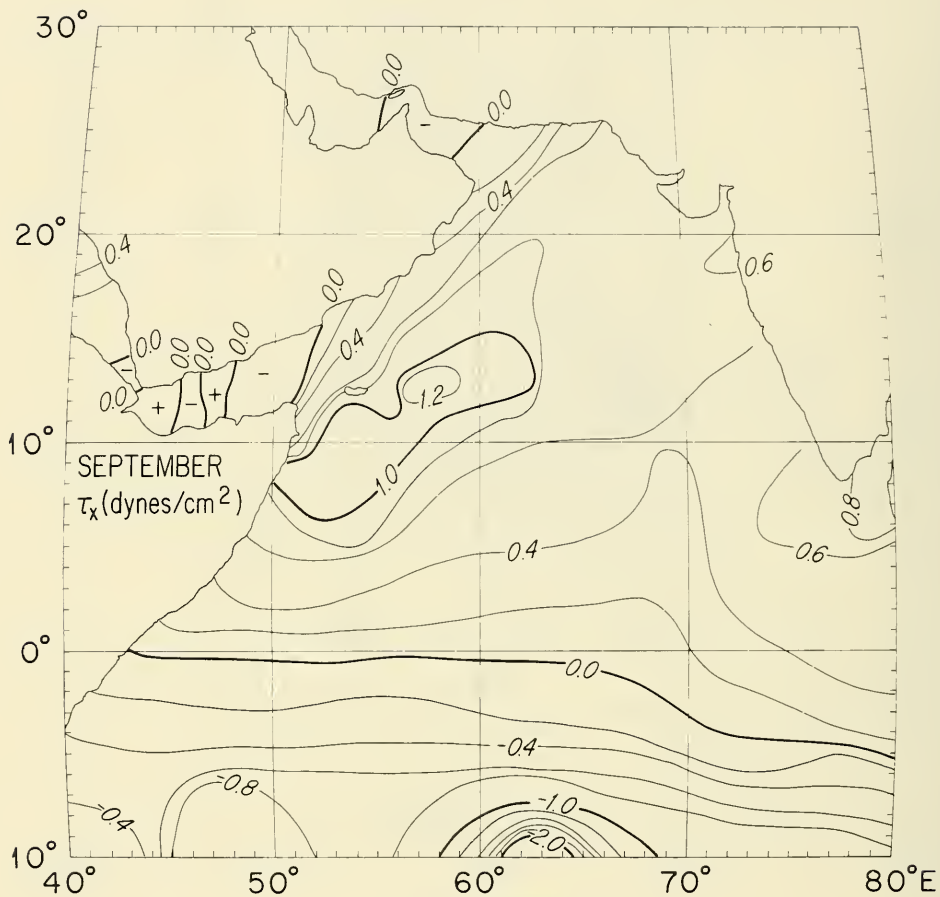


Figure 14. (cont.)

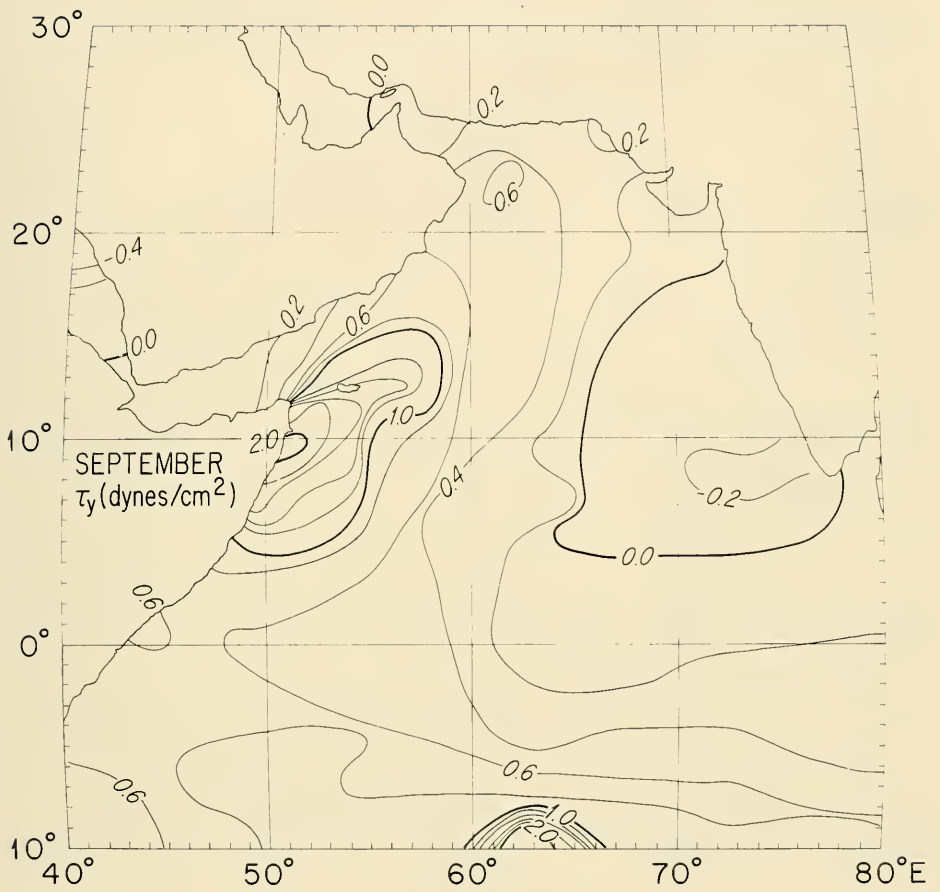


Figure 14. (cont.)

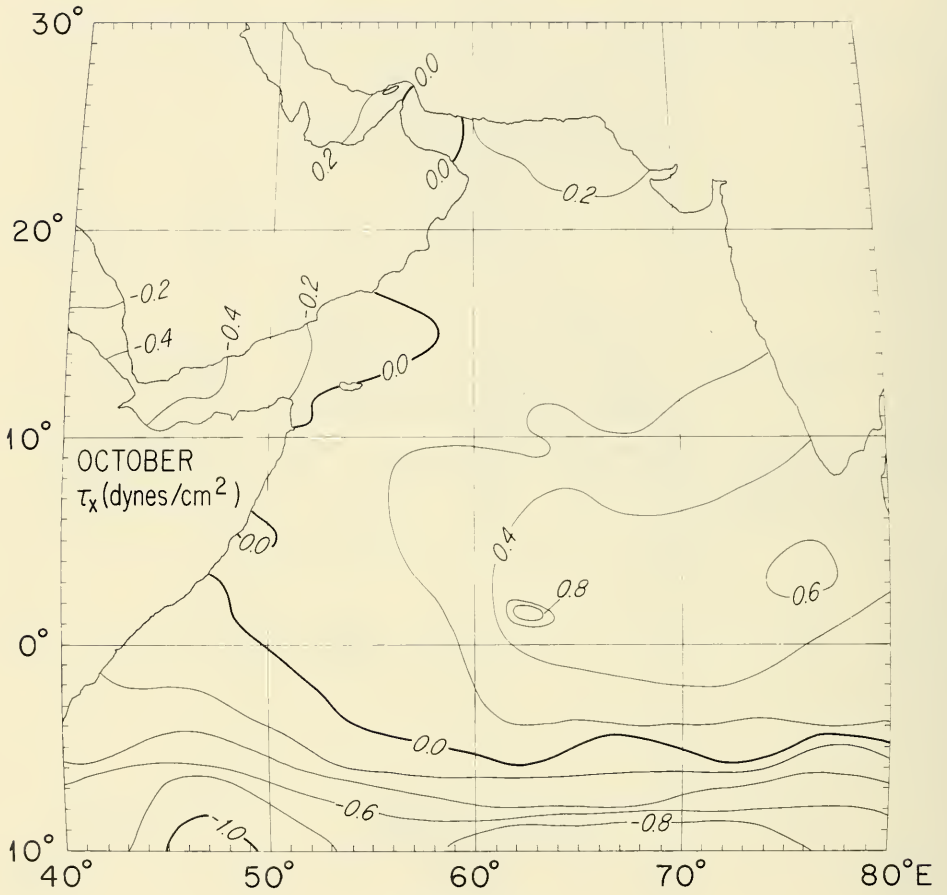


Figure 14. (cont.)

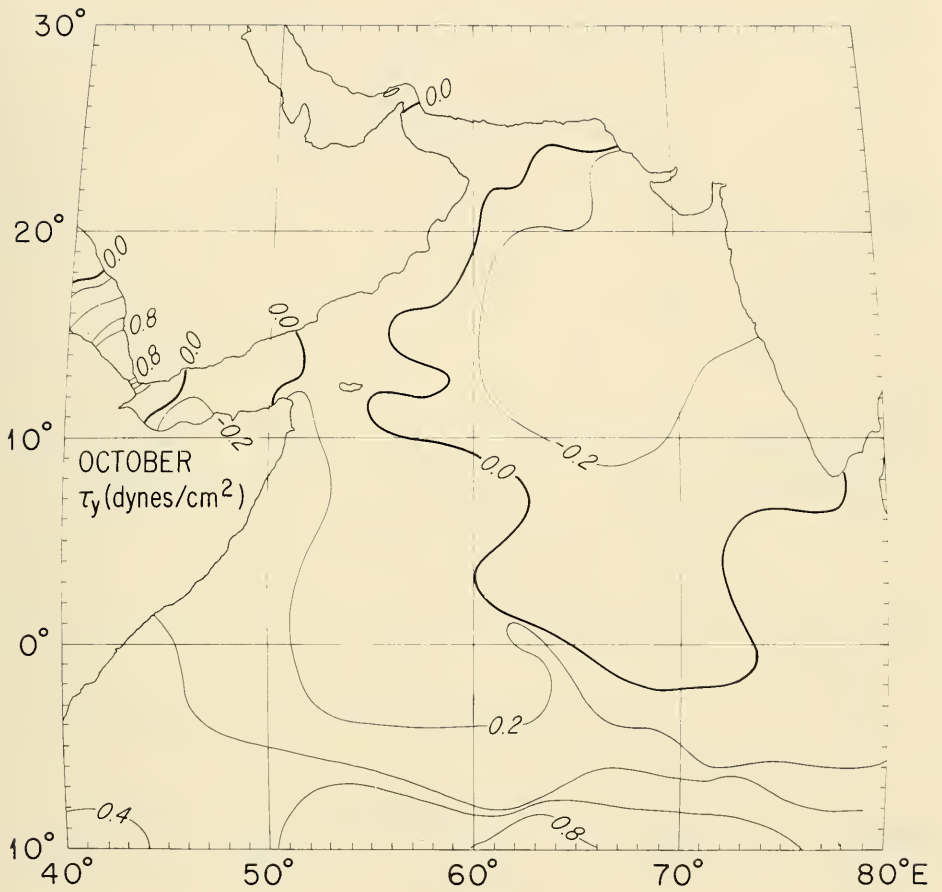


Figure 14. (cont.)

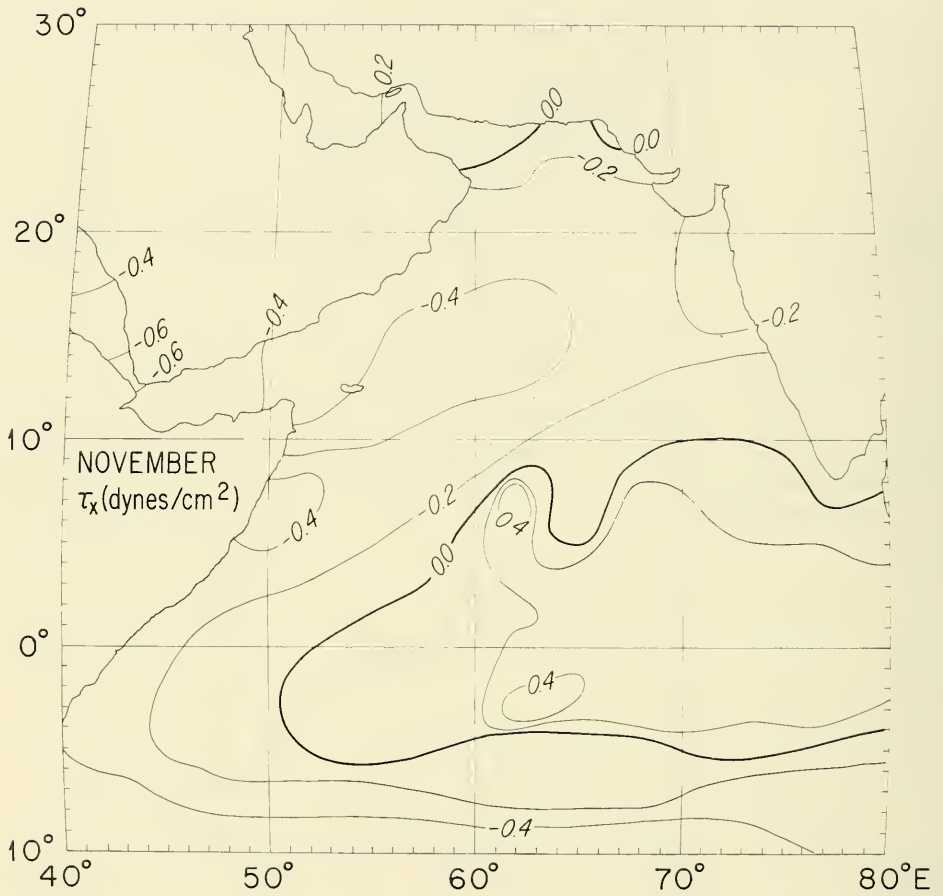


Figure 14. (cont.)

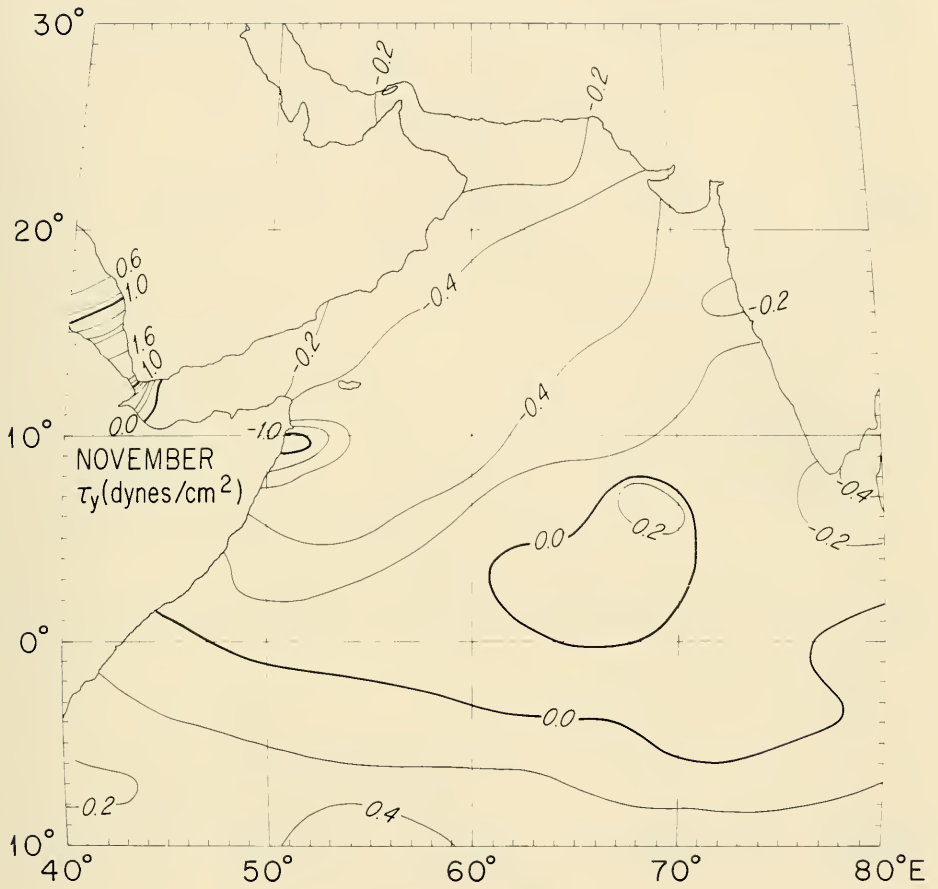


Figure 14. (cont.)

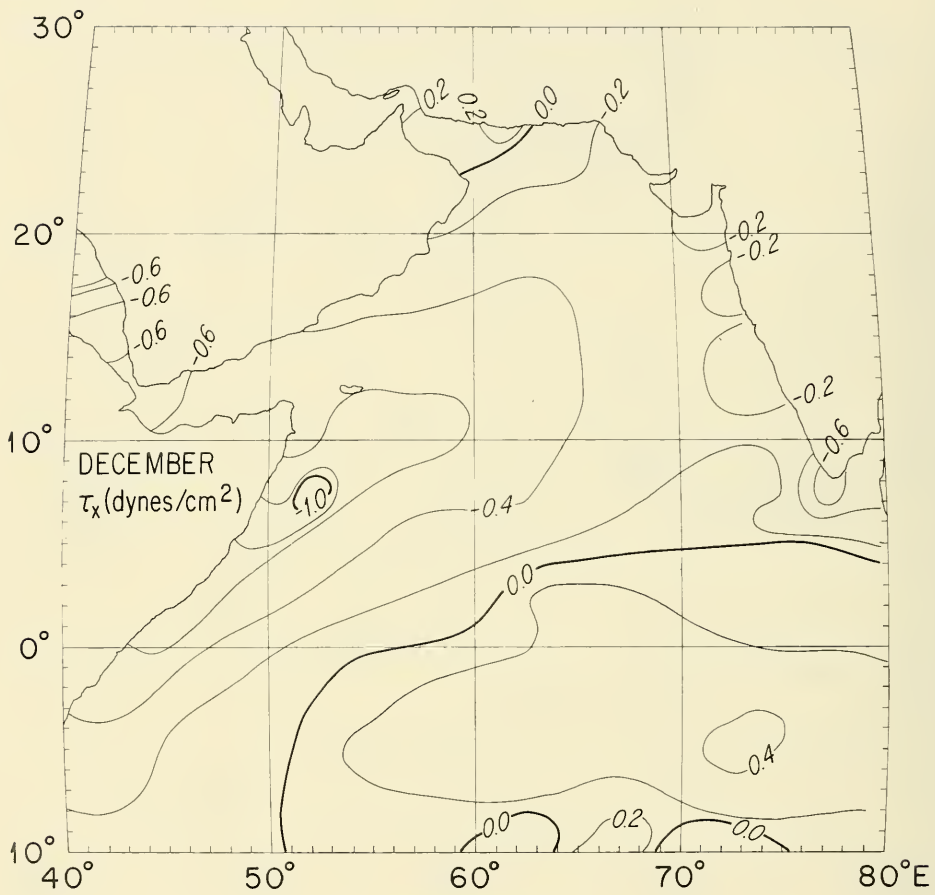


Figure 14. (cont.)

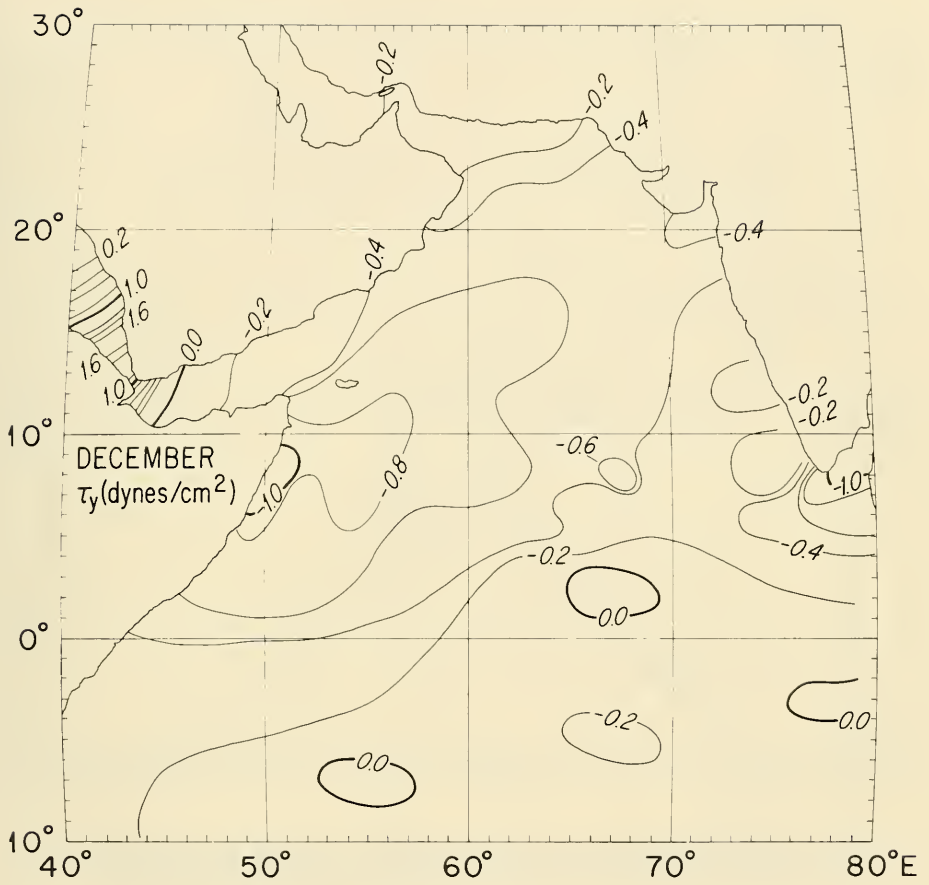


Figure 14. (cont.)

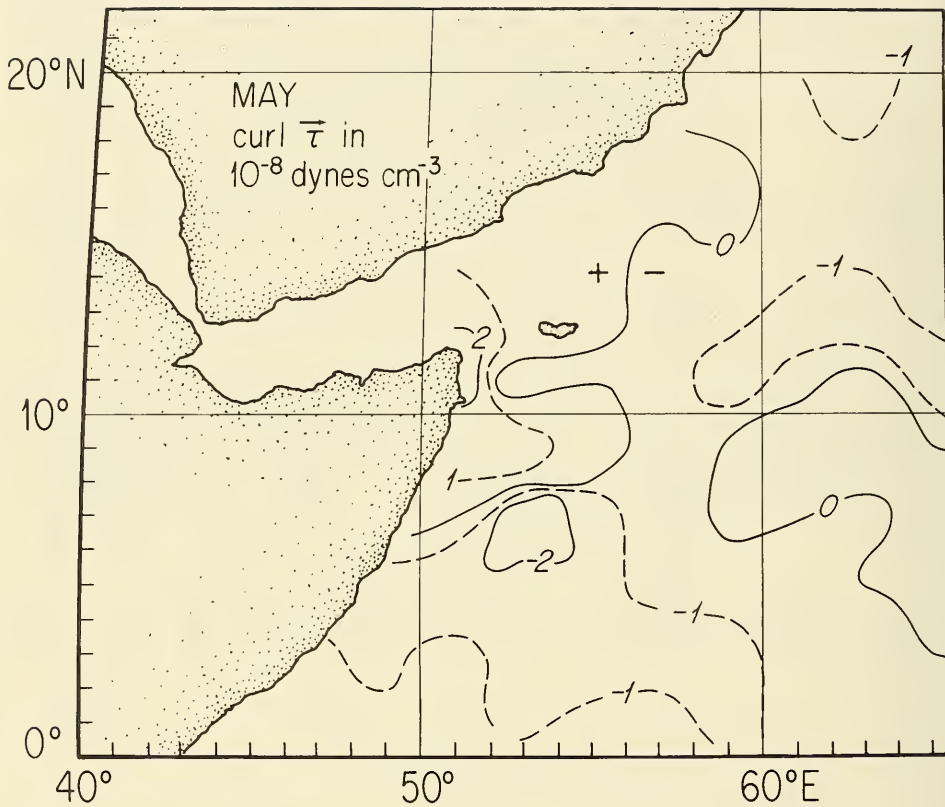


Figure 15. Curl of the wind stress for May in 10^{-8} dynes cm^{-3} from monthly averages (Figure 14) off Somali and Arabian coasts during commencing stage of southwest monsoon.

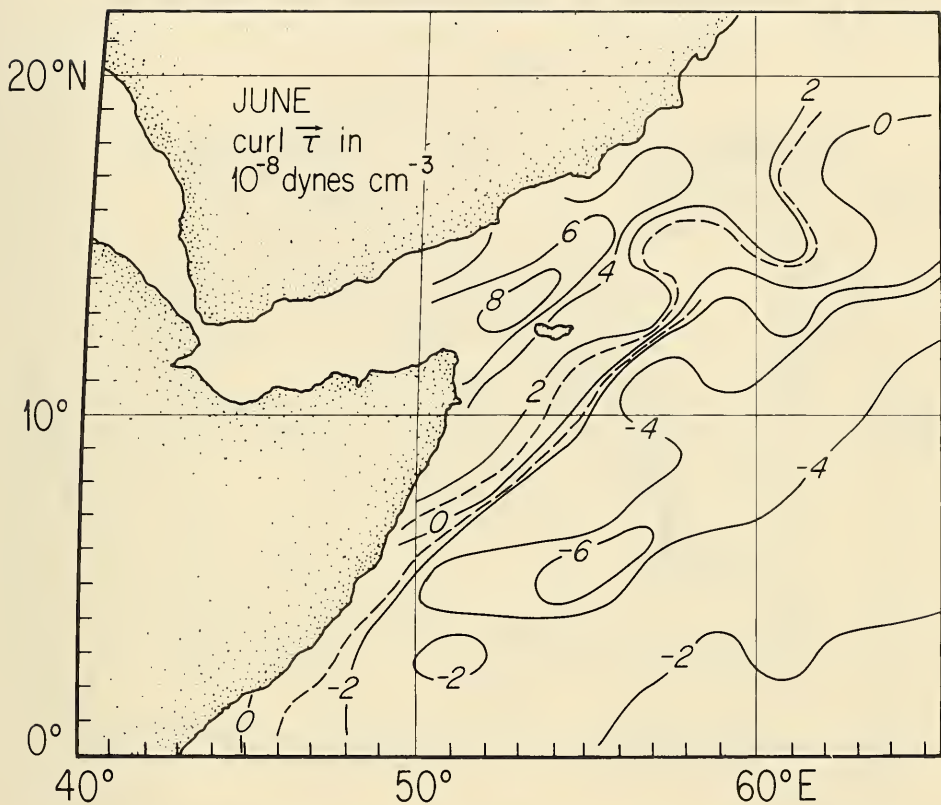


Figure 16. Curl of the wind stress for June in 10^{-8} dynes cm^{-3} from monthly averages (Figure 14) off Somali and Arabian coasts.

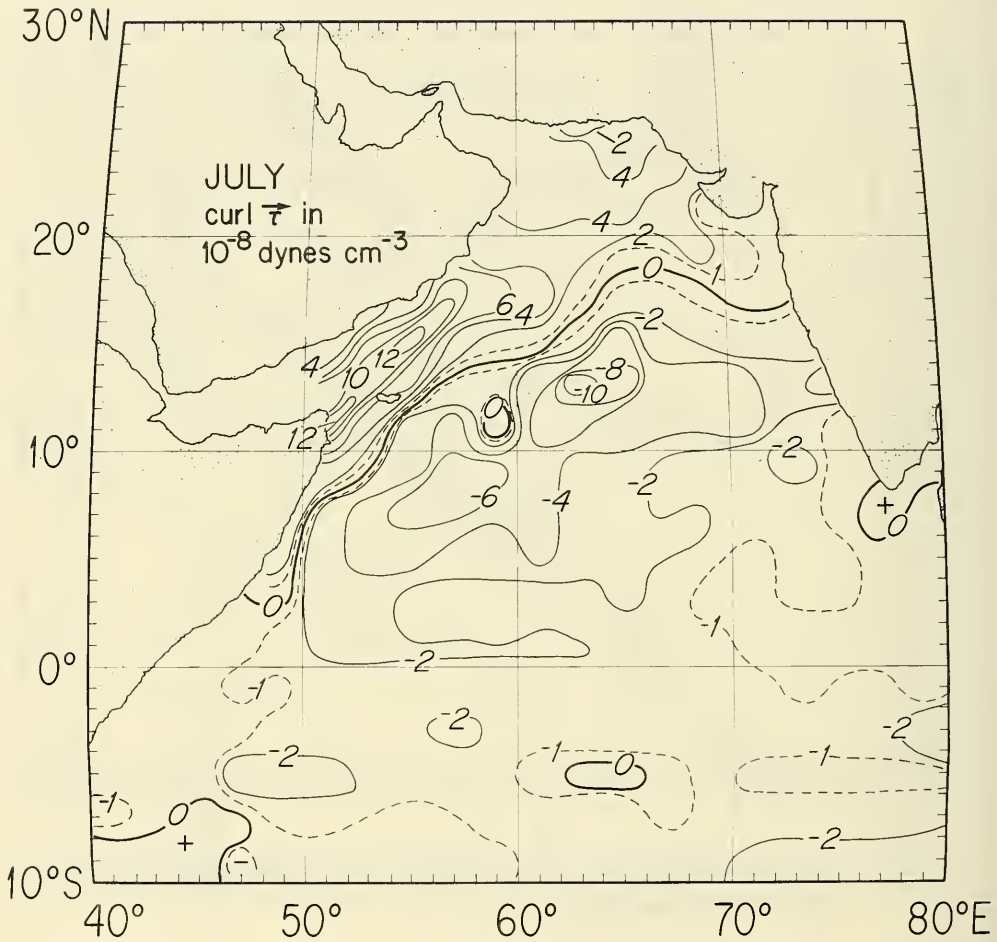


Figure 17. Curl of the wind stress for July in 10^{-8} dynes cm^{-3} from monthly averages (Figure 14) in the western Indian Ocean during the maximum of the southwest monsoon.

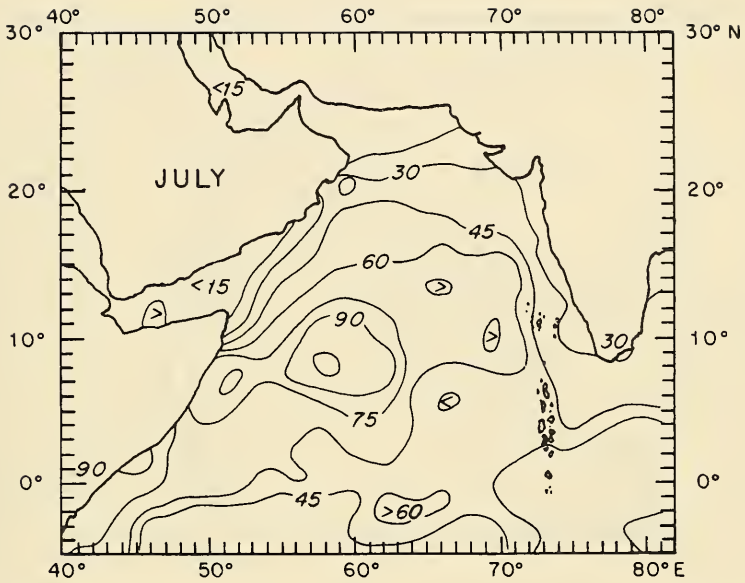


Figure 18. July mean depths (m) to the top of the thermocline (after Robinson *et al.*, 1979).

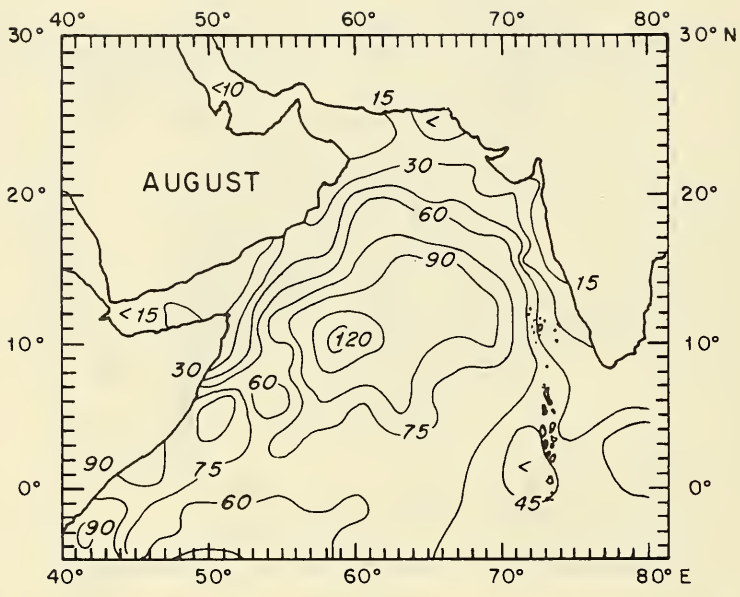


Figure 19. August mean depth (m) to the top of the thermocline (after Robinson *et al.*, 1979).

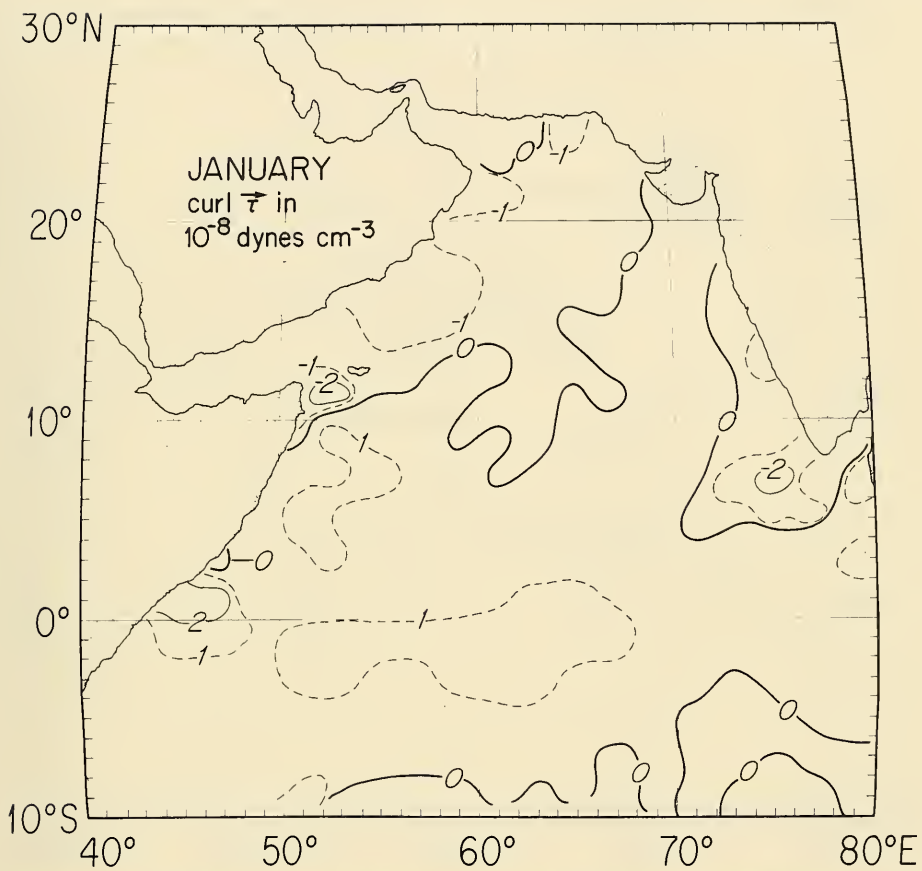


Figure 20. Curl of the wind stress for January in 10^{-8} dynes cm^{-3} from monthly averages (Figure 14) in the western Indian Ocean during the maximum of the northeast monsoon.

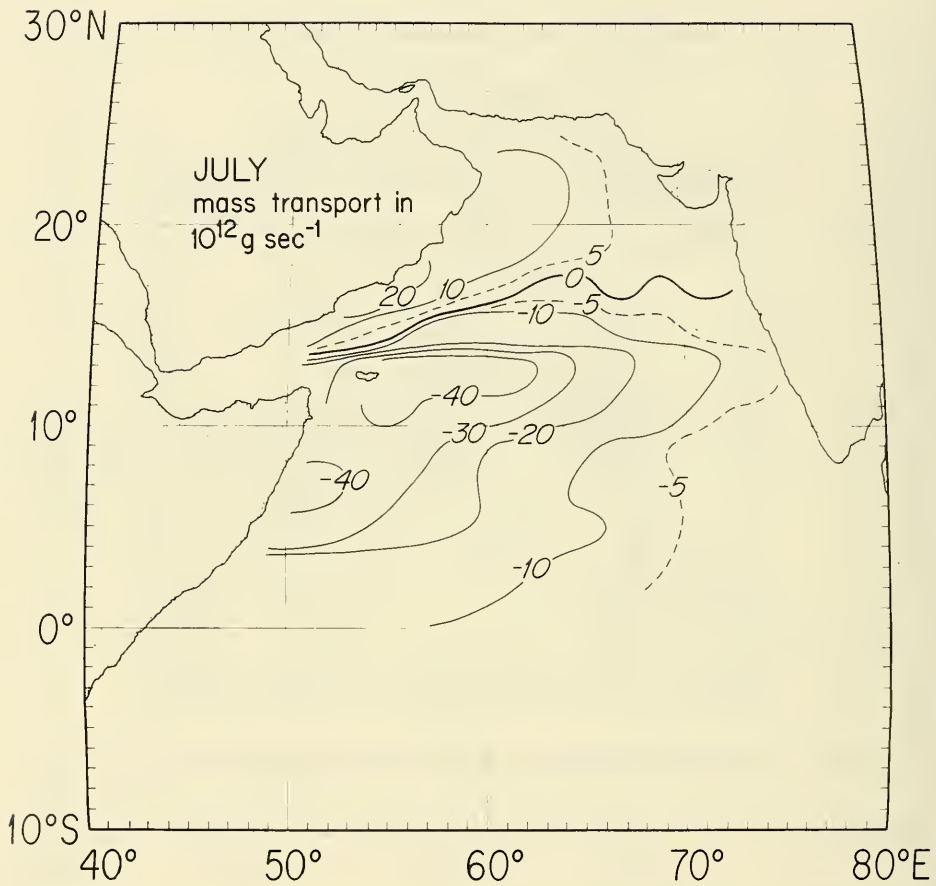


Figure 21. Mean July Sverdrup mass transport in $10^{12} \text{ g sec}^{-1}$, positive to north.

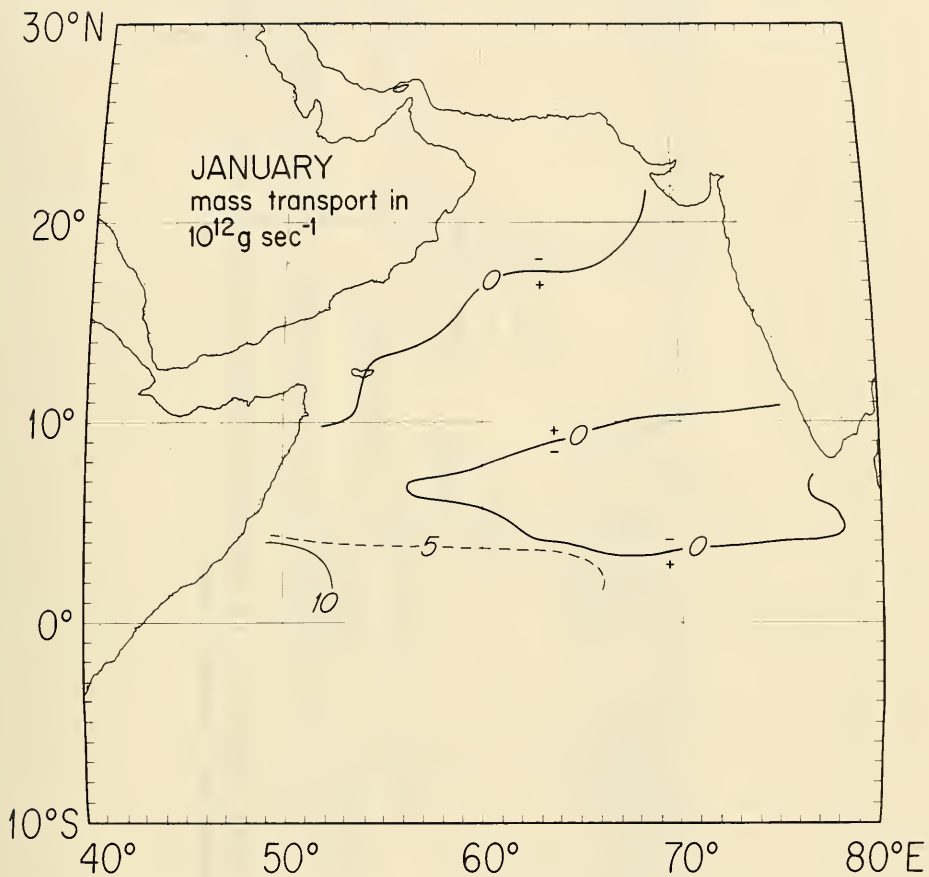


Figure 22. Mean January Sverdrup mass transport in $10^{12} \text{ g sec}^{-1}$, positive to the north.

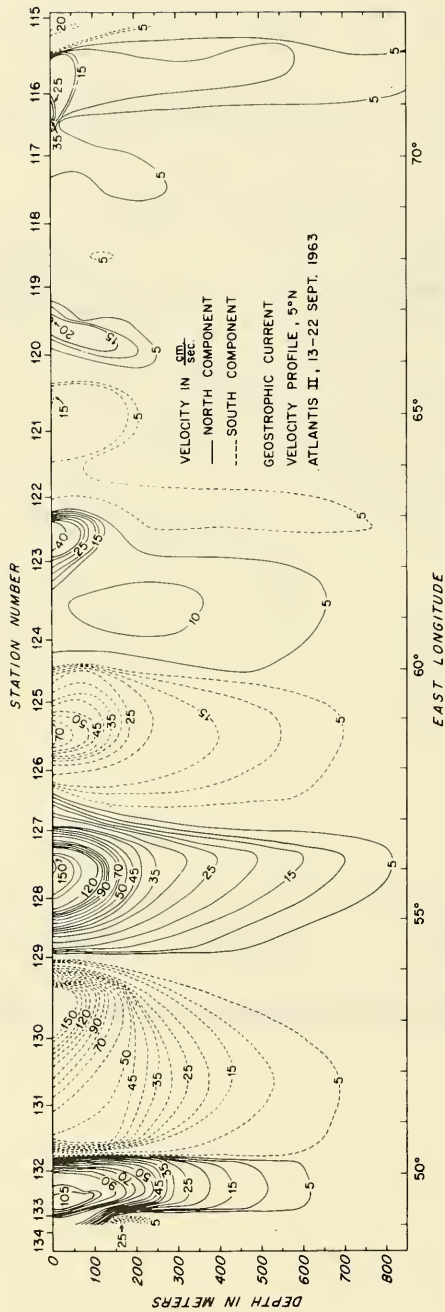


Figure 23. Geostrophic velocity relative to 1000 dbar across 5°N section in the Indian Ocean (between Somali coast, left, to Maldives west slope, right) during latter part of southwest monsoon.

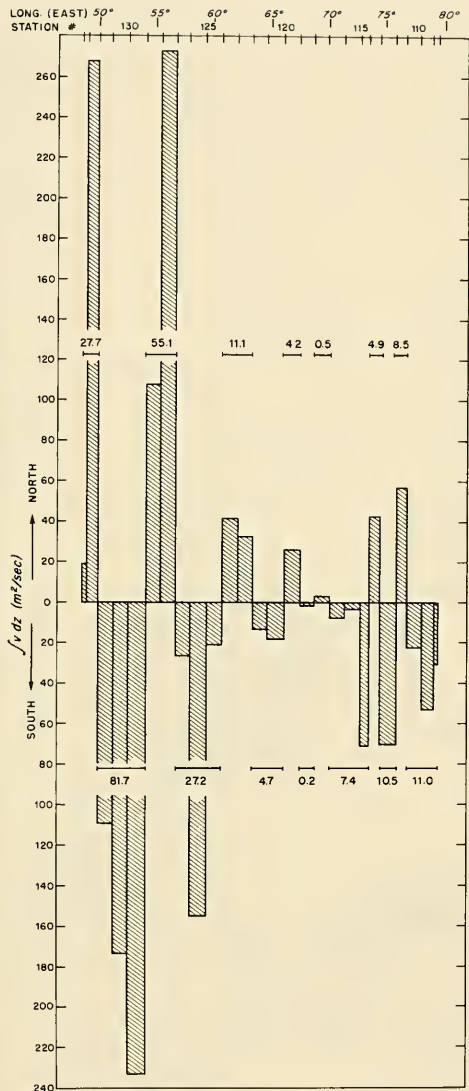


Figure 24. Geostrophic volume transport, 0 - 1000 dbar relative to 1000 dbar, across 5°N section (Figure 23) in the Indian Ocean. Area of columns represents transport, value for each group in $10^6 m^3 sec^{-1}$.

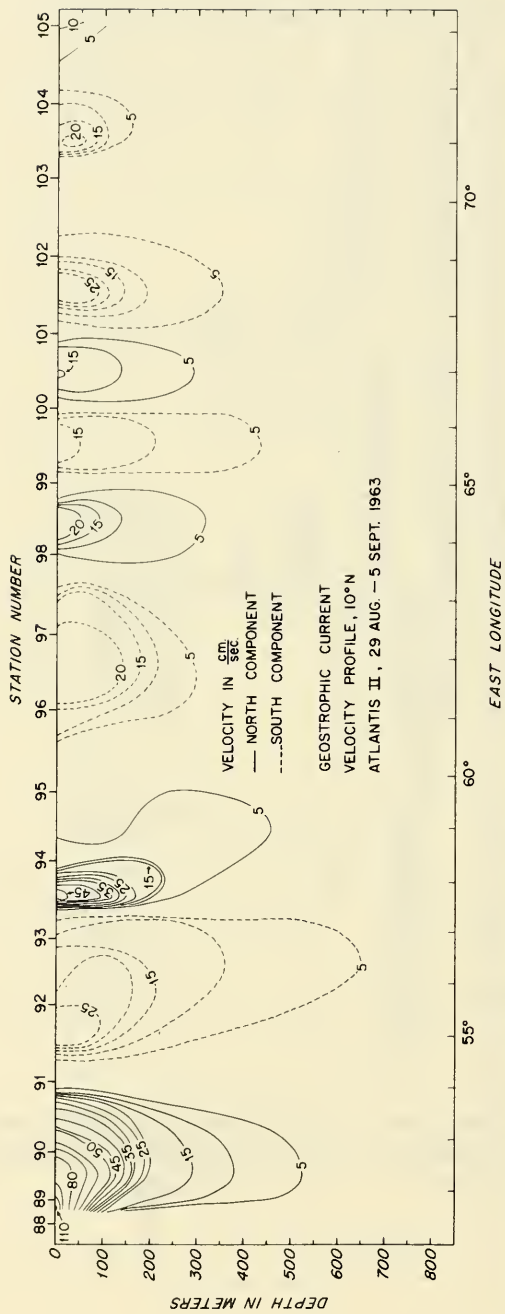


Figure 25. Geostrophic velocity relative to 1000 dbar across 10°N section in the Indian Ocean (between Somali coast, left, and Laccadives, west slope, right) during the southwest monsoon.

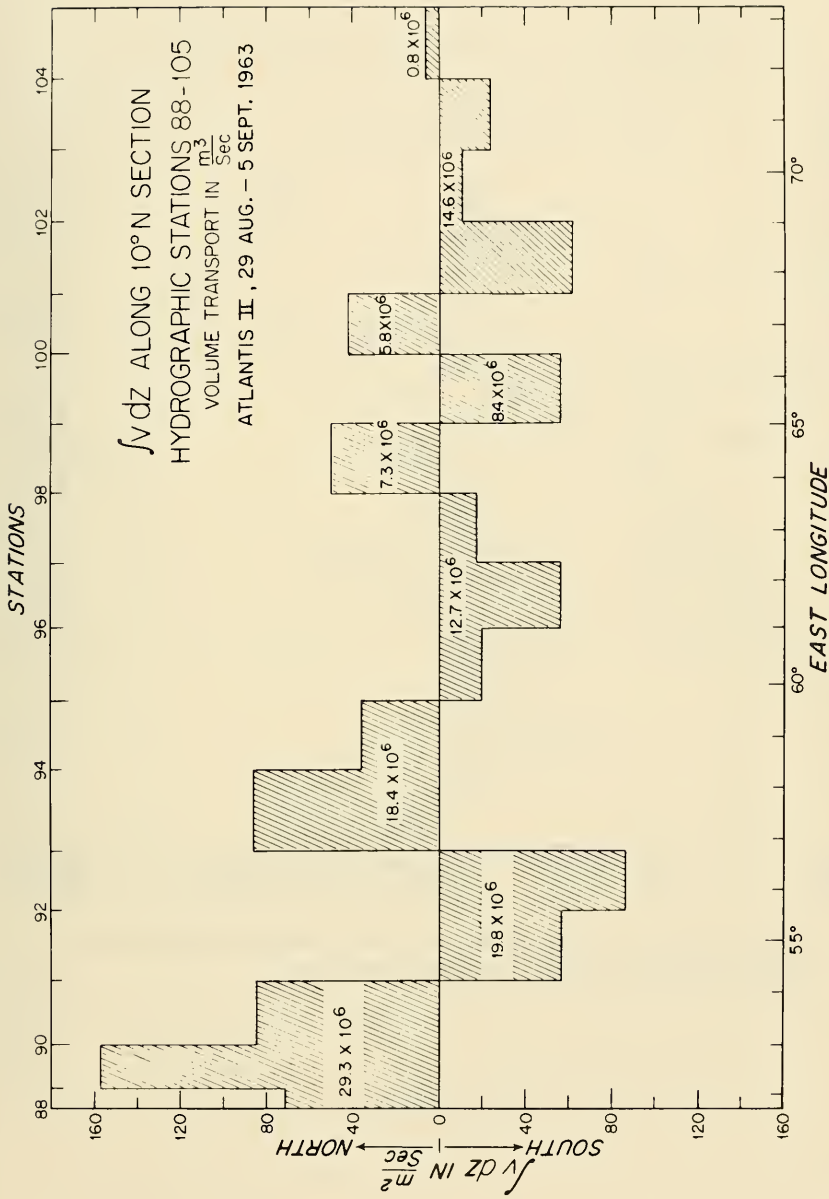


Figure 26. Geostrophic volume transport, 0 - 100 dbar relative to 1000 dbar, across 10°N section (Figure 25) in the Indian Ocean. Area of column represents transport in $m^3 sec^{-1}$.

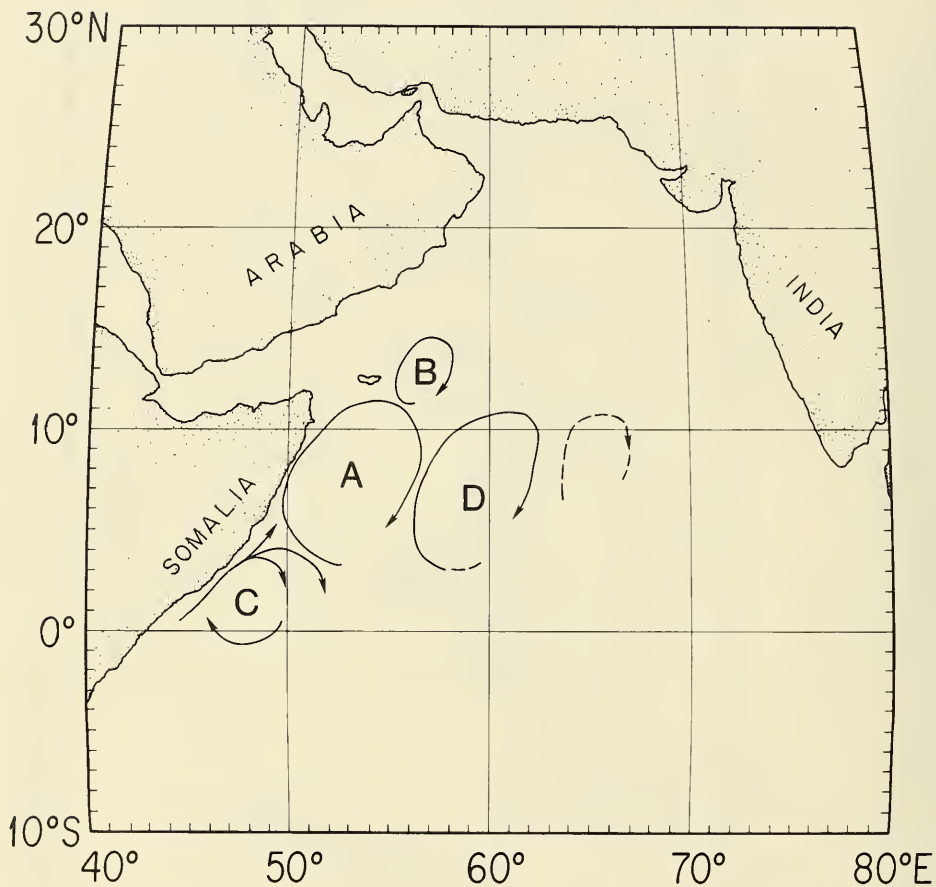


Figure 27. Schematic diagram giving probable circulation pattern of anticyclonic eddies formed during the southwest monsoon in the western Indian Ocean.

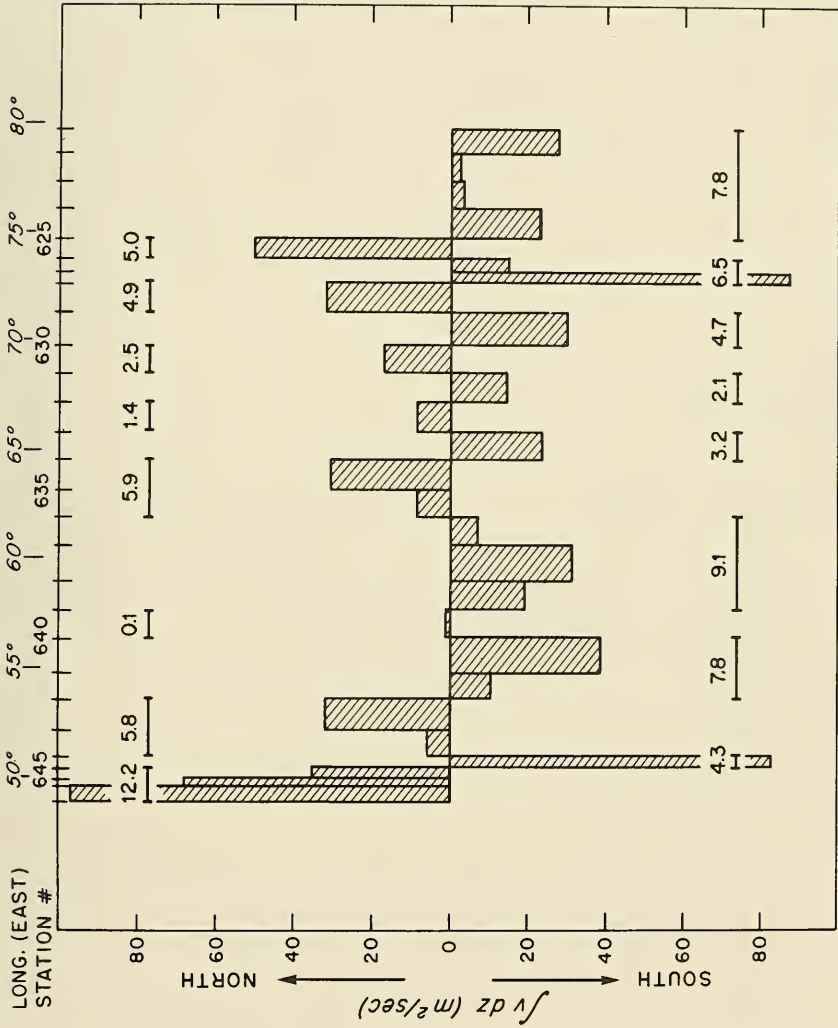


Figure 28. Geostrophic volume transport, 0 - 1000 dbar relative to 1000 dbar, across 5°N section in the Indian Ocean during April 1975 (ATLANTIS II, Cruise 15). Area of column represents transport in $10^6 \text{ m}^3 \text{ sec}^{-1}$.

DISTRIBUTION LIST

<u>Activity</u>	<u>Total No. of Copies</u>
CNO(OP 095, OP 0952)	2
COMNAVOCEANCOM	1
UNSECDEF (R&E)	1
NAVWARCOL	1
CNR (Code 480)	1
NISC	1
NORDA	1
NRL	1
NUSC (Newport)	1
NUSC (New London)	1
NAVPGSCOL	1
NOSC	1
ASN (R&D)	1

TR-272

**VARIATIONS IN THE THERMAL STRUCTURE
AND WIND FIELD OCCURRING IN THE
WESTERN INDIAN OCEAN DURING THE
MONSOONS**